

Biofunctionalized Nanoporous Aluminum Oxide Culture Chips

For Capture and Growth of Bacteria

Aline Debrassi

Thesis committee

Promotors

Prof. Dr H. Zuilhof
Professor of Organic Chemistry
Wageningen University

Prof. Dr W. M. de Vos
Professor of Microbiology
Wageningen University

Co-promotor

Dr T. Wennekes
Assistant Professor, Laboratory of Organic Chemistry
Wageningen University

Other members

Prof. Dr T. Abee, Wageningen University
Prof. Dr J. Huskens, University of Twente, The Netherlands
Prof. Dr T. K. Lindhorst, University of Kiel, Germany
Dr C. J. Ingham, MicroDish BV, Utrecht, The Netherlands

This research was conducted under the auspices of the Graduate School VLAG (Advanced Studies in Food Technology, Agrobiotechnology, Nutrition and Health Sciences).

Biofunctionalized Nanoporous Aluminum Oxide Culture Chips

For Capture and Growth of Bacteria

Aline Debrassi

Thesis

submitted in fulfillment of the requirements for the degree of doctor
at Wageningen University
by the authority of the Rector Magnificus
Prof. Dr A.P.J. Mol,
in the presence of the
Thesis Committee appointed by the Academic Board
to be defended in public
on Monday 25 January 2016
at 4 p.m. in the Aula.

Aline Debrassi

Biofunctionalized Nanoporous Aluminum Oxide Culture Chips for Capture and Growth of Bacteria,
218 pages.

PhD thesis, Wageningen University, Wageningen, NL (2016)
With references, with summary in English

ISBN 978-94-6257-617-9

Contents

Chapter 1

| | |
|---------------------------|---|
| General Introduction..... | 7 |
|---------------------------|---|

Chapter 2

| | |
|---|----|
| Carbohydrate-Presenting Self-Assembled Monolayers: Preparation, Analysis and Applications in Microbiology | 27 |
|---|----|

Chapter 3

| | |
|--|----|
| Stability of (Bio)Functionalized Porous Aluminum Oxide | 77 |
|--|----|

Chapter 4

| | |
|---|-----|
| Versatile (Bio)Functionalization of Bromo-Terminated Phosphonate-Modified Porous Aluminum Oxide | 113 |
|---|-----|

Chapter 5

| | |
|---|-----|
| Carbohydrate-Protein Interactions for the Binding of Bacteria on Porous Aluminum Oxide..... | 147 |
|---|-----|

Chapter 6

| | |
|--|-----|
| Biofunctionalization of Porous Aluminum Oxide With Antibodies for the Binding of Bacteria..... | 171 |
|--|-----|

Chapter 7

| | |
|-------------------------|-----|
| General Discussion..... | 195 |
|-------------------------|-----|

| | |
|---------------|-----|
| Summary | 208 |
|---------------|-----|

| | |
|------------------------|-----|
| Acknowledgements | 211 |
|------------------------|-----|

| | |
|------------------------|-----|
| Curriculum vitae | 214 |
|------------------------|-----|

| | |
|---------------------------|-----|
| List of Publications..... | 215 |
|---------------------------|-----|

| | |
|---|-----|
| Overview of Completed Training Activities | 217 |
|---|-----|

Chapter 1

General Introduction

Aline Debrassi

Introduction

Bacteria can be grown in a culture by allowing them to multiply in a specific growth medium under strictly controlled conditions. Culturing bacteria is the most common method for the detection and identification of bacteria, and is essential to study their phenotype. Moreover, culturing is needed to obtain sufficient cells for other studies, such as expression analysis, transformation or isolation of DNA for genomic characterization. In the case of pathogenic bacteria, culturing is also crucial for assessing their antibiotic susceptibility or resistance.¹ The most frequently used and well-established methods for bacterial cultivation include growth in liquid media or on agar plates. However, these methods present limitations, such as being time-consuming and not allowing for automation and high throughput analysis while it also appeared that the majority of bacterial species cannot be grown in the laboratory.^{2,3}

In recent years, new cultivation and detection approaches have emerged that enable faster and more accurate detection and diagnosis as well as broadening the range of cultivable species. Various point-of-care tests, i.e. tests that can be performed at or near the site of patient care, have been developed to decrease diagnosis time and, consequently, allow for a faster start of antibiotic therapy.⁴⁻⁶ Novel culturing devices for bacteria have also been developed and applied for long-term microscopic observation,⁷ detection,⁸ and cultivation of bacteria that cannot be cultivated using the conventional methods.² One promising, recently developed culturing platform are porous aluminum oxide (PAO) membranes. They can be used for early microcolony detection and to cultivate certain bacteria that cannot be grown with the conventional methods.⁹ The covalent biofunctionalization of PAO surfaces would enhance and expand its application for bacterial culturing and detection, and is the topic of the research described in this thesis. In the next few sections essential background information related to PAO is provided and discussed, including its surface chemistry and (bio)functionalization.

Porous aluminum oxide (PAO)

Porous aluminum oxide (PAO), also known as anodic aluminum oxide, nanoporous alumina, and porous anodic alumina, is a nanoporous material obtained upon electrochemical oxidation of aluminum. Optimization of the anodization

parameters, such as temperature, type and concentration of the electrolyte, voltage and time, can lead to materials with different structural orders, thicknesses, pore sizes, and pore volumes (**Figure 1**).⁹⁻¹⁶ Different nanostructures may influence certain characteristics of the PAO substrate, such as mechanical properties¹¹ or the optical response when used in a flow cell for optical detection of biomolecules.¹⁷ The specifications of the PAO samples used for the research presented in this thesis are shown in **Table 1**.

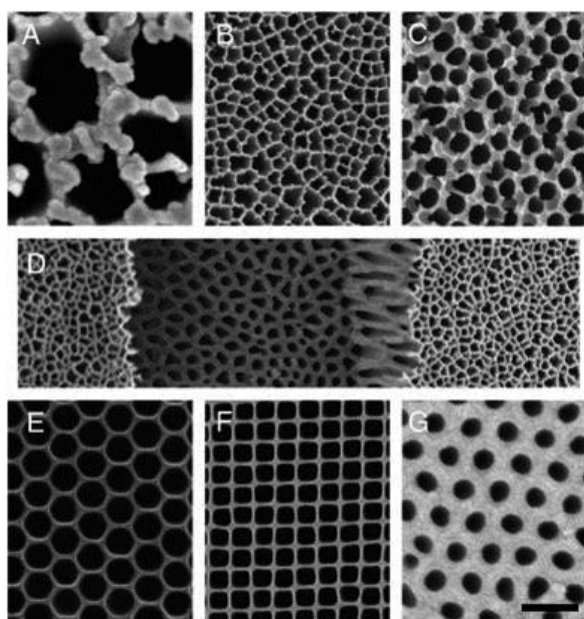
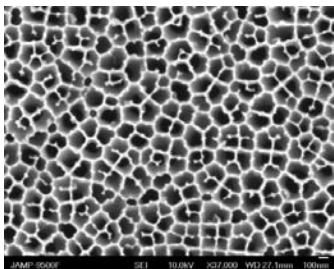
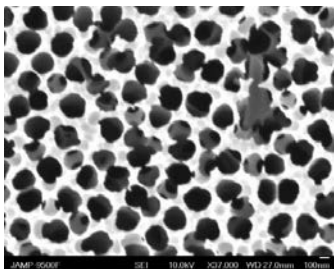


Figure 1. (a) High-resolution SEM of surface of a commercial PAO; (b) Lower resolution SEM of same surface; (c) Reverse side of the sample that comprised panels (a) and (b) with pore diameters from 100 to 200 nm; (d) Surface as panels (a) and (b) with upper surface sheared off in central region revealing structure beneath; (e) More highly ordered PAO with pores around 300 nm; (f) Similar to panel (e), but with square pores; (g) PAO with 40 nm pores. Scale bar in panel (g) indicates the following: 80 nm when applied to panel (a); 350 nm panels (b) and (c); 700 nm panel (d); 550 nm panels (e) and (f); 120 nm

panel (g). Reprinted with permission from reference 9. Copyright (2012) Elsevier.

As a material PAO has many outstanding properties, such as biocompatibility, well-ordered structure, chemical stability, large surface area, controllability of fabrication, optical transparency, and low autofluorescence,^{9, 18-20} and has therefore been applied in various fields of research. It has been used for the development of biosensing systems²⁰⁻³³ and implantable devices for drug delivery,^{18, 34-36} as a template for the fabrication of other microstructures and nanostructures,³⁷⁻⁴⁵ as a support for the immobilization of enzymes for biocatalysis,⁴⁶⁻⁴⁸ as a membrane for filtration,⁴⁹ protein recognition and purification,⁵⁰ and removal of heavy metals.⁵¹ Finally, the most relevant application for the topic of this thesis that takes full advantage of the low autofluorescence and the porous structure of PAO, is its use as a support to culture and

Table 1. Specifications and SEM pictures of the PAO samples used for the research presented in this thesis.

| Characteristic | Dimension |
|---|--|
| Slide size | 8 × 35.6 mm |
| Thickness | 60 µm |
| Pore size | 200 nm |
| SEM picture – smooth side | SEM picture – rough side |
|  |  |

count various cell types,^{19, 52} including a range of different microorganisms.^{9, 53-58} The porous structure enables cellular growth, because the nutrients can easily diffuse from the medium on which the PAO is placed to the other side of the surface, where the cells are located. Additionally, this application of PAO can also be used as a semipermeable barrier between different cell types, maintaining the cell-to-cell communication by the diffusion of soluble molecules through the pores.⁵⁹

The use of PAO or other porous membranes for culturing in microbiology offers the possibility of cultivating certain bacteria that do not grow on traditional agar plates, such as river and soil bacteria.^{54, 60} The possibility of cultivating soil bacteria in the laboratory is important because these less well researched types of bacteria have often been found to be a viable source for new drug candidates. A prime example of this is the recently discovered teixobactin, the first member of a new class of antibiotics that is likely to induce minimal resistance development by target microorganisms.³ Another interesting application of PAO in microbiology is for testing antimicrobial resistance or susceptibility of bacteria and fungi. Because of the possibility of microcolony detection, it is possible to obtain resistance or susceptibility results more rapidly than with conventional tests, such as disc diffusion and Etest.⁶¹⁻⁶⁴ Microcolony detection

techniques have been used to speed up culture-based assays and may be interesting especially for slow-growing pathogenic species, such as *Mycobacterium tuberculosis*.^{65, 66} Additionally, a miniaturized disposable microbial growth chip based on PAO has been developed and is now commercially available, making high throughput-screening of microorganisms possible. The so-called micro-Petri dish (or MicroDish Culture Chip) (**Figure 2**) was produced via deposition of an acrylic film on PAO, followed by reactive ion etching using plasma directed at a shadow mask. The removal of the laminate from defined areas creates a series of microbial growth chips on PAO. The main advantage of this micro-Petri dish is that it allows for the growth (and study) of different microbial species at a high density.⁵⁴

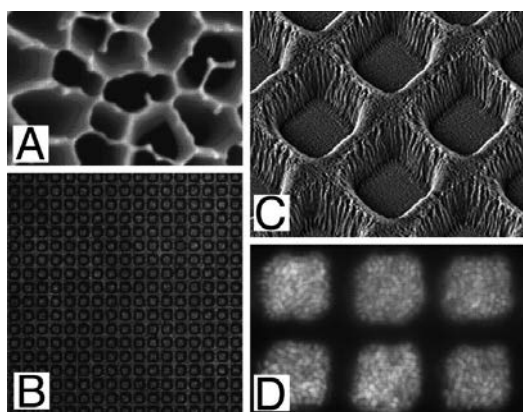


Figure 2. Images of PAO-based materials, growth compartments, and microbial culture on PAO chips. (a) SEM of PAO with pores on average 200 nm diameter; (b) Transmission light microscopy of hundreds of $20 \times 20 \mu\text{m}$ compartments; (c) SEM of $7 \times 7 \mu\text{m}$ compartments at a 30° angle; (d) Culture of *Lactobacillus plantarum* in six compartments stained with a fluorescent dye (Syto 9) after growth. Adapted with permission from reference 54.

Although most of the applications of PAO in microbiology do not require surface modification, the potential (bio)technological applications of PAO can be considerably expanded when the PAO surface can be chemically modified in order to tailor its properties or to immobilize certain biomolecules. The possibility to chemically modify PAO with biomolecules to increase microbial binding has been previously shown by our group.⁶⁷ The techniques currently used to chemically modify aluminum oxide surfaces, including PAO, will be discussed in the following section.

Surface modification of aluminum oxide

The possibility of tuning the surface properties of materials by chemical modification widely expands their range of applications. This is also the case for PAO,

and various functional groups have been used for the modification of (porous) aluminum oxide surfaces (**Figure 3**).⁶⁸

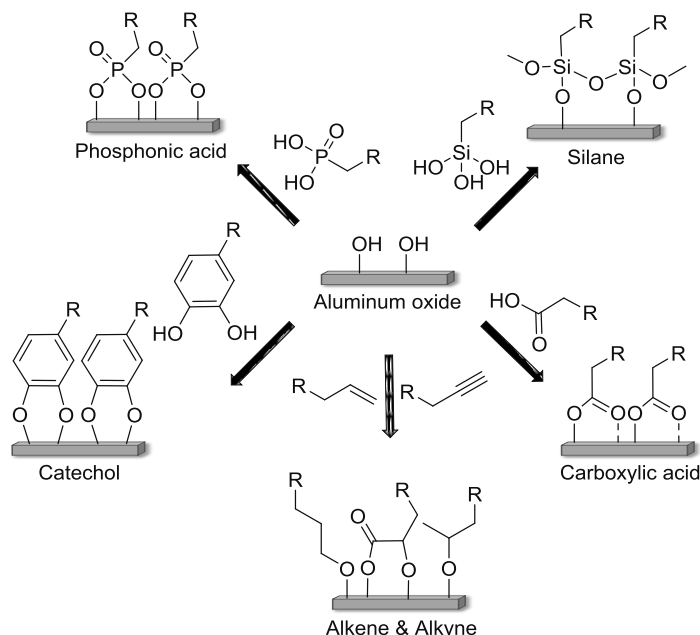


Figure 3. Functionalization methods of (porous) aluminum oxide and the resulting structure on the modified surfaces.

The most commonly used method for the modification of aluminum oxide surfaces is with silane derivatives, presenting chloride, alkoxide or hydride as a leaving group.⁶⁹⁻⁷² The main advantage of this technique is the short reaction time of these molecules with the hydroxyl groups of aluminum oxide surfaces. The main drawback, however, is the difficulty in obtaining uniform monolayers.^{68, 69} Silane derivatives presenting different functional groups have been used for modification of aluminum oxide surfaces, such as perfluorinated,^{70, 73-75} and amine-terminated⁶⁹ silanes. Specifically for PAO surfaces, long hydrocarbon chains have been attached via silane derivatives to generate (super)hydrophobic PAO surfaces.^{71, 76} Additionally, *N*-hydroxysuccinimide-terminated polyethylene glycol²⁹ and epoxy-terminated²¹ silanes have been immobilized on PAO as a first step for surface biofunctionalization.

Another method used for the modification of aluminum oxide surfaces is with carboxylic acids. Although the modification of aluminum oxide with these molecules is simple and various carboxylic acids are commercially available, the resulting modified

surfaces present poor stability, especially in aqueous environment.⁷⁷⁻⁷⁹ Bifunctional carboxylic acids have shown to generate more stable monolayers on aluminum oxide surfaces,⁸⁰ however, their still limited stability will hamper the application of these modified surfaces.

Unsaturated hydrocarbons, namely alkene- and alkyne-containing molecules, can also be used for the modification of aluminum oxide surfaces.^{67, 81-83} In this case, the mechanism likely involves oxygen- and light-dependent oxidation of these molecules to different species, followed by formation of a monolayer with the species that can form stable interactions with the aluminum oxide surface.⁶⁷

Catechol (or 1,2-dihydroxybenzene) derivatives have also been used for surface functionalization of (porous) aluminum oxide surfaces. This type of modification was inspired by the way that mussels adhere to solid surfaces in the sea via mussel byssal proteins that have exceptional adhesive characteristics due to multiple catechol groups.⁸⁴ Modification of PAO surfaces with catechol derivatives has been used to create catalytic membranes via immobilization of asymmetric catalysts,⁸⁵ pH-responsive membranes via immobilization of surface-bound initiators for atom-transfer radical polymerization (ATRP),⁸⁶ and temperature-responsive membranes via immobilization of a poly(*N*-isopropylacrylamide) (PNIPAAm)-catechol derivative.⁸⁷

Finally, phosphonic acids can also be used for modification of (porous) aluminum oxide surfaces.⁸⁸ Most of the research on modification of aluminum oxide surfaces with phosphonic acids has been performed with alkyl phosphonic acids,⁸⁹⁻⁹⁵ but there are also some examples using perfluorinated phosphonic acids,^{88, 93, 96, 97} phenylphosphonic acid,⁹⁸ sulphur-containing phosphonic acids,⁹⁹ and even carbohydrate derivatives containing a phosphonic acid group.¹⁰⁰ This thesis focusses to a large extent on the use of such phosphonic acids because of the high stability of their monolayers on PAO.

The exact contribution of the various binding modes of phosphonic acids to metal oxides surfaces, including aluminum oxide, to form phosphonate monolayers has still not been fully elucidated. Monodentate, bidentate, and tridentate binding modes are possible due to the presence of three oxygen atoms on the phosphonic acids, also possibly combined with electrostatic and hydrogen-bonding interactions. Additionally, all three oxygen atoms can bind to the same metal atom (chelating mode) or to different metal atoms on the surface (bridging mode) (**Figure 4**).

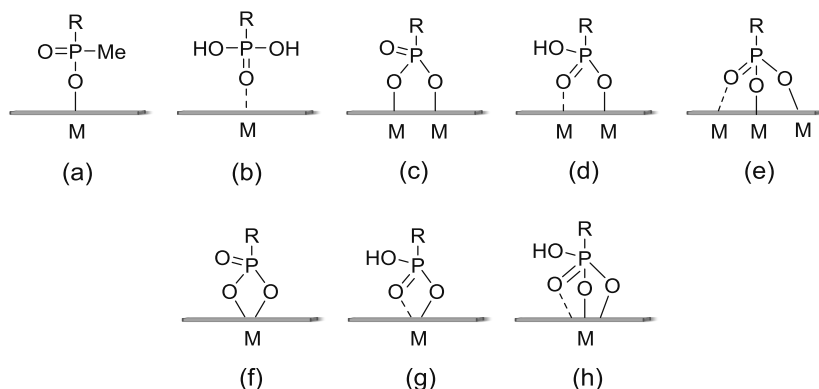


Figure 4. Possible binding modes of phosphonic acids to metal oxide surfaces, including aluminum oxide, where M = metal: monodentate (a and b), bridging bidentate (c and d), bridging tridentate (e), chelating bidentate (f and g), and chelating tridentate (h).^{68, 101}

Biomolecules on surfaces

Over the past few years, the immobilization of biomolecules on surfaces has attracted tremendous attention due to the possibility of extending and refining the application of solid supports, mainly for biosensors and other biotechnological applications. Various biomolecules, such as carbohydrates, proteins (antibodies, lectins, and enzymes), and DNA, can be immobilized onto surfaces and be used as recognition elements. In general, biomolecules can be attached to surfaces via non-covalent immobilization (physical adsorption) or by covalent immobilization (covalent chemical bond formation).¹⁰²⁻¹⁰⁷ The main disadvantage of non-covalent immobilization is the limited stability of the biofunctionalized surfaces.^{103, 105} Covalent immobilization, on the other hand, although is typically more laborious, usually provides more stable surfaces.^{105, 106}

Various non-covalent and covalent immobilization methods have been developed for the immobilization of biomolecules on surfaces. The methods commonly used to immobilize carbohydrates on surfaces can be divided in three distinct approaches: (a) direct formation of carbohydrate-containing self-assembled monolayers (SAMs); (b) use of secondary (or tertiary) reactions to install a carbohydrate on a pre-formed SAM; and (c) non-covalent immobilization of carbohydrates on a surface. An extensive overview of these methods is presented in **Chapter 2**.

Protein immobilization on surfaces can be performed via non-specific (random) or site-specific attachment.^{102, 108, 109} Non-covalent random immobilization of proteins can occur through ionic bonds and hydrophobic and polar interactions. Polystyrene surfaces can be used to immobilize proteins via hydrophobic interactions^{107, 108, 110} Other methods involve surfaces modified to present positively charged amine or negatively charged carboxylate groups.^{108, 111, 112}

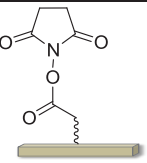

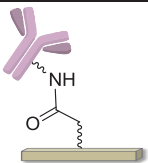
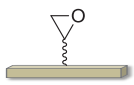

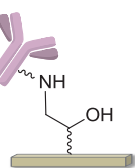
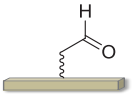

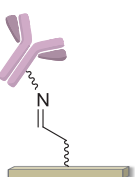


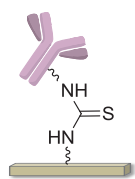
The most common method for covalent immobilization of proteins on surfaces employs the amine group of the lysine side chain, and this was the approach used in this thesis. Various amine-reactive functionalized surfaces can be used for this purpose, such as *N*-hydroxysuccinimide (NHS)-,²⁹ epoxide-²¹ aldehyde-^{113, 114} and isothiocyanate-terminated surfaces¹¹³ (**Table 2**). Although this is an easy and well-established method, the main disadvantage is that it often leads to random orientations in the protein immobilization, due to the high abundance of amine groups on the protein structure.¹⁰⁸

Although the random immobilization of proteins is often relatively simple and does not require prior modification of the target protein, it presents the risk of modifying or blocking the active/binding site of the protein, decreasing its activity. To circumvent this problem, site-specific immobilization techniques have in recent years attracted considerable attention.^{102, 108, 115} Site-specific protein immobilization can also be divided in covalent and non-covalent binding. Non-covalent site-specific immobilization of antibodies, for example, can be performed by first immobilizing an antibody-binding protein on the surface, such as protein A, protein G, or protein A/G, a recombinant fusion protein containing binding domains of both protein A and protein G. These proteins present binding domains that are specific to the Fc portion of antibodies. The antibodies are then immobilized on the protein A or G-containing surfaces, resulting in mainly tail-on orientation.^{102, 108} This approach was used to immobilize anti-galectin antibodies on PAO microarray chips for cancer diagnostics and prognostic purposes.²⁷

Another approach for non-covalent site-specific immobilization of proteins employs the strong and stable interaction between biotin and avidin or streptavidin. In this case, the surface is initially modified with biotin or (strept)avidin and the protein to be attached is previously modified in order to present the complementary molecule.¹⁰⁸ This method was used to attach anti-epithelial cell adhesion molecule (EpCAM) antibodies on PAO surfaces for the detection of circulating tumor cells.²³ Although the biotin-streptavidin interaction is one of the strongest non-covalent interactions, the

main disadvantage is that it requires modification of the protein, biotinylation in most cases, which is not always site-specific.¹¹⁶

Table 2. Immobilization of proteins (here represented by an antibody) using amine-reactive functionalized surfaces: (a) NHS-, (b) epoxide-, (c) aldehyde-, and (d) isothiocyanate-terminated surfaces.

| | Surface Termination | Protein | Immobilized Product |
|-----|--|---|---|
| (a) |  NHS-terminated surface |  ~NH ₂ |  |
| (b) |  Epoxide-terminated surface |  ~NH ₂ |  |
| (c) |  Aldehyde-terminated surface |  ~NH ₂ |  |
| (d) |  Isothiocyanate-terminated surface |  ~NH ₂ |  |

Another non-covalent approach involves the fusion of a polyhistidine (His₆) affinity-tag on the recombinant protein to be immobilized. The His₆ tag presents a high affinity to Ni²⁺, Co²⁺, Zn²⁺, and Cu²⁺ surfaces. These metals can be attached to the surface via a tetradentate ligand nitriloacetate, which occupies three or four binding sites, and the remaining two or three binding sites are chelated by the imidazolyl from the histidine tag.^{102, 107, 117}

Compared to the non-covalent approach, the covalent site-specific methods of protein immobilization usually provide more stable biofunctionalized surfaces, but also in general require protein modification. One exception is the immobilization of antibodies via their carbohydrate moiety at the Fc part on boronic acid-presenting surfaces, which form cyclic boronate ester with 1,2- and 1,3-diols of the *N*-glycan carbohydrate residues.¹¹⁸ The main disadvantage of this method is the reversibility of the bond between boronic acid and the carbohydrates. To overcome this problem, Lin and co-workers designed and synthesized a molecule that presents a boronic acid in combination with a photoactivable reagent, which upon activation form covalent bonds with the antibody near or with the *N*-glycans.¹¹⁹

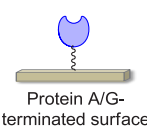

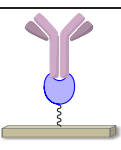
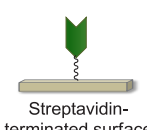

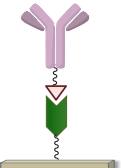
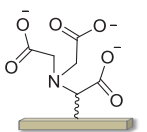
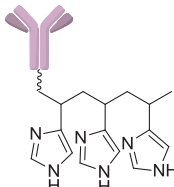
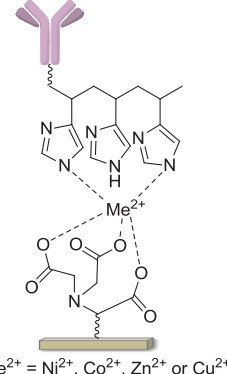
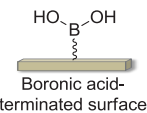
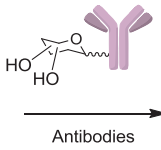
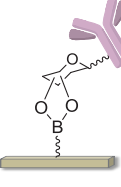
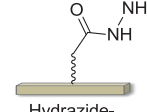
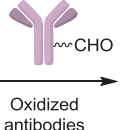
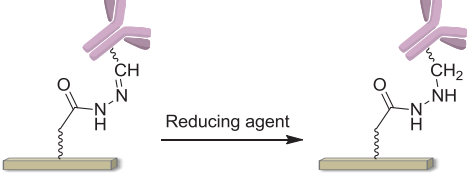
Another method that uses the carbohydrate moieties of the antibodies for the immobilization is via specific oxidation of the vicinal hydroxy groups of the carbohydrates using sodium periodate. The aldehyde groups formed can then react with hydrazide or hydroxylamine-containing reagents.¹²⁰

Additionally, various bio-orthogonal reactions can be used for site-specific covalent immobilization of proteins, such as Diels-Alder cycloaddition,¹²¹ Staudinger ligation,¹²² copper(I)-catalyzed azide-alkyne cycloaddition (CuAAC), strain-promoted azide-alkyne cycloaddition (SPAAC), click sulfonamide reaction (CSR),¹²³ and thiol-ene reaction.^{124, 125} In general, all these reactions form stable covalent bonds. Their main drawback, however, is the necessity of protein modification to install the functional reactive group involved in the bio-orthogonal reaction.^{102, 107, 108, 110, 115}

Bacterial capture and sensing on PAO

Bacterial adhesion to surfaces occurs in many fields of application and can be detrimental or beneficial. Adhesion of probiotic bacteria, such as lactic acid bacteria, to the surface of the gastrointestinal tract is believed to be important to protect the host against pathogenic bacteria.¹²⁶ The molecular details of this process has been worked out in some detail in *Lactobacillus plantarum* WCFS1, which contains a cell-envelope located mannose-specific adhesion and *Lactobacillus rhamnosus* GG, which produces filamentous pili decorated with a mucus-binding protein.^{127, 128} On the other hand, adhesion of bacteria to implants, such as orthopaedic devices, can be extremely dangerous, leading to implant failure.¹²⁹

Table 3. Methods for oriented immobilization of proteins (here represented by an antibody) onto reactive surfaces: (a) Protein A/G, (b) biotin–streptavidin, (c) polyhistidine-conjugated antibodies immobilized onto nitriloacetic acid-terminated surfaces, (d) immobilization via the glycan part of antibodies onto boronic acid-terminated surfaces, and (e) oxidized antibodies onto hydrazide-terminated surfaces.

| | Surface Termination | Protein | Immobilized Product |
|-----|---|---|--|
| (a) |  Protein A/G-terminated surface |  Antibodies |  |
| (b) |  Streptavidin-terminated surface |  Biotin-conjugated antibodies |  |
| (c) |  Nitriloacetic acid-terminated surface |  Polyhistidine-conjugated antibodies |  $\text{Me}^{2+} = \text{Ni}^{2+}, \text{Co}^{2+}, \text{Zn}^{2+} \text{ or } \text{Cu}^{2+}$ |
| (d) |  Boronic acid-terminated surface |  Antibodies |  |
| (e) |  Hydrazide-terminated surface |  Oxidized antibodies |  Reducing agent |

Surfaces have been modified with different coatings in order to prevent detrimental bacterial adhesion.^{130, 131} However, it is also possible to biofunctionalize surfaces in order to specifically capture certain types of bacteria. These surfaces can be modified with carbohydrates, proteins (antibodies, lectins, and enzymes), and DNA, for example, and be used for diagnostic purposes.^{6, 132-135}

PAO surfaces with immobilized antibodies have been used to capture *Escherichia coli* cells in a sensitive and selective manner.¹³⁶ Yang and co-workers also used biofunctionalized PAO to capture and to detect *E. coli* and *Staphylococcus aureus*. In this work, the authors immobilized the antibodies via an epoxy-terminated silane self-assembled monolayer, and detected the captured bacteria using a microfluidic sensor.²¹ Later, the same group also published a work using a different approach to immobilize the antibodies on the PAO surface. This time they used a NHS-terminated silane derivative containing a PEG spacer, known to decrease non-specific adhesion. They also concentrated the *E. coli* cells using antibody-coated magnetic beads and this concentration step increased the sensitivity of the detection method (**Figure 5**).²⁹

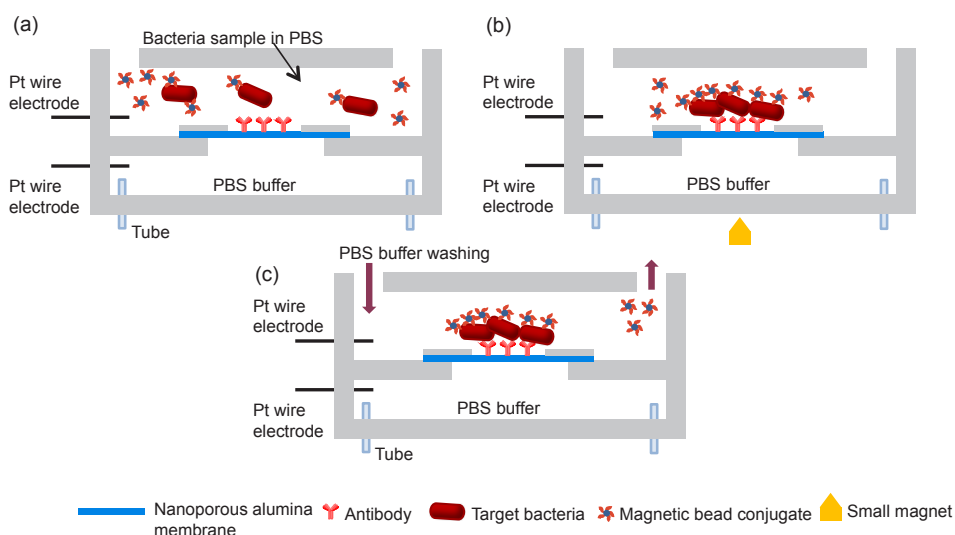


Figure 5. Schematic diagram for biofunctional magnetic bead concentration of bacteria cells in the biochip. (a) Magnetic beads were conjugated with bacteria cells; (b) Bacteria cells were concentrated in a small region by applying an external point magnetic field and captured by the antibody immobilized on nanoporous membrane; and (c) The external magnetic field was released and unbounded magnetic beads were washed away. Adapted with permission from reference 29. Copyright (2013) Elsevier.

PAO surfaces with covalently immobilized DNA have been used to prepare a biosensor for the detection of *Legionella sp.* In this work, the PAO surface was initially modified with an amino-terminated silane, followed by reaction with glutaraldehyde and subsequent immobilization of the DNA probes. The label-free DNA biosensor showed a low detection limit and was able to differentiate the complementary sequence from target sequences with single and triple bases mismatches.²⁵

Outline of the thesis

The previous sections have shown that PAO surfaces can be used for various advanced (bio)technological applications. These applications can be further extended when the surface of PAO is chemically modified and (bio)functionalized with carbohydrates or proteins, for example. The research described in thesis focuses on the (bio)functionalization of PAO surfaces, mainly by using phosphonate chemistry, with carbohydrates, lectins and antibodies to enable the capture and growth of bacteria (Figure 6).

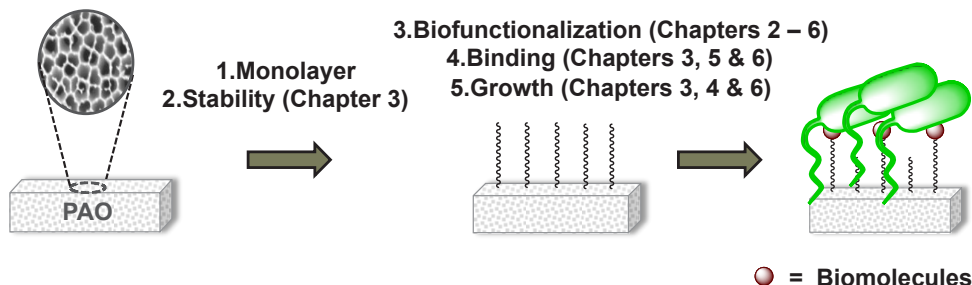


Figure 6. Outline of the thesis.

In **Chapter 2**, an overview is presented of the most commonly used methods to prepare carbohydrate-presenting surfaces. The review of these methods is divided in three different approaches: (a) direct formation of carbohydrate-containing self-assembled monolayers (SAMs); (b) use of secondary (or tertiary) reactions to immobilize a carbohydrate on a pre-formed SAM; and (c) non-covalent immobilization. The chapter also presents several surface analysis techniques that can be used to characterize carbohydrate-presenting surfaces and the applications of these surfaces in microbiology.

Chapter 3 describes the modification of PAO with a range of functional groups and the evaluation of the stability of these modified surfaces under pH and temperature conditions that are relevant for microbial growth. Additionally, a mannose-presenting surface was prepared, and the binding and growth of the mannose-binding bacterium *Lactobacillus plantarum* was studied on this surface.

Chapter 4 presents a straightforward and stable initial modification of the PAO surface, which is followed by subsequent reactions that provide a wide scope of terminal reactive groups. As a proof of principle, we also showed that these reactive surfaces can be further (bio)functionalized with carbohydrate derivatives and fluorescently labelled proteins.

Chapter 5 describes additional studies of binding of lectins and bacteria on PAO surfaces functionalized with carbohydrates. These additional binding studies aim to further explore the variables that can influence the interaction between the carbohydrates and the bacteria. Subsequently, **Chapter 6** presents the immobilization of anti-*E.coli* antibodies on PAO surfaces for the increased binding and growth of this bacterium.

Finally, **Chapter 7** summarizes the most important achievements of the research described in this thesis and discusses future challenges and possibilities for further research.

References

1. Lagier, J. C.; Edouard, S.; Pagnier, I.; Mediannikov, O.; Drancourt, M.; Raoult, D. Current and past strategies for bacterial culture in clinical microbiology. *Clin. Microbiol. Rev.* **2015**, *28*, 208-236.
2. Nichols, D.; Cahoon, N.; Trakhtenberg, E. M.; Pham, L.; Mehta, A.; Belanger, A.; Kanigan, T.; Lewis, K.; Epstein, S. S. Use of ichip for high-throughput in situ cultivation of "uncultivable" microbial species. *Appl. Environ. Microbiol.* **2010**, *76*, 2445-2450.
3. Ling, L. L.; Schneider, T.; Peoples, A. J.; Spoering, A. L.; Engels, I.; Conlon, B. P.; Mueller, A.; Schaeberle, T. F.; Hughes, D. E.; Epstein, S.; Jones, M.; Lazarides, L.; Steadman, V. A.; Cohen, D. R.; Felix, C. R.; Fetterman, K. A.; Millett, W. P.; Nitti, A. G.; Zullo, A. M.; Chen, C.; Lewis, K. A new antibiotic kills pathogens without detectable resistance. *Nature* **2015**, *517*, 455-459.
4. Fournier, P. E.; Drancourt, M.; Colson, P.; Rolain, J. M.; La Scola, B.; Raoult, D. Modern clinical microbiology: new challenges and solutions. *Nature Rev. Microbiol.* **2013**, *11*, 574-585.
5. Rozand, C. Paper-based analytical devices for point-of-care infectious disease testing. *Eur. J. Clin. Microbiol. Infect. Dis.* **2014**, *33*, 147-156.
6. Ahmed, A.; Rushworth, J. V.; Hirst, N. A.; Millner, P. A. Biosensors for whole-cell bacterial detection. *Clin. Microbiol. Rev.* **2014**, *27*, 631-646.
7. Frey, O.; Rudolf, F.; Schmidt, G. W.; Hierlemann, A. Versatile, simple-to-use microfluidic cell-culturing chip for long-term, high-resolution, time-lapse imaging. *Anal. Chem.* **2015**, *87*, 4144-4151.
8. Bouguelia, S.; Roupiez, Y.; Slimani, S.; Mondani, L.; Casabona, M. G.; Durmort, C.; Vernet, T.; Calemczuk, R.; Livache, T. On-chip microbial culture for the specific detection of very low levels of bacteria. *Lab on a Chip* **2013**, *13*, 4024-4032.
9. Ingham, C. J.; ter Maat, J.; de Vos, W. M. Where bio meets nano: The many uses for nanoporous aluminum oxide in biotechnology. *Biotechnol. Adv.* **2012**, *30*, 1089-1099.
10. Poinern, G. E. J.; Ali, N.; Fawcett, D. Progress in nano-engineered anodic aluminum oxide membrane development. *Materials* **2011**, *4*, 487-526.
11. McQuaig, M. K., Jr.; Toro, A.; Van Geertruyden, W.; Misiolek, W. Z. The effect of high temperature heat treatment on the structure and properties of anodic aluminum oxide. *J. Mater. Sci.* **2011**, *46*, 243-253.
12. Zaraska, L.; Sulka, G. D.; Jaskula, M. Anodic alumina membranes with defined pore diameters and thicknesses obtained by adjusting the anodizing duration and pore opening/widening time. *J. Solid State Electrochem.* **2011**, *15*, 2427-2436.

13. Erdogan, P.; Birol, Y. Effect of processing on structural features of anodic aluminum oxides. *Appl. Phys. A Mater. Sci. Process.* **2012**, *108*, 587-592.
14. Lee, W.; Park, S. J. Porous anodic aluminum oxide: anodization and templated synthesis of functional nanostructures. *Chem. Rev.* **2014**, *114*, 7487-7556.
15. Kant, K.; Low, S. P.; Marshal, A.; Shapter, J. G.; Losic, D. Nanopore gradients on porous aluminum oxide generated by nonuniform anodization of aluminum. *ACS Appl. Mater. Inter.* **2010**, *2*, 3447-3454.
16. Petukhov, D. I.; Napolskii, K. S.; Berekchiyan, M. V.; Lebedev, A. G.; Eliseev, A. A. Comparative study of structure and permeability of porous oxide films on aluminum obtained by single- and two-step anodization. *ACS Appl. Mater. Inter.* **2013**, *5*, 7819-7824.
17. Macias, G.; Ferre-Borrull, J.; Pallares, J.; Marsal, L. F. Effect of pore diameter in nanoporous anodic alumina optical biosensors. *Analyst* **2015**, *140*, 4848-4854.
18. Gultepe, E.; Nagesha, D.; Sridhar, S.; Amiji, M. Nanoporous inorganic membranes or coatings for sustained drug delivery in implantable devices. *Adv. Drug Del. Rev.* **2010**, *62*, 305-315.
19. Brueggemann, D. Nanoporous Aluminium Oxide Membranes as Cell Interfaces. *J. Nanomater.* **2013**, 460870.
20. Santos, A.; Kumeria, T.; Losic, D. Nanoporous anodic aluminum oxide for chemical sensing and biosensors. *Trends Anal. Chem.* **2013**, *44*, 25-38.
21. Tan, F.; Leung, P. H. M.; Liu, Z.-b.; Zhang, Y.; Xiao, L.; Ye, W.; Zhang, X.; Yi, L.; Yang, M. A PDMS microfluidic impedance immunosensor for *E. coli* O157:H7 and *Staphylococcus aureus* detection via antibody-immobilized nanoporous membrane. *Sens. Actuat. B-Chem.* **2011**, *159*, 328-335.
22. Pichetsumthorn, P.; Vattipalli, K.; Prasad, S. Nanoporous impedemetric biosensor for detection of trace atrazine from water samples. *Biosens. Bioelectron.* **2012**, *32*, 155-162.
23. Kumeria, T.; Kurkuri, M. D.; Diener, K. R.; Parkinson, L.; Losic, D. Label-free reflectometric interference microchip biosensor based on nanoporous alumina for detection of circulating tumour cells. *Biosens. Bioelectron.* **2012**, *35*, 167-173.
24. Santos, A.; Macias, G.; Ferre-Borrull, J.; Pallares, J.; Marsal, L. F. Photoluminescent enzymatic sensor based on nanoporous anodic alumina. *ACS Appl. Mater. Inter.* **2012**, *4*, 3584-3588.
25. Rai, V.; Deng, J.; Toh, C.-S. Electrochemical nanoporous alumina membrane-based label-free DNA biosensor for the detection of *Legionella* sp. *Talanta* **2012**, *98*, 112-117.
26. Macias, G.; Hernandez-Eguia, L. P.; Ferre-Borrull, J.; Pallares, J.; Marsal, L. F. Gold-coated ordered nanoporous anodic alumina bilayers for future label-free interferometric biosensors. *ACS Appl. Mater. Inter.* **2013**, *5*, 8093-8098.
27. van Hattum, H.; Martin, N. I.; Ruijtenbeek, R.; Pieters, R. J. Development of a microarray detection method for galectin cancer proteins based on ligand binding. *Anal. Biochem.* **2013**, *434*, 99-104.
28. Yeom, S. H.; Han, M. E.; Kang, B. H.; Kim, K. J.; Yuan, H.; Eum, N. S.; Kang, S. W. Enhancement of the sensitivity of LSPR-based CRP immunosensors by Au nanoparticle antibody conjugation. *Sens. Actuat. B-Chem.* **2013**, *177*, 376-383.
29. Chan, K. Y.; Ye, W.; Zhang, Y.; Xiao, L. D.; Leung, P. H. M.; Li, Y.; Yang, M. Ultrasensitive detection of *E. coli* O157:H7 with biofunctional magnetic bead concentration via nanoporous membrane based electrochemical immunosensor. *Biosens. Bioelectron.* **2013**, *41*, 532-537.
30. Deng, J.; Toh, C.-S. Impedimetric DNA biosensor based on a nanoporous alumina membrane for the detection of the specific oligonucleotide sequence of dengue virus. *Sensors* **2013**, *13*, 7774-7785.
31. Kim, Y. J.; Jones, J. E.; Li, H.; Yampara-Iguise, H.; Zheng, G.; Carson, C. A.; Cooperstock, M.; Sherman, M.; Yu, Q. Three-dimensional (3-D) microfluidic-channel-based DNA biosensor for ultra-sensitive electrochemical detection. *J. Electroanal. Chem.* **2013**, *702*, 72-78.
32. Neubacher, H.; Mey, I.; Carnarius, C.; Lazzara, T. D.; Steinem, C. Permeabilization assay for antimicrobial peptides based on pore-spanning lipid membranes on nanoporous alumina. *Langmuir* **2014**, *30*, 4767-4774.
33. Yagur-Kroll, S.; Schreuder, E.; Ingham, C. J.; Heideman, R.; Rosen, R.; Belkin, S. A miniature porous aluminum oxide-based flow-cell for online water quality monitoring using bacterial sensor cells. *Biosens. Bioelectron.* **2015**, *64*, 625-632.
34. Jeon, G.; Yang, S. Y.; Byun, J.; Kim, J. K. Electrically actuatable smart nanoporous membrane for pulsatile drug release. *Nano Lett.* **2011**, *11*, 1284-1288.
35. Kumeria, T.; Gulati, K.; Santos, A.; Losic, D. Real-time and in situ drug release monitoring from nanoporous implants under dynamic flow conditions by reflectometric interference spectroscopy. *ACS Appl. Mater. Inter.* **2013**, *5*, 5436-5442.
36. Szuwarzynski, M.; Zaraska, L.; Sulka, G. D.; Zapotoczny, S. Pulsatile releasing platform of nanocontainers equipped with thermally responsive polymeric nanovalves. *Chem. Mater.* **2013**, *25*, 514-520.
37. Yadlovker, D.; Berger, S. Controlled growth and nucleation of ferroelectric and dielectric single-crystal nano-rods inside nanoporous aluminum oxide. *Sens. Actuat. B-Chem.* **2007**, *126*, 277-282.
38. Schlitt, S.; Greiner, A.; Wendorff, J. H. Cylindrical polymer nanostructures by solution template wetting. *Macromolecules* **2008**, *41*, 3228-3234.
39. Sankar, P. R.; Tiwari, P.; Kumar, R.; Ganguli, T.; Mukherjee, C.; Srivastava, A. K.; Oak, S. M.; Pathak, R. K. Synthesis and characterization of cadmium selenide nanostructures on porous aluminum oxide templates by high frequency alternating current electrolysis. *Appl. Surf. Sci.* **2010**, *256*, 2097-2103.
40. Ding, D.; Cai, W.; Long, M. Controlled growth of spinel CuAl₂O₄/Cu hybrid nanorods array by electrodeposition in porous aluminum oxide template. *J. Alloys Compd.* **2012**, *545*, 53-56.
41. Zhang, D.; Luo, L.; Liao, Q.; Wang, H.; Fu, H.; Yao, J. Polypyrrole/ZnS core/shell coaxial nanowires prepared by anodic aluminum oxide template methods. *J. Phys. Chem. C* **2011**, *115*, 2360-2365.
42. Rana, K.; Kucukayan-Dogu, G.; Bengu, E. Growth of vertically aligned carbon nanotubes over self-ordered nano-porous alumina films and their surface properties. *Appl. Surf. Sci.* **2012**, *258*, 7112-7117.
43. Chi, M. H.; Kao, Y. H.; Wei, T. H.; Lee, C. W.; Chen, J. T. Curved polymer nanodiscs by wetting nanopores of anodic aluminum oxide templates with polymer nanospheres. *Nanoscale* **2014**, *6*, 1340-1346.
44. Martin, J.; Campoy-Quiles, M.; Nogales, A.; Garriga, M.; Alonso, M. I.; Goni, A. R.; Martin-Gonzalez, M. Poly(3-hexylthiophene) nanowires in porous alumina: internal structure under confinement. *Soft Matter* **2014**, *10*, 3335-3346.
45. Sada, T.; Fujigaya, T.; Nakashima, N. Design and fabrication of Ni nanowires having periodically hollow nanostructures. *Nanoscale* **2014**, *6*, 11484-11488.
46. Kjellander, M.; Gotz, K.; Liljeruhm, J.; Boman, M.; Johansson, G. Steady-state generation of hydrogen peroxide: kinetics and stability of alcohol oxidase immobilized on nanoporous alumina. *Biotechnol. Lett.* **2013**, *35*, 585-590.
47. Kjellander, M.; Mazari, A. M. A.; Boman, M.; Mannervik, B.; Johansson, G. Glutathione transferases immobilized on nanoporous alumina: flow system kinetics, screening, and stability. *Anal. Biochem.* **2014**, *446*, 59-63.
48. Chen, Z.; Zhang, J.; Singh, S.; Peltier-Pain, P.; Thorson, J. S.; Hinds, B. J. Functionalized anodic aluminum oxide membrane-electrode system for enzyme immobilization. *ACS Nano* **2014**, *8*, 8104-8112.

49. Lee, K. P.; Mattia, D. Monolithic nanoporous alumina membranes for ultrafiltration applications: characterization, selectivity-permeability analysis and fouling studies. *J. Membr. Sci.* **2013**, *435*, 52-61.
50. Lazzara, T. D.; Behn, D.; Kliesch, T.-T.; Janshoff, A.; Steinem, C. Phospholipids as an alternative to direct covalent coupling: surface functionalization of nanoporous alumina for protein recognition and purification. *J. Colloid. Interface Sci.* **2012**, *366*, 57-63.
51. Song, J.; Oh, H.; Kong, H.; Jang, J. Polyrrhodanine modified anodic aluminum oxide membrane for heavy metal ions removal. *J. Hazard. Mater.* **2011**, *187*, 311-317.
52. Song, Y.; Ju, Y.; Morita, Y.; Xu, B.; Song, G. Surface functionalization of nanoporous alumina with bone morphogenetic protein 2 for inducing osteogenic differentiation of mesenchymal stem cells. *Mater. Sci. Eng. C Mater. Biol. Appl.* **2014**, *37*, 120-126.
53. Ingham, C. J.; van den Ende, M.; Pijnenburg, D.; Wever, P. C.; Schneeberger, P. M. Growth and multiplexed analysis of microorganisms on a subdivided, highly porous, inorganic chip manufactured from anopore. *Appl. Environ. Microbiol.* **2005**, *71*, 8978-8981.
54. Ingham, C. J.; Sprengels, A.; Bomer, J.; Molenaar, D.; van den Berg, A.; Vlieg, J.; de Vos, W. M. The micro-Petri dish, a million-well growth chip for the culture and high-throughput screening of microorganisms. *Proc. Natl. Acad. Sci. U. S. A.* **2007**, *104*, 18217-18222.
55. Hoess, A.; Teuscher, N.; Thormann, A.; Aurich, H.; Heilmann, A. Cultivation of hepatoma cell line HepG2 on nanoporous aluminum oxide membranes. *Acta Biomater.* **2007**, *3*, 43-50.
56. Hu, J.; Tian, J. H.; Shi, J.; Zhang, F.; He, D. L.; Liu, L.; Jung, D. J.; Bai, J. B.; Chen, Y. Cell culture on AAO nanoporous substrates with and without geometry constraints. *Microelectron. Eng.* **2011**, *88*, 1714-1717.
57. Hoess, A.; Thormann, A.; Friedmann, A.; Heilmann, A. Self-supporting nanoporous alumina membranes as substrates for hepatic cell cultures. *J. Biomed. Mater. Res. A* **2012**, *100A*, 2230-2238.
58. Wang, P. Y.; Clements, L. R.; Thissen, H.; Tsai, W. B.; Voelcker, N. H. High-throughput characterisation of osteogenic differentiation of human mesenchymal stem cells using pore size gradients on porous alumina. *Biomater. Sci.* **2013**, *1*, 924-932.
59. Hoess, A.; Thormann, A.; Friedmann, A.; Aurich, H.; Heilmann, A. Co-cultures of primary cells on self-supporting nanoporous alumina membranes. *Adv. Eng. Mater.* **2010**, *12*, B269-B275.
60. Ferrari, B. C.; Binnerup, S. J.; Gillings, M. Microcolony cultivation on a soil substrate membrane system selects for previously uncultured soil bacteria. *Appl. Environ. Microbiol.* **2005**, *71*, 8714-8720.
61. Ingham, C. J.; van den Ende, M.; Wever, P. C.; Schneeberger, P. M. Rapid antibiotic sensitivity testing and trimethoprim-mediated filamentation of clinical isolates of the Enterobacteriaceae assayed on a novel porous culture support. *J. Med. Microbiol.* **2006**, *55*, 1511-1519.
62. Tsou, P. H.; Sreenivasappa, H.; Hong, S. M.; Yasuike, M.; Miyamoto, H.; Nakano, K.; Misawa, T.; Kameoka, J. Rapid antibiotic efficacy screening with aluminum oxide nanoporous membrane filter-chip and optical detection system. *Biosens. Bioelectron.* **2010**, *26*, 289-294.
63. Ingham, C. J.; Boonstra, S.; Levels, S.; de Lange, M.; Meis, J. F.; Schneeberger, P. M. Rapid susceptibility testing and microcolony analysis of *Candida* spp. cultured and imaged on porous aluminum oxide. *Plos One* **2012**, *7*, e33818-e33818.
64. Ingham, C. J.; Schneeberger, P. M. Microcolony imaging of *Aspergillus fumigatus* treated with echinocandins reveals both fungistatic and fungicidal activities. *Plos One* **2012**, *7*, e35478-e35478.
65. den Hertog, A. L.; Visser, D. W.; Ingham, C. J.; Fey, F.; Klatser, P. R.; Anthony, R. M. Simplified automated image analysis for detection and phenotyping of *Mycobacterium tuberculosis* on porous supports by monitoring growing microcolonies. *Plos One* **2010**, *5*.
66. den Hertog, A. L.; Menting, S.; Smienk, E. T.; Werngren, J.; Hoffner, S.; Anthony, R. M. Evaluation of a microcolony growth monitoring method for the rapid determination of ethambutol resistance in *Mycobacterium tuberculosis*. *BMC Infect. Dis.* **2014**, *14*, 9.
67. ter Maat, J.; Regeling, R.; Ingham, C. J.; Weijers, C. A. G. M.; Giesbers, M.; de Vos, W. M.; Zuillhof, H. Organic modification and subsequent biofunctionalization of porous anodic alumina using terminal alkynes. *Langmuir* **2011**, *27*, 13606-13617.
68. Pujari, S. P.; Scheres, L.; Marcelis, A. T. M.; Zuillhof, H. Covalent surface modification of oxide surfaces. *Angew. Chem. Int. Ed.* **2014**, *53*, 6322-6356.
69. Bhushan, B.; Kwak, K. J.; Gupta, S.; Lee, S. C. Nanoscale adhesion, friction and wear studies of biomolecules on silane polymer-coated silica and alumina-based surfaces. *J. R. Soc. Interface* **2009**, *6*, 719-733.
70. Saleema, N.; Sarkar, D. K.; Gallant, D.; Paynter, R. W.; Chen, X. G. Chemical nature of superhydrophobic aluminum alloy surfaces produced via a one-step process using fluoroalkyl-silane in a base medium. *ACS Appl. Mater. Inter.* **2011**, *3*, 4775-4781.
71. Lazzara, T. D.; Kliesch, T.-T.; Janshoff, A.; Steinem, C. Orthogonal functionalization of nanoporous substrates: control of 3D surface functionality. *ACS Appl. Mater. Inter.* **2011**, *3*, 1068-1076.
72. Kelly, D. N.; Wakabayashi, R. H.; Stacy, A. M. A modified sol-gel technique for pore size control in porous aluminum oxide nanowire templates. *ACS Applied Mater. Inter.* **2014**, *6*, 20122-20129.
73. Hoque, E.; DeRose, J. A.; Hoffmann, P.; Bhushan, B.; Mathieu, H. J. Alkylperfluorosilane self-assembled monolayers on aluminum: a comparison with alkylphosphonate self-assembled monolayers. *J. Phys. Chem. C* **2007**, *111*, 3956-3962.
74. DeRose, J. A.; Hoque, E.; Bhushan, B.; Mathieu, H. J. Characterization of perfluorodecanoate self-assembled monolayers on aluminum and comparison of stability with phosphonate and siloxy self-assembled monolayers. *Surf. Sci.* **2008**, *602*, 1360-1367.
75. Finch, D. S.; Oreskovic, T.; Ramadurai, K.; Herrmann, C. F.; George, S. M.; Mahajan, R. L. Biocompatibility of atomic layer-deposited alumina thin films. *J. Biomed. Mater. Res. A* **2008**, *87A*, 100-106.
76. Tasaltin, N.; Sanli, D.; Jonas, A.; Kiraz, A.; Erkey, C. Preparation and characterization of superhydrophobic surfaces based on hexamethyldisilazane-modified nanoporous alumina. *Nanoscale Res. Lett.* **2011**, *6*.
77. Chang, C. S.; Suen, S. Y. Modification of porous alumina membranes with n-alkanoic acids and their application in protein adsorption. *J. Membr. Sci.* **2006**, *275*, 70-81.
78. Liakos, I. L.; Newman, R. C.; McAlpine, E.; Alexander, M. R. Study of the resistance of SAMs on aluminium to acidic and basic solutions using dynamic contact angle measurement. *Langmuir* **2007**, *23*, 995-999.
79. Lim, M. S.; Feng, K.; Chen, X.; Wu, N.; Raman, A.; Nightingale, J.; Gawalt, E. S.; Korakakis, D.; Hornak, L. A.; Timperman, A. T. Adsorption and desorption of stearic acid self-assembled monolayers on aluminum oxide. *Langmuir* **2007**, *23*, 2444-2452.
80. van den Brand, J.; Blajiev, O.; Beentjes, P. C. J.; Terryn, H.; de Wit, J. H. W. Interaction of anhydride and carboxylic acid compounds with aluminum oxide surfaces studied using infrared reflection absorption spectroscopy. *Langmuir* **2004**, *20*, 6308-6317.
81. Lucchesi, P. J.; Carter, J. L.; Yates, D. J. C. Infrared study of chemisorption of ethylene on aluminum oxide. *J. Phys. Chem.* **1962**, *66*, 1451-1456.
82. Ivanov, A. V.; Koklin, A. E.; Uvarova, E. B.; Kustov, L. M. A DRIFT spectroscopic study of acetylene adsorbed on metal oxides. *PCCP* **2003**, *5*, 4718-4723.
83. Muslehiddinoglu, J.; Vannice, M. A. Adsorption of 1,3-butadiene on supported and promoted silver catalysts. *J. Catal.* **2004**, *222*, 214-226.

84. Lee, B. P.; Messersmith, P. B.; Israelachvili, J. N.; Waite, J. H. Mussel-inspired adhesives and coatings. *Annu. Rev. Mater. Res.* **2011**, *41*, 99-132.
85. Cho, S. H.; Walther, N. D.; Nguyen, S. B. T.; Hupp, J. T. Anodic aluminium oxide catalytic membranes for asymmetric epoxidation. *Chem. Commun.* **2005**, 5331-5333.
86. Sugnaux, C.; Lavanant, L.; Klok, H.-A. Aqueous fabrication of pH-gated, polymer-brush-modified alumina hybrid membranes. *Langmuir* **2013**, *29*, 7325-7333.
87. Kim, J. S.; Kim, T. G.; Park, T. G. The surface modification of nano-sized porous membrane with catechol conjugated poly(*n*-isopropyl acrylamide) for thermal responsive diffusion. *J. Control. Release* **2011**, *152*, E215-E216.
88. Brukman, M. J.; Marco, G. O.; Dunbar, T. D.; Boardman, L. D.; Carpick, R. W. Nanotribological properties of alkanephosphonic acid self-assembled monolayers on aluminum oxide: Effects of fluorination and substrate crystallinity. *Langmuir* **2006**, *22*, 3988-3998.
89. McElwee, J.; Helmy, R.; Fadeev, A. Y. Thermal stability of organic monolayers chemically grafted to minerals. *J. Colloid Interface Sci.* **2005**, *285*, 551-556.
90. Liakos, I. L.; McAlpine, E.; Chen, X.; Newman, R.; Alexander, M. R. Assembly of octadecyl phosphonic acid on the α -Al₂O₃ (0001) surface of air annealed alumina: evidence for termination dependent adsorption. *Appl. Surf. Sci.* **2008**, *255*, 3276-3282.
91. Koutsoubas, A. G.; Spiliopoulos, N.; Anastassopoulos, D. L.; Vradis, A. A.; Priftis, G. D. Formation of alkane-phosphonic acid self-assembled monolayers on alumina: an in situ SPR study. *Surf. Interface Anal.* **2009**, *41*, 897-903.
92. Cichomski, M.; Kosla, K.; Grobelny, J.; Kozlowski, W.; Szmaja, W. Tribological and stability investigations of alkylphosphonic acids on alumina surface. *Appl. Surf. Sci.* **2013**, *273*, 570-577.
93. Branch, B.; Dubey, M.; Anderson, S. A.; Artyushkova, K.; Baldwin, J. K.; Petsev, D.; Dattelbaum, A. M. Investigating phosphonate monolayer stability on ALD oxide surfaces. *Appl. Surf. Sci.* **2014**, *288*, 98-108.
94. Sun, S. Q.; Leggett, G. J. Micrometer and nanometer scale photopatterning of self-assembled monolayers of phosphonic acids on aluminum oxide. *Nano Lett.* **2007**, *7*, 3753-3758.
95. Luschtinetz, R.; Oliveira, A. F.; Frenzel, J.; Joswig, J. O.; Seifert, G.; Duarte, H. A. Adsorption of phosphonic and ethylphosphonic acid on aluminum oxide surfaces. *Surf. Sci.* **2008**, *602*, 1347-1359.
96. Rumpel, A.; Novak, M.; Walter, J.; Braunschweig, B.; Halik, M.; Peukert, W. Tuning the molecular order of C-60 functionalized phosphonic acid monolayers. *Langmuir* **2011**, *27*, 15016-15023.
97. Ma, W.; Wu, H.; Higaki, Y.; Otsuka, H.; Takahara, A. A "non-sticky" superhydrophobic surface prepared by self-assembly of fluoroalkyl phosphonic acid on a hierarchically micro/nanostructured alumina gel film. *Chem. Commun.* **2012**, *48*, 6824-6826.
98. Tsud, N.; Yoshitake, M. Vacuum vapour deposition of phenylphosphonic acid on amorphous alumina. *Surf. Sci.* **2007**, *601*, 3060-3066.
99. Fonder, G.; Delhalle, J.; Essahli, M.; Ameduri, B.; Mekhalif, Z. Anchoring of sulfur-containing alkylphosphonic and semifluorinated alkylphosphonic molecules on a polycrystalline aluminum substrate. *Surf. Interface Anal.* **2008**, *40*, 85-96.
100. Chang, S. H.; Han, J. L.; Tseng, S. Y.; Lee, H. Y.; Lin, C. W.; Lin, Y. C.; Jeng, W. Y.; Wang, A. H. J.; Wu, C. Y.; Wong, C. H. Glycan array on aluminum oxide-coated glass slides through phosphonate chemistry. *J. Am. Chem. Soc.* **2010**, *132*, 13371-13380.
101. Hotchkiss, P. J.; Jones, S. C.; Paniagua, S. A.; Sharma, A.; Kippelen, B.; Armstrong, N. R.; Marder, S. R. The modification of indium tin oxide with phosphonic acids: mechanism of binding, tuning of surface properties, and potential for use in organic electronic applications. *Acc. Chem. Res.* **2012**, *45*, 337-346.
102. Trilling, A. K.; Beekwilder, J.; Zuilhof, H. Antibody orientation on biosensor surfaces: a minireview. *Analyst* **2013**, *138*, 1619-1627.
103. Jiang, H.; Xu, F.-J. Biomolecule-functionalized polymer brushes. *Chem. Soc. Rev.* **2013**, *42*, 3394-3426.
104. Clausmeyer, J.; Schuhmann, W.; Plumere, N. Electrochemical patterning as a tool for fabricating biomolecule microarrays. *Trends Anal. Chem.* **2014**, *58*, 23-30.
105. Doncz, B.; Kerekgyarto, J.; Szurmai, Z.; Guttman, A. Glycan microarrays: new angles and new strategies. *Analyst* **2014**, *139*, 2650-2657.
106. Bhakta, S. A.; Evans, E.; Benavidez, T. E.; Garcia, C. D. Protein adsorption onto nanomaterials for the development of biosensors and analytical devices: a review. *Anal. Chim. Acta* **2015**, *872*, 7-25.
107. Wang, C.; Feng, B. Research progress on site-oriented and three-dimensional immobilization of protein. *Mol. Biol.* **2015**, *49*, 1-20.
108. Jonkheijm, P.; Weinrich, D.; Schroeder, H.; Niemeyer, C. M.; Waldmann, H. Chemical strategies for generating protein biochips. *Angew. Chem. Int. Ed.* **2008**, *47*, 9618-9647.
109. Makaraviciute, A.; Ramanaviciene, A. Site-directed antibody immobilization techniques for immunosensors. *Biosens. Bioelectron.* **2013**, *50*, 460-471.
110. Lin, P.-C.; Weinrich, D.; Waldmann, H. Protein biochips: oriented surface immobilization of proteins. *Macromol. Chem. Phys.* **2010**, *211*, 136-144.
111. Wang, S. Y.; Chen, K. M.; Li, L.; Guo, X. H. Binding between proteins and cationic spherical polyelectrolyte brushes: effect of pH, ionic strength, and stoichiometry. *Biomacromolecules* **2013**, *14*, 818-827.
112. Vashist, S. K.; Schneider, E. M.; Lam, E.; Hrapovic, S.; Luong, J. H. T. One-step antibody immobilization-based rapid and highly-sensitive sandwich ELISA procedure for potential in vitro diagnostics. *Sci. Rep.* **2014**, *4*, 7.
113. Aissaoui, N.; Landoulsi, J.; Bergaoui, L.; Boujday, S.; Lambert, J. F. Catalytic activity and thermostability of enzymes immobilized on silanized surface: influence of the crosslinking agent. *Enzyme Microb. Technol.* **2013**, *52*, 336-343.
114. Barbosa, O.; Ortiz, C.; Berenguer-Murcia, A.; Torres, R.; Rodrigues, R. C.; Fernandez-Lafuente, R. Glutaraldehyde in bio-catalysts design: a useful crosslinker and a versatile tool in enzyme immobilization. *RSC Adv.* **2014**, *4*, 1583-1600.
115. Chen, Y.-X.; Triola, G.; Waldmann, H. Bioorthogonal chemistry for site-specific labeling and surface immobilization of proteins. *Acc. Chem. Res.* **2011**, *44*, 762-773.
116. Dundas, C. M.; Demonte, D.; Park, S. Streptavidin-biotin technology: improvements and innovations in chemical and biological applications. *Appl. Microbiol. Biotechnol.* **2013**, *97*, 9343-9353.
117. You, C.; Piehler, J. Multivalent chelators for spatially and temporally controlled protein functionalization. *Anal. Bioanal. Chem.* **2014**, *406*, 3345-3357.
118. Song, L. J.; Zhao, J.; Luan, S. F.; Ma, J.; Liu, J. C.; Xu, X. D.; Yin, J. H. Fabrication of a detection platform with boronic-acid-containing zwitterionic polymer brush. *ACS Appl. Mater. Inter.* **2013**, *5*, 13207-13215.
119. Adak, A. K.; Li, B. Y.; Huang, L. D.; Lin, T. W.; Chang, T. C.; Hwang, K. C.; Lin, C. C. Fabrication of antibody microarrays by light-induced covalent and oriented immobilization. *ACS Appl. Mater. Inter.* **2014**, *6*, 10452-10460.
120. Shrestha, D.; Bagosi, A.; Szollosi, J.; Jenei, A. Comparative study of the three different fluorophore antibody conjugation strategies. *Anal. Bioanal. Chem.* **2012**, *404*, 1449-1463.

121. Palomo, J. M. Diels-Alder cycloaddition in protein chemistry. *Eur. J. Org. Chem.* **2010**, 6303-6314.
122. Kalia, J.; Abbott, N. L.; Raines, R. T. General method for site-specific protein immobilization by Staudinger ligation. *Bioconjugate Chem.* **2007**, *18*, 1064-1069.
123. Govindaraju, T.; Jonkheijm, P.; Gogolin, L.; Schroeder, H.; Becker, C. F. W.; Niemeyer, C. M.; Waldmann, H. Surface immobilization of biomolecules by click sulfonamide reaction. *Chem. Commun.* **2008**, 3723-3725.
124. Jonkheijm, P.; Weinrich, D.; Koehn, M.; Engelkamp, H.; Christianen, P. C. M.; Kuhlmann, J.; Maan, J. C.; Nuesse, D.; Schroeder, H.; Wacker, R.; Breinbauer, R.; Niemeyer, C. M.; Waldmann, H. Photochemical surface patterning by the thiol-ene reaction. *Angew. Chem. Int. Ed.* **2008**, *47*, 4421-4424.
125. Weinrich, D.; Lin, P.-C.; Jonkheijm, P.; Nguyen, U. T. T.; Schroeder, H.; Niemeyer, C. M.; Alexandrov, K.; Goody, R.; Waldmann, H. Oriented immobilization of farnesylated proteins by the thiol-ene reaction. *Angew. Chem. Int. Ed.* **2010**, *49*, 1252-1257.
126. Kanmani, P.; Kumar, R. S.; Yuvaraj, N.; Paari, K. A.; Pattukumar, V.; Arul, V. Probiotics and its functionally valuable products - a review. *Crit. Rev. Food Sci. Nutr.* **2013**, *53*, 641-658.
127. Pretzer, G.; Snel, J.; Molenaar, D.; Wiersma, A.; Bron, P. A.; Lambert, J.; de Vos, W. M.; van der Meer, R.; Smits, M. A.; Kleerebezem, M. Biodiversity-based identification and functional characterization of the mannose-specific adhesin of *Lactobacillus plantarum*. *J. Bacteriol.* **2005**, *187*, 6128-6136.
128. Kankainen, M.; Paulin, L.; Tynkkynen, S.; von Ossowski, I.; Reunanen, J.; Partanen, P.; Satokari, R.; Vesterlund, S.; Hendrickx, A. P. A.; Lebeer, S.; De Keersmaecker, S. C. J.; Vanderleyden, J.; Hamalainen, T.; Laukkanen, S.; Salovuori, N.; Ritari, J.; Alatalo, E.; Korpela, R.; Mattila-Sandholm, T.; Lassig, A.; Hatakka, K.; Kinnunen, K. T.; Karjalainen, H.; Saxelin, M.; Laakso, K.; Surakka, A.; Palva, A.; Salusjarvi, T.; Auvinen, P.; de Vos, W. M. Comparative genomic analysis of *Lactobacillus rhamnosus* GG reveals pili containing a human-mucus binding protein. *Proc. Natl. Acad. Sci. U. S. A.* **2009**, *106*, 17193-17198.
129. Ribeiro, M.; Monteiro, F. J.; Ferraz, M. P. Infection of orthopedic implants with emphasis on bacterial adhesion process and techniques used in studying bacterial-material interactions. *Biomater.* **2012**, *2*, 176-194.
130. Desrousseaux, C.; Sautou, V.; Descamps, S.; Traore, O. Modification of the surfaces of medical devices to prevent microbial adhesion and biofilm formation. *J. Hosp. Infect.* **2013**, *85*, 87-93.
131. Salwiczek, M.; Qu, Y.; Gardiner, J.; Strugnell, R. A.; Lithgow, T.; McLean, K. M.; Thissen, H. Emerging rules for effective antimicrobial coatings. *Trends Biotechnol.* **2014**, *32*, 82-90.
132. Lazcka, O.; Del Campo, F. J.; Munoz, F. X. Pathogen detection: a perspective of traditional methods and biosensors. *Biosens. Bioelectron.* **2007**, *22*, 1205-1217.
133. Skottrup, P. D.; Nicolaisen, M.; Justesen, A. F. Towards on-site pathogen detection using antibody-based sensors. *Biosens. Bioelectron.* **2008**, *24*, 339-348.
134. Dudak, F. C.; Boyaci, I. H. Rapid and label-free bacteria detection by surface plasmon resonance (SPR) biosensors. *Biotechnol. J.* **2009**, *4*, 1003-1011.
135. Arora, P.; Sindhu, A.; Dilbaghi, N.; Chaudhury, A. Biosensors as innovative tools for the detection of food borne pathogens. *Biosens. Bioelectron.* **2011**, *28*, 1-12.
136. Cheng, M. S.; Lau, S. H.; Chow, V. T.; Toh, C. S. Membrane-based electrochemical nanobiosensor for *Escherichia coli* detection and analysis of cells viability. *Environ. Sci. Technol.* **2011**, *45*, 6453-645.

Chapter 2

Carbohydrate-Presenting Self-Assembled Monolayers: Preparation, Analysis and Applications in Microbiology

Aline Debrassi¹, Willem M. de Vos^{2,3}, Han Zuilhof^{1,4}, Tom Wennekes¹

¹ Laboratory of Organic Chemistry, Wageningen University, 6703 HB Wageningen, The Netherlands

² Laboratory of Microbiology, Wageningen University, 6703 HB Wageningen, The Netherlands

³ Department of Bacteriology & Immunology and Department of Veterinary Biosciences, University of Helsinki, Finland

⁴ Department of Chemical and Materials Engineering, King Abdulaziz University, Jeddah, Saudi Arabia

This chapter was published in:

Stine, K. ed. Carbohydrate Nanotechnology. Hoboken, NJ, Wiley (2015)

Introduction

Carbohydrates are a complex class of essential biomolecules that can be considered as the dark matter of the biological universe as they are greatly understudied yet omnipresent in all kingdoms of life, and vital to fully understanding biological processes. The structurally diverse carbohydrates are present both on the cell surface as inside cells. They decorate the cell surface to form the so-called glycocalyx, a dense and complex layer of carbohydrates unique for every type of cell or organism, and as such are key to many important biological recognition events by interacting with carbohydrate-binding proteins. Carbohydrate-protein interactions play an important role in various biological events occurring at the cell surface, such as bacterial and viral infections,^{1, 2} cancer metastasis,^{3, 4} and immune response.⁴ The study of the interactions between carbohydrates and other biomolecules at biological surfaces and interfaces is instrumental in the understanding of these processes and contributing to the development of novel diagnostic methods and medicines. The study of carbohydrates, compared to e.g. nucleic acids and proteins, however, poses unique challenges because their structure is non-linear and their biosynthesis not template driven. The native glycocalyx is too complex, dense and dynamic for studying these interactions individually, with the current techniques at our disposal. Therefore, a simplified version is often created by the placement of well-defined, synthetic carbohydrates on a surface, so-called glycoarrays or glycosurfaces, to study specific carbohydrate-protein interactions. These fabricated glycosurfaces can also be more readily incorporated in a sensor or a nanostructure and as such be used to elicit, detect or quantify binding events, for example in diagnostic devices, molecular imaging and drug delivery applications. Various approaches have been developed to prepare glycosurfaces, each of them with their advantages and drawbacks, and these approaches will be the main focus of this chapter.

We will start the chapter by presenting an overview of the different methods most commonly used to prepare glycosurfaces. These methods will be discussed divided over three sections that each reflect one of the three distinct approaches used to create glycosurfaces: (a) direct formation of carbohydrate-containing self-assembled monolayers (SAMs); (b) use of secondary (or tertiary) reactions to install a carbohydrate on a pre-formed SAM; and (c) non-covalent immobilization of carbohydrates on a surface. The discussion of the secondary reaction approach (b) is subdivided into two

subsections: one addressing the use of unmodified ‘natural’ carbohydrates, and the other the use of synthetic carbohydrate derivatives with a special emphasis on attachment using so-called “click” chemistry. Next, we will focus on several key surface analysis techniques that can be used to characterize a prepared glycosurface and the type of information that can be obtained from each technique. As previously mentioned, carbohydrate-protein interactions are involved in bacterial pathogenesis and symbiosis. A famous example of carbohydrate-mediated bacterial adhesion is between the gut microbiota and the carbohydrates present on the surface of human intestinal cells. Glycosurfaces can be used for the binding, capture, and sensing of gut bacteria. A representative example of this from our own group is the study of interactions between the mannose-specific adhesin of *Lactobacillus plantarum*⁵ – a lactic acid bacterium present in various probiotic products, fermented foods and our gut – and fabricated mannose-terminated glycosurfaces.⁶ At the end of this chapter we will discuss several more applications of glycosurfaces in microbiology, focusing on binding, capture, and sensing of bacteria and bacterial toxins, and on the multivalency effects that exert a large influence on the interaction between carbohydrates and proteins in biological systems and on fabricated glycosurfaces.

Preparation of self-assembled monolayers (SAMs) containing carbohydrates

Self-assembled monolayers (SAMs) are ordered molecular assemblies that spontaneously form on a substrate by chemisorption (or strong interaction) of molecules containing a chemical functionality with a strong affinity for the substrate surface. The chemical structure of molecules that are used to prepare a SAM is usually subdivided in its constituting parts; the part that adsorbs on the substrate surface can be called the attaching group, the part on the opposing end of the molecule that ends up at the top of the monolayer is called the end group or terminal group and the intermediate part is called the chain or backbone.^{7, 8} In this section, we will present an overview of the recent scientific literature on the preparation and properties of SAMs containing carbohydrates as end groups (**Table 1**).

Table 1. Approaches used for the direct preparation of carbohydrate-presenting SAMs. (a) Thiol on gold, (b) disulfide on gold (monovalent binding), (c) disulfide on gold (multidentate binding), (d) alkene on silicon, (e) alkyne on silicon, (f) phosphonic acid on aluminum oxide, and (g) silane on silica.

| | Substrate | Functional Group | Immobilized Product | Immobilized Carbohydrates |
|-----|-------------------------------|---------------------|---------------------|--|
| (a) | Gold surface | Thiol | | Mannose, ⁹⁻¹⁴ glucose, ^{9, 15-17} galactose, ^{13, 16, 17} <i>N</i> -acetylglucosamine, ¹⁸ lactose, ¹⁵ rhamnose, ¹⁷ maltose, ^{17, 19} maltotriose, ¹⁷ abequose, ²⁰ paratose, ²⁰ tyvelose, ²⁰ globotriose, ²¹ xylose, ¹⁷ dimethylated maltose, ¹⁷ GM1, ¹⁵ other disaccharides, ^{22, 23} hexasaccharide ²⁴ |
| (b) | Gold surface | Disulfide | | Globotriose, ²⁵⁻²⁷ maltose, ²⁸ <i>p</i> k trisaccharide, ²⁹ asialo-GM2 disaccharide ²⁹ |
| (c) | Gold surface | Disulfide | | Mannose, ³⁰ glucose, ³⁰⁻³² fucose, ³⁰ galactose, ^{30, 31} <i>N</i> -acetylglucosamine, ³⁰ sialic acid, ³⁰ lactose ³¹ |
| (d) | Silicon | Alkene | | Lactose ³³ |
| (e) | Silicon | Alkyne | | Mannose ³⁴ |
| (f) | Aluminum oxide | Phosphonic acid | | Mannose, Gb3, globo H ³⁵ |
| (g) | Silica-coated stainless steel | Silane | | <i>N</i> -acetylglucosamine, galactose ³⁶ |

One of the most common combinations of substrate and attaching group is the formation of SAMs of thiols on gold (**Table 1; entry a**), and, to our knowledge, this was also the first example of a carbohydrate-presenting SAM. In 1996, Spencer and co-workers reported the formation of SAMs on gold surfaces with a thiol-terminated hexasaccharide. The thiol-terminated hexasaccharide, a truncated amylose derivative consisting of six α -1,4-linked glucopyranosides, was assembled on gold surfaces in its protected (peracetylated) and deprotected form. Both protected and deprotected compounds readily formed SAMs on gold, although the kinetics of SAM formation varied, with the deprotected hexasaccharide achieving a SAM with higher density. The protected hexasaccharide was also successfully deprotected on the surface after the SAM formation, however, the degree of deprotection was slightly lower than when conducted in solution before SAM formation.²⁴ These early studies already indicate that thiol SAMs on gold are best prepared directly with deprotected carbohydrate derivatives in order to circumvent incomplete deprotection of carbohydrates on the surface and degradation of the unstable thiol on gold SAM itself.

Using a similar approach, Russell and co-workers (1998) synthesized protected and deprotected thiol-terminated monosaccharides that were assembled as SAMs on gold-coated glass substrates, and afterwards assessed for their interaction with a series of lectins. The SAM formed with a thiol-terminated mannose derivative was exposed to concanavalin A (Con A), a lectin known to bind strongly with mannose, and a lectin from *Tetragonolobus purpureas*, which specifically binds L-fucose. As expected, the mannose-terminated SAM showed selective interaction with Con A, demonstrating that carbohydrate-presenting SAMs can be used to study interactions between carbohydrates and proteins as a simplified version of natural cell surfaces.⁹

Houseman and Mrksich (1999) were the first to prepare mixed SAMs that consisted of various ratios of a carbohydrate and oligoethylene end group, in which the latter was incorporated to minimize nonspecific interactions. The authors prepared SAMs using *N*-acetylglucosamine and tri(ethylene glycol) with thiol attaching groups, and studied the effect of the concentration of *N*-acetylglucosamine in the monolayer on an enzymatic reaction.¹⁸ Later in this chapter, we will further discuss the strategy of using molecules to “dilute” the amount of carbohydrate on a surface and thereby tune the carbohydrate presentation and concentration (Multivalency effect and optimization of density).

The relatively easy preparation of thiol SAMs on gold and high tolerance for additional functional groups, including carbohydrate hydroxyls, has made it a popular method to immobilize also other carbohydrates with various levels of complexity: monosaccharides (mannose,¹⁰⁻¹⁴ glucose,^{15-17, 32} galactose,^{13, 16, 17, 37} xylose,¹⁷ rhamnose¹⁷), disaccharides (lactose,¹⁵ maltose,^{17, 19} dimethylated maltose¹⁷)^{20, 22, 23} and oligosaccharides (GM1 pentasaccharide,¹⁵ globotriose,²¹ maltotriose¹⁷).³⁷

A general drawback of SAMs created by the adsorption of thiols on gold is their relative limited stability. In order to increase the stability of SAMs on gold, some research groups have prepared SAMs with molecules that can form multiple bonding interactions with the substrate (multidentate adsorbates) (**Table 1; entry c**). The increased stability enables their use under conditions that are not compatible with the monodentate ones.³⁸ Disulfides can be used to generate more stable SAMs on gold (**Figure 1a**) and this strategy has been applied to various carbohydrate derivatives: mannose,^{10, 30} galactose,^{30, 31} glucose,^{30, 31} fucose,³⁰ *N*-acetylglucosamine,³⁰ sialic acid,³⁰ and lactose.³¹ However, some carbohydrate derivatives containing disulfides are designed in a way that does not enable multidentate binding to the surface (**Figure 1b** and **Table 1; entry b**). Although these molecules also form SAMs on gold, their binding mode and presentation of the carbohydrate are comparable to the binding of single thiol attaching groups.²⁵⁻²⁹

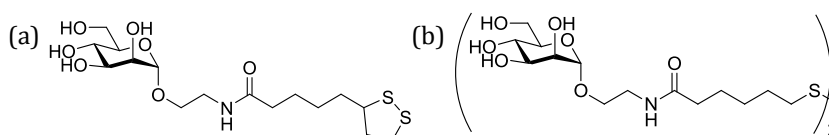


Figure 1. Mannose derivatives containing disulfides: (a) Disulfide that can form multidentate binding on gold and (b) disulfide that results in monodentate binding on gold.

As is clear from the previous paragraphs, carbohydrate-presenting SAMs have up till now been prepared mostly by thiol absorption on gold, but several alternative methods exist which are discussed next. One of these is the formation of SAMs on hydrogen-terminated silicon surfaces using terminal alkenes as attaching group (**Table 1; entry d**). In this case, the SAMs can be obtained by thermal or photochemical radical reaction of the alkene, resulting in the formation of a Si-C bond. Acetyl-protected β -

glucose, a mixture of β and α -sialic acid and a sialic acid derivative were successfully immobilized on hydrogen-terminated silicon surfaces using either thermal or photochemical method, depending on the thermal stability of the carbohydrate.^{39, 40}

Using a similar approach, lactose was immobilized as *p*-vinylbenzylactonoamide on silicon (**Figure 2**). Through a thermal radical reaction, a silicon-centered radical, which was formed by the activation of a Si-H bond, reacted with the terminal alkene of the *p*-vinylbenzylactonoamide molecule in an anti-Markovnikov fashion. After SAM formation, the lactoside-covered surface was patterned by UV irradiation using a copper grid. The authors showed specific binding of a lactose-binding lectin (*Ricinus communis* agglutinin, RCA₁₂₀) on the regions that were not irradiated with UV light, without nonspecific adsorption of the protein on the SiO_x regions. Compared to the earlier SAMs on gold, this technique offers the advantage that an additional resistant SAM, such as a polyethylene glycol chain, is not needed to prevent nonspecific adsorption of proteins on silicon surfaces.³³

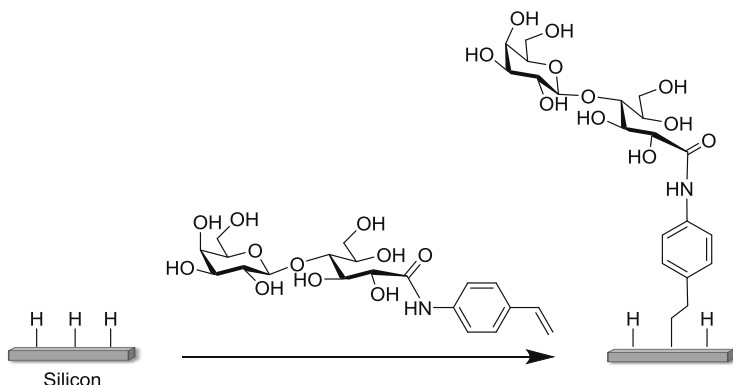


Figure 2. Immobilization of lactose as *p*-vinylbenzylactonoamide on silicon.

In a similar approach, a mannose derivative containing a terminal alkyne group was used to form SAMs on hydrogen-terminated silicon surfaces by a photochemical radical reaction (**Table 1; entry e**). Hydrosilylation of the Si-H surface was achieved by UV/visible light irradiation generated radicals, which initiate the Si-C bond formation that over time generates the SAM. The mannose-presenting SAM was formed on a patterned substrate and displayed specific protein recognition of fluorescently labelled mannose-binding lectin (Con A).³⁴

Another approach to generate covalent SAMs uses carbohydrate derivatives containing a phosphonic acid attaching group that is able to form SAMs on oxide surfaces (**Table 1; entry f**). Using this approach, Wong and co-workers (2010) prepared phosphonic acid-presenting derivatives of simple monosaccharides, like mannose, and more complex carbohydrates, like the trisaccharide Gb3 and the hexasaccharide Globo H that were allowed to form SAMs on aluminum oxide-coated glass slides. The glycan arrays generated by this technique were successfully used to study several carbohydrate-protein interactions.³⁵

Although one of the most common methods to prepare SAMs in general is the modification of surface oxides with alkylsilanes,⁴¹ there are not many examples of carbohydrate derivatives containing alkylsilanes to form SAMs, probably due to the reactivity of silanes with the hydroxyls of unprotected carbohydrates and the consequently laborious synthesis routes required to circumvent this. One of the few existing examples is the synthesis of *N*-acetyl-D-glucosamine and galactose derivatives containing a trialkoxysilane attaching group and their use to form SAMs on silica-coated stainless steel surfaces (**Table 1; entry g**). The presence and availability for biological interactions of the carbohydrates was confirmed by the successful binding of *N*-acetyl-D-glucosamine- and galactose-binding lectins.³⁶

In general, there are not many methods for the direct formation of SAMs with carbohydrate derivatives. It is evident that the most well-known and frequently used method is the formation of SAMs of thiols or disulfides on gold surfaces. Although this is an easy and well established technique for carbohydrate SAMs formation, the limited stability of the thiol SAMs on gold may hamper the scope of their potential applications.⁴² However, the formation of thiol SAMs on gold is the most simple method to immobilize carbohydrates on a surface in only one step and is currently still being used successfully, especially to study carbohydrate-protein interactions by surface plasmon resonance (SPR),¹⁴ electrochemical impedance spectroscopy (EIS),^{12, 13, 21} cyclic voltammetry,¹⁶ quartz crystal microbalance (QCM),³⁰ and a cantilever sensor platform.³⁷ An alternative for the direct formation of SAMs with carbohydrate derivatives is to use a secondary reaction to attach the carbohydrates via the end groups of a previously formed SAM, an approach that is discussed in the following section.

Preparation of glycosurfaces via a secondary reaction on SAMs

Glycosurfaces obtained stepwise using unmodified carbohydrates

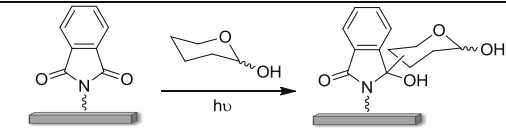
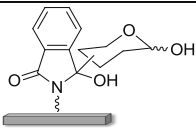
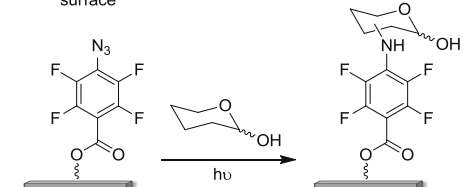
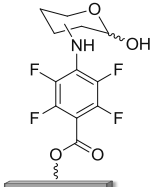
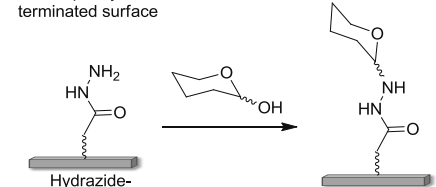
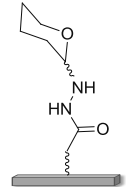
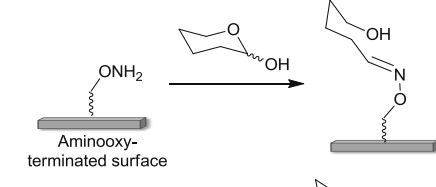
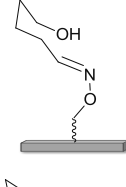
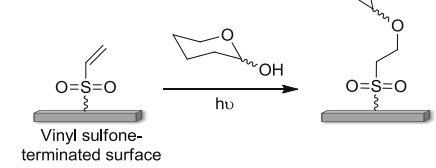
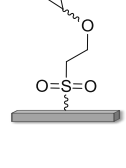
The attachment of unmodified carbohydrates to a reactive surface is the simplest method, because it does not require prior chemical modification of the carbohydrates, which is usually a time-consuming step. For the methods described in this section, in general a preformed SAM presents end groups that react with a functional group of a carbohydrate to form a covalent bond (**Table 2**).

Koberstein and co-workers (2006) described a photochemical method for immobilization of a variety of unmodified mono-, oligo-, and polysaccharides on glass, quartz, and silicon substrates. The authors initially synthesized a phthalimide-derivatized silane, which was self-assembled on the substrates to generate phthalimide-terminated surfaces. Upon exposure to UV light, an excited $n-\pi^*$ state was produced that abstracts a hydrogen atom from a nearby molecule (**Figure 3a** & **Table 2; entry a**). The resulting radicals then recombined and formed a covalent bond that in this case was with a nearby carbohydrate present in the reaction solution. Because of the photochemical nature of the process, this method can be used for direct chemical patterning of surfaces with carbohydrates via a photolithography process. Similar experiments were also successfully performed on benzophenone-terminated surfaces (**Figure 3b**), which also contain aromatic carbonyls that can photochemically react with natural carbohydrates. However, the thickness of these carbohydrate layers was lower and the water contact angle was higher than of the carbohydrates immobilized on the phthalimide-terminated surfaces.⁴³

Another more recently reported application of a photochemical reaction to immobilize unmodified carbohydrates on surfaces employs perfluorophenylazide-terminated SAMs (**Figure 3c** & **Table 2; entry b**). Initially, SAMs were formed on gold with perfluorophenylazide-containing thiol groups. Upon irradiation with UV light, the azide moiety yields perfluorophenylnitrene, which is able to insert into C–H bonds (**Figure 3c**). A series of mono- and oligosaccharides was successfully immobilized in this way onto SPR sensors and used for carbohydrate-protein binding studies. Through these binding studies, it was shown that the surface-bound carbohydrates retained their binding affinities and selectivity. Thus, this technique apparently enables the formation of robust and stable carbohydrate arrays, which can be repeatedly used to study

carbohydrate-protein interactions.⁴⁴ These photochemical reactions form the basis for convenient methods to immobilize various unmodified carbohydrates onto surfaces, although a major drawback is that the carbohydrates are immobilized in an ill-defined way due to the many reactive sites in the same molecule.

Table 2. Immobilization of unmodified carbohydrates on surfaces with different end group terminations. (a) Phthalimide, (b) perfluorophenyl azide, (c) hydrazide, (d) aminoxy, and (e) vinyl sulfone.

| | Surface Termination | Unmodified Carbohydrates | Immobilized Product | Immobilized Carbohydrates |
|-----|--|---|---|---|
| (a) | Phthalimide-terminated surface |  |  | Galactose, <i>N</i> -acetylgalactosamine, arabinose, rhamnose, mannose, glucose, isomaltotriose, isomaltopentose, isomaltoheptaose ⁴³ |
| (b) | Perfluorophenyl azide-terminated surface |  |  | Mannose, glucose, galactose ⁴⁴ |
| (c) | Hydrazide-terminated surface |  |  | <i>N</i> -acetylglucosamine, mannoside, methyl mannopyranoside, mannan, sialyl Lewis x, isomaltopentaose, ⁴⁵ mannose, heparin deca-saccharides ⁴⁶ |
| (d) | Aminoxy-terminated surface |  |  | <i>N</i> -acetylglucosamine, mannoside, methyl mannopyranoside, mannan, sialyl Lewis X, isomaltopentaose ⁴⁵ |
| (e) | Vinyl sulfone-terminated surface |  |  | Mannose, ⁴⁷ various complex carbohydrates ⁴⁸ |

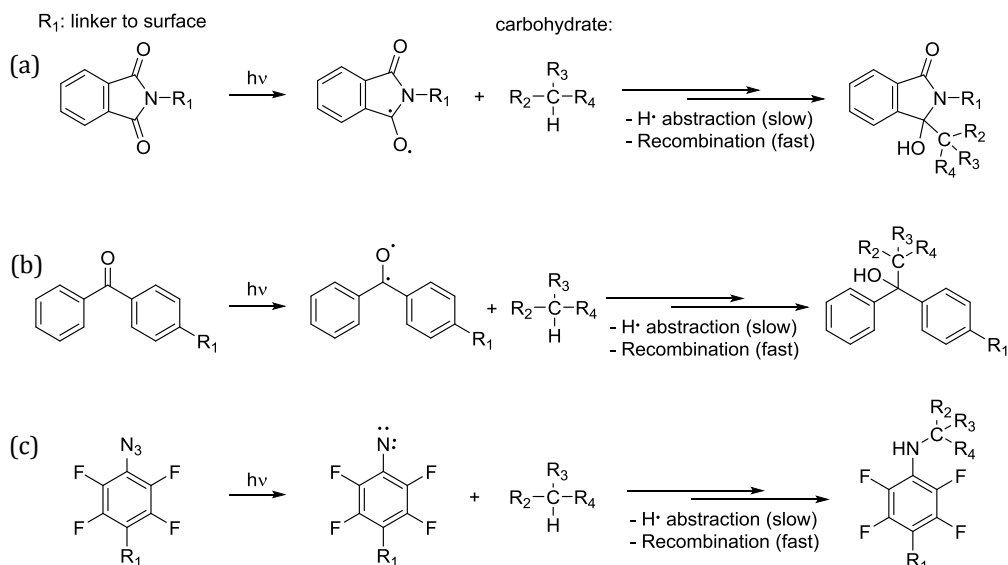


Figure 3. Photochemical reactions used to immobilize unmodified carbohydrates on surfaces with photoactive end groups: (a) phthalimide, (b) benzophenone, and (c) perfluorophenylazide.

A way to overcome this problem and still use unmodified carbohydrates is to use the anomeric hemiacetal present in reducing carbohydrates for the surface immobilization. In solution this functional group is in equilibrium with the open chain form aldehyde that can undergo various selective reactions. Wang and co-workers (2009) used this approach to prepare carbohydrate microarrays on glass slides. They initially immobilized a three-dimensional poly(amidoamine) starburst dendrimer on epoxy-terminated glass, followed by functionalization of the dendrimer with terminal hydrazide (**Table 2; entry c**) and aminooxy (**Table 2; entry d**) groups (**Figure 4**). These functional groups react with the aldehyde of the reducing carbohydrates, leading to site-specific immobilization via oxime and hydrazine formation. Using these techniques, the authors immobilized various unmodified mono-, oligo-, and polysaccharides with preservation of their specific binding activity.⁴⁵

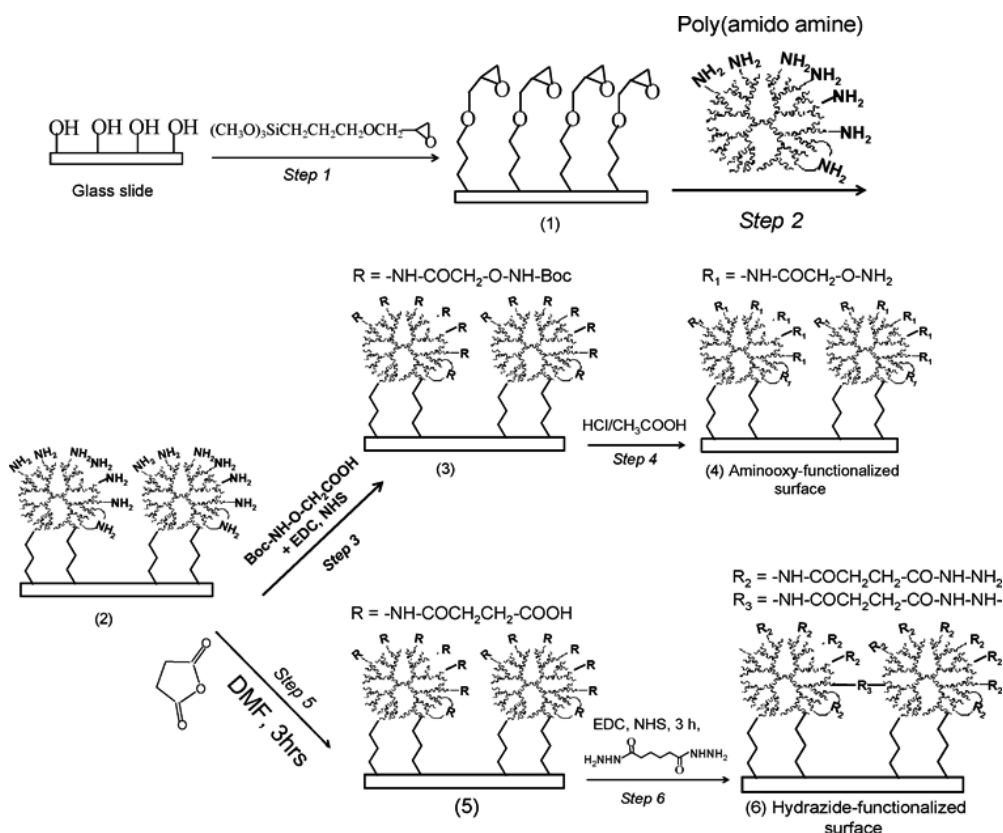


Figure 4. Chemical process for preparation of 3D aminoxy- and hydrazide functionalized glass slides. Reprinted with permission from reference 45. Copyright (2009) American Chemical Society.

In a similar approach, Zhi and co-workers (2006) prepared carbohydrate microarrays by reacting the aldehyde group of a reducing carbohydrate with hydrazide-terminated surfaces. The difference between this approach and the previous one is that the latter uses an additional reduction step of the oligosaccharides to form a reducing end aldehyde moiety, which reacts with the hydrazide groups present on the surface, forming a hydrazone. This hydrazone is then mainly converted into the native β -pyranose form, immobilizing the carbohydrates in a site-specific way.⁴⁶

Another approach that leads to a certain degree of site-specific immobilization of unmodified carbohydrates on surfaces makes use of divinyl sulfone as a crosslinking agent between hydroxy-terminated surfaces and the hydroxyl groups of the carbohydrate (**Table 2; entry e**).^{47, 48} In the first step, a hydroxy-terminated thiol-based SAM is generated on gold, followed by the immobilization of divinyl sulfone and the

unmodified carbohydrate via a Michael addition. The increased nucleophilicity of the anomeric hydroxyl contributes to the immobilization of the carbohydrates mainly via their anomeric center. However, an important drawback of this method is that the carbohydrate may also be immobilized by any of its other multiple hydroxyl groups and can exist as a mixture of α and β anomers, which is difficult to characterize on a surface and can have an effect on subsequent biological assays. To overcome these problems and to improve the reactivity of the carbohydrates, mannose derivatives containing amine and thiol groups were synthesized and immobilized on these vinyl-terminated surfaces (**Table 3; entry i**). The results indeed showed that the aminated and thiolated mannose derivatives are more efficiently immobilized on the vinyl sulfone-terminated surfaces.⁴⁷

Although the approaches described in this section are easy and versatile as they can be applied to a variety of natural carbohydrates, their major drawback is the nonspecific attachment of carbohydrates onto the surface. The use of chemically modified carbohydrates derivatives for site-selective attachment on surfaces is therefore a more commonly used approach to ensure that all molecules present on the surface are immobilized in a well-defined manner and thus have the same orientation. The reactions that are most frequently used for site-selective attachment of carbohydrates on surfaces are discussed in the following section.

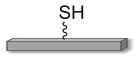
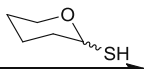
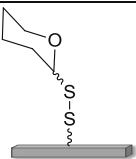
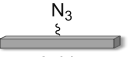
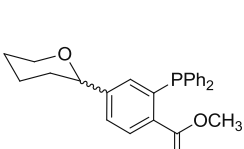
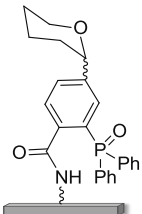
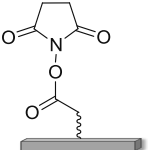
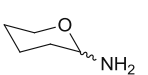
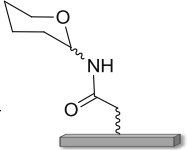
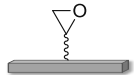
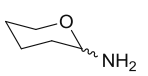
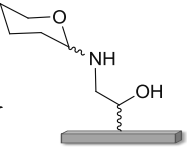
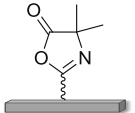
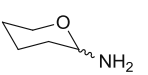
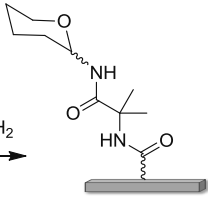
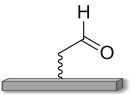
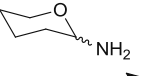
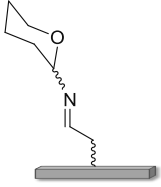
Glycosurfaces obtained stepwise using synthetic carbohydrate derivatives

The most extensively developed method to immobilize carbohydrates on surfaces involves the prior attachment of surface-reactive groups at the anomeric position of carbohydrates, resulting in site-specific immobilization (**Table 3**).⁴⁹ Of course, if one invests the additional time and effort in synthesizing a tailor-made carbohydrate derivative, the subsequent SAM attachment reaction should proceed in a controlled and efficient fashion to allow for a well-defined glycosurface and under mild conditions to allow for a large scope of (complex) carbohydrates.

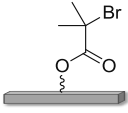
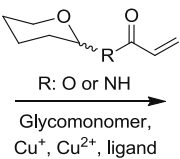
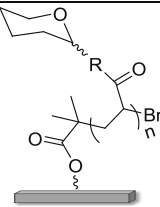

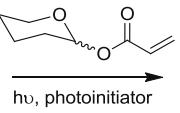
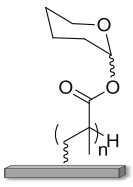
Table 3. Immobilization of synthetic carbohydrates derivatives on surfaces with different end group terminations. (a) CuAAC on alkyne-terminated surfaces, (b) CuAAC on azide-terminated surfaces, (c) SPAAC on azide-terminated surfaces, (d) SPAAC on cyclooctyne-terminated surfaces, (e) nitrile oxide-alkene cycloaddition, (f) thiol-ene, (g) thiol-yne, (h) thiol-maleimide coupling, (i) Michael addition, (j) Diels-Alder on benzoquinone and (k) maleimide-terminated surfaces, (l) Diels-Alder with inverse-electron-demand, (m) disulfide formation, (n) Staudinger ligation, (o) amide coupling on NHS-terminated surfaces, (p) epoxide-amine addition, (q) azlactone-amine coupling, (r) imine formation on aldehyde-terminated surfaces, (s) reductive amination on amine-terminated surfaces, (t) isocyanate-amine coupling on amine-terminated surfaces, (u) isothiocyanate-amine coupling on amine-terminated surfaces, (v) Michael addition on amine-terminated surfaces, (w) benzoquinone-aminoxy reaction, (x) enzymatic transglycosylation, (y) surface-initiated atom transfer radical polymerization (SI-ATRP), and (z) UV-induced graft polymerization on polypropylene membranes.

| | Surface Termination | Functionalized Carbohydrates | Immobilized Product | Immobilized Carbohydrates |
|-----|--------------------------------|------------------------------|---------------------|--|
| (a) | Alkyne-terminated surface | Azide, Cu^+ | | Mannose, ^{6, 50-54} galactose, ⁵² glucose, ^{52, 55} <i>N</i> -acetylglucosamine, ⁵² sulfo- <i>N</i> -acetylglucosamine, ⁵² sialic acid, ⁵² lactose, ^{50, 53} α -Gal trisaccharide, ⁵⁰ |
| (b) | Azide-terminated surface | Alkyne, Cu^+ | | Mucin mimic glycopolymer, ⁵⁶ maltoheptaose ⁵⁷ |
| (c) | Azide-terminated surface | Cyclooctyne | | Mannose ⁵⁸ Lactose ⁵⁹ |
| (d) | Cyclooctyne-terminated surface | Azide | | |
| (e) | Oxime-terminated surface | Norbornene, Oxidation | | Galactose ⁵⁸ |
| (f) | Alkene-terminated surface | Thiol, $h\nu$ | | Mannose, ^{60, 61} glucose, ⁶² galactose ^{61, 62} |

| | Surface Termination | Functionalized Carbohydrates | Immobilized Product | Immobilized Carbohydrates |
|-----|--------------------------------------|--|------------------------------|---|
| (g) | Alkyne-terminated surface | Thiol, $h\nu$ | | Mannose, ⁶¹ galactose, ⁶¹ glucose ^{63, 64} |
| (h) | Maleimide-terminated surface | Thiol | | Mannose, ⁶⁵⁻⁶⁷ galactose, ⁶⁵ glucose, ^{65, 68} <i>N</i> -acetylglucosamine ⁶⁵ |
| (i) | Vinyl sulfone-terminated surface | R: SH or NH ₂ Thiol or amine, $h\nu$ | R ₁ : S or NH | Mannose, ^{47, 69} galactose, ⁶⁹ complex carbohydrates ⁶⁹ |
| (j) | Benzoquinone-terminated surface | Cyclopentadiene | | Mannose, galactose, glucose, fucose, rhamnose, <i>N</i> -acetylglucosamine ⁷⁰ |
| (k) | Maleimide-terminated surface | Cyclopentadiene | | Mannose, galactose, glucose, lactose, maltose ⁷¹ |
| (l) | Tetrazine-terminated surface | Alkene | | Mannose, lactose, <i>N</i> -acetylglucosamine ⁷² |

| | Surface Termination | Functionalized Carbohydrates | Immobilized Product | Immobilized Carbohydrates |
|-----|---|--|---|---|
| (m) |  Thiol-terminated surface |  Thiol |  | Mannose, ⁷³ galactose, ^{73, 74} maltose ⁷⁴ |
| (n) |  Azide-terminated surface |  Phosphine |  | Galactose, lactose, <i>N</i> -acetyl-lactosamine ⁷⁵ |
| (o) |  NHS-terminated surface |  Amine |  | Galactose, ^{76, 77} glucose, ^{76, 78, 79} mannose, ^{76, 80} <i>N</i> -acetylglucosamine, ^{76, 77} <i>N</i> -acetylgalactosamine, ⁷⁸ sialic acid, ^{77, 81} lactose, ^{60, 76} <i>N</i> -acetyl-lactosamine, ^{79, 81} manno- biose, ⁷⁹ heparin decasaccharide, ⁷⁶ Globo H, ⁸² complex carbohydrates ^{76, 80-84} |
| (p) |  Epoxide-terminated surface |  Amine |  | Complex carbohydrates ^{84, 85} |
| (q) |  Azlactone-terminated surface |  Amine |  | Glucamine ⁸⁶ |
| (r) |  Aldehyde-terminated surface |  Amine |  | Mannose, galactose, glucose ⁸⁷ |

| | Surface Termination | Functionalized Carbohydrates | Immobilized Product | Immobilized Carbohydrates |
|-----|-------------------------------------|-------------------------------------|---------------------|--|
| (s) | Amine-terminated surface | Aldehyde | | Mannose, galactose, glucose, glucosamine, cellobiose, lactose, lactosamine ⁸⁸ |
| (t) | Isocyanate-terminated surface | Amine | | <i>N</i> -acetylglucosamine, <i>N</i> -acetyl-lactosamine ⁸⁹ |
| (u) | Amine-terminated surface | Isothiocyanate | | Mannose ⁹⁰ |
| (v) | Amine-terminated surface | Vinyl sulfone | | Mannose, glucose, <i>N</i> -acetylglucosamine, fucose, lactose, maltose, melibiose ⁹¹ |
| (w) | Hydroquinone-terminated surface | Aminooxy, Reduction | | Galactose, glucose ⁹² |
| (x) | Hydroxy-terminated surface | Lactose, β -galactosidase | | Galactose ⁹³ |

| | Surface Termination | Functionalized Carbohydrates | Immobilized Product | Immobilized Carbohydrates |
|-----|---|--|---|--|
| (y) |  Initiator-terminated surface |  R: O or NH Glycomonomer, Cu ⁺ , Cu ²⁺ , ligand |  | Glucose, ⁹⁴⁻⁹⁷ sulfonated glucose, ⁹⁵ mannose, ^{97, 98} galactose ⁹⁷ |
| (z) |  Polypropylene membrane |  hv, photoinitiator |  | Galactose ⁹⁹ |

In view of these desired reaction characteristics, the most frequently used reactions to immobilize carbohydrates on surfaces via this approach belong to the popular so-called “click” reactions. The most used is the copper(I)-catalyzed azide-alkyne cycloaddition (CuAAC) reaction (**Table 3; entries a & b**), which can be performed in various solvents and tolerates most functionalities. One of the first examples of immobilization of carbohydrates on surfaces using a CuAAC reaction was reported by Wang and co-workers (2006). In their study, azide-containing carbohydrate derivatives (mannoside, lactoside, and a galactose-containing trisaccharide) were successfully immobilized on alkyne-terminated gold surfaces via the CuAAC reaction. The immobilized carbohydrates presented specific binding towards proteins, as analyzed by SPR and QCM.⁵⁰ Overall two different approaches have been used to immobilize carbohydrates on surfaces via CuAAC: the alkyne functionality is either present on the surface and reacts with azide-containing carbohydrate derivatives^{6, 51-53, 55, 100-102}, or the azide group is on the surface and reacts with an alkyne-containing carbohydrate.^{56, 57} While the yield of CuAAC is typically high, a significant drawback of this reaction is the requirement of the toxic copper catalyst, which cannot always be completely removed and might limit the use of the resulting glycosurfaces for diagnostic and other biotechnological applications.^{103, 104}

An interesting alternative to circumvent the toxicity of copper is the use of strained cyclic alkynes that are able to react with azides via a copper-free strain-promoted azide-alkyne cycloaddition (SPAAC) reaction (**Table 3; entries c & d**)¹⁰⁵. The SPAAC reaction was first described by Bertozzi and co-workers (2004)¹⁰⁶ and has been used by our group to attach lactose derivatives containing azide groups on cyclooctyne-terminated Si₃N₄ surfaces. The bioactivity of the lactoside immobilized on Si₃N₄ was analyzed by binding studies with a fluorescently labeled lectin.⁵⁹ In the same year, Ravoo and co-workers (2012) immobilized a mannose derivative containing a cyclooctyne group on azide-terminated surfaces.⁵⁸ The main disadvantage of the SPAAC reaction is the more challenging synthesis of carbohydrate derivatives containing cyclooctynes when compared with the ones containing linear terminal alkynes. The limited stability of cyclooctyne-terminated monolayers also needs to be considered when using the SPAAC reaction to immobilize biomolecules on surfaces.

Another reaction used by Ravoo and co-workers (2012) to immobilize carbohydrates on surfaces involves *in situ* generation of nitrile oxide moieties on the surface, which react with alkenes or alkynes, forming isoxazolines (**Table 3; entry e**). The nitrile oxide groups on the surface were generated by oxidation of oxime-terminated surfaces using diacetoxy iodobenzene as the oxidizing agent. Using this approach, the authors immobilized a galactose derivative containing a norbornene group, and the galactose-terminated surfaces were shown to bind fluorescently labeled peanut agglutinin (PNA).⁵⁸

Another approach immobilizes carbohydrates on surfaces using a “click” reaction between thiols and alkenes or alkynes, called the thiol-ene or thiol-yne reaction (**Table 3; entries f & g**), respectively. The radical thiol-ene and thiol-yne reactions are usually carried out under UV light using a photoinitiator such as 2,2-dimethoxy-2-phenylacetophenone (DMPA). Ravoo and co-workers (2012) used the thiol-ene photochemical reaction to attach a thiol-containing mannose derivative on alkene-terminated surfaces.⁶⁰ The same type of reaction was also used by Ramström and co-workers (2012) to attach mannose and galactose derivatives on polymer-coated quartz surfaces functionalized with alkenes or alkynes. The authors carried out the reactions at room temperature and in aqueous solutions of the thiol-containing carbohydrates, *i.e.* using nonpolar solvents. The addition of a radical initiator was not necessary for the

reactions and, as expected, the thiol-ene reaction proceeded at a higher rate than the thiol-yne. The carbohydrate-terminated surfaces were then tested for their binding affinity to various lectins, showing good selectivity.⁶¹ The thiol-yne reaction was also used to immobilize glucose derivatives on an alkyne-presenting microporous polypropylene membrane^{63, 64} and on an alkyne-terminated silicon surface.¹⁰⁷ In the latter example, the consecutive double addition of thiol-terminated carbohydrates onto the alkyne in the thiol-yne reaction resulted in a higher surface density of carbohydrates when compared with the thiol-ene reaction.

Thiol-containing carbohydrate derivatives can also be used for immobilization onto maleimide-terminated surfaces (**Table 3; entry h**). Mrksich and co-workers (2003) used thiol-maleimide coupling to attach mannose, galactose, glucose, and *N*-acetylglucosamine derivatives on mixed disulfide monolayers on gold.⁶⁵ The same approach was also used later to prepare mannose-terminated surfaces, which were used to compare the binding responses with Con A of propagating SPR and localized SPR sensors.⁶⁶ Glucose-⁶⁸ and mannose⁶⁷-terminated surfaces were also prepared using the same reaction.

Another reaction used to immobilize carbohydrates on surfaces is the Diels-Alder reaction. Diels-Alder was used to attach various carbohydrate-diene conjugates on benzoquinone- (**Table 3; entry j**)⁷⁰ and maleimide- (**Table 3; entry k**)⁷¹ terminated surfaces. The Diels-Alder reaction with inverse-electron-demand (**Table 3; entry l**) was also successfully used to immobilize alkene-containing carbohydrate derivatives on tetrazine-terminated surfaces.⁷²

Thiol-containing carbohydrate derivatives have also been used for immobilization on thiol-terminated monolayers by formation of disulfides (**Table 3; entry m**). Based on this method, Corn and co-workers (2003) attached mannose and galactose derivatives on gold surfaces to fabricate carbohydrate arrays for imaging SPR.⁷³ Badyal and co-workers (2009) also used the formation of disulfides as a method to immobilize galactose and maltose on thiol-terminated surfaces.⁷⁴ An advantage of this immobilization method is the possibility of reducing the disulfide bonds and reusing the same thiol-terminated surfaces to attach other carbohydrates, if the initial monolayer is stable enough to survive the reduction step.

Cairo and co-workers (2010) prepared galactose, lactose, and *N*-acetyl-lactosamine-terminated surfaces using the Staudinger ligation as immobilization

method (**Table 3; entry n**). For this technique, the authors initially introduced an azide functionality to a carboxymethyl-dextran surface, which reacted with phosphane-containing carbohydrate derivatives. The modified surfaces were then used to analyze carbohydrate-lectin interactions by SPR.⁷⁵

Another functional group frequently used for attachment of carbohydrates on surfaces is the amine group, which can either be present on the surface or in the carbohydrate derivative. Amine-containing carbohydrate derivatives can be attached to carboxy-terminated surfaces using carbodiimide chemistry (e.g. *dicyclohexylcarbodiimide*, DCC) or *N*-hydroxysuccinimide (NHS) coupling chemistry (**Table 3; entry o**). Using this latter technique, a series of mono- and disaccharide derivatives containing an amine group was synthesized and attached on NHS-terminated monolayers on gold surfaces. The specific binding of proteins on the carbohydrate arrays was analyzed by SPR, matrix-assisted laser desorption/ionization time-of-flight mass spectrometry (MALDI-ToF-MS), and on-chip enzymatic modification.⁷⁶ This NHS-approach has also been used to immobilize a variety of monosaccharides,^{77, 79, 80} disaccharides,^{60, 77, 81} and also more complex carbohydrates,⁸⁰⁻⁸⁴ and has been used by the Consortium for Functional Glycomics (CFG) for the surface immobilization of carbohydrates for years.¹⁰⁸ The resulting surfaces were used to prepare arrays used for various biotechnological applications such as profiling diverse glycan binding proteins⁸³ and studying carbohydrate-specific cell adhesion.⁷⁷

Carbohydrate derivatives containing amine groups have also been immobilized on epoxy-terminated surfaces (**Table 3; entry p**). De Boer and co-workers (2007) used this technique to immobilize a series of complex carbohydrates, and prepare an array to study carbohydrate-protein interactions.⁸⁵ Cummings and co-workers (2009) compared the immobilization of amine-containing complex carbohydrate derivatives on epoxy and NHS-terminated surfaces. The authors observed that the minimum detectable printing concentrations are lower on the epoxy slides, but that this reaction is less specific when compared with printing on NHS-terminated surfaces.⁸⁴

Amine-containing molecules can also be immobilized on azlactone-terminated surfaces (**Table 3; entry q**). Using this approach, Lynn and co-workers (2009) immobilized D-glucamine on polymeric films with terminal azlactones and the resulting surfaces prevented the adhesion and growth of mammalian cells *in vitro*.⁸⁶ Another technique to immobilize amine-containing carbohydrate derivatives is by reacting with

aldehyde-terminated surfaces, forming an imine bond (**Table 3; entry r**). Wang and co-workers (2014) used this approach to attach monosaccharides onto a polyacrylamide hydrogel activated with glutaraldehyde, and employed the resulting surfaces for bacterial capture.⁸⁷ The use of carbohydrate-terminated surfaces to capture microorganisms will be discussed in more detail at the end of this chapter. The formation of an imine bond can also be used to attach aldehyde-functionalized carbohydrates on amine-terminated surfaces. The imine bond can then be reduced with mild reducing agents such as sodium cyanoborohydride to obtain irreversible immobilization (**Table 3; entry s**).⁸⁸ The reaction between amines and isocyanate or isothiocyanate groups (**Table 3; entries t & u**) have also been used to immobilize carbohydrate derivatives on surfaces. Amine-functionalized carbohydrates were successfully immobilized onto 96-well plates coated with an isocyanate-presenting polymer.⁸⁹ Using a similar reaction, a mannose derivative containing an isothiocyanate group was attached to amine-terminated surfaces and the resulting surfaces were used for bacterial capture.⁹⁰ Another strategy that has been used to prepare glycosurfaces involves the reaction between amines and vinyl sulfones (**Table 3; entry v**). Ratner and co-workers (2012) used this reaction to immobilize carbohydrates on the surface of silicon photonic microring resonators, used for label-free detection of glycan–protein and glycan–virus interactions.⁶⁹ Another possibility is to synthesize carbohydrate derivatives with a vinyl sulfone group, which then reacts with amine-terminated surfaces such as commercially available amine-functionalized glass slides or microwell plates.⁹¹

Another strategy used to prepare glycosurfaces is to synthesize carbohydrates presenting an oxyamine group, which reacts with the ketone group in electroactive quinone-terminated monolayers (**Table 3; entry w**). A remarkable advantage of this approach is the possibility to release the immobilized carbohydrate by applying a constant potential under reducing conditions to regenerate the original surface. Using this technique, glucose, galactose, and mannose derivatives were immobilized on gold surfaces, which were used to prepare microarrays to analyze binding of lectins.⁹²

Carbohydrates can also be attached on surfaces via enzymatic reactions. In a recent work, Xu and co-workers (2012) immobilized lactose on QCM chips modified with hydroxyl-terminated poly(ethylene glycol) (PEG) brushes via enzymatic transglycosylation (**Table 3; entry x**). The β -galactosidase enzyme catalyzed the

transfer of the galactose unit from lactose to the hydroxyl acceptor, yielding the glycoside compound with a β -1,4-glycosidic bond. The modified surface was used to selectively bind a lectin, while it displayed minimal non-specific adsorption of bovine serum albumin (BSA).⁹³

Finally, another quite distinct method to prepare glycosurfaces is the use of polymerization reactions with carbohydrate-containing monomers. The most commonly used polymerization method is the surface-initiated atom transfer radical polymerization (SI-ATRP) (**Table 3; entry y**), a powerful and versatile controlled radical polymerization method that enables control over polymer thickness and functionality.¹⁰⁹ Using this method, Fukuda and co-workers (2000) prepared glucose-terminated surfaces with protected glucose-functionalized monomers. The glucose units were subsequently deprotected quantitatively by removing the isopropylidenyl protecting groups, which did not result in degrafting or chain breaking of the glycopolymers.⁹⁴ The same monomer was later also used by Ayres and co-workers (2008) and Yoon and co-workers (2009), but with different surface-bound initiators.^{95, 96} Additionally, Ayres and co-workers (2008) performed a sulfonation reaction to also obtain glycosurfaces that may mimic heparin, a naturally occurring sulfonated glycosaminoglycan.⁹⁵ Another example using SI-ATRP to functionalize surfaces with glycopolymers employs D-gluconamidoethyl methacrylate as the glycomonomer used for the polymerization. The capability of preventing the binding of nonspecific proteins, such as lysozyme, BSA, and fibrinogen, on this glycopolymer was shown by SPR studies.¹¹⁰ The property of certain glycopolymers to prevent nonspecific protein adsorption on surfaces was also explored by Yu and Kizhakkedathu (2010). In their work, the authors prepared glycopolymer brushes by SI-ATRP using unprotected mannoside, glucoside, and galactoside *N*-substituted acrylamide derivatives as the monomers. The surfaces modified with the glycopolymers showed low BSA and fibrinogen adsorption, but also preserved the specific protein interaction as shown in the binding study with Con A.⁹⁷ Another example of a mannose-containing polymer was prepared by free radical polymerization on a gold surface and binding with Con A was studied by QCM, atomic force microscopy (AFM), and SPR techniques.⁹⁸ A galactose-containing monomer was synthesized by Ulbricht and co-workers (2010) and grafted on a polypropylene microfiltration membrane surface by UV-induced graft polymerization (**Table 3; entry z**). The galactose-presenting glycopolymer was successfully recognized by the bacterium

Enterococcus faecalis, increasing the adhesion of bacteria (by a factor of 39) when compared with the unmodified polypropylene surfaces.⁹⁹ The main advantage of preparing glycopolymers on surfaces is that the orientations in which they are presented probably better resembles the complex natural presentation of carbohydrates when compared to SAMs. However, one current challenge is to limit the polydispersity in order to obtain well-defined glycosurfaces.

The chemo-selective reactions discussed in this section are the most frequently used approach to immobilize carbohydrates on surfaces in a well-defined and controlled manner. In general, the main benefit of this approach is the possibility of obtaining a homogeneous carbohydrate layer, in which all the carbohydrate units are presented in the same orientation. They are usually bound to the surface via a linker connected to the anomeric carbon of the carbohydrate, yielding a carbohydrate layer with defined anomeric centers and thus hopefully similar properties compared to the glycosurfaces present in nature. However, this approach also has the disadvantage of requiring chemical modification of the carbohydrates for the immobilization on the previously prepared initial SAM. The synthetic methods required for the modification of the carbohydrates might limit the wider applicability of these chemo-selective reactions in the carbohydrate nanotechnology scientific community.

Non-covalent immobilization of carbohydrates to prepare glycosurfaces.

The preparation of glycosurfaces using secondary reactions, either using unmodified carbohydrates or in a chemo-selective way, usually has the advantage of yielding stable modifications due to the covalent nature of the bond used for the immobilization of the carbohydrate. Non-covalent immobilization (**Table 4**) is a quick and easy alternative to immobilize carbohydrates on surfaces, although it usually yields less stable glycosurfaces.

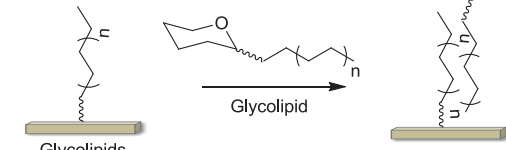
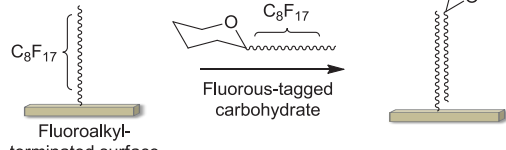
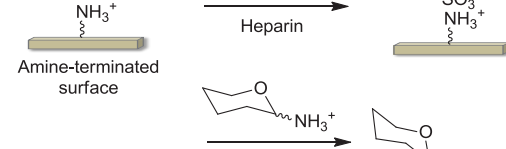
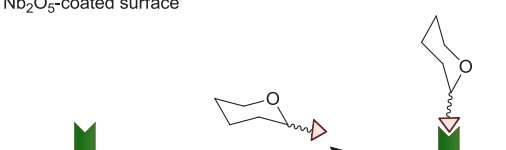
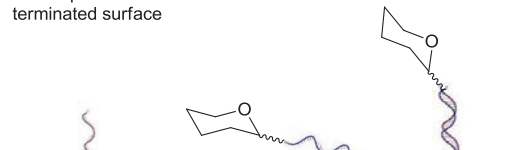
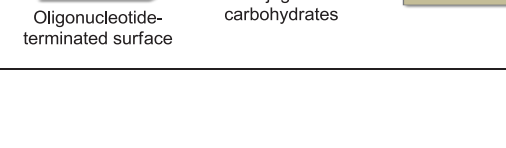
An interesting approach to prepare glycosurfaces using non-covalent immobilization methods is using glycolipids (**Table 4; entry a**), which can interact with surfaces presenting hydrophobic monolayers or also with surfaces that are intrinsically hydrophobic.^{115, 126} Using this approach, Kiessling and co-workers (1998) prepared a mannose-presenting glycolipid, which interacted with a previously prepared hydrophobic SAM. The carbohydrate density on the glycolipid bilayer was varied by using different percentages of the mannose glycolipid relative to phosphatidylcholine.

The modified surfaces were then used to investigate the specific binding of Con A by SPR.¹¹¹ Mannose glycolipids with two hydrophobic alkyl chains were also immobilized on surfaces by a similar technique.¹¹³⁻¹¹⁵ More complex carbohydrates such as gangliosides were also immobilized on surfaces using a similar approach and used to investigate the binding of cholera toxin.^{112, 119, 127} The same technique was also used to prepare glycosurfaces with C-lactose and C-galactose glycolipids on a commercially available HPA hydrophobic chip (Biacore).¹¹⁷ Natural glycolipids secreted by *Pseudozyma* yeast, known as mannosylerythritol lipids, were also immobilized on the HPA hydrophobic chip.¹²⁸ Using a slightly different technique, but also with a carbohydrate derivative containing hydrophobic chains, Liu and co-workers (2007) prepared *N*-acetylglucosamine-terminated surfaces. In their approach (**Figure 5**), a glass slide was initially functionalized to present amino groups. The amino-terminated glass slide was then covered with gold nanoparticles and these nanoparticles were then functionalized with thiols containing hydrophobic chains, which were used to interact with the glycolipids.¹¹⁸

Non-covalent immobilization of carbohydrates by hydrophobic interactions is not restricted to long alkyl chains. Other groups that provide hydrophobic or fluorophase interactions can be bound to carbohydrates and used to prepare glycosurfaces, such as aromatic rings and perfluorinated hydrocarbon chains (**Table 4; entry b**). Lindhorst and co-workers (2012) prepared mannose-terminated surfaces using trityl-containing mannose derivatives, which were immobilized onto polystyrene microplates.^{67, 116} Complex carbohydrates were also immobilized on aluminum oxide-coated glass surfaces via interaction between perfluorinated hydrocarbon chains immobilized on the surface and the ones present on the carbohydrate derivative.³⁵

Another type of interaction that can be used to prepare glycosurfaces via non-covalent immobilization is ionic interaction between surfaces and molecules with opposite charges (**Table 4; entries c & d**). The anionic polysaccharide heparin was immobilized on a positively charged amine-terminated surface.¹²⁰ Coullerez and co-workers (2008) also prepared a glycosurface based on the polycationic graft copolymer poly(L-lysine)-*graft*-poly(ethylene glycol) (PLL-g-PEG), which was modified to present mannose units and immobilized via ionic interactions on a negatively charged surface.¹²¹

Table 4. Methods of non-covalent immobilization of carbohydrates on surfaces. (a) Glycolipids, (b) Perfluorinated hydrocarbon chains, ionic interactions on (c) positively and (d) negatively charged surfaces, (e) biotin-streptavidin interaction, and (f) DNA-directed immobilization.

| | Substrate | Functional Group | Immobilized Product | Immobilized Carbohydrates |
|-----|---|--|---|---|
| (a) | Glycolipids-terminated or other hydrophobic surface | Glycolipid |  | Mannose, ¹¹¹⁻¹¹⁶ galactose, ¹¹⁷ <i>N</i> -acetylglucosamine, ^{116, 118} lactose, ¹¹⁷ cellobiose, ¹¹⁷ maltose, ¹¹⁷ GM1, ^{112, 119} other complex carbohydrates ¹¹² |
| (b) | Fluoroalkyl-terminated surface | Fluorous-tagged carbohydrate |  | Mannose, lactose, cellobiose, cellotriose, cellotetraose, Gb5, Globo H ³⁵ |
| (c) | Amine-terminated surface | Heparin |  | Heparin ¹²⁰ |
| (d) | Nb2O5-coated surface | PLL-g-PEG/PEG-mannoside |  | Mannose ¹²¹ |
| (e) | Streptavidin-terminated surface | Biotin-conjugated carbohydrates |  | Complex carbohydrates ¹²²⁻¹²⁴ |
| (f) | Oligonucleotide-terminated surface | Oligonucleotide-conjugated carbohydrates |  | Mannose, galactose ¹²⁵ |

Additionally, DNA-directed immobilization can also be used to prepare glycosurfaces (**Table 4; entry f**). Chevolot and co-workers (2009) successfully immobilized galactose derivatives on borosilicate glass slides using this technique.¹²⁵

The carbohydrates present on the cell surface in nature are usually present in the fluid lipid bilayer of membranes as glycoconjugates of proteins or lipids and, consequently, are exposed to their interaction partner in a dynamic fashion. In order to better mimic this aspect of natural glycosurfaces, some non-covalent immobilization techniques can be used, such as solid-supported lipid bilayers.^{115, 126} In this case, the carbohydrates may be exposed in a more dynamic way and may behave more similarly to the natural glycosurfaces.

In general, various techniques to prepare glycosurfaces have been developed in the past few decades. These techniques can be divided in four main groups: SAMs of molecules containing carbohydrates, covalent immobilization of unmodified carbohydrates by secondary reactions, chemo-selective covalent immobilization of carbohydrate derivatives, and non-covalent immobilization of carbohydrates. All the approaches discussed have their advantages and their drawbacks, and the optimal technique usually depends on the application of the glycosurfaces and the expertise of the scientists responsible for their design and preparation. However, what all these techniques have in common is the need to comprehensively characterize the obtained glycosurfaces. The main techniques used for characterization of glycosurfaces, including a few examples, will be discussed in the following section.

Characterization of glycosurfaces

Various methods are reported in the literature for preparation of glycosurfaces, as described in the previous sections. Glycosurfaces generated via all these methods need to be characterized to prove the successful modification of the surface. In this section, we provide an overview of the most frequently used techniques to characterize glycosurfaces (**Figure 7**), including the type of information that can possibly be obtained with each of these techniques.

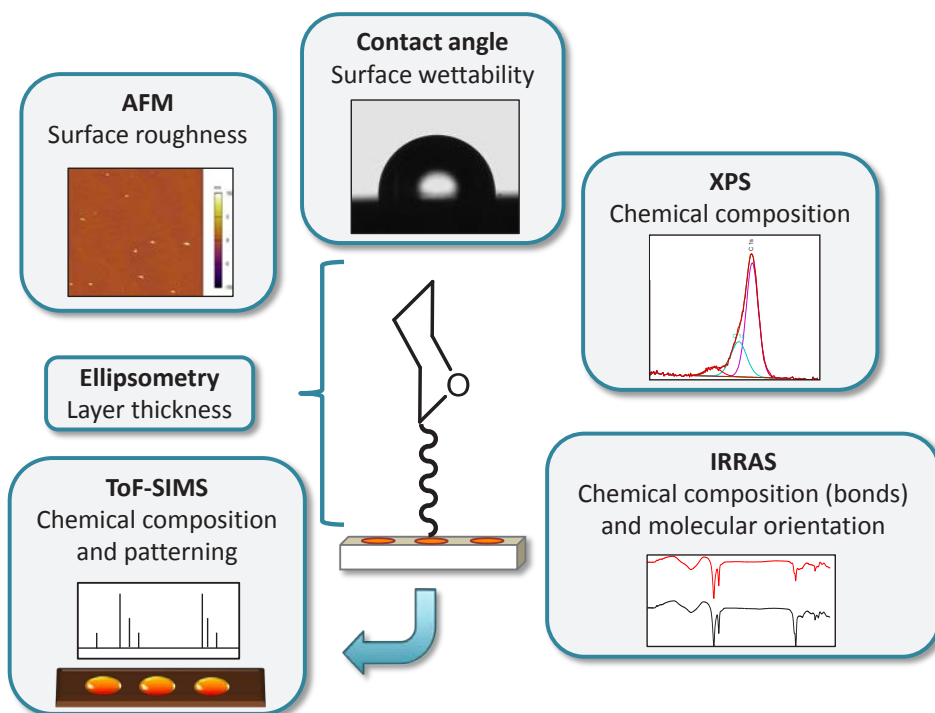


Figure 7. Main analysis techniques used to characterize glycosurfaces.

Contact angle measurements (wettability)

One of the most often used techniques for characterization of modified surfaces, including glycosurfaces, is the measurement of the surface wettability. The surface wettability is measured statically by placing a small drop of liquid on a surface and measuring the angle formed between the liquid and the solid surface, named contact angle. Nowadays, these measurements are obtained using a camera to record the image of the drop and a software that provides different fitting models to calculate the contact angle.^{131, 132} The main solvent used for contact angle measurements is water, but more apolar solvents can also be used. In general, according to the values of the static water contact angle the surfaces can be divided in hydrophilic ($\theta_{CA} < 90^\circ$) or hydrophobic ($\theta_{CA} > 90^\circ$).¹³² A surface after functionalization with carbohydrates typically displays a low water contact angle due to the hydrophilicity of the unprotected carbohydrates. The most frequently used contact angle measurement is the static contact angle, however advancing and receding contact angles can also be measured. The difference between the advancing and receding contact angles, called contact angle hysteresis, represents

the “non-ideality” of a surface and is related to the adhesion of materials on the surface.

132

Water contact angle measurements have been used by many researchers as the first technique to quickly and easily follow reactions with carbohydrates on surfaces. Yu and Kizhakkedathu (2010), for example, compared the water contact angles of glycopolymers on surface generated both with protected carbohydrate derivatives and deprotected ones. The surfaces generated with the protected carbohydrates presented a contact angle of 53.8°, whereas the ones generated with the deprotected carbohydrates had a contact angle of 7.2°. When the deprotection step was performed on the surface after generation of the glycopolymer, the contact angle of the resulting surfaces was 33.5°, showing that the deprotection on the surface was incomplete.⁹⁷ Xu and co-workers (2013) used water contact angle measurements to evaluate the effect of glycosyl density on the hydrophilicity of a polypropylene membrane. The authors observed a significant decrease of the contact angle with increase of the glycosyl density.⁶⁴

Although other techniques need to be used to analyse the functionalization of a surface with carbohydrates at the molecular/structural level, the contact angle measurement is an easy and quick method that provides a good indication about whether a functionalization step succeeded and the overall surface wettability.

X-ray photoelectron spectroscopy (XPS)

Another technique that has been frequently used for characterization of glycosurfaces is X-ray photoelectron spectroscopy (XPS), which provides quantitative information on the elemental and chemical composition of a surface to a depth of a few nanometers.¹³³ In XPS, a X-ray source induces the emission of photoelectrons from the surface. The emitted photoelectrons are collected, identified, and quantified according to their energy. The method is quantitative because the binding energies of the core levels that are analyzed are element-specific, while the signal intensities are not influenced significantly by the precise nature of chemical bonding.¹³⁴ An important advantage of XPS when compared to other techniques that provide elemental and chemical composition information is that it is essentially a non-destructive technique.¹³⁵ Two different types of surface analysis can be performed in XPS: wide-scan analysis, which provides (quantitative) information on the elemental composition, and high resolution

analysis (yielding a narrow-scan spectrum), which provides chemical bond information.¹³⁶

Many authors have used XPS to characterize glycosurfaces made with mixed SAMs of molecules containing carbohydrates and oligoethylene glycol or hydrocarbon units. In this case, the elemental analysis (wide-scan spectrum) is not sufficient to distinguish between the carbon and oxygen atoms of the carbohydrates and those of the ethylene glycol or hydrocarbon units. However, in the C1s narrow scan spectrum it is possible to obtain quantitative information about the chemical bonds that are present on the glycosurface. One can conveniently identify a XPS signal that is characteristic of carbohydrates, corresponding to the anomeric acetal carbon (O-C-O), that is present around 288 eV.^{6, 137-139} Dhayal and Ratner (2009), for example, used this signal to quantify the relative coverage of carbohydrate in mixed monolayers with ethylene glycol units.¹³⁷

Overall XPS provides very useful information on the composition and chemical state of elements present on surfaces. Although it has been used for the characterization of glycosurfaces, its more restricted availability to laboratories specialized in surface chemistry has limited its widespread application.

Infrared reflection-absorption spectroscopy (IRRAS)

Infrared reflection-absorption spectroscopy (IRRAS) is another technique that has been used for characterization of glycosurfaces. IRRAS is a truly non-destructive technique that provides information about the chemical composition of surfaces, based on frequencies and intensities of molecular vibrations.¹⁴⁰ IRRAS measurements can, in principle, also provide information about the molecular orientation within the layer, using polarized light,^{141, 142} but the short-range disorder of glycosurfaces will typically hamper providing such detailed information.

An advantage of infrared spectroscopy is that it does not require ultrahigh vacuum conditions, as opposed to XPS. Most IRRAS analysis of SAMs can be performed in air or inert atmosphere.¹⁴¹ Depending on the substrate, transmission infrared spectroscopy can be used instead of IRRAS, e.g. for glass¹⁴³ and porous aluminum oxide.^{6, 101}

The characteristic bands of carbohydrates are present at around 3300–3500 cm⁻¹, related to the stretching of intramolecular and intermolecular OH groups; and as

three shoulders at around 1147, 1090, and 1045 cm^{-1} , related to the hemiacetal of carbohydrates (O–C–O).^{55, 141} Some other IR bands that can often be found on prepared glycosurfaces are found at around 2850 cm^{-1} and 2920 cm^{-1} . They relate to the symmetric and antisymmetric stretching vibrations of the CH_2 chain, respectively, which are present when the carbohydrates are attached to a hydrocarbon chain.^{55, 141} The position of these bands may give information about how ordered the monolayer is.^{141, 144}

IRRAS is an useful and accessible technique for characterization of glycosurfaces. However, quantification of the carbohydrate density is challenging and another technique is probably required for more comprehensive characterization of a glycosurface.

Mass spectrometry

Mass spectrometry techniques, such as time-of-flight secondary ion mass spectrometry (ToF-SIMS) and direct analysis in real time high-resolution mass spectrometry (DART-HRMS) have also been used to obtain information about the composition of glycosurfaces. ToF-SIMS is a highly sensitive technique that can be used for surface chemical mapping and also enables the elucidation of molecular orientation.¹⁴⁵ In SIMS, a pulsed ion beam removes molecular fragments from the surface and the secondary ion fragments are accelerated by an electrical field. The ToF detector measures the velocity of the ions, which depends on the mass-to-charge ratio.¹⁴⁶

Some characteristic peaks that can be observed in ToF-SIMS analysis of glycosurfaces are related to oxygen rich anions, namely $\text{C}_3\text{H}_3\text{O}_2^-$, $\text{C}_2\text{H}_3\text{O}_2^-$, $\text{C}_2\text{H}_2\text{O}_2^-$, CHO_2^- , C_2HO^- ,⁷¹ and $\text{C}_3\text{H}_5\text{O}_2^+$.⁴⁷ Other signals mostly depend on the type of SAM present on the surface, such as CH_2AuS , $\text{C}_2\text{H}_4\text{AuS}$, and $\text{C}_4\text{H}_8\text{AuS}$ for alkanethiol SAMs on gold, for example.¹³⁸ ToF-SIMS has also been used for characterization of patterned glycosurfaces, with detection of characteristic carbohydrate ions depending on the surface localization.^{71, 141}

Another mass spectrometry technique, which has recently been studied in detail in our group, for the characterization of glycosurfaces is DART-HRMS. In DART-HRMS excited He gas is impinged onto the surface under ambient conditions. This affects an interaction between such excited He and the surface, or between atmospheric species obtained from ionization by excited He, and the surface. Surface-bound groups are in

this process removed from the surface, and ionized.¹⁴⁷ We used DART-HRMS to characterize lactose, mannose, and fucose-functionalized porous aluminum oxide surfaces. Using the tremendous structural power of HRMS, it is thus easily possible to discriminate between the immobilized monosaccharides, and between various disaccharides.¹⁰⁰ In this way DART-HRMS provides structural information about glycosurfaces that is not easy to obtain otherwise.

Mass spectrometry techniques, such as ToF-SIMS and DART-HRMS are useful to obtain information about chemical composition of glycosurfaces and also to prove the localization of carbohydrates on patterned surfaces. A drawback is that these techniques are destructive, so the glycosurfaces that are analyzed cannot be further used for biological tests.

Ellipsometry

Ellipsometry is a powerful optical tool to measure the thickness of thin films, including glycosurfaces. Ellipsometric measurements are usually performed with a light beam that propagates in air (or vacuum) and is reflected by (or transmitted through) the sample, eventually arriving at the detector. This technique can determine the thickness of monolayers or glycopolymers on surfaces, because the light reflected by the interface of an initial layer interferes with the light reflected by the interface of a second layer on top of it.¹⁴⁸

Ellipsometry has usually been used in combination with other techniques to characterize glycosurfaces, because it does not provide information on chemical composition. An interesting characteristic of ellipsometry is the possibility of measuring layer thickness in various conditions, including the presence of different solvents. This technique is useful to measure SAMs directly prepared with carbohydrate derivatives,^{17, 25, 34} glycosurfaces in which the carbohydrate is immobilized via a secondary (or tertiary reaction),⁹⁰ and also for glycopolymers on surfaces.^{96, 97, 110}

Atomic force microscopy (AFM)

Atomic force microscopy (AFM) is a scanning probe microscopy imaging technique used to investigate roughness of surfaces, size, shape, structure, dispersion, and aggregation of nanomaterials. The equipment consists of a micro-machined cantilever, usually made of silicon or silicon nitride, with a sharp tip at one end. This tip

detects the deflection of the cantilever caused by repulsion or attraction between the tip and the analysed surface. It presents different scanning modes: noncontact or static mode, contact mode, and intermittent sample contact mode (or dynamic and tapping mode).¹⁴⁹

AFM can also be used as a highly sensitive force machine that can measure forces as small as 10 to 20 pN. This property enables the use of AFM to measure nano-adhesive properties of samples. By using a (bio)functionalized cantilever tip it is even possible to measure the attraction or binding event between a (bio)molecule and a (bio)functionalized surface.^{150, 151}

For the characterization of glycosurfaces, AFM has mainly been used to investigate surface roughness, especially for glycopolymers on surfaces.^{28, 32, 97, 124} AFM is an interesting technique to investigate how the carbohydrates are distributed on a surface, however, it provides limited information on the nature of the carbohydrate molecule. One way to increase the information provided by AFM is the use of specific lectins at its cantilever tip. In addition, AFM can be combined with other characterization techniques, such as XPS, ToF-SIMS, and IR, for confirmation of the biofunctionalization of the surface with carbohydrates.

Various techniques have been used for characterization of glycosurfaces and each of them provides different types of information. It is usually necessary to apply a combination of two or three techniques to properly characterize a glycosurface. The best selection of characterization methods often depends on the material of the modified substrate, the type of modification (SAMs, glycopolymers or non-covalent immobilization), and the intended final application of the glycosurface.

Application of Glycosurfaces in Microbiology

As mentioned in the introduction, carbohydrates are present on the surface of most multicellular and single cell organisms and their interaction with other biomolecules, especially receptor proteins are critical in many biological processes, but currently only poorly understood. Glycosylated surfaces are an emerging type of biomaterial that can be used in the investigation of interactions between carbohydrates and other biomolecules, mainly proteins, either in isolation or on microbial cells. The study of these interactions can contribute to the discovery of novel carbohydrate-

protein (usually lectins) binding partners, which can for instance be useful to identify disease biomarkers or to better characterize certain microorganisms.¹⁵² The main application of prepared glycosurfaces is currently for carbohydrate microarrays.^{49, 153} When compared to antibodies or DNA-based sensors, the carbohydrate-based sensors have the advantages of being more stable under various conditions.¹⁵⁴ However, the main drawbacks are the lower selectivity and lower binding affinity of the carbohydrate-based sensors.

Glycosurfaces have also been used for binding, capture, and sensing of bacteria via the interaction with the lectins present on the surface of many bacterial species. In bacterial infections, a well-known carbohydrate-protein interaction is the one between mannosides and the type 1 fimbrial lectin (FimH), present on the cell surface of *Enterobacteriaceae* species, including the uropathogenic *Escherichia coli* (UPEC). This interaction is responsible for the adhesion of UPEC on the luminal surface of the bladder epithelium, causing bladder infection and inflammation. In this case, mannose-presenting surfaces can be used to detect these pathogenic bacteria.¹

In this section, we will focus on some examples of applications that use glycosurfaces for binding, capture, and sensing of bacteria and bacterial toxins, as well as the multivalency effect that plays an important part in carbohydrate-protein interactions on glycosurfaces.

Binding, capture, and sensing of bacteria

The genetic model bacterium *E. coli* has been frequently used as a model for microbial capture using glycosurfaces due to the well-known interaction between their fimbrial adhesins and the glycocalyx of their host cells. The interaction between α -D-mannoside residues and the FimH adhesin present on the type 1 fimbriae of many strains of *E. coli* is the most investigated bacterial adhesion process so far.¹ Wang and co-workers (2007) used two different approaches for *E. coli* detection via carbohydrate-adhesin interactions: direct detection and Con A-mediated detection (**Figure 8**). The direct detection involved detecting the interaction between a mannose-terminated SAM and the adhesin units present on the fimbriae of the bacteria. The Con A-mediated detection, on the other hand, involved the initial binding of the lipopolysaccharide present on the bacterial surface to Con A that in turn binds to the mannose-terminated SAM. The signal response was around eight times larger when the Con A-mediated

detection was used. This is attributed to the formation of bridges between *E. coli* and the mannose-presenting surface, leading to a relatively rigid and strong attachment.¹¹ Most studies using glycosurfaces for binding, capture or sensing of *E. coli*, however, use the direct detection approach,^{13, 90, 121, 155-157} as the use of the multivalent binding capacity of Con A as in intermediate adds additional complexity to interpreting the already complex carbohydrate-protein interaction of interest.⁸⁷ In general, the bacterial binding can be detected and/or quantified by, for example, (fluorescence) microscopy (**Figure 9**),^{90, 121} faradaic electrochemical impedance spectroscopy (EIS),¹³ metal mesh device (MMD) sensors,¹⁵⁵ or quartz crystal microbalance with dissipation (QCM-D) techniques.¹⁵⁶

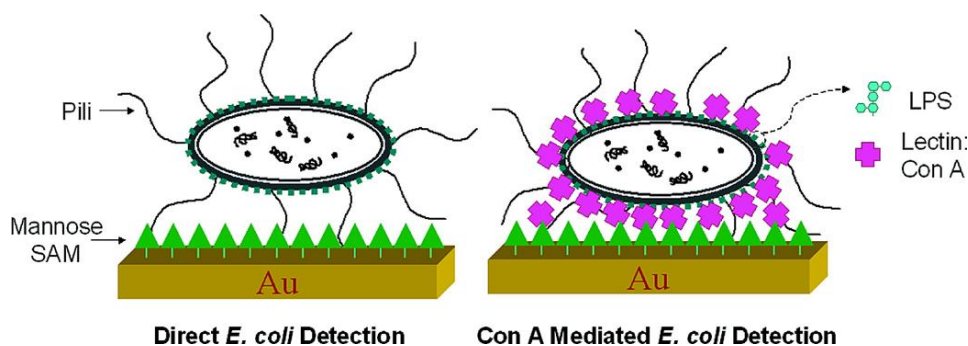


Figure 8. Schematic representation of direct *E. coli* detection and Con A-mediated *E. coli* detection. Reprinted with permission from reference 11. Copyright (2007) American Chemical Society.

Different *E. coli* strains have been used as a model for investigating this binding, such as the ORN178^{13, 115, 155} and DH5 α ¹⁵⁷ strains – which both possess the wild type FimH domain – or a fluorescently GFP-expressing strain (*E. coli* pPKL1162) that also overexpresses the type 1 fimbriae on its surface.⁹⁰ The interaction between bacteria and glycosurfaces is a complex process, and proper negative controls are therefore required. Some *E. coli* strains that do not present the type 1 fimbriae have been used as a negative control, such as AAEC191A¹²¹ and HB101 strains (non-fimbriated *E. coli*), a strain lacking the plasmid for FimH expression (but expressing the rest of the *fim* gene cluster),¹²¹ and the ORN 208 strain (expresses abnormal type 1 pili that fail to mediate mannose-specific binding).^{13, 115, 155} The use of these strains as negative controls is important to show that the binding process is mostly due to the interaction between the

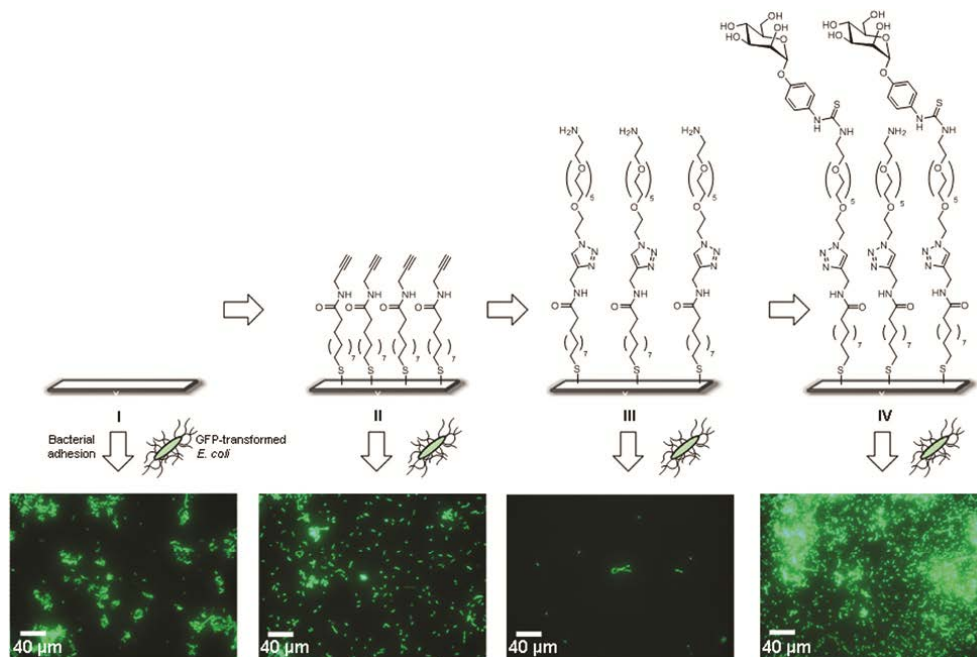


Figure 9. Adhesion of fluorescent bacteria to the different stages of the SAM during the “dual click” approach. The GFP-transformed *E. coli* bacteria (pPKL1162) enable a fast, direct fluorescence readout to investigate bacterial adhesion on surfaces. The native gold surface (I) was used as reference in each of the other experiments. As can be seen in the epifluorescence micrographs, the (non-specific) adhesivity of the alkyne-terminated SAM II is comparable to the one of the native Au surface. Introduction of the OEG chain reduces the adhesion significantly, while the α -mannosyl-terminated SAM is effectively recognized by the *E. coli* leading to heavy adhesion. Reproduced from reference 90 with permission from The Royal Society of Chemistry.

carbohydrates and the adhesins, partially excluding non-specific interactions as the source for any observed binding. Another option for a negative control is the addition of soluble carbohydrates to the suspension of bacteria before the binding to the glycosurface. If the soluble carbohydrate is the same as the one present on the glycosurface, it will saturate the carbohydrate binding sites of any present bacterial adhesins, and thereby strongly decreases the bacterial glycosurface binding when compared with the experiments in the absence of the soluble carbohydrate.^{6, 87}

Another bacterium known to have adhesins that are related to its binding of natural glycosurfaces and the formation of biofilms is *Pseudomonas aeruginosa*. *P. aeruginosa* synthesizes two surface adhesins, named PA-IL (or LecA), which specifically binds galactose, and PA-IIL (or LecB), which specifically binds fucose.^{158, 159} Wei and co-

workers (2010) studied the binding of *P. aeruginosa* on glycosurfaces with trisaccharides containing β -D-*N*-acetylgalactosamine or α -L-fucose. The bacteria adhered to both glycosurfaces, however, they displayed a lower adhesion to the surface with the fucose-containing trisaccharide than on the one containing *N*-acetylgalactosamine, which naturally occurs on the epithelium of the pulmonary tract. This difference might be due to the fact that the fucose-binding adhesin PA-IIL is regulated in an environmentally-dependent fashion, requiring certain compounds in the culture medium for proper expression.¹⁶⁰ More recently, Liu and co-workers (2014) investigated the binding of *P. aeruginosa* by QCM-D using surfaces coated with glycopolymers generated with glucose and lactose-containing monomers. The bacteria showed an increased and calcium-dependent adhesion to the lactose-presenting surface, probably due to the interaction between PA-IL and the galactose unit.¹⁵⁶

Surfaces coated with glycopolymers containing lactose were also used to increase the binding of *E. faecalis* via interaction between an adhesin on its surface and the galactose unit.⁹⁹ It was shown that the presence of soluble galactose decreased the bacterial binding, whereas a soluble glucose negative control did not influence the binding. The binding of *E. faecalis* was also significantly affected by the blocking of the carbohydrates with peanut agglutinin (PNA), a lectin that specifically binds galactose. Prior exposure of the glycosurface to BSA or Con A had considerably less influence on the bacterial binding when compared with PNA.⁹⁹

Glycosurfaces were also recently used by us for increased binding of *L. plantarum*, a probiotic bacterium that presents a mannose-binding adhesin on the cell surface.¹⁶¹ Mannose-terminated porous aluminum oxide (PAO) was used for binding and subsequent growth of *L. plantarum* on the same surface. PAO is a cheap nanoporous surface that has been used for various biotechnological applications. Bacterial growth is possible on PAO because nutrients can diffuse from the medium on which PAO is placed to the top surface via the pores present on the surface.¹⁶² We also showed in a control experiment that a soluble mannose derivative was able to reduce the binding of *L. plantarum* to the mannose-terminated glycosurface by blocking the mannose-binding adhesin.⁶

Binding and sensing of bacterial toxins

Although the use of glycosurfaces for detection of bacterial cells is still limited, there are various examples of detection of bacterial toxins using glycosurfaces. This is probably because the interaction between carbohydrates and whole cells is more complex and challenging to characterize than the interaction between carbohydrates and toxins. The detection of bacterial toxins using glycosurfaces is possible because a large number of bacterial toxins target carbohydrate derivatives on host cell surfaces to enter into the cells. Some examples of bacterial toxins that target carbohydrates of the host cell surface include cholera toxin, shiga and shiga-like toxins, tetanus toxin, botulinum toxin, and pertussis toxin.¹⁶³

Cholera toxin, secreted by *Vibrio cholerae*, is the cause of the pathology observed in cholera, mainly watery diarrhoea and vomiting, that can lead to lethal dehydration and is still a common illness in many developing countries. The natural ligand of cholera toxin is the glycosphingolipid ganglioside GM1, which is present on the cellular membrane of the intestinal epithelial surface of the host. The major contributors to the binding are the galactose and the *N*-acetylneuraminic acid units of the GM1 ganglioside.¹⁶⁴ Glycosurfaces containing these carbohydrates may therefore be useful for detection of cholera toxin. GM1-terminated surfaces have been used for detection of cholera toxin,^{112, 119, 165-167} and also to study the inhibition of cholera toxin binding by soluble carbohydrate derivatives.¹²⁷ Ligler and co-workers (2006) detected cholera toxin on both *N*-acetylneuraminic acid and *N*-acetylgalactosamine-terminated surfaces, with a limit of detection of 100 ng/mL. As expected, the binding of the toxin to the *N*-acetylneuraminic acid-terminated surface was more intense than to the *N*-acetylgalactosamine-terminated one.¹⁶³ Even more simple carbohydrates, such as galactose, showed interaction with cholera toxin when immobilized on a surface used to generate carbohydrate microarrays.¹⁶⁸

Shiga toxin and shiga-like toxins have also been detected using glycosurfaces. These toxins are known to cause gastrointestinal diseases after invading mammalian cells through binding to the carbohydrate portion of glycolipids on the cell surface. A shiga-like toxin produced by *E. coli* O157:H7 presents specificity towards globotriaosylceramide (Gb3), which contains the trisaccharide $\alpha\text{Gal}(1\rightarrow4)\beta\text{Gal}(1\rightarrow4)\beta\text{Glc}$.¹⁶⁹ Consequently, Gb3 derivatives and more simple carbohydrates that are part of

Gb3 have been immobilized on surfaces and used for the binding of shiga-like toxins as detected by QCM^{26, 170} and SPR.^{29, 171-173}

Other glycosurfaces have been used to investigate the interactions between carbohydrates and other bacterial toxins,^{108, 174} such as *E. coli* heat-labile enterotoxin,¹²⁹ and tetanus toxin.¹⁶³

Multivalency effect

Although single interactions between carbohydrates and proteins are in general very weak, multiple interactions can reinforce one another and together achieve avidities that result in strong binding. Almost all carbohydrate-protein interactions in nature are multivalent, including the interactions between carbohydrates and bacterial adhesins or toxins discussed in the previous sections. The avidity and even the selectivity of carbohydrate-protein interactions clearly depend on the density of the carbohydrate units on a studied surface.¹⁷⁵ In this case, for an optimal binding of a protein on a glycosurface, it is important that the carbohydrate is homogeneously distributed on the surface and present in a suitable density. Obviously, even when surfaces are functionalized with monovalent ligands, they can act as a multivalent system based only on the immobilization of the monovalent agents on the surface.¹⁷⁶

Kahne and co-workers (1999) investigated the influence of carbohydrate surface density on protein-binding selectivity. They showed that the *Bauhinia purpurea* lectin switches its selectivity from one carbohydrate to another depending on the surface density of the ligands in a mixed SAM.²² Houseman and Mrksich (1999) investigated the influence of the surface density of carbohydrates on an enzymatic glycosylation reaction. In their system, the optimal density of carbohydrate for the enzymatic glycosylation was an intermediate density, around 70%, with significant decrease of glycosylation rates at higher densities of carbohydrates.¹⁸ The influence of the carbohydrate density on antibody binding was investigated by SPR. When the carbohydrate was present on the SAM at a high density, the antibody binding was minimal. The carbohydrate density needed to be reduced to around 25% to obtain an increase of antibody binding.²⁰ Similar results were found for binding of Con A on maltose-terminated surfaces, with increase of the binding being observed when the carbohydrate density decreased (**Figure 10**). The binding also changed from monovalent recognition to bivalent recognition when the carbohydrate was diluted to 10%.¹⁷⁷ One explanation for the low binding of proteins to

glycosurfaces with a high carbohydrate density is attributed to the tight packing of the end groups in the SAM, resulting in limited access of the carbohydrates to the protein binding pocket.²⁰

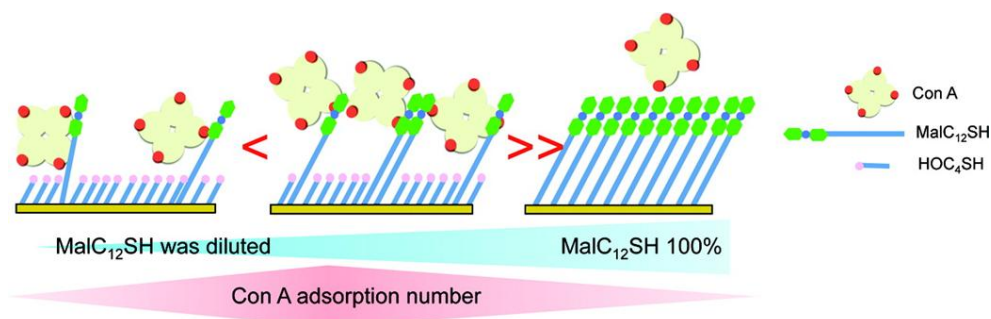


Figure 10. Model structure of three-dimensional carbohydrate positioning in the interface provides the best strategy for overcoming the weak binding detection. The maltoside–OH terminated hybrid monolayer represents multivalent binding for Con A when the maltoside was diluted. The affinity of Con A and maltoside on the surface was enhanced in ~10 mol % surfaces. Reprinted with permission from reference 177. Copyright (2012) American Chemical Society.

Ratner and co-workers (2009) showed that the effect of the carbohydrate density in the binding of proteins also depends on the type of molecule used for the dilution (**Figure 11**). When a molecule with a long chain (longer than the carbohydrate) was used for dilution, the increase of carbohydrate density increased the lectin binding. On the other hand, when a short molecule was used for the dilution, the maximum lectin binding was found around 40 – 60% carbohydrate density, followed by a plateau and a slight decrease of binding.¹³⁷

Stine and co-workers (2012) observed a difference in the optimal mannose density for Con A binding on flat gold and nanoporous gold. Although the dilution of the carbohydrate in the SAM increased the Con A binding for both surfaces, the optimal mannose density proved lower for nanoporous gold. Whereas the optimal mannose density for Con A binding was 1:9 ratio (mannoside/alkane thiol) for flat gold, the best Con A binding was found to be 1:19 for nanoporous gold.¹²

Buriak and co-workers (2011) did not find a decrease of protein binding with an increase of carbohydrate density, but rather an optimal protein binding when the carbohydrate is present at 30% density, followed by a plateau when the carbohydrate density was increased.³⁶ Szunerits and co-workers (2010) obtained similar results for binding of *Lens culinaris* lectin on mannose-terminated surfaces, with a maximum

response for carbohydrate density of 60%, with a plateau of response when increasing the mannose density.⁵³

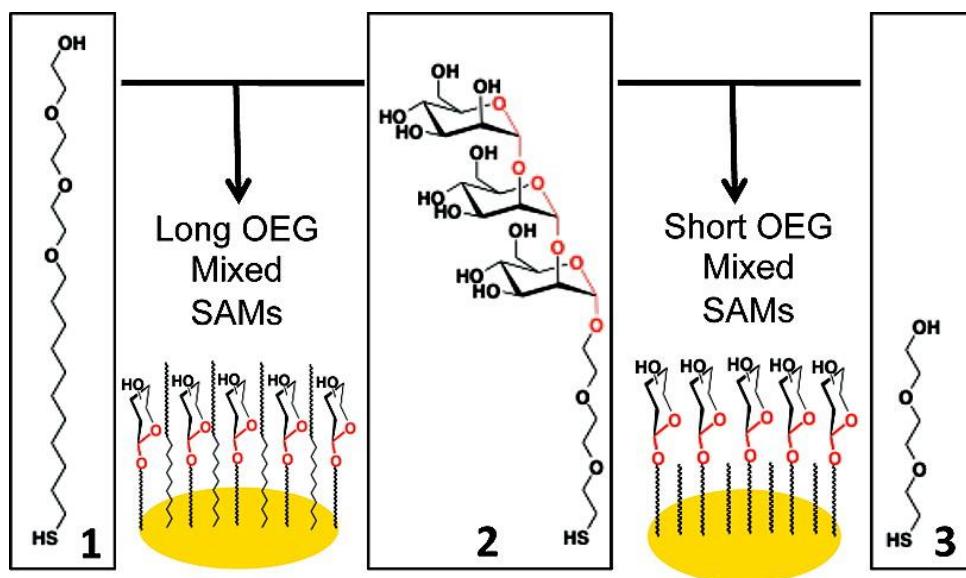


Figure 11. Assembly of mixed sugar/oligoethylene glycol (OEG) SAMs on gold. Reprinted with permission from reference 137. Copyright (2009) American Chemical Society.

Another way of studying the effect of multivalency on the binding of lectins to glycosurfaces is using carbohydrate derivatives with different valencies. Pieters and co-workers (2010) investigated the binding of a series of lectins to five different carbohydrates presenting valencies ranging from one to eight. Using a microarray it was possible to investigate the lectin specificity and the multivalency effect for each carbohydrate in a single experiment. The authors found various profiles, depending on the carbohydrate and the lectin, but with maintenance of specificity.¹⁶⁸

Changes in the carbohydrate density of SAMs or in the way of presenting the carbohydrate units can also interfere in the bacterial binding to glycosurfaces. Carbohydrate derivatives with different valencies were immobilized on a surface and the binding of *E. coli* was investigated. The bacterial binding increased when the amount of carbohydrate units per molecule increased from one to three. However, when the carbohydrate units further increased to six and nine, there was a decrease in bacterial binding.¹²¹ The binding of *E. coli* to dynamic glycosurfaces with different densities showed a change in the avidity from monovalent to multivalent as the mannose density

increased (**Figure 12**).¹¹⁵ Recently, Lindhorst and co-workers (2013) investigated the influence on bacterial binding to mannose-presenting surfaces of both the carbohydrate density and of different ways of presenting mannose. The authors showed that at high densities of carbohydrate the simple monovalent mannoside provided a more adhesive surface for *E. coli* than the bivalent and trivalent ones. However, at lower densities the binding of *E. coli* was higher on the surfaces with bivalent and trivalent mannosides when compared to the monovalent one. The highest binding affinity was found for the lowest concentration tested with the trivalent mannoside.¹⁷⁸

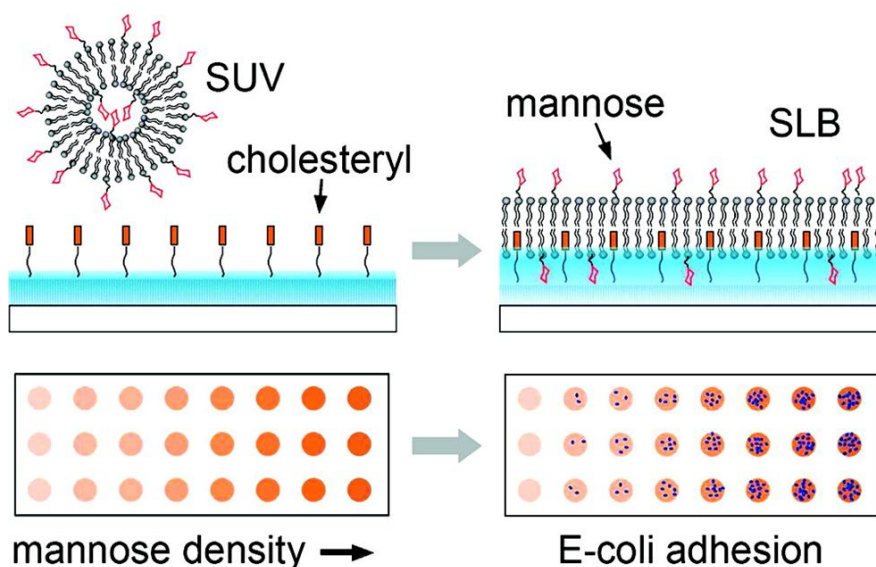


Figure 12. (Upper) Formation of a glycan presenting supported lipid bilayer (SLB) surface from a small unilamellar vesicle (SUV) solution. (Lower) Schematic illustration of a glycan density gradient microarray for pathogen adhesion. Reprinted with permission from reference 115. Copyright (2009) American Chemical Society.

It is interesting to notice that a higher carbohydrate density on a SAM does not necessarily result in greater binding of lectins or bacteria. It can either not provide any improvement in binding, resulting in waste of the excess of carbohydrate or, in the worst case, decrease the binding.³⁶ For this reason, it is important to determine the optimal carbohydrate density in a glycosurface to maximize the biological effect and also to reduce the waste of carbohydrate derivative.

Outlook

In the previous sections, we presented an overview of the methods frequently used to prepare glycosurfaces via three different general approaches: (a) direct formation of self-assembled monolayers (SAMs) containing carbohydrates, (b) secondary reactions (with unmodified and modified carbohydrates), and (c) non-covalent immobilization. The main challenge in the modification of surfaces with carbohydrates is to develop an approach that yields well-defined and stable glycosurfaces using the minimal number of steps. These steps should ideally be reproducible, simple, cheap, and available to a great number of scientists. Additionally, the ideal glycosurface should be stable to a wide range of conditions and for certain applications it should be resistant to multiple cycles of regeneration, without loss of its original properties. For industrial applications, it would also be important to consider the possibilities of scaling-up the production process. The currently most used approach for straightforward glycosurfaces is still the method that was first developed, formation of thiol-based SAMs of carbohydrate derivatives on gold, mainly because of their easy preparation. As the study and utilization of the biological role of carbohydrates has been rapidly increasing over the past decades, glycosurfaces are required that enable an ever increasing amount of sensitivity, complexity and precise control over their composition. In general the trend is therefore to explore other approaches that enable stable and controlled site-specific immobilization of unprotected carbohydrates via an attaching group on their anomeric position.

Besides the often applied copper(I)-catalyzed azide-alkyne cycloaddition (CuAAC), an increasing range of other “click” reactions^{179, 180} have become available also for use in surface attachment of carbohydrates. The full potential of these reactions for the preparation of glycosurfaces has not yet been reached, but over the coming years will allow for more advanced glycosurfaces and perhaps the ideal one. When preparing a glycosurface it is of course essential to know what it looks like before using it. Various characterization techniques have been applied for glycosurfaces, namely contact angle measurements, X-ray photoelectron spectroscopy (XPS), infrared reflection-absorption spectroscopy (IRRAS), mass spectrometry, ellipsometry, and atomic force microscopy (AFM). All these methods provide different types of information and the main challenge is to select what is the best combination of techniques to characterize a glycosurface. This selection usually depends on the substrate used to prepare the glycosurface, the

type of modification, and the application of the glycosurface. It should give the highest level of information in the shortest time possible, ideally without destroying the glycosurface.

Glycosurfaces have already proven to be very useful in increasing our understanding of the binding between carbohydrates and other biomolecules, mainly proteins, and have been successfully used for detection of known carbohydrate-protein interactions and helping the discovery of new binding partners and the development of novel therapies. Because of the enormous number and diversity of carbohydrate-containing biomolecules and the fact that most are still uncharted, there is a great need for reliable and sensitive methods for their high throughput characterization and it is evident that the next-generation glycosurfaces will be instrumental in this.¹⁸¹ What is needed now is a focus on developing and optimizing immobilization techniques that yield well-defined and stable complex glycosurfaces and also on developing and optimizing automated (chemo-enzymatic) synthetic methods¹⁸²⁻¹⁸⁴ to prepare the required complex carbohydrates with suitable reactive functional groups at the anomeric position for surface immobilization. Well established automated synthetic methods may eventually make the synthesis and application of complex carbohydrate derivatives a routine procedure that is more accessible to non-specialists and thereby widen their application to slowly but surely illuminate this complex dark matter-world.

Acknowledgements

Part of this research was supported by the NanoNext programme, a micro and nanotechnology consortium of the Government of the Netherlands and 130 partners, the Netherlands Organization for Scientific Research (VENI grant 722.011.006 & Spinoza grant) and the European Research Council (ERC 250172).

References

1. Hartmann, M.; Lindhorst, T. K. The bacterial lectin FimH, a target for drug discovery - carbohydrate inhibitors of type 1 fimbriae-mediated bacterial adhesion. *Eur. J. Org. Chem.* **2011**, *2011*, 3583-3609.
2. Kamhi, E.; Joo, E. J.; Dordick, J. S.; Linhardt, R. J. Glycosaminoglycans in infectious disease. *Biol. Rev.* **2013**, *88*, 928-943.
3. Berois, N.; Osinaga, E. Glycobiology of neuroblastoma: Impact on tumor behavior, prognosis, and therapeutic strategies. *Front. Oncol.* **2014**, *4*, 114.
4. Krengel, U.; Bousquet, P. A. Molecular recognition of gangliosides and their potential for cancer immunotherapies. *Front. Immunol.* **2014**, *5*, 325.
5. Pretzer, G.; Snel, J.; Molenaar, D.; Wiersma, A.; Bron, P. A.; Lambert, J.; de Vos, W. M.; van der Meer, R.; Smits, M. A.; Kleerebezem, M. Biodiversity-based identification and functional characterization of the mannose-specific adhesin of *Lactobacillus plantarum*. *J. Bacteriol.* **2005**, *187*, 6128-6136.
6. Debrassi, A.; Ribbera, A.; de Vos, W. M.; Wennekes, T.; Zuilhof, H. Stability of (bio)functionalized porous aluminum oxide. *Langmuir* **2014**, *30*, 1311-1320.
7. Schreiber, F. Structure and growth of self-assembling monolayers. *Prog. Surf. Sci.* **2000**, *65*, 151-256.

8. Love, J. C.; Estroff, L. A.; Kriebel, J. K.; Nuzzo, R. G.; Whitesides, G. M. Self-assembled monolayers of thiolates on metals as a form of nanotechnology. *Chem. Rev.* **2005**, *105*, 1103-1169.
9. Revell, D. J.; Knight, J. R.; Blyth, D. J.; Haines, A. H.; Russell, D. A. Self-assembled carbohydrate monolayers: Formation and surface selective molecular recognition. *Langmuir* **1998**, *14*, 4517-4524.
10. Karamanska, R.; Mukhopadhyay, B.; Russell, D. A.; Field, R. A. Thioctic acid amides: Convenient tethers for achieving low nonspecific protein binding to carbohydrates presented on gold surfaces. *Chem. Commun.* **2005**, 3334-3336.
11. Shen, Z.; Huang, M.; Xiao, C.; Zhang, Y.; Zeng, X.; Wang, P. G. Nonlabeled quartz crystal microbalance biosensor for bacterial detection using carbohydrate and lectin recognitions. *Anal. Chem.* **2007**, *79*, 2312-2319.
12. Pandey, B.; Tan, Y. H.; Fujikawa, K.; Demchenko, A. V.; Stine, K. J. Comparative study of the binding of concanavalin A to self-assembled monolayers containing a thiolated alpha-mannoside on flat gold and on nanoporous gold. *J. Carbohydr. Chem.* **2012**, *31*, 466-503.
13. Guo, X.; Kulkarni, A.; Doepke, A.; Halsall, H. B.; Iyer, S.; Heineman, W. R. Carbohydrate-based label-free detection of *Escherichia coli* ORN 178 using electrochemical impedance spectroscopy. *Anal. Chem.* **2012**, *84*, 241-246.
14. Kaplan, J. M.; Shang, J.; Gobbo, P.; Antonello, S.; Armelao, L.; Chatare, V.; Ratner, D. M.; Andrade, R. B.; Maran, F. Conformationally constrained functional peptide monolayers for the controlled display of bioactive carbohydrate ligands. *Langmuir* **2013**, *29*, 8187-8192.
15. Seo, J. H.; Adachi, K.; Lee, B. K.; Kang, D. G.; Kim, Y. K.; Kim, K. R.; Lee, H. Y.; Kawai, T.; Cha, H. J. Facile and rapid direct gold surface immobilization with controlled orientation for carbohydrates. *Bioconjugate Chem.* **2007**, *18*, 2197-2201.
16. He, X. P.; Wang, X. W.; Jin, X. P.; Zhou, H.; Shi, X. X.; Chen, G. R.; Long, Y. T. Epimeric monosaccharide-quinone hybrids on gold electrodes toward the electrochemical probing of specific carbohydrate-protein recognitions. *J. Am. Chem. Soc.* **2011**, *133*, 3649-3657.
17. Fyrner, T.; Lee, H.-H.; Mangone, A.; Ekblad, T.; Pettitt, M. E.; Callow, M. E.; Callow, J. A.; Conlan, S. L.; Mutton, R.; Clare, A. S.; Konradsson, P.; Liedberg, B.; Ederth, T. Saccharide-functionalized alkanethiols for fouling-resistant self-assembled monolayers: Synthesis, monolayer properties, and antifouling behavior. *Langmuir* **2011**, *27*, 15034-15047.
18. Houseman, B. T.; Mrksich, M. The role of ligand density in the enzymatic glycosylation of carbohydrates presented on self-assembled monolayers of alkanethiolates on gold. *Angew. Chem. Int. Ed.* **1999**, *38*, 782-785.
19. Sato, Y.; Yoshioka, K.; Tanaka, M.; Murakami, T.; Ishida, M. N.; Niwa, O. Recognition of lectin with a high signal to noise ratio: Carbohydrate-tri(ethylene glycol)-alkanethiol co-adsorbed monolayer. *Chem. Commun.* **2008**, 4909-4911.
20. Grant, C. F.; Kanda, V.; Yu, H.; Bundle, D. R.; McDermott, M. T. Optimization of immobilized bacterial disaccharides for surface plasmon resonance imaging measurements of antibody binding. *Langmuir* **2008**, *24*, 14125-14132.
21. Pandey, B.; Tan, Y. H.; Parameswar, A. R.; Pornsuriyasak, P.; Demchenko, A. V.; Stine, K. J. Electrochemical characterization of globotriose-containing self-assembled monolayers on nanoporous gold and their binding of soybean agglutinin. *Carbohydr. Res.* **2013**, *373*, 9-17.
22. Horan, N.; Yan, L.; Isobe, H.; Whitesides, G. M.; Kahne, D. Nonstatistical binding of a protein to clustered carbohydrates. *Proc. Natl. Acad. Sci. U. S. A.* **1999**, *96*, 11782-11786.
23. Hederos, M.; Konradsson, P.; Borgh, A.; Liedberg, B. Mimicking the properties of antifreeze glycoproteins: Synthesis and characterization of a model system for ice nucleation and antifreeze studies. *J. Phys. Chem. B* **2005**, *109*, 15849-15859.
24. Fritz, M. C.; Hahner, G.; Spencer, N. D.; Burli, R.; Vasella, A. Self-assembled hexasaccharides: Surface characterization of thiol-terminated sugars adsorbed on a gold surface. *Langmuir* **1996**, *12*, 6074-6082.
25. Svedhem, S.; Ohberg, L.; Borrelli, S.; Valiokas, R.; Andersson, M.; Oscarson, S.; Svensson, S. C. T.; Liedberg, B.; Konradsson, P. Synthesis and self-assembly of globotriose derivatives: A model system for studies of carbohydrate-protein interactions. *Langmuir* **2002**, *18*, 2848-2858.
26. Miura, Y.; Sasao, Y.; Dohi, H.; Nishida, Y.; Kobayashi, K. Self-assembled monolayers of globotriaosylceramide (gb3) mimics: Surface-specific affinity with shiga toxins. *Anal. Biochem.* **2002**, *310*, 27-35.
27. Miura, Y.; Sasao, Y.; Kamihira, M.; Sakaki, A.; Iijima, S.; Kobayashi, K. Peptides binding to a gb3 mimic selected from a phage library. *Biochim. Biophys. Acta* **2004**, *1673*, 131-138.
28. Tromas, C.; Eaton, P.; Mimault, J.; Rojo, J.; Penades, S. Structural characterization of self-assembled monolayers of neoglycoconjugates using atomic force microscopy. *Langmuir* **2005**, *21*, 6142-6144.
29. Kanda, V.; Kitov, P.; Bundle, D. R.; McDermott, M. T. Surface plasmon resonance imaging measurements of the inhibition of shiga-like toxin by synthetic multivalent inhibitors. *Anal. Chem.* **2005**, *77*, 7497-7504.
30. Wang, Y.; El-Boubbou, K.; Kouyoumdjian, H.; Sun, B.; Huang, X.; Zeng, X. Lipic acid glyco-conjugates, a new class of agents for controlling nonspecific adsorption of blood serum at biointerfaces for biosensor and biomedical applications. *Langmuir* **2010**, *26*, 4119-4125.
31. Uzawa, H.; Ohga, K.; Shinozaki, Y.; Ohsawa, I.; Nagatsuka, T.; Seto, Y.; Nishida, Y. A novel sugar-probe biosensor for the deadly plant protein toxin, ricin. *Biosens. Bioelectron.* **2008**, *24*, 923-927.
32. Kadalbajoo, M.; Park, J.; Opdahl, A.; Suda, H.; Kitchens, C. A.; Garino, J. C.; Batteas, J. D.; Tarlov, M. J.; DeShong, P. Synthesis and structural characterization of glucopyranosylamide films on gold. *Langmuir* **2007**, *23*, 700-707.
33. Shirahata, N.; Hozumi, A.; Miura, Y.; Kobayashi, K.; Sakka, Y.; Yonezawa, T. An efficient matrix that resists the nonspecific adsorption of protein to fabricate carbohydrate arrays on silicon. *Thin Solid Films* **2006**, *499*, 213-218.
34. Funato, K.; Shirahata, N.; Miura, Y. Alpha-Man monolayer formation via Si-C bond formation and protein recognition. *Thin Solid Films* **2009**, *518*, 699-702.
35. Chang, S. H.; Han, J. L.; Tseng, S. Y.; Lee, H. Y.; Lin, C. W.; Lin, Y. C.; Jeng, W. Y.; Wang, A. H. J.; Wu, C. Y.; Wong, C. H. Glycan array on aluminum oxide-coated glass slides through phosphonate chemistry. *J. Am. Chem. Soc.* **2010**, *132*, 13371-13380.
36. Slaney, A. M.; Wright, V. A.; Meloncelli, P. J.; Harris, K. D.; West, L. J.; Lowary, T. L.; Buriak, J. M. Biocompatible carbohydrate-functionalized stainless steel surfaces: A new method for passivating biomedical implants. *ACS Appl. Mater. Interfaces* **2011**, *3*, 1601-1612.
37. Gruber, K.; Horlacher, T.; Castelli, R.; Mader, A.; Seeberger, P. H.; Hermann, B. A. Cantilever array sensors detect specific carbohydrate-protein interactions with picomolar sensitivity. *ACS Nano* **2011**, *5*, 3670-3678.
38. Chinwangso, P.; Jamison, A. C.; Lee, T. R. Multidentate adsorbates for self-assembled monolayer films. *Acc. Chem. Res.* **2011**, *44*, 511-519.
39. de Smet, L.; Stork, G. A.; Hurenkamp, G. H. F.; Sun, Q. Y.; Topal, H.; Vronen, P. J. E.; Sieval, A. B.; Wright, A.; Visser, G. M.; Zuilhof, H.; Sudholter, E. J. R. Covalently attached saccharides on silicon surfaces. *J. Am. Chem. Soc.* **2003**, *125*, 13916-13917.
40. de Smet, L.; Pukin, A. V.; Sun, Q. Y.; Eves, B. J.; Lopinski, G. P.; Visser, G. M.; Zuilhof, H.; Sudholter, E. J. R. Visible-light attachment of Si-C linked functionalized organic monolayers on silicon surfaces. *Appl. Surf. Sci.* **2005**, *252*, 24-30.

41. Pujari, S. P.; Scheres, L.; Marcelis, A. T. M.; Zuilhof, H. Covalent surface modification of oxide surfaces. *Angew. Chem. Int. Ed.* **2014**, *53*, 6322-6356.
42. Bhairamagdi, N. S.; Pujari, S. P.; Trovela, F. G.; Debrassi, A.; Khamis, A. A.; Alonso, J. M.; Al Zahrani, A. A.; Wennekes, T.; Al-Turaif, H. A.; van Rijn, C.; Alhamed, Y. A.; Zuilhof, H. Hydrolytic and thermal stability of organic monolayers on various inorganic substrates. *Langmuir* **2014**, *30*, 5829-5839.
43. Carroll, G. T.; Wang, D. N.; Turro, N. J.; Koberstein, J. T. Photochemical micropatterning of carbohydrates on a surface. *Langmuir* **2006**, *22*, 2899-2905.
44. Tyagi, A.; Wang, X.; Deng, L.; Ramstrom, O.; Yan, M. Photogenerated carbohydrate microarrays to study carbohydrate-protein interactions using surface plasmon resonance imaging. *Biosens. Bioelectron.* **2010**, *26*, 344-350.
45. Zhou, X.; Turchi, C.; Wang, D. Carbohydrate cluster microarrays fabricated on three-dimensional dendrimeric platforms for functional glycomics exploration. *J. Proteome Res.* **2009**, *8*, 5031-5040.
46. Zhi, Z.-l.; Powell, A. K.; Turnbull, J. E. Fabrication of carbohydrate microarrays on gold surfaces: Direct attachment of nonderivatized oligosaccharides to hydrazide-modified self-assembled monolayers. *Anal. Chem.* **2006**, *78*, 4786-4793.
47. Cheng, F.; Shang, J.; Ratner, D. M. A versatile method for functionalizing surfaces with bioactive glycans. *Bioconjugate Chem.* **2011**, *22*, 50-57.
48. Shang, J.; Piskarev, V. E.; Xia, M.; Huang, P.; Jiang, X.; Likhoshershtov, L. M.; Novikova, O. S.; Newburg, D. S.; Ratner, D. M. Identifying human milk glycans that inhibit norovirus binding using surface plasmon resonance. *Glycobiology* **2013**, *23*, 1491-1498.
49. Park, S.; Gildersleeve, J. C.; Blixt, O.; Shin, I. Carbohydrate microarrays. *Chem. Soc. Rev.* **2013**, *42*, 4310-4326.
50. Zhang, Y.; Luo, S. Z.; Tang, Y. J.; Yu, L.; Hou, K. Y.; Cheng, J. P.; Zeng, X. Q.; Wang, P. G. Carbohydrate-protein interactions by "clicked" carbohydrate self-assembled monolayers. *Anal. Chem.* **2006**, *78*, 2001-2008.
51. Kleiner, M.; Winkler, T.; Terfort, A.; Lindhorst, T. K. A modular approach for the construction and modification of glyco-SAMs utilizing 1,3-dipolar cycloaddition. *Org. Biomol. Chem.* **2008**, *6*, 2118-2132.
52. Matsumoto, E.; Yamauchi, T.; Fukuda, T.; Miura, Y. Sugar microarray via click chemistry: Molecular recognition with lectins and amyloid β (1-42). *Sci. Technol. Adv. Mater.* **2009**, *10*, 034605.
53. Szunerits, S.; Niedziolka-Joensson, J.; Boukherroub, R.; Woisel, P.; Baumann, J. S.; Siriwardena, A. Label-free detection of lectins on carbohydrate-modified boron-doped diamond surfaces. *Anal. Chem.* **2010**, *82*, 8203-8210.
54. Yang, J.; Chazalviel, J. N.; Siriwardena, A.; Boukherroub, R.; Ozanam, F.; Szunerits, S.; Gouget-Laemmel, A. C. Quantitative assessment of the multivalent protein-carbohydrate interactions on silicon. *Anal. Chem.* **2014**, *86*, 10340-10349.
55. Leone, G.; Consumi, M.; Tognazzi, A.; Magnani, A. Realisation and chemical characterisation of a model system for saccharide-based biosensor. *Thin Solid Films* **2010**, *519*, 462-470.
56. Godula, K.; Rabuka, D.; Nam, K. T.; Bertozzi, C. R. Synthesis and microcontact printing of dual end-functionalized mucin-like glycopolymers for microarray applications. *Angew. Chem. Int. Ed.* **2009**, *48*, 4973-4976.
57. Bouchet-Spinelli, A.; Reuillard, B.; Coche-Guerente, L.; Armand, S.; Labbe, P.; Fort, S. Oligosaccharide biosensor for direct monitoring of enzymatic activities using QCM-D. *Biosens. Bioelectron.* **2013**, *49*, 290-296.
58. Wendeln, C.; Singh, I.; Rinnen, S.; Schulz, C.; Arlinghaus, H. F.; Burley, G. A.; Ravoo, B. J. Orthogonal, metal-free surface modification by strain-promoted azide-alkyne and nitrile oxide-alkene/alkyne cycloadditions. *Chem. Sci.* **2012**, *3*, 2479-2484.
59. Manova, R. K.; Pujari, S. P.; Weijers, C. A. G. M.; Zuilhof, H.; van Beek, T. A. Copper-free click biofunctionalization of silicon nitride surfaces via strain-promoted alkyne-azide cycloaddition reactions. *Langmuir* **2012**, *28*, 8651-8663.
60. Wendeln, C.; Rinnen, S.; Schulz, C.; Kaufmann, T.; Arlinghaus, H. F.; Ravoo, B. J. Rapid preparation of multifunctional surfaces for orthogonal ligation by microcontact chemistry. *Chem. Eur. J.* **2012**, *18*, 5880-5888.
61. Norberg, O.; Lee, I. H.; Aastrup, T.; Yan, M.; Ramstrom, O. Photogenerated lectin sensors produced by thiol-ene/yne photo-click chemistry in aqueous solution. *Biosens. Bioelectron.* **2012**, *34*, 51-56.
62. Biggs, C. I.; Edmondson, S.; Gibson, M. I. Thiol-ene immobilisation of carbohydrates onto glass slides as a simple alternative to gold-thiol monolayers, amines or lipid binding. *Biomater. Sci.* **2015**, *3*, 175-181.
63. Wang, C.; Ren, P.-F.; Huang, X.-J.; Wu, J.; Xu, Z.-K. Surface glycosylation of polymer membrane by thiol-yne click chemistry for affinity adsorption of lectin. *Chem. Commun.* **2011**, *47*, 3930-3932.
64. Wang, C.; Fan, Y.; Hu, M.-X.; Xu, W.; Wu, J.; Ren, P.-F.; Xu, Z.-K. Glycosylation of the polypropylene membrane surface via thiol-yne click chemistry for lectin adsorption. *Colloid. Surf. B* **2013**, *110*, 105-112.
65. Houseman, B. T.; Gwalt, E. S.; Mrksich, M. Maleimide-functionalized self-assembled monolayers for the preparation of peptide and carbohydrate biochips. *Langmuir* **2003**, *19*, 1522-1531.
66. Yonzon, C. R.; Jeoung, E.; Zou, S. L.; Schatz, G. C.; Mrksich, M.; Van Duyne, R. P. A comparative analysis of localized and propagating surface plasmon resonance sensors: The binding of concanavalin A to a monosaccharide functionalized self-assembled monolayer. *J. Am. Chem. Soc.* **2004**, *126*, 12669-12676.
67. Wehner, J. W.; Weissenborn, M. J.; Hartmann, M.; Gray, C. J.; Sardzik, R.; Evers, C. E.; Flitsch, S. L.; Lindhorst, T. K. Dual purpose S-trityl-linkers for glycoarray fabrication on both polystyrene and gold. *Org. Biomol. Chem.* **2012**, *10*, 8919-8926.
68. Yatawara, A. K.; Tiruchinapally, G.; Bordenyuk, A. N.; Andreana, P. R.; Benderskii, A. V. Carbohydrate surface attachment characterized by sum frequency generation spectroscopy. *Langmuir* **2009**, *25*, 1901-1904.
69. Shang, J.; Cheng, F.; Dubey, M.; Kaplan, J. M.; Rawal, M.; Jiang, X.; Newburg, D. S.; Sullivan, P. A.; Andrade, R. B.; Ratner, D. M. An organophosphonate strategy for functionalizing silicon photonic biosensors. *Langmuir* **2012**, *28*, 3338-3344.
70. Houseman, B. T.; Mrksich, M. Carbohydrate arrays for the evaluation of protein binding and enzymatic modification. *Chem. Biol.* **2002**, *9*, 443-454.
71. Wendeln, C.; Heile, A.; Arlinghaus, H. F.; Ravoo, B. J. Carbohydrate microarrays by microcontact printing. *Langmuir* **2010**, *26*, 4933-4940.
72. Beckmann, H. S. G.; Niederwieser, A.; Wiessler, M.; Wittmann, V. Preparation of carbohydrate arrays by using Diels-Alder reactions with inverse electron demand. *Chem. Eur. J.* **2012**, *18*, 6548-6554.
73. Smith, E. A.; Thomas, W. D.; Kiessling, L. L.; Corn, R. M. Surface plasmon resonance imaging studies of protein-carbohydrate interactions. *J. Am. Chem. Soc.* **2003**, *125*, 6140-6148.
74. Harris, L. G.; Schofield, W. C. E.; Doores, K. J.; Davis, B. G.; Badyal, J. P. S. Rewritable glycochips. *J. Am. Chem. Soc.* **2009**, *131*, 7755-7761.
75. Loka, R. S.; Cairo, C. W. Immobilization of carbohydrate epitopes for surface plasmon resonance using the Staudinger ligation. *Carbohydr. Res.* **2010**, *345*, 2641-2647.
76. Zhi, Z. L.; Laurent, N.; Powel, A. K.; Karamanska, R.; Fais, M.; Voglmeir, J.; Wright, A.; Blackburn, J. M.; Crocker, P. R.; Russell, D. A.; Flitsch, S.; Field, R. A.; Turnbull, J. E. A versatile gold surface approach for fabrication and interrogation of glycoarrays. *ChemBioChem* **2008**, *9*, 1568-1575.

77. Sardzik, R.; Sharma, R.; Kaloo, S.; Voglmeir, J.; Crocker, P. R.; Flitsch, S. L. Chemoenzymatic synthesis of sialooligosaccharides on arrays for studies of cell surface adhesion. *Chem. Commun.* **2011**, 47, 5425-5427.
78. Javier Munoz, F.; Andre, S.; Gabius, H.-J.; Sinisterra, J. V.; Hernaiz, M. J.; Linhardt, R. J. Green glycosylation using ionic liquid to prepare alkyl glycosides for studying carbohydrate-protein interactions by SPR. *Green Chem.* **2009**, 11, 373-379.
79. Clo, E.; Blixt, O.; Jensen, K. J. Chemoselective reagents for covalent capture and display of glycans in microarrays. *Eur. J. Org. Chem.* **2010**, 2010, 540-554.
80. Liang, P.-H.; Wang, S.-K.; Wong, C.-H. Quantitative analysis of carbohydrate-protein interactions using glycan microarrays: Determination of surface and solution dissociation constants. *J. Am. Chem. Soc.* **2007**, 129, 11177-11184.
81. Bohorov, O.; Andersson-Sand, H.; Hoffmann, J.; Blixt, O. Arraying glycomics: A novel bi-functional spacer for one-step microscale derivatization of free reducing glycans. *Glycobiology* **2006**, 16, 21C-27C.
82. Wang, C. C.; Huang, Y. L.; Ren, C. T.; Lin, C. W.; Hung, J. T.; Yu, J. C.; Yu, A. L.; Wu, C. Y.; Wong, C. H. Glycan microarray of Globo H and related structures for quantitative analysis of breast cancer. *Proc. Natl. Acad. Sci. U. S. A.* **2008**, 105, 11661-11666.
83. Blixt, O.; Head, S.; Mondala, T.; Scanlan, C.; Huflejt, M. E.; Alvarez, R.; Bryan, M. C.; Fazio, F.; Calarese, D.; Stevens, J.; Razi, N.; Stevens, D. J.; Skehel, J. J.; van Die, I.; Burton, D. R.; Wilson, I. A.; Cummings, R.; Bovin, N.; Wong, C. H.; Paulson, J. C. Printed covalent glycan array for ligand profiling of diverse glycan binding proteins. *Proc. Natl. Acad. Sci. U. S. A.* **2004**, 101, 17033-17038.
84. Song, X.; Xia, B.; Stowell, S. R.; Lasanajak, Y.; Smith, D. F.; Cummings, R. D. Novel fluorescent glycan microarray strategy reveals ligands for galectins. *Chem. Biol.* **2009**, 16, 36-47.
85. de Boer, A. R.; Hokke, C. H.; Deelder, A. M.; Wührer, M. General microarray technique for immobilization and screening of natural glycans. *Anal. Chem.* **2007**, 79, 8107-8113.
86. Buck, M. E.; Breitbach, A. S.; Belgrade, S. K.; Blackwell, H. E.; Lynn, D. M. Chemical modification of reactive multilayered films fabricated from poly(2-alkenyl azlactone)s: Design of surfaces that prevent or promote mammalian cell adhesion and bacterial biofilm growth. *Biomacromolecules* **2009**, 10, 1564-1574.
87. Liu, X.; Lei, Z.; Liu, F.; Liu, D.; Wang, Z. Fabricating three-dimensional carbohydrate hydrogel microarray for lectin-mediated bacterium capturing. *Biosens. Bioelectron.* **2014**, 58, 92-100.
88. Kopitzki, S.; Jensen, K. J.; Thiem, J. Synthesis of benzaldehyde-functionalized glycans: A novel approach towards glyco-SAMs as a tool for surface plasmon resonance studies. *Chem. Eur. J.* **2010**, 16, 7017-7029.
89. Beer, M. V.; Rech, C.; Diederichs, S.; Hahn, K.; Bruellhoff, K.; Moeller, M.; Elling, L.; Groll, J. A hydrogel-based versatile screening platform for specific biomolecular recognition in a well plate format. *Anal. Bioanal. Chem.* **2012**, 403, 517-526.
90. Grabosch, C.; Kind, M.; Gies, Y.; Schweighoefer, F.; Terfort, A.; Lindhorst, T. K. A 'dual click' strategy for the fabrication of bioselective, glycosylated self-assembled monolayers as glycocalyx models. *Org. Biomol. Chem.* **2013**, 11, 4006-4015.
91. Javier Lopez-Jaramillo, F.; Ortega-Munoz, M.; Megia-Fernandez, A.; Hernandez-Mateo, F.; Santoyo-Gonzalez, F. Vinyl sulfone functionalization: A feasible approach for the study of the lectin-carbohydrate interactions. *Bioconjugate Chem.* **2012**, 23, 846-855.
92. Pulsipher, A.; Yousaf, M. N. A renewable, chemoselective, and quantitative ligand density microarray for the study of biospecific interactions. *Chem. Commun.* **2011**, 47, 523-525.
93. Fang, Y.; Xu, W.; Wu, J.; Xu, Z. K. Enzymatic transglycosylation of PEG brushes by beta-galactosidase. *Chem. Commun.* **2012**, 48, 11208-11210.
94. Ejaz, M.; Ohno, K.; Tsujii, Y.; Fukuda, T. Controlled grafting of a well-defined glycopolymer on a solid surface by surface-initiated atom transfer radical polymerization. *Macromolecules* **2000**, 33, 2870-2874.
95. Ayres, N.; Holt, D. J.; Jones, C. F.; Corum, L. E.; Grainger, D. W. Polymer brushes containing sulfonated sugar repeat units: Synthesis, characterization, and in vitro testing of blood coagulation activation. *J. Polym. Sci. A* **2008**, 46, 7713-7724.
96. Yoon, K. R.; Ramaraj, B.; Lee, S.; Yu, J.-S.; Choi, I. S. Surface-initiated atom-transfer radical polymerization of 3-O-methacryloyl-1,2,5,6-di-O-isopropylidene- α -D-glucopyranoside onto gold surface. *J. Biomed. Mater. Res. A* **2009**, 88A, 735-740.
97. Yu, K.; Kizhakkeedathu, J. N. Synthesis of functional polymer brushes containing carbohydrate residues in the pyranose form and their specific and nonspecific interactions with proteins. *Biomacromolecules* **2010**, 11, 3073-3085.
98. Yu, L.; Huang, M.; Wang, P. G.; Zeng, X. Cross-linked surface-grafted glycopolymer for multivalent recognition of lectin. *Anal. Chem.* **2007**, 79, 8979-8986.
99. Yang, Q.; Strathmann, M.; Rumpf, A.; Schaule, G.; Ulbricht, M. Grafted glycopolymer-based receptor mimics on polymer support for selective adhesion of bacteria. *ACS Appl. Mater. Interf.* **2010**, 2, 3555-3562.
100. Manova, R. K.; Joshi, S.; Debrassi, A.; Bhairamadgi, N. S.; Roeven, E.; Gagnon, J.; Tahir, M. N.; Claassen, F. W.; Scheres, L. M. W.; Wennekes, T.; Schroen, K.; van Beek, T. A.; Zuilhof, H.; Nielen, M. W. F. Ambient surface analysis of organic monolayers using direct analysis in real time orbitrap mass spectrometry. *Anal. Chem.* **2014**, 86, 2403-2411.
101. ter Maat, J.; Regeling, R.; Ingham, C. J.; Weijers, C. A. G. M.; Giesbers, M.; de Vos, W. M.; Zuilhof, H. Organic modification and subsequent biofunctionalization of porous anodic alumina using terminal alkynes. *Langmuir* **2011**, 27, 13606-13617.
102. Sun, X. L.; Stabler, C. L.; Cazalis, C. S.; Chaikof, E. L. Carbohydrate and protein immobilization onto solid surfaces by sequential Diels-Alder and azide-alkyne cycloadditions. *Bioconjugate Chem.* **2006**, 17, 52-57.
103. Patterson, D. M.; Nazarova, L. A.; Prescher, J. A. Finding the right (bio)orthogonal chemistry. *ACS Chem. Biol.* **2014**, 9, 592-605.
104. King, M.; Wagner, A. Developments in the field of bioorthogonal bond forming reactions-past and present trends. *Bioconjugate Chem.* **2014**, 25, 825-839.
105. Manova, R.; van Beek, T. A.; Zuilhof, H. Surface functionalization by strain-promoted alkyne-azide click reactions. *Angew. Chem. Int. Ed.* **2011**, 50, 5428-5430.
106. Agard, N. J.; Prescher, J. A.; Bertozzi, C. R. A strain-promoted [3+2] azide-alkyne cycloaddition for covalent modification of biomolecules in living systems. *J. Am. Chem. Soc.* **2004**, 126, 15046-15047.
107. Bhairamadgi, N. S.; Gangarapu, S.; Campos, M. A. C.; Paulusse, J. M. J.; van Rijn, C. J. M.; Zuilhof, H. Efficient functionalization of oxide-free silicon(111) surfaces: Thiol-yne versus thiol-ene click chemistry. *Langmuir* **2013**, 29, 4535-4542.
108. Rillahan, C. D.; Paulson, J. C. Glycan microarrays for decoding the glycome. *Annu. Rev. Biochem.* **2011**, 80, 797-823.
109. Siegwart, D. J.; Oh, J. K.; Matyjaszewski, K. ATRP in the design of functional materials for biomedical applications. *Prog. Polym. Sci.* **2012**, 37, 18-37.
110. Yang, Q.; Kaul, C.; Ulbricht, M. Anti-nonspecific protein adsorption properties of biomimetic glycocalyx-like glycopolymer layers: Effects of glycopolymer chain density and protein size. *Langmuir* **2010**, 26, 5746-5752.
111. Mann, D. A.; Kanai, M.; Maly, D. J.; Kiessling, L. L. Probing low affinity and multivalent interactions with surface plasmon resonance: Ligands for concanavalin A. *J. Am. Chem. Soc.* **1998**, 120, 10575-10582.
112. Liebau, M.; Hildebrand, A.; Neubert, R. H. H. Bioadhesion of supramolecular structures at supported planar bilayers as studied by the quartz crystal microbalance. *Eur. Biophys. J. Biophys.* **2001**, 30, 42-52.

113. Zheng, H.; Du, X. Enhanced binding and biosensing of carbohydrate-functionalized monolayers to target proteins by surface molecular imprinting. *J. Phys. Chem. B* **2009**, *113*, 11330-11337.
114. Zheng, H.; Du, X. Protein-directed spatial rearrangement of glycolipids at the air-water interface for bivalent protein binding: In situ infrared reflection absorption spectroscopy. *J. Phys. Chem. B* **2010**, *114*, 577-584.
115. Zhu, X. Y.; Holtz, B.; Wang, Y.; Wang, L.-X.; Orndorff, P. E.; Guo, A. Quantitative glycomics from fluidic glycan microarrays. *J. Am. Chem. Soc.* **2009**, *131*, 13646-13650.
116. Weissenborn, M. J.; Wehner, J. W.; Gray, C. J.; Sardzik, R.; Evers, C. E.; Lindhorst, T. K.; Flitsch, S. L. Formation of carbohydrate-functionalised polystyrene and glass slides and their analysis by MALDI-TOF MS. *Beilstein J. Org. Chem.* **2012**, *8*, 753-762.
117. Critchley, P.; Clarkson, G. J. Carbohydrate-protein interactions at interfaces: Comparison of the binding of ricinus communis lectin to two series of synthetic glycolipids using surface plasmon resonance studies. *Org. Biomol. Chem.* **2003**, *1*, 4148-4159.
118. Guo, C.; Boullanger, P.; Jiang, L.; Liu, T. Highly sensitive gold nanoparticles biosensor chips modified with a self-assembled bilayer for detection of con A. *Biosens. Bioelectron.* **2007**, *22*, 1830-1834.
119. Parikh, A. N.; Beers, J. D.; Shreve, A. P.; Swanson, B. I. Infrared spectroscopic characterization of lipid-alkylsiloxane hybrid bilayer membranes at oxide substrates. *Langmuir* **1999**, *15*, 5369-5381.
120. Sato, H.; Miura, Y.; Saito, N.; Kobayashi, K.; Takai, O. A micropatterned carbohydrate display for tissue engineering by self-assembly of heparin. *Surf. Sci.* **2007**, *601*, 3871-3875.
121. Barth, K. A.; Coullerez, G.; Nilsson, L. M.; Castelli, R.; Seeberger, P. H.; Vogel, V.; Textor, M. An engineered mannoside presenting platform: *Escherichia coli* adhesion under static and dynamic conditions. *Adv. Funct. Mater.* **2008**, *18*, 1459-1469.
122. Guo, Y.; Feinberg, H.; Conroy, E.; Mitchell, D. A.; Alvarez, R.; Blixt, O.; Taylor, M. E.; Weis, W. I.; Drickamer, K. Structural basis for distinct ligand-binding and targeting properties of the receptors DC-SIGN and DC-SIGNR. *Nat. Struct. Mol. Biol.* **2004**, *11*, 591-598.
123. Bochner, B. S.; Alvarez, R. A.; Mehta, P.; Bovin, N. V.; Blixt, O.; White, J. R.; Schnaar, R. L. Glycan array screening reveals a candidate ligand for Siglec-8. *J. Biol. Chem.* **2005**, *280*, 4307-4312.
124. Linman, M. J.; Yu, H.; Chen, X.; Cheng, Q. Fabrication and characterization of a sialoside-based carbohydrate microarray biointerface for protein binding analysis with surface plasmon resonance imaging. *ACS Appl. Mater. Interf.* **2009**, *1*, 1755-1762.
125. Zhang, J.; Pourceau, G.; Meyer, A.; Vidal, S.; Praly, J. P.; Souteyrand, E.; Vasseur, J. J.; Morvan, F.; Chevolot, Y. DNA-directed immobilisation of glycomimetics for glycoarrays application: Comparison with covalent immobilisation, and development of an on-chip IC50 measurement assay. *Biosens. Bioelectron.* **2009**, *24*, 2515-2521.
126. Castellana, E. T.; Cremer, P. S. Solid supported lipid bilayers: From biophysical studies to sensor design. *Surf. Sci. Rep.* **2006**, *61*, 429-444.
127. Sinclair, H. R.; Kemp, F.; de Slegte, J.; Gibson, G. R.; Rastall, R. A. Carbohydrate-based anti-adhesive inhibition of *Vibrio cholerae* toxin binding to GM1-OS immobilized into artificial planar lipid membranes. *Carbohydr. Res.* **2009**, *344*, 1968-1974.
128. Konishi, M.; Imura, T.; Fukuoka, T.; Morita, T.; Kitamoto, D. A yeast glycolipid biosurfactant, mannosylerythritol lipid, shows high binding affinity towards lectins on a self-assembled monolayer system. *Biotechnol. Lett.* **2007**, *29*, 473-480.
129. Pukin, A. V.; Florack, D. E. A.; Brochu, D.; van Lagen, B.; Visser, G. M.; Wennekes, T.; Gilbert, M.; Zuilhof, H. Chemoenzymatic synthesis of biotin-appended analogues of gangliosides GM2, GM1, GD1a and GalNAc-GD1a for solid-phase applications and improved ELISA tests. *Org. Biomol. Chem.* **2011**, *9*, 5809-5815.
130. Linman, M. J.; Taylor, J. D.; Yu, H.; Chen, X.; Cheng, Q. Surface plasmon resonance study of protein-carbohydrate interactions using biotinylated sialosides. *Anal. Chem.* **2008**, *80*, 4007-4013.
131. Dorrer, C.; Ruehe, J. Some thoughts on superhydrophobic wetting. *Soft Matter* **2009**, *5*, 51-61.
132. Chu, Z.; Seeger, S. Superamphiphobic surfaces. *Chem. Soc. Rev.* **2014**, *43*, 2784-2798.
133. Kingshott, P.; Andersson, G.; McArthur, S. L.; Griesser, H. J. Surface modification and chemical surface analysis of biomaterials. *Curr. Opin. Chem. Biol.* **2011**, *15*, 667-676.
134. Papp, C.; Steinrueck, H. P. In situ high-resolution X-ray photoelectron spectroscopy: Fundamental insights in surface reactions. *Surf. Sci. Rep.* **2013**, *68*, 446-487.
135. Hajati, S.; Tougaard, S. XPS for non-destructive depth profiling and 3D imaging of surface nanostructures. *Anal. Bioanal. Chem.* **2010**, *396*, 2741-2755.
136. Rabanel, J.-M.; Hildgen, P.; Banquy, X. Assessment of peg on polymeric particles surface, a key step in drug carrier translation. *J. Control. Release* **2014**, *185*, 71-87.
137. Dhayal, M.; Ratner, D. A. XPS and SPR analysis of glycoarray surface density. *Langmuir* **2009**, *25*, 2181-2187.
138. Dietrich, P. M.; Horlacher, T.; Girard-Lauriault, P. L.; Gross, T.; Lippitz, A.; Min, H.; Wirth, T.; Castelli, R.; Seeberger, P. H.; Unger, W. E. S. Adlayers of dimannoside thiols on gold: Surface chemical analysis. *Langmuir* **2011**, *27*, 4808-4815.
139. Chernyy, S.; Jensen, B. E. B.; Shimizu, K.; Ceccato, M.; Pedersen, S. U.; Zelikin, A. N.; Daasbjerg, K.; Iruthayaraj, J. Surface grafted glycopolymer brushes to enhance selective adhesion of HepG2 cells. *J. Colloid Interf. Sci.* **2013**, *404*, 207-214.
140. Mendelsohn, R.; Mao, G.; Flach, C. R. Infrared reflection-absorption spectroscopy: Principles and applications to lipid-protein interaction in Langmuir films. *Biochim. Biophys. Acta* **2010**, *1798*, 788-800.
141. Leone, G.; Consumi, M.; Lamponi, S.; Magnani, A. Combination of static time of flight secondary ion mass spectrometry and infrared reflection-adsorption spectroscopy for the characterisation of a four steps built-up carbohydrate array. *Appl. Surf. Sci.* **2012**, *258*, 6302-6315.
142. Ramin, M. A.; Le Bourdon, G.; Daugey, N.; Bennetau, B.; Vellutini, L.; Buffeteau, T. PM-IRRAS investigation of self-assembled monolayers grafted onto SiO₂/Au substrates. *Langmuir* **2011**, *27*, 6076-6084.
143. Dinh, D. H.; Vellutini, L.; Bennetau, B.; Dejous, C.; Rebiere, D.; Pascal, E.; Moynet, D.; Belin, C.; Desbat, B.; Labrugere, C.; Pillot, J.-P. Route to smooth silica-based surfaces decorated with novel self-assembled monolayers (SAMs) containing glycidyl-terminated very long hydrocarbon chains. *Langmuir* **2009**, *25*, 5526-5535.
144. Pujari, S. P.; Spruijt, E.; Stuart, M. A. C.; van Rijn, C. J. M.; Paulusse, J. M. J.; Zuilhof, H. Ultralow adhesion and friction of fluoro-hydro alkyne-derived self-assembled monolayers on H-terminated Si(111). *Langmuir* **2012**, *28*, 17690-17700.
145. Barnes, T. J.; Kempson, I. M.; Prestidge, C. A. Surface analysis for compositional, chemical and structural imaging in pharmaceuticals with mass spectrometry: A tof-sims perspective. *Int. J. Pharm.* **2011**, *417*, 61-69.
146. Wei, Q.; Becherer, T.; Angioletti-Uberti, S.; Dzubiella, J.; Wischke, C.; Neffe, A. T.; Lendlein, A.; Ballauff, M.; Haag, R. Protein interactions with polymer coatings and biomaterials. *Angew. Chem. Int. Ed.* **2014**, *53*, 8004-8031.
147. Manova, R. K.; Claassen, F. W.; Nielen, M. W. F.; Zuilhof, H.; van Beek, T. A. Ambient mass spectrometry of covalently bound organic monolayers. *Chem. Commun.* **2013**, *49*, 922-924.
148. Garcia-Caurel, E.; De Martino, A.; Gaston, J.-P.; Yan, L. Application of spectroscopic ellipsometry and Mueller ellipsometry to optical characterization. *Appl. Spectrosc.* **2013**, *67*, 1-21.

149. Lin, P. C.; Lin, S.; Wang, P. C.; Sridhar, R. Techniques for physicochemical characterization of nanomaterials. *Biotechnol. Adv.* **2014**, *32*, 711-726.
150. Pillet, F.; Chopinet, L.; Formosa, C.; Dague, E. Atomic force microscopy and pharmacology: From microbiology to cancerology. *Biochim. Biophys. Acta* **2014**, *1840*, 1028-1050.
151. Wang, C.; Yadavalli, V. K. Investigating biomolecular recognition at the cell surface using atomic force microscopy. *Micron* **2014**, *60*, 5-17.
152. Kennedy, D. C.; Gruenstein, D.; Lai, C. H.; Seeberger, P. H. Glycosylated nanoscale surfaces: Preparation and applications in medicine and molecular biology. *Chem. Eur. J.* **2013**, *19*, 3794-3800.
153. Paulson, J. C.; Blixt, O.; Collins, B. E. Sweet spots in functional glycomics. *Nat. Chem. Biol.* **2006**, *2*, 238-248.
154. Zeng, X.; Andrade, C. A. S.; Oliveira, M. D. L.; Sun, X. L. Carbohydrate-protein interactions and their biosensing applications. *Anal. Bioanal. Chem.* **2012**, *402*, 3161-3176.
155. Seto, H.; Kamba, S.; Kondo, T.; Hasegawa, M.; Nashima, S.; Ehara, Y.; Ogawa, Y.; Hoshino, Y.; Miura, Y. Metal mesh device sensor immobilized with a trimethoxysilane-containing glycopolymer for label-free detection of proteins and bacteria. *ACS Appl. Mater. Interf.* **2014**, *6*, 13234-13241.
156. Wang, Y.; Narain, R.; Liu, Y. Study of bacterial adhesion on different glycopolymer surfaces by quartz crystal microbalance with dissipation. *Langmuir* **2014**, *30*, 7377-7387.
157. Dechtrirat, D.; Gajovic-Eichmann, N.; Wojcik, F.; Hartmann, L.; Bier, F. F.; Scheller, F. W. Electrochemical displacement sensor based on ferrocene boronic acid tracer and immobilized glycan for saccharide binding proteins and *E. coli*. *Biosens. Bioelectron.* **2014**, *58*, 1-8.
158. Winzer, K.; Falconer, C.; Garber, N. C.; Diggle, S. P.; Camara, M.; Williams, P. The *Pseudomonas aeruginosa* lectins PA-IL and PA-III are controlled by quorum sensing and by RpoS. *J. Bacteriol.* **2000**, *182*, 6401-6411.
159. Chemani, C.; Imberty, A.; de Bentzmann, S.; Pierre, M.; Wimmerova, M.; Guery, B. P.; Faure, K. Role of LecA and LecB lectins in *Pseudomonas aeruginosa*-induced lung injury and effect of carbohydrate ligands. *Infect. Immun.* **2009**, *77*, 2065-2075.
160. Adak, A. K.; Leonov, A. P.; Ding, N.; Thundimadathil, J.; Kularatne, S.; Low, P. S.; Wei, A. Bishydrazide glycoconjugates for lectin recognition and capture of bacterial pathogens. *Bioconjugate Chem.* **2010**, *21*, 2065-2075.
161. Gross, G.; Snel, J.; Boekhorst, J.; Smits, M. A.; Kleerebezem, M. Biodiversity of mannose-specific adhesion in *Lactobacillus plantarum* revisited: Strain-specific domain composition of the mannose-adhesin. *Benef. Microb.* **2010**, *1*, 61-66.
162. Ingham, C. J.; ter Maat, J.; de Vos, W. M. Where bio meets nano: The many uses for nanoporous aluminum oxide in biotechnology. *Biotechnol. Adv.* **2012**, *30*, 1089-1099.
163. Ngundi, M. M.; Taitt, C. R.; McMurry, S. A.; Kahne, D.; Ligler, F. S. Detection of bacterial toxins with monosaccharide arrays. *Biosens. Bioelectron.* **2006**, *21*, 1195-1201.
164. Garcia-Hartjes, J.; Bernardi, S.; Weijers, C. A. G. M.; Wennekes, T.; Gilbert, M.; Sansone, F.; Casnati, A.; Zuilhof, H. Picomolar inhibition of cholera toxin by a pentavalent ganglioside GM1OS-calix[5]arene. *Org. Biomol. Chem.* **2013**, *11*, 4340-4349.
165. Arigi, E.; Blixt, O.; Buschard, K.; Clausen, H.; Levery, S. B. Design of a covalently bonded glycosphingolipid microarray. *Glycoconjugate J.* **2012**, *29*, 1-12.
166. Seo, J. H.; Lee, H. Y.; Cha, H. J. Characterization of the GM1 pentasaccharide-*Vibrio cholera* toxin interaction using a carbohydrate-based electrochemical system. *Analyst* **2012**, *137*, 2860-2865.
167. Seo, J. H.; Kim, C. S.; Cha, H. J. Structural evaluation of GM1-related carbohydrate-cholera toxin interactions through surface plasmon resonance kinetic analysis. *Analyst* **2013**, *138*, 6924-6929.
168. Pera, N. P.; Branderhorst, H. M.; Kooij, R.; Maierhofer, C.; van der Kaaden, M.; Liskamp, R. M. J.; Wittmann, V.; Ruijtenbeek, R.; Pieters, R. J. Rapid screening of lectins for multivalency effects with a glycodendrimer microarray. *ChemBioChem* **2010**, *11*, 1896-1904.
169. Chien, Y. Y.; Jan, M. D.; Adak, A. K.; Tzeng, H. C.; Lin, Y. P.; Chen, Y. J.; Wang, K. T.; Chen, C. T.; Chen, C. C.; Lin, C. C. Globotriose-functionalized gold nanoparticles as multivalent probes for shiga-like toxin. *ChemBioChem* **2008**, *9*, 1100-1109.
170. Mori, T.; Ohtsuka, T.; Okahata, Y. Kinetic analyses of bindings of shiga-like toxin to clustered and dispersed GB(3) glyco-arrays on a quartz-crystal microbalance. *Langmuir* **2010**, *26*, 14118-14125.
171. Uzawa, H.; Ito, H.; Neri, P.; Mori, H.; Nishida, Y. Glycochips from polyanionic glycopolymers as tools for detecting shiga toxins. *ChemBioChem* **2007**, *8*, 2117-2124.
172. Toyoshima, M.; Oura, T.; Fukuda, T.; Matsumoto, E.; Miura, Y. Biological specific recognition of glycopolymer-modified interfaces by RAFT living radical polymerization. *Polym. J.* **2010**, *42*, 172-178.
173. Nagatsuka, T.; Uzawa, H.; Sato, K.; Kondo, S.; Izumi, M.; Yokoyama, K.; Ohsawa, I.; Seto, Y.; Neri, P.; Mori, H.; Nishida, Y.; Saito, M.; Tamiya, E. Localized surface plasmon resonance detection of biological toxins using cell surface oligosaccharides on glyco chips. *ACS Appl. Mater. Interf.* **2013**, *5*, 4173-4180.
174. Haseley, S. R. Carbohydrate recognition: A nascent technology for the detection of bioanalytes. *Anal. Chim. Acta* **2002**, *457*, 39-45.
175. Bernardi, A.; Jimenez-Barbero, J.; Casnati, A.; De Castro, C.; Darbre, T.; Fieschi, F.; Finne, J.; Funken, H.; Jaeger, K. E.; Lahmann, M.; Lindhorst, T. K.; Marradi, M.; Messner, P.; Molinaro, A.; Murphy, P. V.; Nativi, C.; Oscarson, S.; Penades, S.; Peri, F.; Pieters, R. J.; Renaudet, O.; Reymond, J. L.; Richichi, B.; Rojo, J.; Sansone, F.; Schaffer, C.; Turnbull, W. B.; Velasco-Torrijos, T.; Vidal, S.; Vincent, S.; Wennekes, T.; Zuilhof, H.; Imberty, A. Multivalent glycoconjugates as anti-pathogenic agents. *Chem. Soc. Rev.* **2013**, *42*, 4709-4727.
176. Huskens, J. Multivalent interactions at interfaces. *Curr. Opin. Chem. Biol.* **2006**, *10*, 537-543.
177. Sato, Y.; Yoshioka, K.; Murakami, T.; Yoshimoto, S.; Niwa, O. Design of biomolecular interface for detecting carbohydrate and lectin weak interactions. *Langmuir* **2012**, *28*, 1846-1851.
178. Wehner, J. W.; Hartmann, M.; Lindhorst, T. K. Are multivalent cluster glycosides a means of controlling ligand density of glycoarrays? *Carbohydr. Res.* **2013**, *371*, 22-31.
179. Nebhani, L.; Barner-Kowollik, C. Orthogonal transformations on solid substrates: Efficient avenues to surface modification. *Adv. Mater.* **2009**, *21*, 3442-3468.
180. Xi, W.; Scott, T. F.; Kloxin, C. J.; Bowman, C. N. Click chemistry in materials science. *Adv. Funct. Mater.* **2014**, *24*, 2572-2590.
181. Wang, L.-X.; Davis, B. G. Realizing the promise of chemical glycobiology. *Chem. Sci.* **2013**, *4*, 3381-3394.
182. Seeberger, P. H. Automated oligosaccharide synthesis. *Chem. Soc. Rev.* **2008**, *37*, 19-28.
183. Wang, Z.; Chinyo, Z. S.; Ambre, S. G.; Peng, W.; McBride, R.; de Vries, R. P.; Glushka, J.; Paulson, J. C.; Boons, G. J. A general strategy for the chemoenzymatic synthesis of asymmetrically branched N-glycans. *Science* **2013**, *341*, 379-383.
184. Bennett, C. S. Principles of modern solid-phase oligosaccharide synthesis. *Org. Biomol. Chem.* **2014**, *12*, 1686-1698.

Chapter 3

Stability of (Bio)Functionalized Porous Aluminum Oxide

**Aline Debrassi¹, Angela Ribbera², Willem M. de Vos^{2,3}, Tom Wennekes¹, Han
Zuilhof^{1,4}**

¹ Laboratory of Organic Chemistry, Wageningen University, 6703 HB Wageningen, The
Netherlands

² Laboratory of Microbiology, Wageningen University, 6703 HB Wageningen, The
Netherlands

³ Department of Bacteriology & Immunology and Department of Veterinary Biosciences,
University of Helsinki, Finland

⁴ Department of Chemical and Materials Engineering, King Abdulaziz University, Jeddah,
Saudi Arabia

This chapter was published as:
Langmuir **30**, 1311-1320 (2014)

Abstract

Porous aluminum oxide (PAO), a nanostructured support for, among others, culturing microorganisms, was chemically modified in order to attach biomolecules that can selectively interact with target bacteria. We present the first comprehensive study of monolayer-modified PAO using conditions that are relevant to microbial growth with a range of functional groups, (carboxylic acid, α -hydroxycarboxylic acid, alkyne, alkene, phosphonic acid, and silane). Their stability was initially assessed in phosphate-buffered saline (pH 7.0) at room temperature. The most stable combination (PAO with phosphonic acids) was further studied at a range of physiological pHs (4–8), and temperatures (up to 80 °C). Varying the pH had no significant effect on the stability, but it gradually decreased with increasing temperature. The stability of phosphonic acid-modified PAO surfaces was shown to depend strongly on the other terminal group of the monolayer structure: in general, hydrophilic monolayers were less stable than hydrophobic monolayers. Finally, an alkyne-terminated PAO surface was reacted with an azide-linked mannose derivative. The resulting mannose-presenting PAO surface showed a clearly increased adherence of a mannose-binding bacterium, *Lactobacillus plantarum*, and also allowed for bacterial outgrowth.

Introduction

Porous aluminum oxide (PAO) is a nanostructured material that has been used for various applications, such as the development of biosensors,¹ implantable devices for drug delivery,² glycoarrays,³ immobilization of enzymes for biocatalysis,⁴ and as a support to generate other micro and nanostructures.⁵ PAO is obtained via an electrochemical oxidation of aluminum. Different structural orders, thicknesses, pore sizes, and pore volumes can be generated by varying parameters such as the temperature, type and concentration of the electrolyte, voltage, and anodization time during its fabrication.^{6, 7}

One of the most recent applications of PAO that takes full advantage of its highly defined porous structure is as support to culture and count microorganisms and other types of cells.⁸⁻¹⁴ Cellular growth can proceed smoothly because many cells respond favorably to the PAO substrate and because nutrients can diffuse from the media on which the PAO is placed to the top surface via the orthogonally aligned pores. The use of

PAO in this application presents many advantages, such as the possibility to cultivate certain bacteria that do not grow on traditional agar plates (e.g. soil and river bacteria),^{10, 13} moving microcolonies from one culture medium to another, and the low autofluorescence of PAO that allows easy visualization of the cell growth by fluorescence microscopy. A commercially available microbial growth chip based on PAO, presenting up to one million compartments, even makes high-throughput screening of microorganisms possible.^{9, 13} PAO has also been applied for antimicrobial resistance or susceptibility testing of bacteria and fungi, giving more rapid results when compared with the conventional tests, such as disc diffusion or Etest.^{15, 16}

The potential applications for PAO in microbiology and especially in culturing will expand if the PAO surface can be chemically modified to enable the attachment of biomolecules that can specifically interact with and bind to target bacteria. We have recently reported a modification approach that uses 1, ω -dialkynes to generate an alkyne-terminated monolayer on the PAO surface, which could be lactosylated via the copper(I)-catalyzed alkyne-azide cycloaddition (CuAAC), “click” reaction. The lactosylated PAO surface showed increased adhesion of *Candida albicans*.¹⁷ After this proof of principle, we are now interested in further developing the bio(functionalization) of PAO for microbiological applications. Biofunctionalization of surfaces usually requires two or more steps. In most cases it starts by generating an initial monolayer that is subsequently used to attach the biomolecules needed for the application. It is important that this initial monolayer is connected to the PAO surface via a covalent bond that is well-defined and stable under the conditions of the target application, in this case the culture of microorganisms.

Different functional groups have been used for the surface modification of aluminum oxide such as carboxylic acids,¹⁸⁻²⁰ silane derivatives,²¹⁻²³ alkynes,¹⁷ alkenes,^{17, 24} and phosphonic acids.^{18, 25-31} However, the stability of the resulting surfaces significantly differs for all of them. Choosing the appropriate modification method for an application on PAO is difficult because no study has been reported that systematically compares the stability of all these different methods, on PAO, under various conditions.

Our objective in this study (**Figure 1**) was therefore to modify PAO with most of the surface-reactive functional groups known from the literature, and to compare the stability of the modified surfaces under ambient aqueous conditions. The modification that proved most stable in this comparison was further studied at different physiological

pH values and temperatures that are important for microbial growth. Moreover, because previous stability studies mostly compare only simple alkyl-terminated monolayers, we also systematically evaluated the stability of monolayers on PAO with various chain lengths, compositions, and terminal reactive groups. To demonstrate that the most stable PAO monolayer can indeed be biofunctionalized, alkyne-functionalized PAO surfaces were subjected to the CuAAC click reaction with an azide-terminated mannose derivative to obtain a mannose-presenting PAO surface. Finally, we showed the usefulness of the thus-biofunctionalized PAO by the binding and growth of *Lactobacillus plantarum*, a well-characterized bacterium commonly found in fermented food products that is decorated with mannose-binding proteins.^{32, 33}

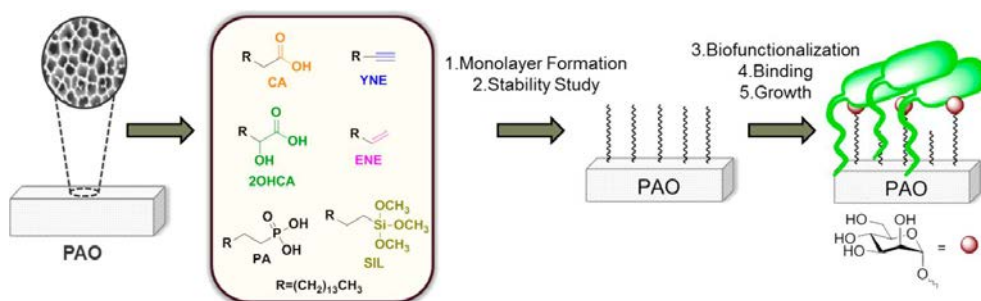


Figure 1. Biofunctionalization of PAO surfaces for application in microbial culturing, with the different functional groups assessed in the current study.

Materials and Methods

Materials

PAO substrates with dimensions of $36 \times 8 \text{ mm}^2$ and average pore size of 200 nm were purchased from MicroDish BV (Netherlands). All of the phosphonic acids were purchased from SiKÉMIA (France), except the alkylphosphonic acids. Dodecylphosphonic acid was obtained from PlasmaChem (Germany). 1-Hexadecyne was synthesized as previously described.³⁴ 1-Hexadecyne and 1-hexadecene were purified by column chromatography and vacuum distillation. The other chemicals were obtained from Sigma-Aldrich and used without further purification. Solvents used were of analytical grade. Dichloromethane was distilled over calcium hydride prior to use. All of the buffer solutions were prepared with demineralized water. Sonication steps were

performed in an Elmasonic P 30 H ultrasonic unit at frequency of 80 kHz. Optical rotation was measured at 589 nm on a PerkinElmer 241 polarimeter. Nuclear magnetic resonance (NMR) spectra were recorded on a Bruker 400 MHz spectrometer. NMR peak assignments were made on the basis of COSY and HSQC experiments. HRMS data were recorded on an Exactive high-resolution MS instrument (Thermo Scientific) equipped with a DART or ESI probe.

Surface modification

For all the surface modifications, the substrate preparation procedure was the same as previously reported by us.¹⁷ Briefly, a PAO substrate was rinsed three times and sonicated in acetone (5 min) and ultrapure water (5 min). It was next immersed in a fresh mixture of 37% hydrochloric acid and methanol (1:1, v/v) for 30 min. The substrate was rinsed three times and sonicated with ultrapure water (5 min) and absolute ethanol (5 min). It is known that the pore diameter of PAO differs on both sides of the surface (rough and smooth sides).^{17, 35} After the chemical modification, the sides are visually distinguishable because of the increased opacity of the rough side, although the XPS spectra does not show any difference in the chemical composition. In this study, all of the water contact angle measurements were performed on the rough side of the PAO surface because this is the side that is in contact with the bacteria in the microbiological experiments.

The PAO surface was modified with 1-hexadecylphosphonic acid (PA), 1-hexadecylcarboxylic acid (CA), 2-hydroxyhexadecylcarboxylic acid (2OHCA), 1-hexadecyne (YNE), 1-hexadecene (ENE), and 1-hexadecyltrimethoxysilane (SIL). The surface modification with CA and 2OHCA was carried out by immersing the prepared PAO in a 1 mM solution of the modifying agents in absolute ethanol at 65 °C for 16 h. For the modification with YNE and ENE, the modifying agent was frozen with liquid nitrogen in the reaction flask after which the PAO substrate was transferred on top of the frozen alkyne or alkene. When the compound had melted, the flask was held at 80 °C for 16 h.¹⁷ For the PAO modification with PA, the substrate was immersed in a 1 mM solution of the modifying agent in absolute ethanol at room temperature for the desired time (from 5 min to 16 h for the kinetic study). Unless stated otherwise, all of the samples modified with phosphonic acid derivatives were modified for 16 h and submitted to an additional curing step (holding at 140 °C under vacuum for 6 h). The azide-terminated PAO was

prepared by the modification of the PAO surface with 12-bromophosphonic acid followed by immersion of the bromo-terminated PAO in a 1 M NaN_3 solution in DMF for 16 h at 60 °C. Afterward, the surface was extensively washed and sonicated in water for 5 min. For the modification of PAO with SIL, the substrate was immersed in a 5% solution of the modifying agent in acetone for 1 h. Subsequently, the surface was washed in acetone and cured by heating the modified PAO at 120 °C under vacuum for 30 min.³⁶ After the modification, all of the samples were rinsed and sonicated in ethanol (5 min) and dichloromethane (5 min) and dried in air, except for the samples modified with phosphonic acids, which were sonicated twice for 5 min in ethanol and then in dichloromethane (5 min).

Monolayer characterization

The monolayers were characterized by static water contact angle measurements and infrared (IR) and X-ray photoelectron spectroscopy (XPS) as previously described.¹⁷ The wetting properties of the modified surfaces were analyzed by automated static water contact angle using a Krüss DSA-100 goniometer (volume of drop of demineralized water = 3.0 μL). At least three small droplets of water were used per sample, and the contact angle of each droplet was measured 10 times.

IR spectra were measured with a Bruker Tensor 27 FT-IR spectrometer. Spectra were obtained in transmission mode using a spectral resolution of 2 cm^{-1} and 256 scans in each measurement. The raw spectra were divided by the spectrum of a freshly cleaned and etched bare PAO reference substrate.

XPS measurements were performed using a JPS-9200 photoelectron spectrometer (JEOL). The spectra were obtained under ultrahigh vacuum conditions using a monochromatic Al $K\alpha$ X-ray radiation at 12 kV and 20 mA, with an analyzer pass energy of 10 eV. The binding energies were calibrated at 285.0 eV for the C 1s peak as a reference. To prevent surface charging, the samples were irradiated with electrons with a kinetic energy of 2.8 eV. High-resolution spectra were corrected using a linear background subtraction before fitting. The spectra were processed using CasaXPS software (version 2.3.15).

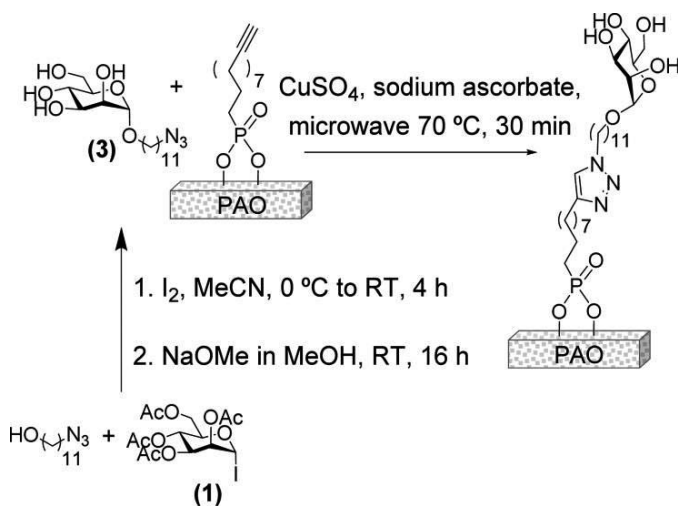
Stability study

The stability of a monolayer was assessed by immersing the modified surface in various buffer solutions. At various time points, the samples were removed, thoroughly washed with ultrapure water, ethanol and distilled dichloromethane, and dried under vacuum for 15 min. The stability was measured using water contact angle at all the time points and XPS at specific time points. The stability of the PAO surfaces modified with the various functional groups known in literature was studied in pH 7.0 phosphate-buffered saline (PBS) at room temperature. The most stable group was then studied at pH 4.0 (acetate buffer, 0.1 M), 6.0 (potassium phosphate buffer, 0.1 M), and 8.0 (tris(hydroxymethyl)aminomethane, 0.1 M). Additionally, this PAO modification was also studied in PBS at different temperatures (40, 60, and 80 °C) in a water bath.

Synthesis of 1-(11-azidoundecanyl)- α -D-mannopyranoside (3)

Acetyl-protected mannosyl iodide **1** was prepared according to a method previously described in the literature.³⁷ Compound **1** was coupled to 11-azido-1-undecanol, and the product was deprotected with basic methanol to yield the target compound (3) (**Scheme 1**). Complete synthetic procedures and characterization can be found in the Supporting Information.

Scheme 1. Synthesis of azido-mannoside 3 and the CuAAC click reaction with PAO-ynePA.



CuAAC click reaction

The CuAAC click reaction was performed on the PAO surface modified with 10-undecynylphosphonic acid, analogous to a procedure previously described by us.¹⁷ A solution containing mannoside **3** (0.1 mM), copper sulfate (0.2 mM), and sodium ascorbate (0.2 mM) was prepared in ultrapure water and added to a reaction tube. The reaction tube was equipped with a stirring bar and a platform to protect the fragile surface from the stirring bar. The alkyne-terminated surface was immersed in the solution and heated in a microwave oven (CEM Discover) for 30 min at 70 °C under stirring. After the reaction, the substrate was thoroughly washed and sonicated in water, ethanol, and dichloromethane (5 min per solvent) and dried in air. For the microbiological tests, PAO was modified with a mixture of 1-octylphosphonic acid and 10-undecynylphosphonic acid 50:50 (w/w) (PAO-ynemix), and the same CuAAC click reaction was performed either with mannoside **3** (PAO-mix-Man) or 11-azido-1-undecanol (PAO-mix-OH).

Microbiological tests

A 100-fold dilution in ultrapure water of an overnight culture of *L. plantarum* WCFS1³² in MRS broth (Difco Lactobacilli MRS broth, BD, Amsterdam, The Netherlands) containing approximately 10⁷ CFU/mL was prepared, and 3 µL of this was added to three samples of both PAO-mix-Man and PAO-mix-OH. The resulting PAO samples were incubated for 30 min at 37 °C and subsequently the top surface of two samples was washed with PBS buffer pH 7.4 containing 0.05% of Tween 20 (PBST). The washing was performed by adding 150 µL of PBST to the top surface of the samples and removing the solution using a micropipet. This washing procedure was repeated three times for each sample. One of each type of surface was not washed for further comparison and was used as a control. Both washed and nonwashed surfaces were transferred to an MRS agar plate and incubated for 5 h at 37 °C. The bacteria on the surface were fluorescently stained with 5-carboxyfluorescein diacetate (cFDA) by placing the PAO surfaces on low-melting-point agarose (BioRad, CA, USA) that contained 50 µM cFDA for 30 min. As a control experiment, the same experiment was done with three samples of PAO-mix-Man using an initial dilution of *L. plantarum* that now also contained 25 mM methyl- α -D-mannopyranoside. The surfaces with bacteria were imaged directly using an Olympus BX-41 fluorescence microscope. The microscope was equipped with U-MWIBA filters

(Olympus) for fluorescence imaging of the bacteria stained with cFDA, and images were taken using a Kappa CCD camera. The area occupied by bacteria was calculated using CellProfiler version 2 (Broad Institute).

Results and Discussion

Stability of porous aluminum oxide (PAO) modifications with different functional groups

The first goal of this study was to identify which of the various possible surface modification reactions for PAO result in the most stable functionalization under aqueous ambient conditions. The compounds used for modification of the PAO surface at this stage were selected to have a constant alkyl chain length (C_{16}) (**Figure 1**) to ensure that the effect on stability of the functional group bound to the PAO surface was only due to the surface-binding moiety. PAO was therefore modified with 1-hexadecylphosphonic acid (PA), 1-hexadecylcarboxylic acid (CA), 2-hydroxyhexadecylcarboxylic acid (2OHCA), 1-hexadecyne (YNE), 1-hexadecene (ENE), and 1-hexadecyltrimethoxysilane (SIL). All of the modified surfaces presented a layer thickness of ~ 2 nm (**Table SI-1**, Supporting Information), indicating a monolayer, except the surface modified with ENE, which presented a thickness approaching that of a bilayer (3.6 nm). The stability of the modified PAO surfaces was studied in PBS pH 7.0 and monitored over time by water static contact angle (**Figure 2**) and XPS (**Table 1**) measurements.

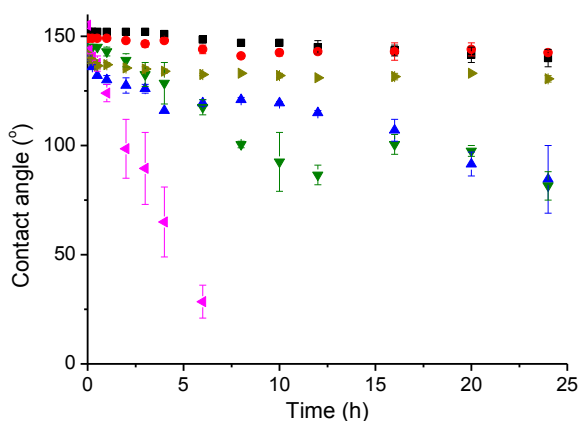


Figure 2. Stability of PAO modified with different functional groups at room temperature in PBS pH 7.0 measured by the static water contact angle: PA cured (■), PA noncured (●), YNE (▲), 2OHCA (▼), ENE (◄), and SIL (◄).

Table 1. Carbon (%) of PAO surface modified with different functional groups after immersion in PBS pH 7.0 at room temperature.^a

| Functional groups | %C, t ₀ | %C, 24 h | %C, 1 week | %C, 2 weeks |
|-------------------|--------------------|----------|------------|-------------|
| PA cur | 83 ± 1 | 83 ± 1 | 82 ± 1 | 81 ± 2 |
| PA non cur | 82 ± 1 | 79 ± 1 | 80 ± 1 | 78 ± 2 |
| YNE | 77 ± 1 | 57 ± 1 | 50 ± 1 | 44 ± 2 |
| 2OHCA | 70 ± 1 | 53 ± 4 | 42 ± 2 | 42 ± 3 |
| SIL ^b | 65 ± 1 | 65 ± 1 | 67 ± 1 | 65 ± 1 |

^a %C was determined by integrating the XPS signals of C 1s and Al 2p.

^b Additional sonication step (1 min in hexane).

The initially high static water contact angles (>141°) and carbon content (>70%) of the modified PAO surfaces indicate a successful modification because the nonmodified PAO surface presents a low contact angle (<15°) and carbon content (<5%). All of the modified PAO surfaces presented a decrease in the contact angles after prolonged exposure to the PBS buffer. The order of stability of the modified PAO surfaces was PA > SIL > YNE ≈ 2OHCA >> ENE > CA. PAO surfaces modified with CA and ENE initially presented high contact angles (153° for CA and 155° for ENE) and carbon content, but the monolayer rapidly degraded when placed in PBS buffer, indicating they are not stable. The initial carbon contents (considering the XPS signals of C 1s and Al 2p) of the samples modified with CA and ENE were 63% and 77%, respectively. The carbon content decreased to 29% (CA) and 41% (ENE) after 30 min and 8 h of immersion, respectively. This is in line with the known low stability of alkyl carboxylic acids modifications on flat aluminum oxide in water.^{19, 20, 38} Although its stability varies depending on both the conditions of monolayer generation and the alkyl chain length,⁵⁴ relatively rapid desorption has been previously observed in various media.¹⁹

The stability of aluminum surfaces modified with unsaturated hydrocarbons has not been extensively investigated. Although there have been some studies that report the adsorption of alkenes and alkynes on aluminum surfaces,^{39, 40} their use for the modification of PAO was only recently studied in more detail by our group.¹⁷ The results observed here in PBS are comparable to the results obtained in water during our

previous study,¹⁷ with PAO modifications with YNE being significantly more stable than with ENE. However, both modified PAO surfaces are slightly less stable in PBS than in water. The differences between alkenes and alkynes indicate that they yield different species when they are reacted with and bound to the PAO surface.

Considering that the probable surface species formed in the modification of PAO with alkynes is an alkyl carboxylate with a hydroxyl group in the α position,¹⁷ we decided to include a sample modified with 2OHCA in the stability study. The results of water contact angle and XPS show that the samples modified with YNE and 2OHCA indeed have comparable stability. The slightly better stability of PAO modified with YNE may be attributed to the fact that the modification with YNE is performed at a higher temperature and under neat conditions, whereas the modification with 2OHCA is performed in an ethanol solution. The conditions used for the modification of PAO with YNE lead to a denser monolayer with increased stability. Another comparison that deserves attention is the different stabilities of the PAO surfaces modified with CA and 2OHCA. Although the reactive group is the same, the significant difference in the stability of these modified PAO surfaces indicates the participation of the α -hydroxy group in the bidentate attachment to the PAO surface.¹⁷

The PAO surface modified with SIL showed considerably better stability than the above mentioned PAO surfaces when analyzed by contact angle. However, an additional sonication step was needed in the washing procedure of this modified PAO after removing it from the PBS buffer (**Table 1**). Without this sonication step, the carbon content of the PAO modified with SIL increased after exposure to the PBS buffer (data not shown). The final contact angle of the PAO modified with SIL was also lower when the sonication step was included (102°) than without the sonication step (122°). This different behavior of the PAO modified with SIL might be due to the formation of disordered structures that attract more organic contamination than the PAO surfaces modified with other molecules.

Finally, the PAO surfaces modified with PA both with and without curing proved to be the most stable. This is in accordance with previous stability studies that showed substrates modified with phosphonic acids to be more stable than substrates modified with carboxylic acids or silane derivatives.^{18, 41, 42}

The influence of the curing step in the stability of the surfaces modified with PA was also assessed. The curing step consists of heating the modified PAO to high

temperature (usually 140 °C) under vacuum to allow for better chemisorption of the phosphonic acid on the surface.^{31, 43} The curing of phosphonate monolayers on silicon oxide surfaces is known to increase their order and stability.^{44, 45} However, in our study no significant difference was observed in the stability of PA-modified PAO with or without a curing step. After 2 weeks in PBS buffer, the remaining carbon for the noncured PAO was 95% of the initial content, whereas for the cured PAO it was 97%. However, considering the reports that show increased order and stability upon curing for analogous monolayers on silicon oxide,^{46, 49} we decided to apply the curing step for all further modifications of the PAO surface with phosphonic acids.

PAO modified with hexadecylphosphonic acid (PA)

After our finding that the modification of the PAO surface with PA was the most stable at room temperature, we further investigated this modification and its stability. First, the kinetics of the modification of the PAO surface with PA in a 1 mM ethanolic solution was studied (**Figure 3a**). The percentage of carbon on the modified PAO surface increases until one hour after immersion in the solution of PA and remains constant upon prolonged immersion. This result is comparable to the kinetics of the modification of flat Al₂O₃ with other alkylphosphonic acids in ethanol solutions.⁴⁶

Next, we assessed its stability over a range of pHs (4.0–8.0) (**Figure 3b** and **Table SI-3**) and temperatures (25–80 °C) (**Figure 3c** and **Table 2**) that are important for microbial growth. The selected range of pH takes into consideration the application of the modified PAO surface for a wide range of bacteria, including some genera that decrease the pH of the medium during growth (e.g., lactobacilli)⁴⁷ or require high temperatures to grow (e.g., thermophiles).⁴⁸ Most importantly, the PAO surface modified with PA showed good stability for 2 weeks in PBS for all of the tested pH values, with contact angles between 147° and 152° and no significant difference in the carbon content. This is in line with the reported stability at pH 1–10 for monolayers of phosphonic acids on magnetron-sputtered aluminum for 1 h, although those samples rapidly degraded when exposed to a pH 11 solution.¹⁸

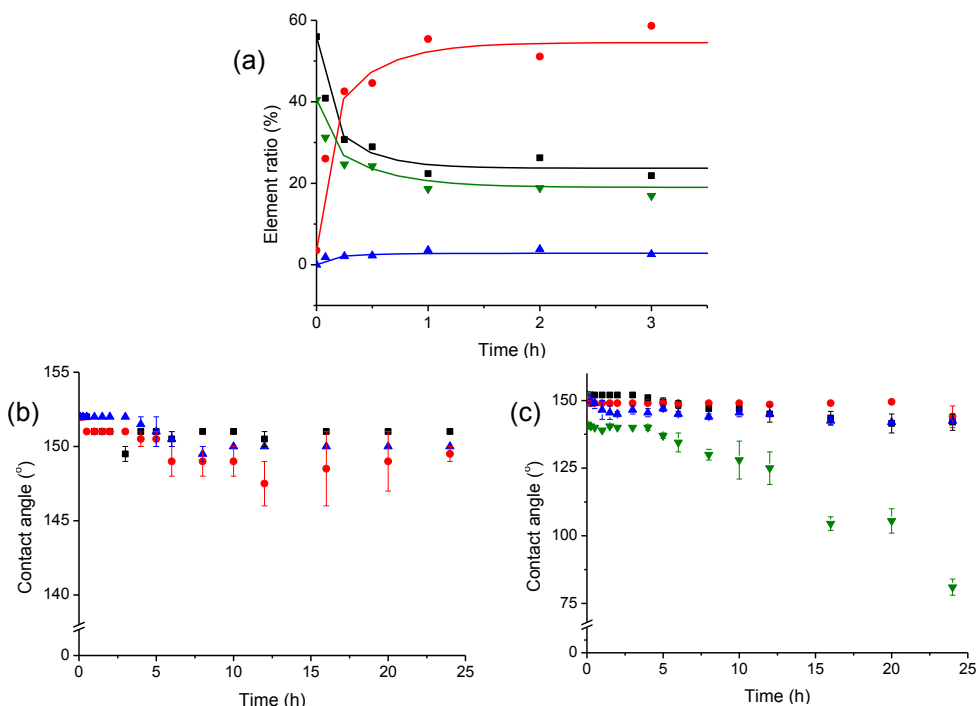


Figure 3. (a) Surface composition of PAO-PA at different reaction times determined by XPS: O 1s (■), C 1s (●), P 2s (▲), Al 2p (▼). The continuous lines serve as a guide to the eye. (b) Stability of PAO-PA at room temperature at different pH values measured via the static water contact angle: pH 4.0 (■), 6.0 (●), 8.0 (▲). (c) Stability of PAO-PA in PBS pH 7.0 at different temperatures measured via the static water contact angle: 25 (■), 40 (●), 60 (▲), 80 °C (▼).

The PAO surface modified with PA was stable for 24 h at temperatures up to 60 °C (Figure 3c and Table 2), and only started to show some degradation at 80 °C. Such temperature effects are more pronounced upon prolonged immersion: whereas the carbon content decreases only slightly at 25 °C and 40 °C even after two weeks, it significantly decreases at 60 °C and 80 °C, indicating gradual degradation (Table 2, data for 1 and 2 weeks).

Table 2. Carbon (%) of PAO-PA after immersion in PBS pH 7.0 at different temperatures.^a

| Temperature | %C, t0 | %C, 24 h | %C, 1 week | %C, 2 weeks |
|-------------|--------|----------|------------|-------------|
| 25 °C | 83 ± 1 | 84 ± 1 | 82 ± 1 | 81 ± 2 |
| 40 °C | 83 ± 1 | 83 ± 1 | 81 ± 1 | 78 ± 3 |
| 60 °C | 82 ± 1 | 85 ± 1 | 61 ± 4 | 50 ± 2 |
| 80 °C | 83 ± 1 | 80 ± 1 | 37 ± 14 | 31 ± 3 |

^a %C was determined by integrating the XPS signals of C 1s and Al 2p.

Finally, we also assessed the stability of the PAO surface modified with phosphonic acids with shorter alkyl chain lengths (1-octylphosphonic acid and 1-dodecylphosphonic acid) in PBS pH 7.0 at room temperature. Also, these shorter-chain phosphonic acids were stable up to at least two weeks (data not shown).

PAO modified with phosphonic acids presenting different terminal groups

Biofunctionalization of surfaces usually requires a stepwise approach. In most cases, the initial monolayer has to react further with the biomolecule needed for the application. For this reason, we also modified the PAO surface with phosphonic acids presenting different terminal groups that are frequently used to attach biomolecules (mainly via click reactions):⁴⁹⁻⁵² alkyne (PAO-ynePA), alkene (PAO-enePA), azide (PAO-N3PA), hydroxyl (PAO-OHPA), and triethyleneglycol (PAO-TEGPA) (**Figure 4a**).

After the modification of PAO with the selected phosphonic acids, the different terminal groups could be conveniently differentiated via their IR spectra (**Figure 4b**). All of the modified PAO surfaces present asymmetric (ν_a) and symmetric (ν_s) C-H methylene stretching vibrations at around 2926 cm⁻¹ and 2855 cm⁻¹, respectively. All of the spectra also show an oscillatory pattern attributed to internal reflections or optical effects due to the nanopores.¹⁷ PAO-ynePA presents the alkyne \equiv C-H stretching at 3323 cm⁻¹, whereas PAO-enePA displays an alkene =C-H stretching at 3082 cm⁻¹. PAO-N3PA shows an azide stretching vibration at 2098 cm⁻¹, and PAO-TEGPA presents different intensity and a wider frequency range of the ν_a and ν_s methylene stretching vibrations compared to those of the other modified PAO surfaces, which is attributed to the additional presence of the highly flexible and disordered ethylene oxide moieties. In

addition, a broad O–H stretching vibration from 3670 to 3160 cm^{-1} confirms the presence of the terminal hydroxyl group, similar to what is observed for PAO-OHPA.

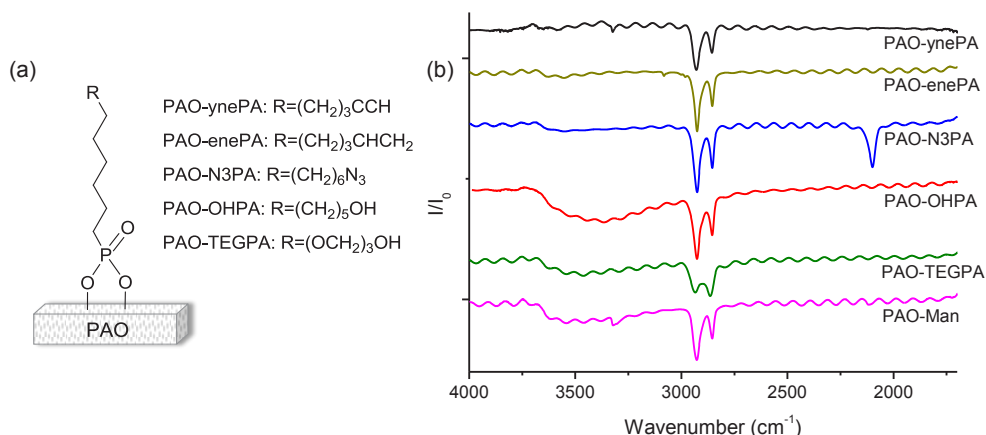
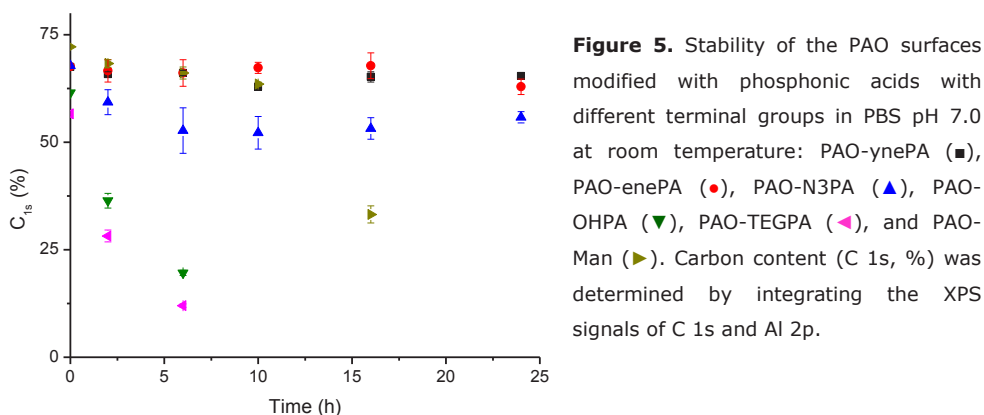


Figure 4. (a) PAO surface modified with phosphonic acids presenting different terminal groups. (b) IR spectra of the modified PAO surfaces listed above.

Next, the stability of these modified PAO surfaces was assessed in pH 7.0 PBS at room temperature (**Figure 5**) for up to 2 weeks, and this yielded the following stability order: PAO-ynePA \approx PAO-enePA $>$ PAO-N3PA $>$ PAO-OHPA and PAO-TEGPA. The alkyne and alkene-modified surfaces were the most stable, with no significant decrease in the carbon content even after 2 weeks (data not shown). PAO-N3PA presented an initial small decrease of the carbon content from 68% to 53% after 6 h, but this remained constant after this initial change, even after 2 weeks of immersion in PBS (data not shown). The hydroxy-terminated PAO modifications (PAO-OHPA and PAO-TEGPA) proved to be the least stable, with about a 35–50% reduction in carbon content after 2 h of immersion in PBS, and a further decrease after 6 h of immersion in PBS.



The lower stability of these hydroxy-terminated modified PAO surfaces may be attributed to two factors: hydrophilic characteristic and possible upside-down interaction. Considering that the degradation of the PAO surfaces modified with phosphonic acids occurs via hydrolysis, the presence of a hydrophilic moiety will likely increase the degradation by actively attracting water molecules to the surface. In addition, during the initial PAO modification step the hydroxyl-terminated phosphonic acids may also attach to the PAO surface through the hydroxyl group, instead of the phosphonic acid group (upside-down interaction). Although substantially less favorable, the reversal of this process in the phase of an almost completely formed monolayer may be slow, given the significant stabilization by the Van der Waals forces in such monolayers. However, in aqueous media such modified PAO surfaces are rapidly degraded by the weak interaction between the hydroxyl group and the PAO surface.⁵³

Biofunctionalization and bacterial binding

The next objective was to demonstrate that phosphonic acid-bound monolayers can be used to attach a target biomolecule so that modified PAO can function as an improved bacteria binding substrate. For this proof of principle biofunctionalization, we selected a carbohydrate, mannose, that we aimed to attach to PAO-ynePA via a CuAAC reaction. The CuAAC reaction has already been successfully employed by others for the biofunctionalization of, for example, the surface of diamonds,⁵⁴ SPR chips,⁵⁵ and silicon wafers⁵⁶ with carbohydrates. Therefore, a mannoside derivative (**3**) equipped with an azido-terminated anomeric linker was prepared according to the synthesis route depicted in **Scheme 1**. Briefly, azido-mannoside **3** was synthesized by a glycosylation between known protected mannose iodide **1**³⁷ and 11-azido-1-undecanol, followed by deprotection of the peracetylated intermediate.

Next, PAO-ynePA was exposed to the CuAAC reaction conditions in the presence of **3** to generate the mannose-terminated PAO surface (PAO-Man). This is shown via the decrease in the contact angle of PAO-Man (from 137° to <20°) and the occurrence of a broad O–H stretching vibration in the IR spectrum (**Figure 4b**). In addition, the development of a N signal in the XPS spectrum that shows the presence of nitrogen (as expected for PAO-Man, **Figure 6c**), which was not present on PAO-ynePA (**Figure 6a**), and an increase in the carbon content after the CuAAC reaction provide conclusive evidence for the successful attachment. The XPS spectrum of the C 1s region of PAO-Man

(Figure 6d) presents three regions corresponding to the three types of carbon [C-C (285.0 eV), C-O/C-N (286.5 eV), and O-C-O (288.6 eV)] whereas the spectrum of PAO-ynePA (Figure 6b) presents only one type of carbon (C-C). It is not possible to distinguish between C-C and C-P carbons or between C-O and C-N carbons. The ratio of C to N in the wide-scan spectrum was used to estimate the efficiency of the CuAAC reaction, which turned out to be around 70%. This efficiency of the CuAAC reaction was greater than what was previously observed for the CuAAC reaction of a lactosyl azide on the alkyne-terminated PAO modified with 1,15-hexadecyne (45%).¹⁷

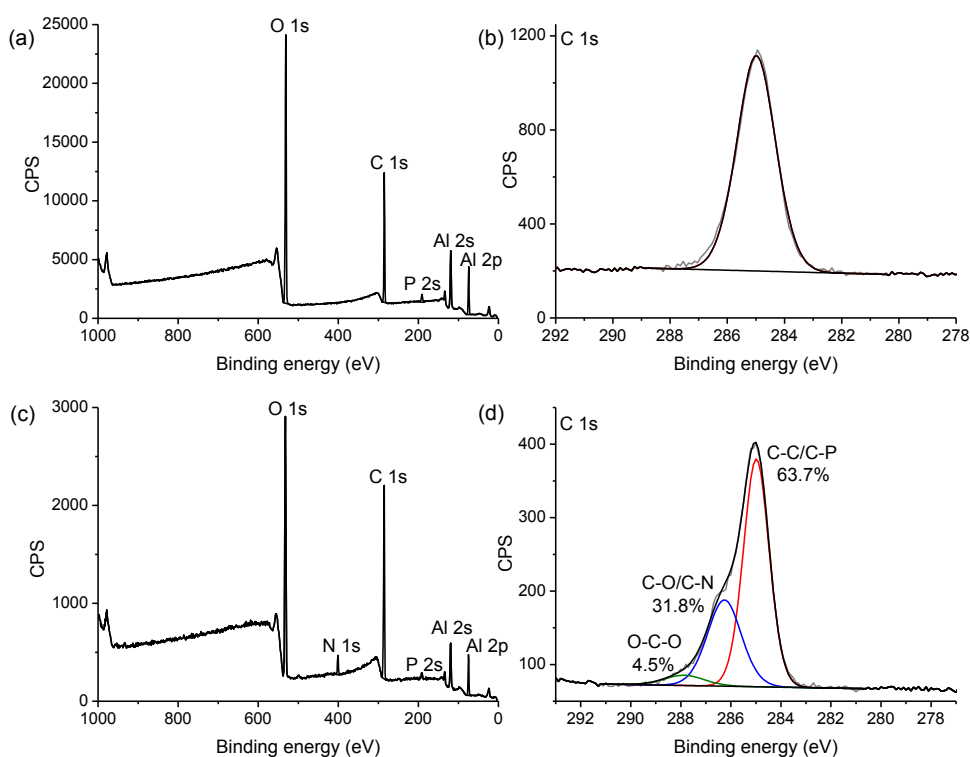


Figure 6. XPS spectra of alkyne-terminated PAO before (a, b) and after (c, d) the CuAAC reaction with azide-terminated mannose. (a) PAO-ynePA, wide-range scan; (b) PAO-ynePA C 1s narrow scans; (c) PAO-Man wide-range scan; and (d) PAO-Man C 1s narrow scans.

Before using PAO-Man for binding and growth, we first investigated its stability in pH 7.0 PBS at room temperature (Figure 5). For bacterial binding, PAO-Man needs to be stable only for the time required for the interaction between the bacterial adhesin and the surface (<1 h). PAO-Man presented an initial carbon content of 72%, which

slightly decreased to 68% after 2 h. After that, the carbon content gradually decreased to 64% during 10 h of immersion in PBS. The degradation of PAO-Man may be attributed to the hydrophilic characteristic of the modified PAO surface, which may favor hydrolysis. Although PAO-Man is more hydrophilic than PAO-OHPA (110°) and PAO-TEGPA (46°), it is more stable. The better stability of PAO-Man when compared to that of PAO-OHPA and PAO-TEGPA also reinforces the hypothesis that the upside-down interaction during the modification with the hydroxyl-terminated phosphonic acids is the cause of the low stability of PAO-OHPA and PAO-TEGPA.

By confirming that PAO-Man was stable enough for use under culturing conditions, we tested the ability of a mannose-terminated PAO to increase the binding of *L. plantarum*. It is known that *L. plantarum* is decorated with multiple copies of a mannose-binding protein that functions as an adhesin – a cell surface component of bacteria that facilitates bacterial adhesion – and is probably involved in the interaction with the intestinal epithelial surface of its host.^{32, 57} For the binding studies, a mannose-terminated PAO was obtained by using a mixture of 10-undecynylphosphonic acid and 1-octylphosphonic acid to generate the initial mixed alkyne-containing monolayer (PAO-ynemix). A mixed monolayer was used to provide better accessibility for the subsequent CuAAC reaction⁵⁸ and bacterial binding.⁵⁹ PAO-ynemix was further used to perform the CuAAC reaction with mannoside **3** (to yield PAO-mix-Man) or with 11-azido-1-undecanol (to yield PAO-mix-OH). PAO-mix-OH was used as a negative control in the binding studies because it lacks the mannose necessary for binding the bacterial adhesin, but presents a hydrophilic surface that is similar to that of PAO-mix-Man.

PAO-mix-Man showed increased binding of *L. plantarum* compared to PAO-mix-OH (95% of the bacteria bound to PAO-mix-Man compared to only 14% for PAO-mix-OH), indicating that the interaction between the mannose-binding adhesin of *L. plantarum* plays an important role in the increased adsorption of this bacterium to the biofunctionalized surface (**Figure 7**). It was also observed that the binding of *L. plantarum* to PAO-mix-Man was reduced 20-fold (to only 5%) when methyl- α -D-mannopyranoside was added to the bacterial suspension before exposing it to the PAO surface (**Figure 7c, d**). This mannose derivative is known to block the mannose-binding adhesin of *L. plantarum*³² and therefore proves that the increased adsorption of *L. plantarum* on PAO-mix-Man was indeed due to the biofunctionalization of PAO with mannose. Finally, we showed that the bound *L. plantarum* cells were capable of further

growth to microcolonies (**Figure 8**). These results showed that the modification of PAO with carbohydrates is feasible and can be used to achieve enhanced binding and the subsequent growth of certain type of bacteria.

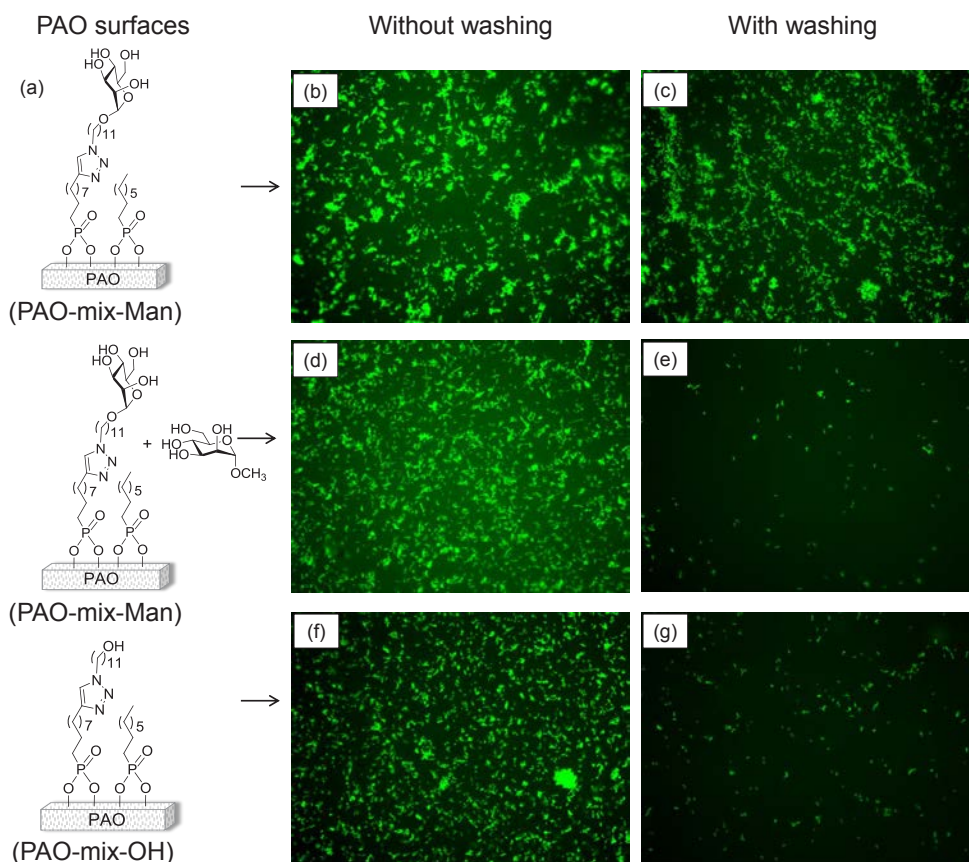


Figure 7. Binding of *L. plantarum* on modified PAO surfaces: (a) PAO surfaces used for the binding studies, (b) PAO-mix-Man without washing, (c) PAO-mix-Man after washing, (d) PAO-mix-Man and methyl- α -D-mannopyranoside without washing, (e) PAO-mix-Man and methyl- α -D-mannopyranoside after washing, (f) PAO-mix-OH without washing, and (g) PAO-mix-OH after washing. Total magnification is 200 \times , and the cell length of *L. plantarum* is 1 to 3 μm .⁶⁰

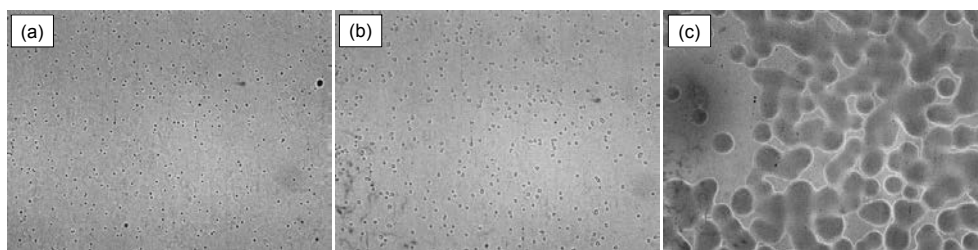


Figure 8. *Lactobacillus plantarum* on mannose-terminated PAO after incubation at 37 °C: (a) 2.5 h; (b) 5 h; and (c) 24 h. Total magnification 40 ×.

Conclusions

We present a comprehensive stability study of porous aluminum oxide (PAO) modified with most attachment chemistries known from literature. Surface modification with phosphonic acids yielded the most stable surfaces over a wide range of pH and temperature, with monolayers that are fully stable up to 2 weeks in PBS buffer. We also successfully attached a mannose derivative to the PAO surface that resulted in the adherence of bacterium *L. plantarum* via a bacterial mannose-specific adhesin. These results show that biofunctionalized PAO surfaces can be used to integrate the binding and subsequent growth of bacteria. Future work involves the modification of PAO with various carbohydrates and the use of these modified surfaces to study the interaction with different pathogenic and probiotic bacteria.

Supporting Information

Layer thickness and initial contact angles of the modified surfaces, synthetic procedure and NMR spectra of mannoside **3**, effect of the pH on the stability of PAO-PA, XPS spectra, bacteria counting, and bacterial growth not given in the main text. This material is available free of charge via the Internet at <http://pubs.acs.org>.

Acknowledgements

This work is supported by NanoNextNL, a micro and nanotechnology consortium of the Government of the Netherlands and 130 partners and ERC grant 250712 (MicrobesInside). The authors thank Zalan Szabo and Colin Ingham (MicroDish BV) and Luc Scheres and Esther Roeven (Surfix BV) for fruitful discussions, and Steven Aalvink (Wageningen University) for help with the microbiological experiments.

Supporting Information

Layer thickness

The layer thickness was calculated on the basis of the attenuation of the XPS O 1s signal, using the following equation:

$$I_o = I_o^{\infty} \exp\left(\frac{-d}{\lambda_{o,c} \cos \theta}\right)$$

with I_o = the absolute oxygen peak intensity, I_o^{∞} = the absolute oxygen peak intensity of an unmodified, cleaned substrate, d = the thickness of the adsorbed layer, $\lambda_{o,c}$ = the attenuation length of O 1s electrons in the hydrocarbon layer (3.5 nm), and θ = the electron takeoff angle (10°).¹⁷

Table SI-1. Thickness of the layers on PAO used for the stability study.

| Functional groups | Layer thickness (nm) |
|-------------------|----------------------|
| PA cur | 2.1 |
| PA non cur | 2.2 |
| CA | 1.8 |
| YNE | 2.3 |
| 2OHCA | 2.0 |
| ENE | 3.6 |
| SIL | 2.2 |

Initial contact angles of the modified surfaces**Table SI-2.** Initial contact angles of rough and smooth sides of the modified PAO surfaces.

| Modified PAO | Rough side (°) | Smooth side (°) |
|--------------|----------------|-----------------|
| PA cur | 152 | 149 |
| PA non cur | 149 | 145 |
| CA | 153 | 135 |
| YNE | 144 | 141 |
| 2OHCA | 145 | 140 |
| ENE | 155 | 141 |
| SIL | 142 | 126 |

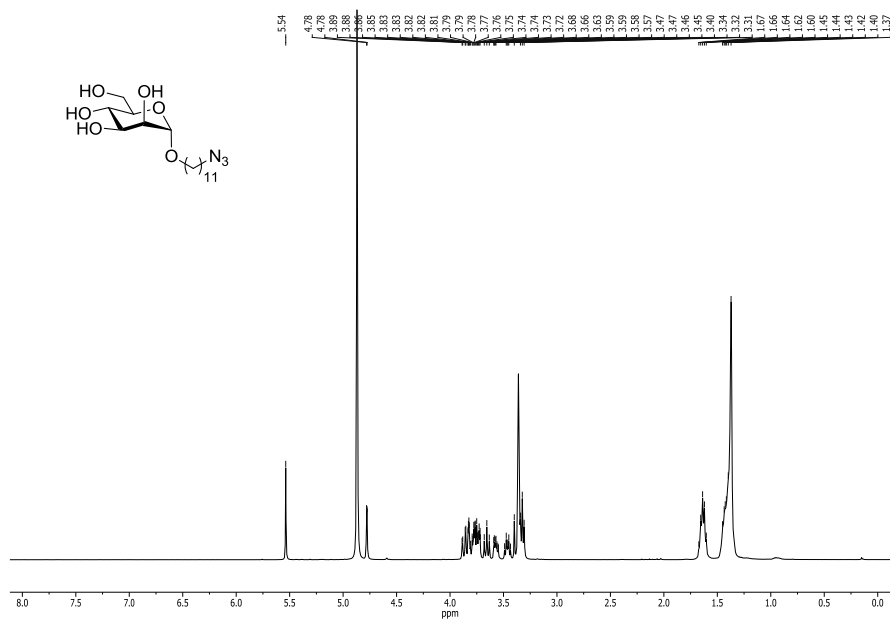
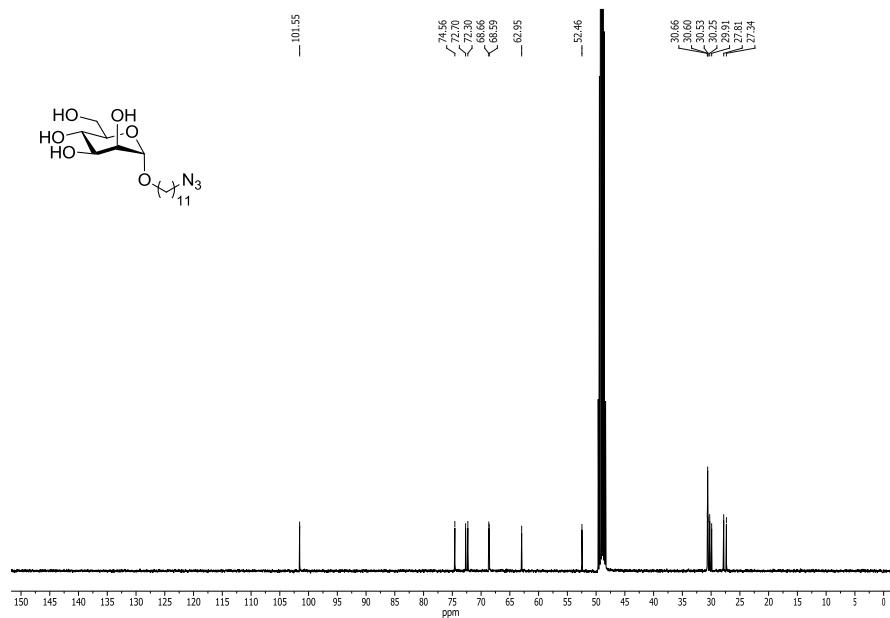
Stability study

The %C listed in **Tables 1** and **2** and **Figure 5** (Results & Discussion section) and **Table SI-3** (Supporting Information) were determined by integration of the C 1s and Al 2p XPS signals in the wide area spectra. Example: in **Table 1**, the sample PA cured at time 0 is listed as having 83% of C. This means that the remaining 17% correspond to Al. Only these two elements are compared because they are unique for the surface (Al) and for the monolayer (C), and degradation of the monolayers causes changes in the ratio of these two elements.

Synthesis of 1-(11-azidoundecanyl)- α -D-mannopyranoside (3)

Acetyl-protected mannosyl iodide **1** was prepared according to a method previously described in the literature.³⁷ A solution of donor **1** (0.86 g, 1.9 mmol), the 11-azido-1-undecanol acceptor (0.80 g, 3.75 mmol), and activated molecular sieves (1.15 g, 4 Å) in acetonitrile (12 mL) was cooled to 0 °C under argon atmosphere. Iodine (0.95 g, 3.75 mmol) was added and the mixture was stirred for 4 h, slowly warming up to room temperature. The dark brown suspension was diluted with ethyl acetate (90 mL) and filtered to remove the molecular sieves. The filtrate was washed successively with 1 M Na₂S₂O₃ (2 × 70 mL) and saturated NaCl solution (30 mL), dried over Na₂SO₄, filtered, and concentrated under reduced pressure. The crude product was purified by column

chromatography (eluent petroleum ether/ethyl acetate, 80:20) to yield 2,3,4,6-tetra-*O*-acetyl-1-(11-azidoundecanyl)- α -D-mannopyranoside (**2**) as a yellowish syrup in 29% yield (0.30 g, 0.55 mmol). Intermediate **2** (0.30 g, 0.55 mmol) was then dissolved in dry methanol (3 mL) and a solution of sodium methoxide in methanol (0.5 M, 60 μ L) was added. The mixture was stirred for 16 h and after complete conversion (monitored by TLC, eluent ethyl acetate), additional methanol (6 mL) was added to completely dissolve the product. Afterwards, Dowex 50 (H^+ form) was added to the solution until the pH was 7, and the suspension was filtered over a Celite layer. The solution was concentrated under reduced pressure to yield 1-(11-azidoundecanyl)- α -D-mannopyranoside (**3**) as an off-white solid in 72% yield (0.15 g, 0.4 mmol). $[\alpha]_D^{20} +40.7$ (*c* 1.0, MeOH). 1H NMR (400 MHz, MeOD): δ 5.54 (1H, s, OH), 4.78 (1H, d, H-1, $J = 1.8$ Hz), 3.86 (1H, dd, H-6a, $J = 2.1$ Hz, 11.8 Hz), 3.80 (1H, m, $-OCHa-$), 3.76 – 3.70 (3H, m, H-2, H-3, H-6b), 3.66 (1H, t, H-4, $J = 9.4$ Hz), 3.57 (1H, m, H-5), 3.45 (1H, m, $-OCHb-$), 3.32 (2H, t, $-CH_2-N_3$, $J = 6.8$ Hz), 1.68 – 1.59 (4H, m, $-CH_2CH_2N_3$, $-OCH_2CH_2-$), 1.49 – 1.32 (14H, m, $-(CH_2)_7-$). ^{13}C NMR (100 MHz, MeOD): δ 101.6 (CH, C-1), 74.6 (CH, C-5), 72.7, 72.3 (2 \times CH, C-2, C-3), 68.7 (CH, C-4), 68.6 (CH_2 , $-CH_2O-$), 62.9 (CH_2 , C-6), 52.5 (CH_2 , $-CH_2N_3$), 30.7, 30.6, 30.6, 30.6, 30.5, 30.2, 29.9, 27.8, 27.3 (9 \times CH_2 , $-(CH_2)_9-$, overlap of three peaks). HRMS: m/z 374.2291; calcd for $C_{17}H_{32}N_3O_6$ ($[M - H]^-$), 374.2286.

1-(11-azidoundecanyl)- α -D-mannopyranoside (3**)** ^1H NMR spectrum**Figure SI-1.** ^1H NMR spectrum of 1-(11-azidoundecanyl)- α -D-mannopyranoside (**3**). ^{13}C NMR spectrum**Figure SI-2.** ^{13}C NMR spectrum of 1-(11-azidoundecanyl)- α -D-mannopyranoside (**3**).

Effect of pH on the stability of porous aluminum oxide modified with hexadecylphosphonic acid (PAO-PA)

Table SI-3. Carbon (%) of PAO-PA after immersion in buffer solutions with different pHs at room temperature. %C was determined by integrating the XPS signals of C_{1s} and Al_{2p}.

| pH | %C t0 | %C 24 h | %C 1 week | %C 2 weeks |
|-----|--------|---------|-----------|------------|
| 4.0 | 84 ± 1 | 84 ± 1 | 84 ± 1 | 84 ± 1 |
| 6.0 | 84 ± 1 | 85 ± 1 | 82 ± 2 | 82 ± 1 |
| 8.0 | 83 ± 1 | 83 ± 1 | 85 ± 1 | 85 ± 1 |

XPS spectra of the modified PAO surfaces

PA cured

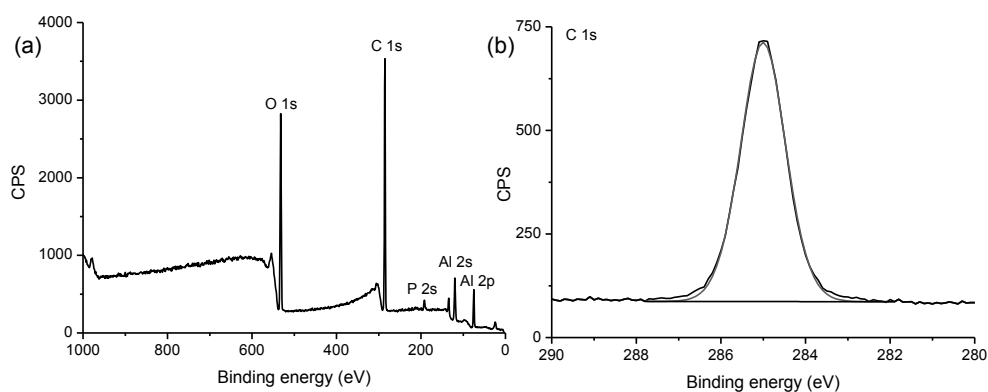


Figure SI-3. XPS spectra of PAO modified with 1-hexadecylphosphonic acid with curing step (PA cured): (a) wide area and (b) C 1s narrow scans.

PA cured: smooth side

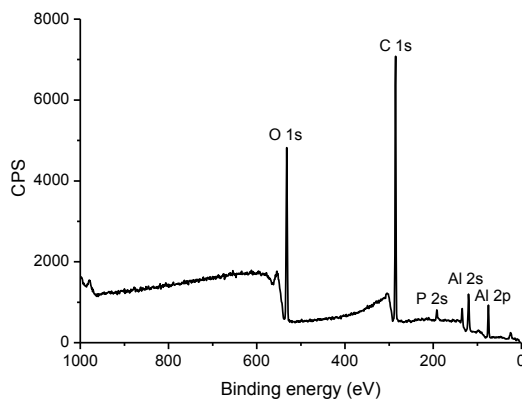


Figure SI-4. XPS spectra (wide area) of the smooth side of PAO modified with 1-hexadecylphosphonic acid with curing step (PA cured).

PA non-cured

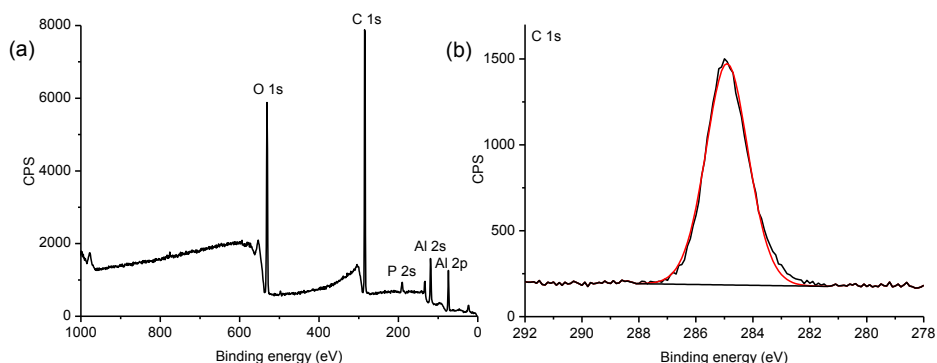


Figure SI-5. XPS spectra of PAO modified with 1-hexadecylphosphonic acid without curing step (PA non-cured): (a) wide area and (b) C 1s narrow scans.

YNE

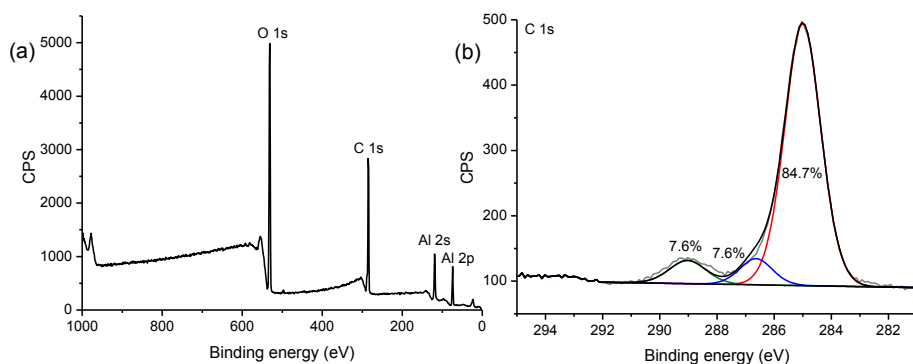


Figure SI-6. XPS spectra of PAO modified with 1-hexadecyne (YNE): (a) wide area and (b) C 1s narrow scans.

2OHCA

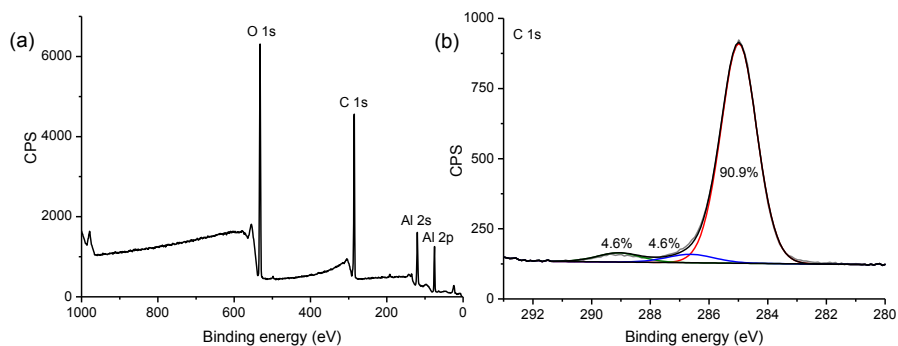


Figure SI-7. XPS spectra of PAO modified with 2-hydroxyhexadecylcarboxylic acid (2OHCA): (a) wide area and (b) C 1s narrow scans.

ENE

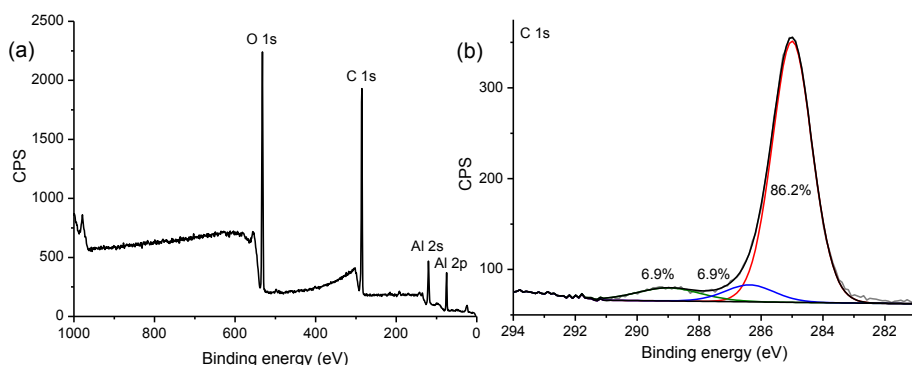


Figure SI-8. XPS spectra of PAO modified with 1-hexadecene (ENE): (a) wide area and (b) C 1s narrow scans.

SIL

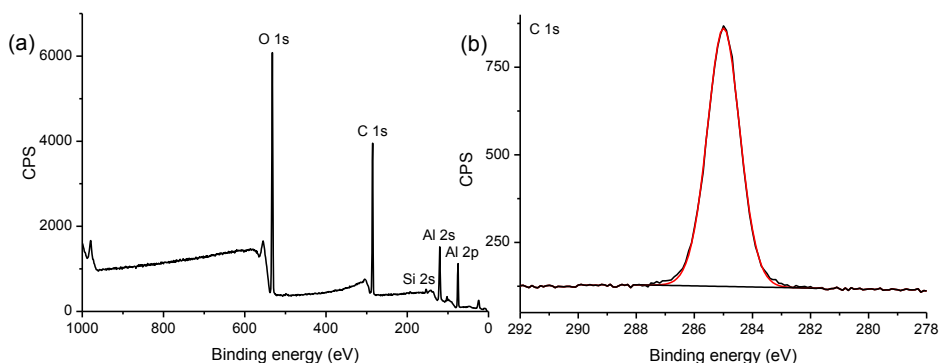


Figure SI-9. XPS spectra of PAO modified with 1-hexadecyltrimethoxysilane (SIL): (a) wide area and (b) C 1s narrow scans.

CA

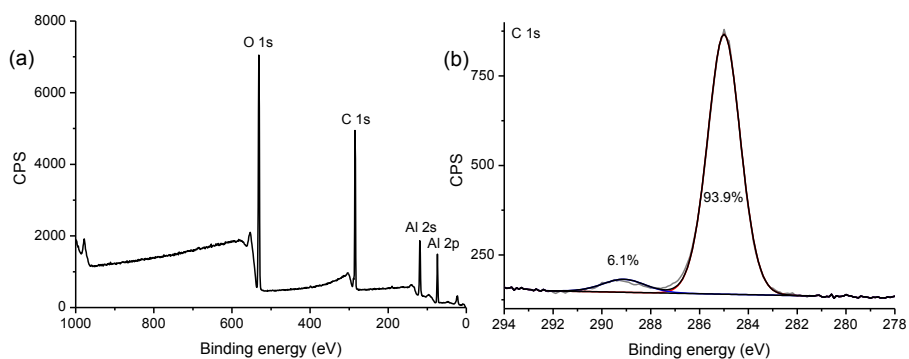


Figure SI-10. XPS spectra of PAO modified with 1-hexadecylcarboxylic acid (CA): (a) wide area and (b) C 1s narrow scans.

PAO-ynePA

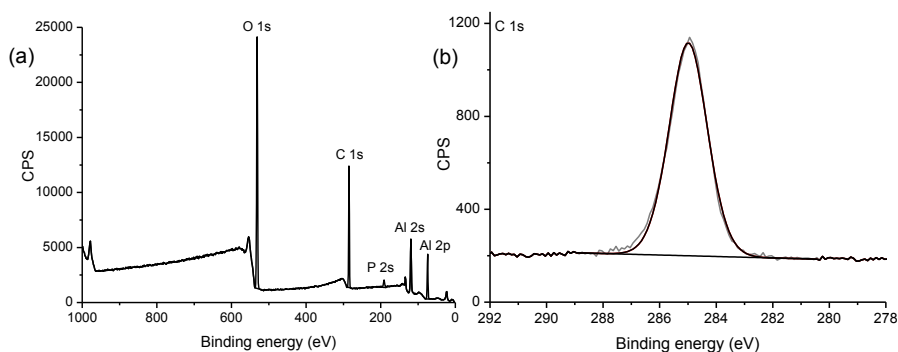


Figure SI-11. XPS spectra of alkyne-terminated PAO (PAO-ynePA): (a) wide area and (b) C 1s narrow scans.

PAO-enePA

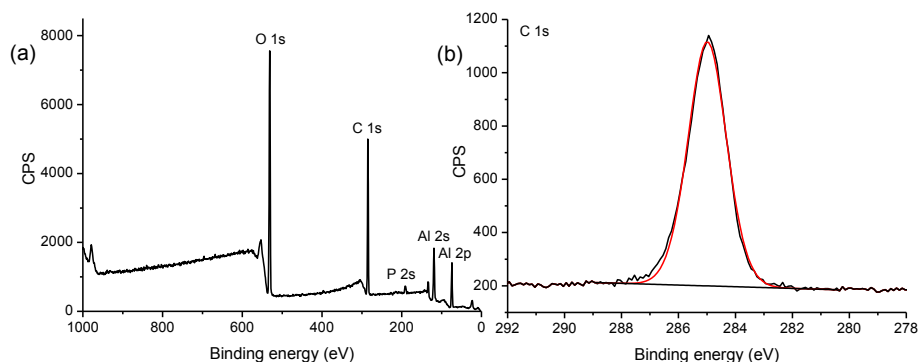


Figure SI-12. XPS spectra of alkene-terminated PAO (PAO-enePA): (a) wide area and (b) C 1s narrow scans.

PAO-N3PA

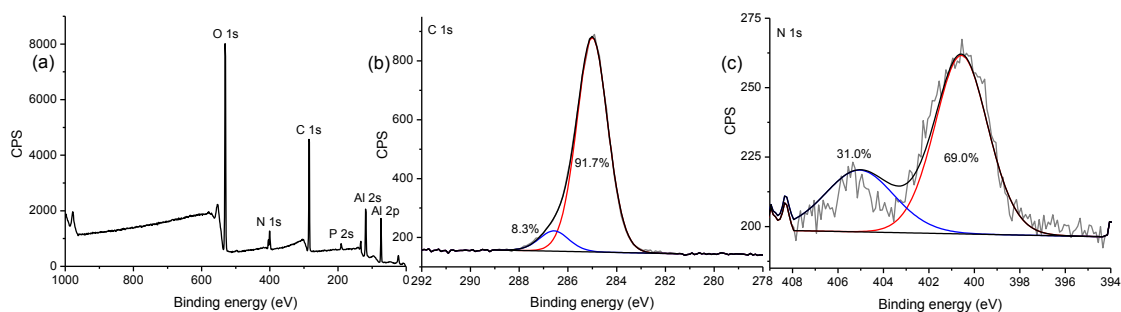


Figure SI-13. XPS spectra of azide-terminated PAO (PAO-N3PA): (a) wide area; (b) C 1s; and (c) N 1s narrow scans.

PAO-OHPA

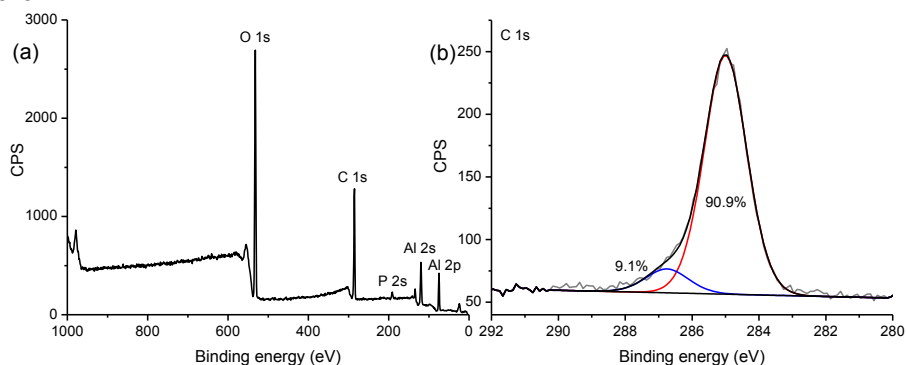


Figure SI-14. XPS spectra of hydroxy-terminated PAO (PAO-OHPA): (a) wide area and (b) C 1s narrow scans.

PAO-TEGPA

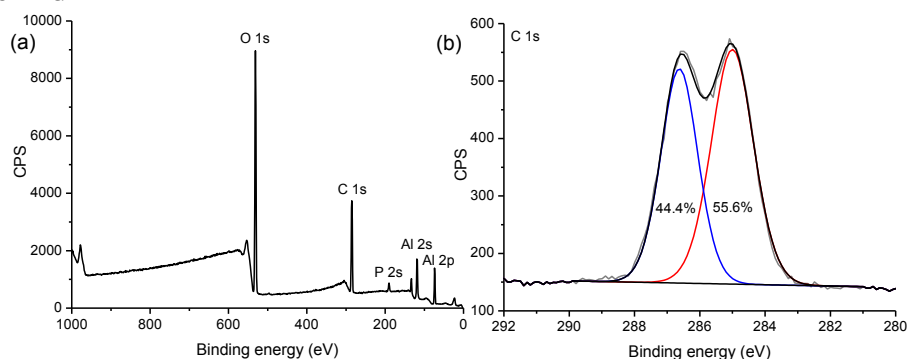


Figure SI-15. XPS spectra of triethyleneglycol-terminated PAO (PAO-TEGPA): (a) wide area and (b) C 1s narrow scans.

PAO-ynemix

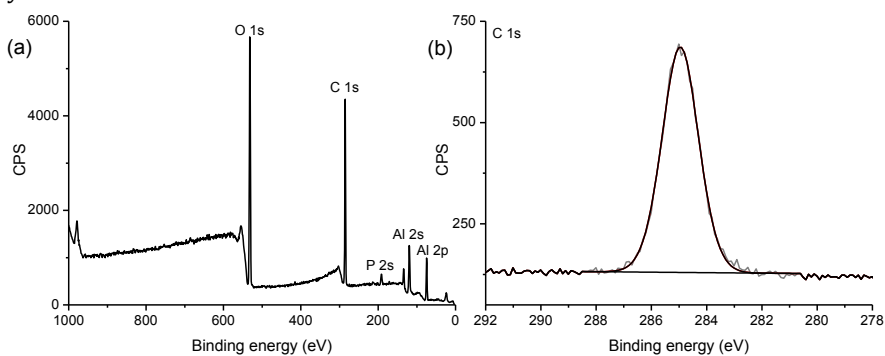


Figure SI-16. XPS spectra of PAO modified with a mixture of 1-octylphosphonic acid and 10-undecynylphosphonic acid 50:50 (w/w) (PAO-ynemix): (a) wide area and (b) C 1s narrow scans.

PAO-mix-Man

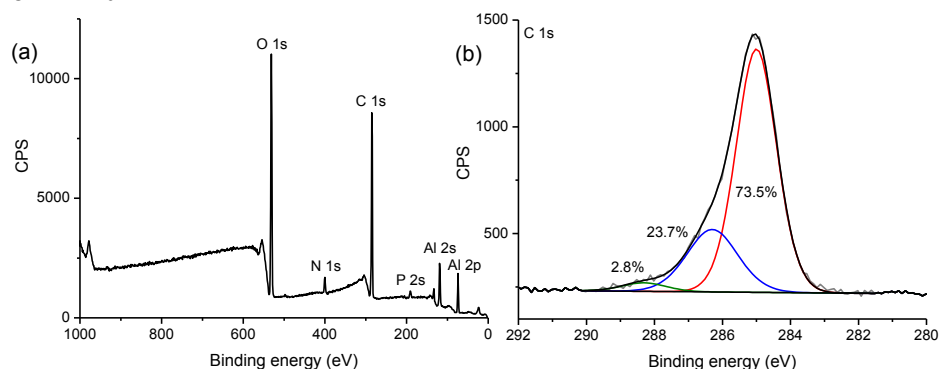


Figure SI-17. XPS spectra of mannose-terminated PAO obtained from PAO-ynemix (PAO-mix-Man): (a) wide area and (b) C 1s narrow scans.

PAO-mix-OH

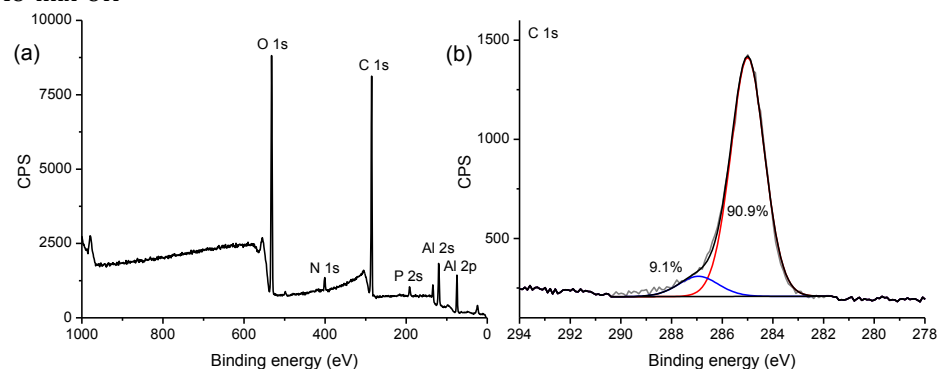


Figure SI-18. XPS spectra of hydroxy-terminated PAO obtained from PAO-ynemix (PAO-mix-OH): (a) wide area and (b) C 1s narrow scans.

PAO-Man stability 2 h

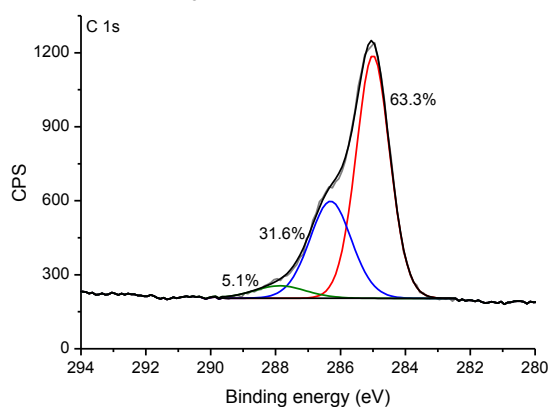


Figure SI-19. XPS C 1s narrow scans of mannose-terminated PAO (PAO-Man) after 2 h of immersion in PBS at room temperature.

Bacteria counting using CellProfiler

PAO-mix-Man without washing

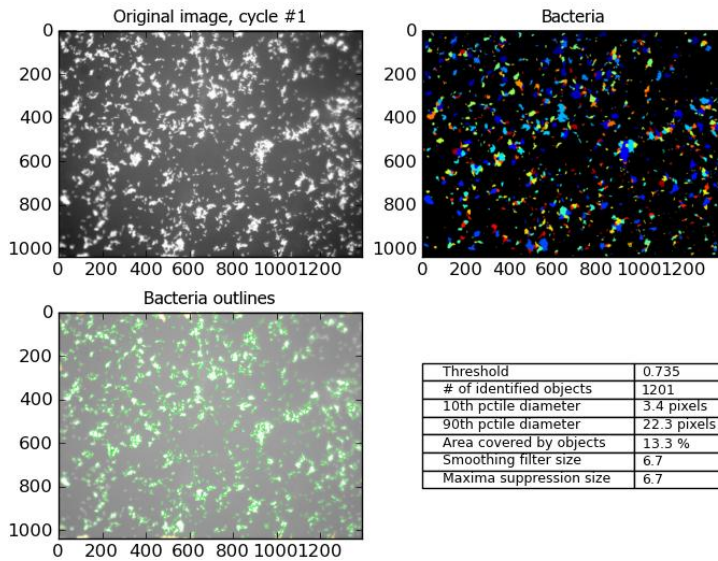


Figure SI-20. Bacteria counting on PAO-mix-Man without washing.

PAO-mix-Man after washing

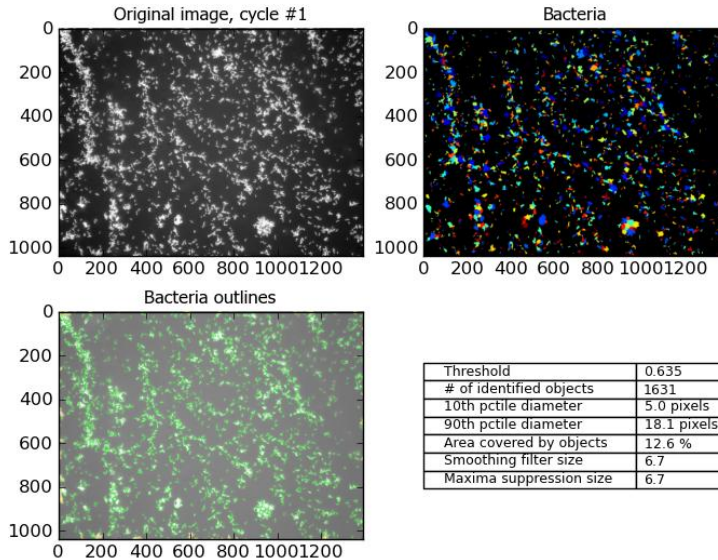


Figure SI-21. Bacteria counting on PAO-mix-Man after washing.

PAO-mix-Man with methyl- α -D-mannopyranoside without washing

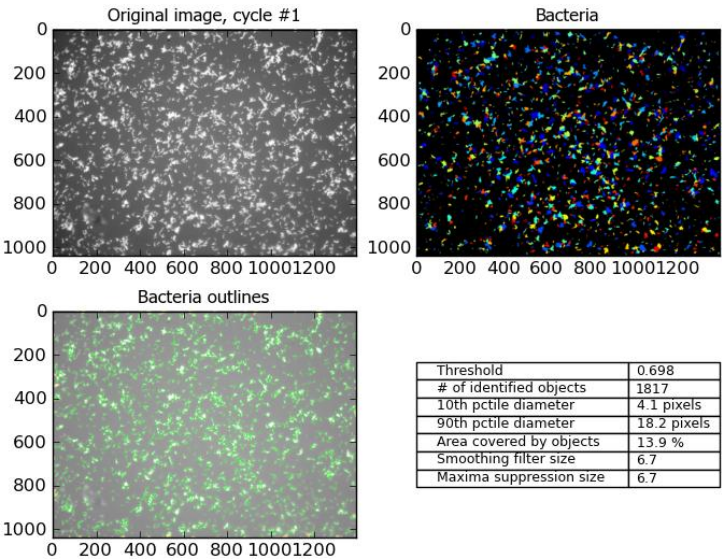


Figure SI-22. Bacteria counting on PAO-mix-Man with methyl- α -D-mannopyranoside without washing.

PAO-mix-Man with methyl- α -D-mannopyranoside after washing

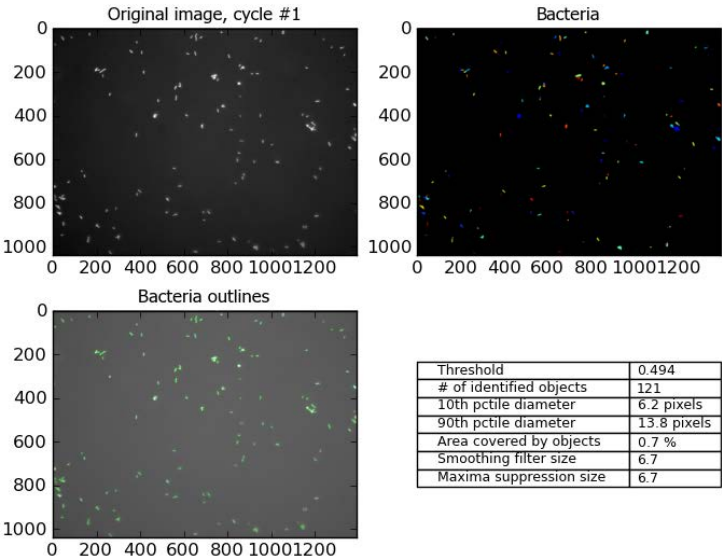


Figure SI-23. Bacteria counting on PAO-mix-Man with methyl- α -D-mannopyranoside after washing.

PAO-mix-OH without washing

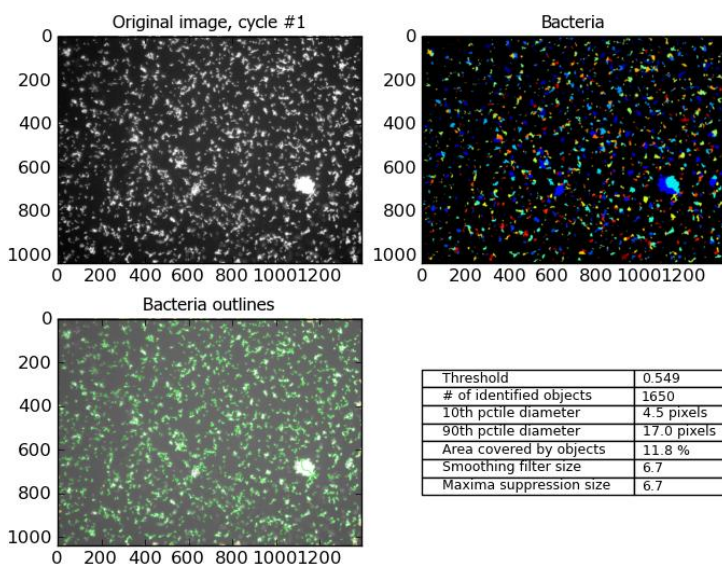


Figure SI-24. Bacteria counting on PAO-mix-OH without washing.

PAO-mix-OH after washing

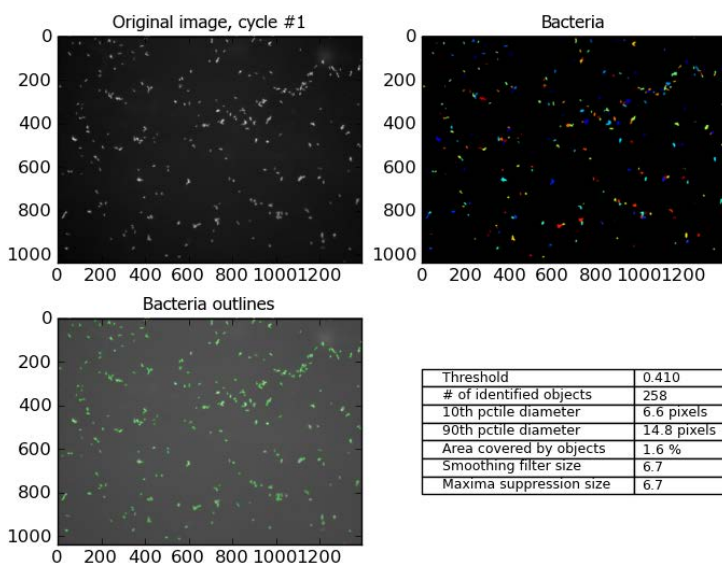


Figure SI-25. Bacteria counting on PAO-mix-OH after washing.

References

1. Rai, V.; Deng, J.; Toh, C.S. Electrochemical nanoporous alumina membrane-based label-free DNA biosensor for the detection of *Legionella* sp. *Talanta* **2012**, *98*, 112-117.
2. Gultepe, E.; Nagesha, D.; Sridhar, S.; Amiji, M. Nanoporous inorganic membranes or coatings for sustained drug delivery in implantable devices. *Adv. Drug Del. Rev.* **2010**, *62*, 305-315.
3. Pera, N. P.; Branderhorst, H. M.; Kooij, R.; Maierhofer, C.; van der Kaaden, M.; Liskamp, R. M. J.; Wittmann, V.; Ruijtenbeek, R.;

- Pieters, R. J. Rapid screening of lectins for multivalency effects with a glycodendrimer microarray. *ChemBioChem* **2010**, *11*, 1896-1904.
4. Lu, S.; An, Z.; He, J.; Li, B. Hierarchically-structured immobilized enzyme displaying the multi-functions of bio-membranes. *J. Mater. Chem.* **2012**, *22*, 3882-3888.
5. Rana, K.; Kucukayan-Dogu, G.; Bengu, E. Growth of vertically aligned carbon nanotubes over self-ordered nano-porous alumina films and their surface properties. *Appl. Surf. Sci.* **2012**, *258*, 7112-7117.
6. Erdogan, P.; Birol, Y. Effect of processing on structural features of anodic aluminum oxides. *Appl. Phys. A: Mater. Sci. Process.* **2012**, *108*, 587-592.
7. Poinern, G. E. J.; Ali, N.; Fawcett, D. Progress in nano-engineered anodic aluminum oxide membrane development. *Materials* **2011**, *4*, 487-526.
8. Ingham, C. J.; ter Maat, J.; de Vos, W. M. Where bio meets nano: The many uses for nanoporous aluminum oxide in biotechnology. *Biotechnol. Adv.* **2012**, *30*, 1089-1099.
9. Ingham, C. J.; van den Ende, M.; Pijnenburg, D.; Wever, P. C.; Schneeberger, P. M. Growth and multiplexed analysis of microorganisms on a subdivided, highly porous, inorganic chip manufactured from Anopore. *Appl. Environ. Microbiol.* **2005**, *71*, 8978-8981.
10. Ferrari, B. C.; Binnerup, S. J.; Gillings, M. Microcolony cultivation on a soil substrate membrane system selects for previously uncultured soil bacteria. *Appl. Environ. Microbiol.* **2005**, *71*, 8714-8720.
11. Hoess, A.; Teuscher, N.; Thormann, A.; Aurich, H.; Heilmann, A. Cultivation of hepatoma cell line HepG2 on nanoporous aluminum oxide membranes. *Acta Biomater.* **2007**, *3*, 43-50.
12. Hu, J.; Tian, J. H.; Shi, J.; Zhang, F.; He, D. L.; Liu, L.; Jung, D. J.; Bai, J. B.; Chen, Y. Cell culture on AAO nanoporous substrates with and without geometry constraints. *Microelectron. Eng.* **2011**, *88*, 1714-1717.
13. Ingham, C. J.; Sprengels, A.; Bomer, J.; Molenaar, D.; van den Berg, A.; Vlieg, J.; de Vos, W. M. The micro-Petri dish, a million-well growth chip for the culture and high-throughput screening of microorganisms. *Proc. Natl. Acad. Sci. U S A* **2007**, *104*, 18217-18222.
14. Wang, P. Y.; Clements, L. R.; Thissen, H.; Tsai, W. B.; Voelcker, N. H. High-throughput characterisation of osteogenic differentiation of human mesenchymal stem cells using pore size gradients on porous alumina. *Biomater. Sci.* **2013**, *1*, 924-932.
15. Tsou, P. H.; Sreenivasappa, H.; Hong, S. M.; Yasuike, M.; Miyamoto, H.; Nakano, K.; Misawa, T.; Kameoka, J. Rapid antibiotic efficacy screening with aluminum oxide nanoporous membrane filter-chip and optical detection system. *Biosens. Bioelectron.* **2010**, *26*, 289-294.
16. Ingham, C. J.; Schneeberger, P. M. Microcolony imaging of *Aspergillus fumigatus* treated with echinocandins reveals both fungistatic and fungicidal activities. *Plos One* **2012**, *7*, e35478-e35478.
17. ter Maat, J.; Regeling, R.; Ingham, C. J.; Weijers, C. A. G. M.; Giesbers, M.; de Vos, W. M.; Zuilhof, H. Organic modification and subsequent biofunctionalization of porous anodic alumina using terminal alkynes. *Langmuir* **2011**, *27*, 13606-13617.
18. Liakos, I. L.; Newman, R. C.; McAlpine, E.; Alexander, M. R. Study of the resistance of SAMs on aluminium to acidic and basic solutions using dynamic contact angle measurement. *Langmuir* **2007**, *23*, 995-999.
19. Chang, C. S.; Suen, S. Y. Modification of porous alumina membranes with *n*-alkanoic acids and their application in protein adsorption. *J. Membr. Sci.* **2006**, *275*, 70-81.
20. Lim, M. S.; Feng, K.; Chen, X.; Wu, N.; Raman, A.; Nightingale, J.; Gawalt, E. S.; Korakakis, D.; Hornak, L. A.; Timperman, A. T. Adsorption and desorption of stearic acid self-assembled monolayers on aluminum oxide. *Langmuir* **2007**, *23*, 2444-2452.
21. Tasaltin, N.; Sanli, D.; Jonas, A.; Kiraz, A.; Erkey, C. Preparation and characterization of superhydrophobic surfaces based on hexamethyldisilazane-modified nanoporous alumina. *Nanoscale Res. Lett.* **2011**, *6*, 487-494.
22. Santos, A.; Macias, G.; Ferre-Borrull, J.; Pallares, J.; Marsal, L. F. Photoluminescent enzymatic sensor based on nanoporous anodic alumina. *ACS Appl. Mater. Interfaces* **2012**, *4*, 3584-3588.
23. Tan, F.; Leung, P. H. M.; Liu, Z.-b.; Zhang, Y.; Xiao, L.; Ye, W.; Zhang, X.; Yi, L.; Yang, M. A PDMS microfluidic impedance immunosensor for *E. coli* O157:H7 and *Staphylococcus aureus* detection via antibody-immobilized nanoporous membrane. *Sensor. Actuat. B-Chem.* **2011**, *159*, 328-335.
24. Muslehiddinoglu, J.; Vannice, M. A. Adsorption of 1,3-butadiene on supported and promoted silver catalysts. *J. Catal.* **2004**, *222*, 214-226.
25. Hauffman, T.; Blajiev, O.; Snauwaert, J.; van Haesendonck, C.; Hubin, A.; Terryn, H. Study of the self-assembling of *n*-octylphosphonic acid layers on aluminum oxide. *Langmuir* **2008**, *24*, 13450-13456.
26. Lushtinetz, R.; Oliveira, A. F.; Frenzel, J.; Joswig, J.-O.; Seifert, G.; Duarte, H. A. Adsorption of phosphonic and ethylphosphonic acid on aluminum oxide surfaces. *Surf. Sci.* **2008**, *602*, 1347-1359.
27. Hauffman, T.; Van Lokeren, L.; Willem, R.; Hubin, A.; Terryn, H. *In situ* study of the deposition of (ultra)thin organic phosphonic acid layers on the oxide of aluminum. *Langmuir* **2012**, *28*, 3167-3173.
28. Chang, S. H.; Han, J. L.; Tseng, S. Y.; Lee, H. Y.; Lin, C. W.; Lin, Y. C.; Jeng, W. Y.; Wang, A. H. J.; Wu, C. Y.; Wong, C. H. Glycan array on aluminum oxide-coated glass slides through phosphonate chemistry. *J. Am. Chem. Soc.* **2010**, *132*, 13371-13380.
29. Yah, W. O.; Takahara, A.; Lvov, Y. M. Selective modification of halloysite lumen with octadecylphosphonic acid: New inorganic tubular micelle. *J. Am. Chem. Soc.* **2012**, *134*, 1853-1859.
30. Hoque, E.; DeRose, J. A.; Kulik, G.; Hoffmann, P.; Mathieu, H. J.; Bhushan, B. Alkylphosphonate modified aluminum oxide surfaces. *J. Phys. Chem. B* **2006**, *110*, 10855-10861.
31. Queffelec, C.; Petit, M.; Janvier, P.; Knight, D. A.; Bujoli, B. Surface modification using phosphonic acids and esters. *Chem. Rev.* **2012**, *112*, 3777-3807.
32. Pretzer, G.; Snel, J.; Molenaar, D.; Wiersma, A.; Bron, P. A.; Lambert, J.; de Vos, W. M.; van der Meer, R.; Smits, M. A.; Kleerebezem, M. Biodiversity-based identification and functional characterization of the mannose-specific adhesin of *Lactobacillus plantarum*. *J. Bacteriol.* **2005**, *187*, 6128-6136.
33. de Vos, W. M. Systems solutions by lactic acid bacteria: From paradigms to practice. *Micr. Cell Fact.* **2011**, *10*, S2-S20.
34. Smith, W. N.; Beumel, O. F. Preparation of alkynes and dialkynes by reaction of monohalo-alkanes and dihaloalkanes with lithium acetylenide-ethylenediamine complex. *Synthesis* **1974**, *6*, 441-442.
35. Urteaga, R.; Acquaroli, L. N.; Koropec, R. R.; Santos, A.; Alba, M.; Pallares, J.; Marsal, L. F.; Berli, C. L. A. Optofluidic characterization of nanoporous membranes. *Langmuir* **2013**, *29*, 2784-2789.
36. Vlassiok, I.; Krasnoslobodtsev, A.; Smirnov, S.; Germann, M. "Direct" detection and separation of DNA using nanoporous alumina filters. *Langmuir* **2004**, *20*, 9913-9915.
37. Mukhopadhyay, B.; Kartha, K. P. R.; Russell, D. A.; Field, R. A. Streamlined synthesis of per-*O*-acetylated sugars, glycosyl iodides, or thioglycosides from unprotected reducing sugars. *J. Org. Chem.* **2004**, *69*, 7758-7760.

38. Karaman, M. E.; Antelmi, D. A.; Pashley, R. M. The production of stable hydrophobic surfaces by the adsorption of hydrocarbon and fluorocarbon carboxylic acids onto alumina substrates. *Colloid. Surface. A* **2001**, *182*, 285-298.
39. Lucchesi, P. J.; Carter, J. L.; Yates, D. J. C. Infrared study of chemisorption of ethylene on aluminum oxide. *J. Phys. Chem.* **1962**, *66*, 1451-1456.
40. Ivanov, A. V.; Koklin, A. E.; Uvarova, E. B.; Kustov, L. M. A drift spectroscopic study of acetylene adsorbed on metal oxides. *PCCP Phys. Chem. Ch. Ph.* **2003**, *5*, 4718-4723.
41. Hoque, E.; DeRose, J. A.; Hoffmann, P.; Bhushan, B.; Mathieu, H. J. Alkylperfluorosilane self-assembled monolayers on aluminum: A comparison with alkylphosphonate self-assembled monolayers. *J. Phys. Chem. C* **2007**, *111*, 3956-3962.
42. DeRose, J. A.; Hoque, E.; Bhushan, B.; Mathieu, H. J. Characterization of perfluorodecanoate self-assembled monolayers on aluminum and comparison of stability with phosphonate and siloxy self-assembled monolayers. *Surf. Sci.* **2008**, *602*, 1360-1367.
43. Vega, A.; Thissen, P.; Chabal, Y. J. Environment-controlled tethering by aggregation and growth of phosphonic acid monolayers on silicon oxide. *Langmuir* **2012**, *28*, 8046-8051.
44. Hanson, E. L.; Schwartz, J.; Nickel, B.; Koch, N.; Danisman, M. F. Bonding self-assembled, compact organophosphonate monolayers to the native oxide surface of silicon. *J. Am. Chem. Soc.* **2003**, *125*, 16074-16080.
45. Gouzman, I.; Dubey, M.; Carolus, M. D.; Schwartz, J.; Bernasek, S. L. Monolayer vs. Multilayer self-assembled alkylphosphonate films: X-ray photoelectron spectroscopy studies. *Surf. Sci.* **2006**, *600*, 773-781.
46. Koutsoubas, A. G.; Spiliopoulos, N.; Anastassopoulos, D. L.; Vradis, A. A.; Priftis, G. D. Formation of alkane-phosphonic acid self-assembled monolayers on alumina: An *in situ* SPR study. *Surf. Interface Anal.* **2009**, *41*, 897-903.
47. Hutkins, R. W.; Nannen, N. L. pH homeostasis in lactic-acid bacteria. *J. Dairy Sci.* **1993**, *76*, 2354-2365.
48. Borglin, S.; Joyner, D.; DeAngelis, K. M.; Khudyakov, J.; D'Haeseleer, P.; Joachimiak, M. P.; Hazen, T. Application of phenotypic microarrays to environmental microbiology. *Curr. Opin. Biotechnol.* **2012**, *23*, 41-48.
49. Hoyle, C. E.; Bowman, C. N. Thiol-ene click chemistry. *Angew. Chem. Int. Ed.* **2010**, *49*, 1540-1573.
50. Zeng, X.; Andrade, C. A. S.; Oliveira, M. D. L.; Sun, X.-L. Carbohydrate-protein interactions and their biosensing applications. *Anal. Bioanal. Chem.* **2012**, *402*, 3161-3176.
51. Lallana, E.; Sousa-Herves, A.; Fernandez-Trillo, F.; Riguera, R.; Fernandez-Megia, E. Click chemistry for drug delivery nanosystems. *Pharm. Res.* **2012**, *29*, 1-34.
52. Yilmaz, M. D.; Huskens, J. Orthogonal supramolecular interaction motifs for functional monolayer architectures. *Soft Matter* **2012**, *8*, 11768-11780.
53. Kim, H.; Colavita, P. E.; Paoprasert, P.; Gopalan, P.; Kuech, T. F.; Hamers, R. J. Grafting of molecular layers to oxidized gallium nitride surfaces via phosphonic acid linkages. *Surf. Sci.* **2008**, *602*, 2382-2388.
54. Szunerits, S.; Niedziolka-Joensson, J.; Boukherroub, R.; Woisel, P.; Baumann, J.-S.; Siriwardena, A. Label-free detection of lectins on carbohydrate-modified boron-doped diamond surfaces. *Anal. Chem.* **2010**, *82*, 8203-8210.
55. Maaloul, N.; Barras, A.; Siriwardena, A.; Bouazaoui, M.; Boukherroub, R.; Szunerits, S. Comparison of photo- and Cu(I)-catalyzed "click" chemistries for the formation of carbohydrate SPR interfaces. *Analyst* **2013**, *138*, 805-812.
56. Gouget-Laemmel, A. C.; Yang, J.; Lodhi, M. A.; Siriwardena, A.; Aureau, D.; Boukherroub, R.; Chazalviel, J. N.; Ozanam, F.; Szunerits, S. Functionalization of azide-terminated silicon surfaces with glycans using click chemistry: XPS and FTIR study. *J. Phys. Chem. C* **2013**, *117*, 368-375.
57. Gross, G.; Snel, J.; Boekhorst, J.; Smits, M. A.; Kleerebezem, M. Biodiversity of mannose-specific adhesion in *Lactobacillus plantarum* revisited: Strain-specific domain composition of the mannose-adhesin. *Benef. Microbes* **2010**, *1*, 61-66.
58. Kleinert, M.; Winkler, T.; Terfort, A.; Lindhorst, T. K. A modular approach for the construction and modification of glyco-SAMs utilizing 1,3-dipolar cycloaddition. *Org. Biomol. Chem.* **2008**, *6*, 2118-2132.
59. Sato, Y.; Yoshioka, K.; Murakami, T.; Yoshimoto, S.; Niwa, O. Design of biomolecular interface for detecting carbohydrate and lectin weak interactions. *Langmuir* **2012**, *28*, 1846-1851.
60. Ingham, C. J.; Beerthuyzen, M.; Vlieg, J. v. H. Population heterogeneity of *Lactobacillus plantarum* WCFS1 microcolonies in response to and recovery from acid stress. *Appl. Environ. Microbiol.* **2008**, *74*, 7750-7758.

Chapter 4

Versatile (Bio)Functionalization of Bromo-Terminated Phosphonate-Modified Porous Aluminum Oxide

Aline Debrassi¹, Esther Roeven², Selina Thijssen¹, Luc Scheres², Willem M. de Vos^{3,4}, Tom Wennekes¹, Han Zuilhof^{1,5}

¹ Laboratory of Organic Chemistry, Wageningen University, 6703 HB Wageningen, The Netherlands

² Surfix BV, Dreijenplein 8, 6703 HB, Wageningen, The Netherlands

³ Laboratory of Microbiology, Wageningen University, 6703 HB Wageningen, The Netherlands

⁴ Department of Bacteriology & Immunology and Department of Veterinary Biosciences, University of Helsinki, 00014 Helsinki, Finland

⁵ Department of Chemical and Materials Engineering, King Abdulaziz University, 21589 Jeddah, Saudi Arabia

This chapter was published as:
Langmuir **31**, 5633-5644 (2015)

Abstract

Porous aluminum oxide (PAO) is a nanoporous material used for various (bio)technological applications, and tailoring its surface properties via covalent modification is a way to expand and refine its application. Specific and complex chemical modification of the PAO surface requires a stepwise approach in which a secondary reaction on a stable initial modification is necessary to achieve the desired terminal molecular architecture and reactivity. We here show that the straightforward initial modification of the bare PAO surface with bromo-terminated phosphonic acid allows for the subsequent preparation of PAO with a wide scope of terminal reactive groups, making it suitable for (bio)functionalization. Starting from the initial bromo-terminated PAO, we prepared PAO surfaces presenting various terminal functional groups, such as azide, alkyne, alkene, thiol, isothiocyanate, and *N*-hydroxysuccinimide (NHS). We also show that this wide scope of easily accessible tailored reactive PAO surfaces can be used for subsequent modification with (bio)molecules, including carbohydrate derivatives and fluorescently labeled proteins.

Introduction

Porous aluminum oxide (PAO) is a nanoporous support used for various advanced (bio)technological applications. These applications can be considerably extended and refined when the surface properties of PAO are tailored by chemical modification.¹ PAO has previously been chemically modified in various ways, including with hydrophobic molecules to prepare corrosion-resistant surfaces,² with antibodies to detect pathogenic bacteria^{3, 4} or biomarkers linked to cancer progression,⁵ with single-stranded DNA probes for DNA sensing,⁶ and with carbohydrates to study the binding of lectins.⁷ We are interested in the covalent biofunctionalization of PAO for the selective capture and growth of microorganisms and have previously reported on this using carbohydrates on PAO.^{8, 9}

In order to attach a biomolecule of interest, such as a carbohydrate, to the PAO surface, a secondary chemical modification of an initial self-assembled PAO monolayer is often required. In view of this, we were interested in identifying a specific stable PAO monolayer that could be used as a starting platform to subsequently generate surfaces with a wide range of terminal reactive groups and thereby allow for a tailored choice in

the final biofunctionalization step. The first prerequisite in this is that the initial chemical modification of PAO is stable under the conditions of its intended application, the field of microbiology in our case. We have recently reported the first comprehensive stability study of PAO modified with a wide range of functional groups known to chemically bind to aluminum oxide. This study showed that PAO modified with phosphonic acids possesses remarkable stability over a range of pH values and temperatures encountered during biotechnological applications. In that work, a stable azide-terminated PAO surface was prepared from a Br-terminated PAO via a substitution reaction.⁹ This prompted us to further investigate the scope of such Br-terminated monolayers. The potential of halide-terminated monolayers to obtain other terminal groups is significant and has been reviewed by Haensch et al.¹⁰ For example, on silicon oxide surfaces, azide,¹¹⁻¹⁶ thiocyanate,^{11, 12} sulfide,¹² amine,^{13, 17} sulfonate,^{14, 18} thioacetate,¹⁴ nitrile,¹⁴ and alkyne¹⁶-terminated monolayers have been prepared from bromo-terminated monolayers,¹¹⁻¹⁶ whereas analogous reactions have been performed using chlorine¹⁷ or iodine^{17, 18}-terminated silane monolayers. Considering this wide array of chemical modification options for bromo-terminated monolayers combined with the excellent stability of phosphonic acid PAO modification, we decided to investigate a bromo-terminated phosphonic acid PAO modification as the starting point to further explore its versatility to enable the (bio)functionalization of PAO.

Our objective in this study was therefore to explore the scope of reactions that would allow a subsequent mild and facile (bio)functionalization of the PAO surface starting from a stable and well-defined initial Br-terminated PAO surface (**PAO-Br**), itself easily prepared using a bromo-terminated phosphonic acid. To this aim, we evaluated seven terminal functional groups, the selection of which is explained below, namely, alkyne, azide, alkene and thiol to enable click reactions; amine, *N*-hydroxysuccinimide and isothiocyanate for protein immobilization (**Figure 1**). The most popular click reaction used to immobilize (bio)molecules on surfaces is the copper-catalyzed azide-alkyne cycloaddition (CuAAC) reaction,¹⁹⁻²³ which can be performed under various reaction conditions and tolerates most functionalities. The CuAAC reaction on the PAO surface can be performed using two approaches: surface-bound azide moieties to react with alkynes in solution, and surface-bound alkyne moieties to react with azides in solution. The main drawback of the CuAAC reaction is the necessity of a copper catalyst, which cannot always be removed and might be toxic to cells. One

way to circumvent the use of a metal catalyst is the strain-promoted azide-alkyne cycloaddition (SPAAC) reaction, which would require the conjugation of cyclooctynes onto the surface or to the (bio)molecule of interest.^{24, 25} Another click reaction that does not require any metal catalysis and which we investigated in this study is the reaction between thiols and alkenes, called the thiol-ene reaction, on the PAO surface. Apart from the absence of metal catalysts, thiol-ene reactions by virtue of their light-initiated nature, also allow for photopatterning of the surface, including the site-specific immobilization of proteins through the thiol groups of their cysteine residues.²⁶ In a similar manner as in the CuAAC reaction, the thiol-ene reaction can also be performed using two different approaches: with the alkene on the surface and the thiol in solution, or with the thiol on the surface and the alkene in solution. The thiol-terminated surface used for the thiol-ene reaction can also be used to attach maleimide-containing (bio)molecules. The maleimide-thiol coupling is a well-established and popular bioconjugation method and various maleimide-containing (bio)molecules, including many proteins, are commercially available. Two other popular methods for protein bioconjugation are the use of *N*-hydroxysuccinimide (NHS) or isothiocyanate activated (bio)molecules.²⁷ The amide coupling between the amine groups of a protein and a NHS-terminated surface is one of the most frequently used methods to immobilize proteins on a surface.²⁸ Isothiocyanate-terminated surfaces, on the other hand, have not been extensively investigated for immobilization of biomolecules on surfaces,²⁹ although they are more stable than NHS-terminated surfaces but are also correspondingly less reactive.

The current article presents a study of the efficacy of these surface modifications starting from **PAO-Br** by a series of optimized preparation protocols and a detailed analysis of the resulting surfaces using a range of surface-sensitive techniques, including X-ray photoelectron spectroscopy (XPS), transmission infrared spectroscopy (IR), and fluorescence microscopy. The resulting set of surfaces displays the potential of this two-step modification of PAO to obtain a very wide range of biologically relevant surface modifications of this surface.

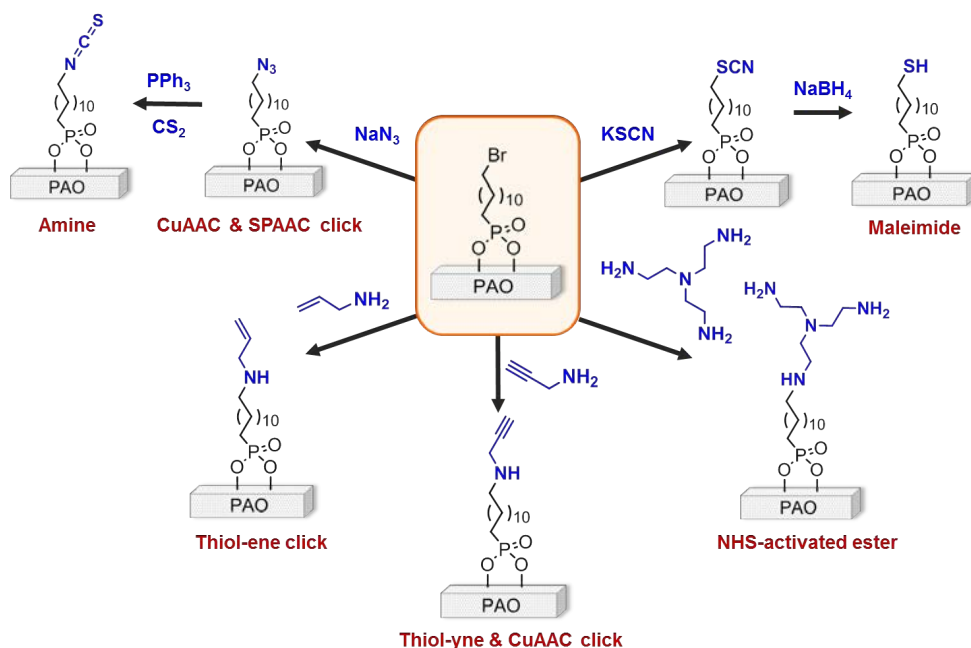


Figure 1. Scope of reactions to functionalize PAO starting from the **PAO-Br** surface and (in red) their potential for further (bio)functionalization reactions.

Materials and Methods

Materials

Porous aluminum oxide (PAO) substrates with dimensions of $36 \times 8 \text{ mm}^2$ and average pore size of 200 nm were purchased from MicroDish BV (Netherlands). 12-Bromododecylphosphonic acid was purchased from SiKÉMIA (France). 16-Fluorohexadec-1-yne,³⁰ 1-(11-azidoundecanyl)- α -D-mannopyranoside,⁹ and 3-(2,2,2-trifluoroethoxy)prop-1-ene³¹ were synthesized as previously described. Streptavidin-fluorescein isothiocyanate conjugate (strep-FITC) was purchased from Thermo Fisher Scientific (USA). Dichloromethane and THF were purified using a Pure Solv 400 solvent purification system (Innovative Technology, USA). Dry DMF was purchased in SureSeal™ bottles and stored under argon. Ultrapure water was produced using a Milli-Q Integral 3 system (Millipore, France). Other solvents used were of analytical grade. The other chemicals were obtained from Sigma-Aldrich and used without further purification. Molecular sieves (10 Å) were oven-dried (120 °C, overnight) directly prior to use. For

the thiol-ene reactions, a 6 W 365 nm UV lamp was used. Sonication steps were performed in an Elmasonic P 30 H ultrasonic unit at a frequency of 80 kHz (at a lower frequency setting, the PAO breaks).

Characterization of modified PAO surfaces

The modified PAO substrates were characterized by infrared (IR) and X-ray photoelectron spectroscopy (XPS). IR spectra were measured with a Bruker Tensor 27 FT-IR spectrometer. Spectra were obtained in transmission mode using a spectral resolution of 2 cm⁻¹ and 256 scans in each measurement. The raw spectra were divided by the spectrum of a freshly cleaned and etched bare PAO reference substrate. XPS measurements were performed using a JPS-9200 photoelectron spectrometer (JEOL). The spectra were obtained using a monochromatic Al K α X-ray radiation at 12 kV and 20 mA under ultrahigh vacuum conditions. The binding energies were calibrated at 285.0 eV for the C 1s peak as a reference. Because of electrostatic surface charging, charge neutralization was used with electrons with a kinetic energy of 2.8 eV and a filament current of 4.8 A. High-resolution spectra were corrected using a linear background subtraction before fitting. The spectra were processed using CasaXPS software (version 2.3.15). In the case of attachment of proteins, for fluorescence microscopy, an Olympus BX-41 fluorescence microscope equipped with U-MWIBA filters (Olympus) and a Kappa CCD camera was used.

Modification of PAO with 12-bromododecylphosphonic acid

The substrate preparation procedure was the same as previously reported by us.⁹ Briefly, a PAO substrate was rinsed and sonicated in acetone (5 min) and ultrapure water (5 min). Next, the substrate was immersed in a freshly prepared mixture of 37% hydrochloric acid and methanol (1:1 v/v) for 30 min. It was then rinsed and sonicated in ultrapure water (5 min) and absolute ethanol (5 min). The PAO substrate was immersed in a 1 mM solution of 12-bromododecylphosphonic acid in absolute ethanol for 16 h at room temperature. Afterward, it was rinsed with absolute ethanol and heated at 140 °C under vacuum for 6 h. The substrate was rinsed and sonicated in absolute ethanol (twice for 5 min) and dichloromethane (5 min) and dried in air to obtain the bromo-terminated PAO (**PAO-Br**).

Substitution reactions on PAO-Br

To obtain the azide-terminated PAO (**PAO-N₃**), the **PAO-Br** substrate was immersed in a 0.1 M NaN₃ solution in dry DMF for 16 h at 60 °C under argon. To obtain the alkene- and alkyne-terminated PAO (**PAO-ene** and **PAO-yne**, respectively), the **PAO-Br** substrate was immersed in a 2.0 M solution of allylamine (for **PAO-ene**) or propargylamine (for **PAO-yne**) in DMF for 16 h at 45 °C. To obtain the thiocyanate-terminated PAO (**PAO-SCN**), the **PAO-Br** substrate was immersed in a 0.5 M solution of KSCN in DMF for 16 h at 45 °C. **PAO-SCN** was then used to prepare the thiol-terminated PAO (**PAO-SH**) by reducing the thiocyanate group. For the reduction step, the **PAO-SCN** substrate was immersed in a 0.5 M solution of NaBH₄ in ethanol for 3 h at room temperature. After the reaction, the substrate was rinsed, sonicated in ethanol (5 min) and dichloromethane (5 min), and dried in air. To obtain the amine-terminated PAO (**PAO-NH₂**), the **PAO-Br** substrate was immersed in a 1.0 M solution of tris(2-aminoethyl)amine in DMF for 16 h at room temperature. After all substitution reactions on **PAO-Br**, the substrates were rinsed, sonicated in DMF (5 min), ethanol (5 min), and dichloromethane (5 min) and dried in air.

Copper-catalyzed azide-alkyne cycloaddition (CuAAC) reaction on azide-terminated PAO (PAO-N₃)

A solution containing 2.5 mM 16-fluorohexadec-1-yne, 5 mM CuSO₄ and 5 mM sodium ascorbate was prepared in DMF. A reaction tube was equipped with a stirring bar and a custom-made Teflon platform to prevent the stirring bar from breaking the fragile PAO substrate. The **PAO-N₃** substrate was placed on top of the platform in the reaction tube, and the solution was added and heated in a microwave oven (CEM Discover) at 50 °C for 30 min under stirring. After the reaction, the substrate was thoroughly rinsed, sonicated in DMF (5 min), ethanol (5 min), and dichloromethane (5 min), and dried in air.

Strain-promoted azide-alkyne cycloaddition (SPAAC) on PAO-N₃

A diluted version of the **PAO-N₃** surface (azide-, octylphosphonic acid-terminated 50:50) was immersed in a solution containing 5.0 mM 2,5-dioxopyrrolidin-1-yl 1-(bicyclo[6.1.0]non-4-yn-9-yl)-3,14-dioxo-2,7,10-trioxa-4,13-diazaoctadecan-18-oate

BCN-NHS) in dichloromethane for 4 h at room temperature. After the reaction, the substrate was rinsed, sonicated in dichloromethane (5 min), and dried in air.

CuAAC reaction on alkyne-terminated PAO (PAO-yne)

The CuAAC reaction was performed on the **PAO-yne** substrate as previously reported by us,⁹ using the same reaction tube, stirring bar, and platform as described for the CuAAC reaction on **PAO-N₃**. The **PAO-yne** substrate was immersed in a solution containing 0.1 mM 1-(11-azidoundecanyl)- α -D-mannopyranoside, 0.2 mM CuSO₄, and 0.2 mM sodium ascorbate in ultrapure water and heated in a microwave oven at 70 °C for 30 min under stirring. After the reaction, the substrate was thoroughly rinsed, sonicated in ultrapure water (5 min), ethanol (5 min), and dichloromethane (5 min), and dried in air.

Thiol-ene reaction on alkene-terminated PAO (PAO-ene)

A **PAO-ene** substrate was immersed in a solution containing 0.4 M 1-thio- β -D-glucose tetraacetate and 0.1 M 2,2-dimethoxy-2-phenylacetophenone (DMPA) in dichloromethane and irradiated with a 365 nm UV light for 2 h. After the reaction, the substrate was rinsed, sonicated in dichloromethane (twice for 5 min), and dried in air. After immobilization on the PAO surface, the surface-bound tetraacetate glucoside was deacetylated by immersion of the surface in a 2.0 mM solution of sodium methoxide in methanol for 4 h at room temperature, followed by addition of Dowex 50 (H⁺ form) to this solution and stirring until the pH was 7. Subsequently, the substrate was taken out of the solution, rinsed, sonicated in methanol (5 min), ethanol (5 min), and dichloromethane (5 min), and dried in air.

Thiol-ene reaction on thiol-terminated PAO (PAO-SH)

A **PAO-SH** substrate was immersed in a solution containing 0.5 M 3-(2,2,2-trifluoroethoxy)prop-1-ene and 0.01 M DMPA in dichloromethane and irradiated with a 365 nm UV lamp for 1 h. After the reaction, the substrate was rinsed and sonicated in dichloromethane (twice for 5 min).

Maleimide-thiol coupling reaction on thiol-terminated PAO

A **PAO-SH** substrate was immersed in a 5 mM solution of alkyne-PEG4-maleimide in phosphate-buffered saline (PBS), pH 7.0, for 16 h at room temperature. After the

reaction, the substrate was rinsed, sonicated in water (5 min), ethanol (5 min), and dichloromethane (5 min), and dried in air.

Transformation of PAO-N₃ into isothiocyanate-terminated PAO (PAO-NCS) and reaction with fluorinated amine

A **PAO-N₃** substrate was immersed in a 0.5 M solution of triphenylphosphine in dry THF (2 mL) with approximately 0.4 g of oven-dried 10 Å molecular sieves. Immediately, 3 mL of carbon disulfide was added, and the substrate was allowed to stay in this mixture for 1.5 h at room temperature. Afterward, the mixture with the substrate was kept at 50 °C for 2.5 h. Subsequently, the substrate was rinsed, sonicated in THF (5 min) and dichloromethane (5 min), and dried in air. For the subsequent reaction with a fluorinated amine, a **PAO-NCS** substrate was immersed in a solution containing 1 M trifluoroethylamine and 1 M DIPEA in dichloromethane for 16 h at room temperature. The substrate was then rinsed and sonicated in dichloromethane (5 min).

Immobilization of protein on N-hydroxysuccinimide-terminated PAO (PAO-NHS)

The first step was to generate the **PAO-NHS** substrate. For this reaction, the **PAO-NH₂** substrate was immersed in a solution containing 0.1 M *N,N'*-disuccinimidyl carbonate (DSC) and 0.1 M *N,N*-diisopropylethylamine (DIPEA) in DMF at 40 °C for 16 h. After the reaction, the substrate was rinsed, sonicated in DMF (5 min) and dichloromethane (5 min), and dried in air to obtain the **PAO-NHS** substrate. For the immobilization of the protein on the **PAO-NHS** substrate, a solution of fluorescently labeled bovine serum albumin (with fluorescein isothiocyanate: BSA-FITC; 0.1 mg/mL) was prepared in PBS, pH 7.0, containing 0.05% Tween 20. The substrate was immersed in the BSA-FITC solution for 30 min at room temperature, thoroughly washed with PBS, and immersed in a 1.0 M solution of ethanolamine in PBS for 30 min at room temperature. The substrate was thoroughly washed with PBS, dried under vacuum for 15 min, and imaged by fluorescence microscopy. A **PAO-NHS** substrate previously blocked with a 1.0 M solution of ethanolamine in PBS for 30 min at room temperature was used as the negative control for this experiment. The negative control was treated in the same way as the **PAO-NHS** substrate for the immobilization of the protein. The same procedure was also performed with BSA (nonfluorescently labeled) to obtain the **PAO-BSA** surfaces and the resulting samples were used for the bacterial growth experiment.

Immobilization of biotin on PAO and binding of streptavidin

To obtain the biotin-terminated PAO (**PAO-biotin**), the **PAO-NH₂** substrate was immersed in a solution containing 10 mM biotinamido hexanoic acid *N*-hydroxysuccinimide ester and 20 mM DIPEA in DMF at 40 °C for 16 h. After the reaction, the substrate was rinsed, sonicated in DMF (5 min), ethanol (5 min), and dichloromethane (5 min), and dried in air to obtain the **PAO-biotin** substrate. The **PAO-biotin** substrate was then immersed in a solution containing 0.1 M *N,N'*-disuccinimidyl carbonate (DSC) and 0.1 M DIPEA in DMF at 40 °C for 16 h, and then in a 1.0 M solution of ethanolamine in PBS for 30 min at room temperature to block the remaining amino groups. Finally, the substrate was rinsed, sonicated in water (5 min), ethanol (5 min), and dichloromethane (5 min), and dried in air. For the binding of strep-FITC, the **PAO-biotin** substrate was immersed in a solution containing 0.05 mg/mL of strep-FITC in PBS, pH 7.0, containing 0.05% Tween 20 for 30 min at room temperature. The substrate was thoroughly washed with PBS, dried under vacuum for 15 min, and imaged using fluorescence microscopy. The negative control used for this experiment was the same as that described in section above, and it was treated in the same way as the **PAO-biotin** substrate for the binding of strep-FITC.

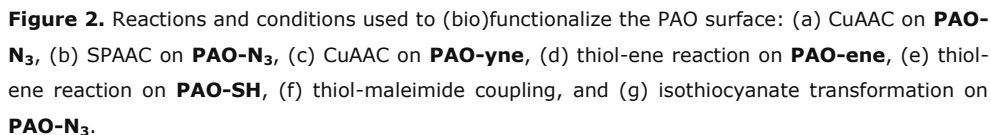
Bacterial growth on PAO-BSA

An overnight culture of *Lactobacillus plantarum* WCFS1³² in MRS broth (Difco Lactobacilli MRS broth, BD, Amsterdam, The Netherlands) was diluted with ultrapure water to obtain an optical density at 600 nm (OD₆₀₀) of 0.5. The **PAO-BSA** surfaces were cut in pieces of approximately 9 × 8 mm² and placed on MRS agar plates. The bacterial suspension at OD₆₀₀ = 0.5 was placed on the **PAO-BSA** surfaces (3 µL per sample) and incubated at 37 °C. The samples were imaged after 0, 5, and 7 h using transmission light. One sample was also stained with 5-carboxyfluorescein diacetate (cFDA) at each time point by placing the **PAO-BSA** surfaces on low-melting point agarose (BioRad, USA) that contained 50 µM cFDA for 30 min. The cFDA-stained samples were also imaged using fluorescence microscopy. The contrast and the color of the fluorescence images were adjusted using ImageJ.

Results and Discussion

Modification of porous aluminum oxide (PAO) with 12-bromododecylphosphonic acid

The first step involves modification of acid-activated PAO with 12-bromododecylphosphonic acid (1 mM in EtOH, 16 h, rt, followed by vacuum drying at 140 °C for 6 h) to produce the bromo-terminated PAO (**PAO-Br**), the starting point for all subsequent reactions (**Figure 2**). The X-ray photoelectron spectroscopy (XPS) survey scan of **PAO-Br** (**Figure 3a**) clearly shows the presence of a Br 3s peak at 257 eV, in addition to the peaks corresponding to the other components of the phosphonic acid and the PAO substrate (O at 531 eV, C at 285 eV, P at 134 eV, and Al at 119 eV), confirming the modification of PAO. The XPS C 1s narrow scan (**Figure 3b**) presents two types of carbon: \underline{C} -C (285.0 eV) and carbon bound to an electronegative element, in this case \underline{C} -Br (286.5 eV), and the ratio between them is as expected for an intact Br-terminated monolayer (11 \underline{C} -C or \underline{C} -P,⁹ 1 \underline{C} -Br). This initial monolayer showed good stability upon immersion of the surface in PBS, pH 7.0, with less than 10 and 20% degradation after 2 and 24 h, respectively. The stable **PAO-Br** surface was then used as the starting point for all the subsequent reactions explored in this work (**Figure 2**).



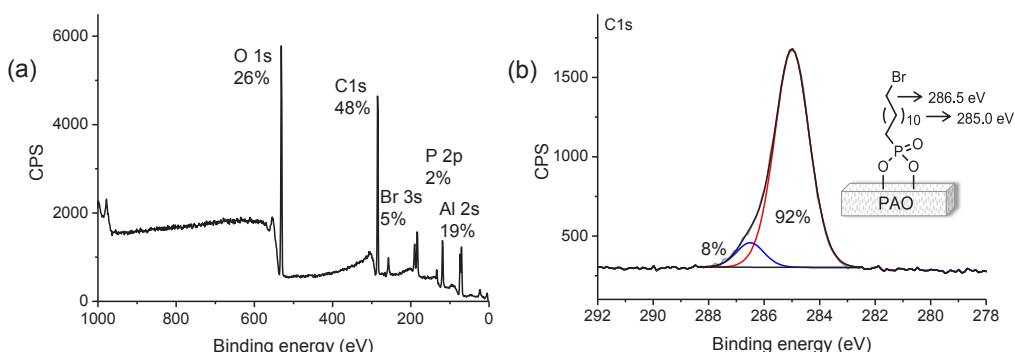


Figure 3. XPS spectra of **PAO-Br**: (a) survey scan and (b) C 1s narrow scan.

Copper-catalyzed azide-alkyne cycloaddition (CuAAC) on azide-terminated PAO (PAO-N₃)

For the first approach, the initial step was a substitution reaction with NaN₃ on the **PAO-Br** substrate. In this work, the concentration of the NaN₃ solution was decreased from 1.0 M in our previous study to 0.1 M without any change in the resulting **PAO-N₃** surface,⁹ according to the XPS spectra. The XPS spectra show the absence of bromine remaining on the surface, indicating the full conversion to **PAO-N₃**, and two separated peaks in the N 1s narrow spectrum at 400.5 and 404.4 eV with a 2:1 ratio, respectively, characteristic of the azide group³³ (**Figure SI-1** for XPS data).

The **PAO-N₃** substrate was then used to react with a fluorinated alkyne (1-fluorohexadec-1-yne) as a model system, using the high sensitivity of fluorine in XPS. The yield of this reaction was near-quantitative based on the C 1s spectrum of the reacted surface, which shows the presence of three types of carbon: C-C (285.0 eV), C-N (286.5 eV), and C-F (288.0 eV), with an experimental ratio of 84 / 12 / 4%, which matches the theoretical ratio (85 / 11 / 4%). The N 1s spectrum shows the characteristic peaks of the triazole ring at 400.5 and 401.8 eV,³³ which appear as a broad peak instead of the two separated peaks from the **PAO-N₃** surface (**Figure 4**). In combination with the nearly complete loss of the 404.5 eV peak, this indicates that most of the azide present on the surface reacted with the alkyne (**Figure SI-1** for corresponding wide scan XPS).

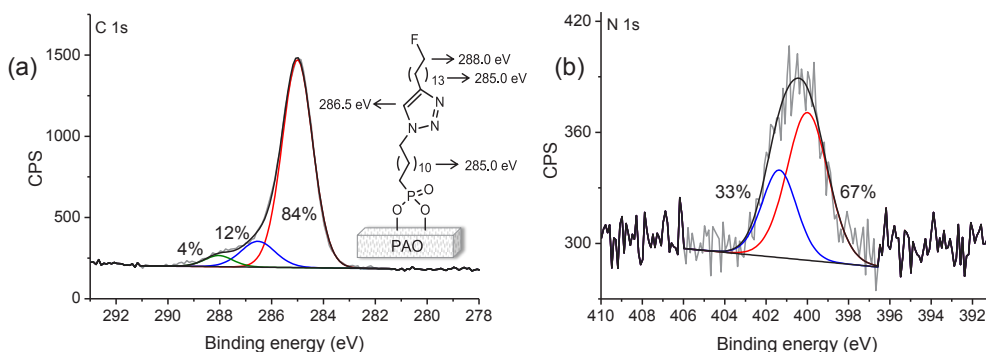


Figure 4. XPS spectra of modified PAO after the CuAAC reaction between **PAO-N₃** and 1-fluorohexadec-1-yne: (a) C 1s and (b) N 1s narrow scans.

The infrared (IR) spectra of **PAO-Br**, **PAO-N₃**, and **PAO-N₃** after CuAAC reaction with the fluorinated alkyne can also be used to monitor this sequence of reactions. The IR spectrum of the **PAO-N₃** surface shows the presence of the azide, with a strong band at around 2100 cm⁻¹.³⁴ From the decrease of this signal after the CuAAC reaction (**Figure SI-1**), a reaction efficiency of ~80% can be calculated for the CuAAC reaction, i.e., within experimental error, in line with the XPS data.

The CuAAC reaction of an alkyne molecule in solution with the **PAO-N₃** surface can be easily monitored by the characteristic peaks of the azide in the XPS spectrum of nitrogen and also by the strong azide band in IR spectra. The main advantage of this approach when compared to the reaction between an alkyne-terminated surface and an azide-containing (bio)molecule is the easy characterization of the modified surface via the distinct N₃ signals.

Strain-promoted azide-alkyne cycloaddition (SPAAC) on PAO-N₃

The **PAO-N₃** surface can also be used to immobilize (bio)molecules containing a strained cyclooctyne group via the SPAAC reaction, which does not require any catalyst. This reaction presented near quantitative conversion, based on the absence of the azide band in the IR spectrum (at around 2100 cm⁻¹) and the loss of the peak at 404.5 eV in the N 1s XPS spectrum (**Figure SI-1**).

CuAAC on alkyne-terminated PAO (PAO-yne)

The other approach for the CuAAC is the reaction between a surface-bound alkyne with azide-containing (bio)molecules in solution.¹⁹ The required alkyne-

terminated PAO (**PAO-yne**) can also be obtained starting from the **PAO-Br** surface, via a substitution reaction with propargylamine. The XPS spectrum of the **PAO-yne** surface indicates full conversion to the alkyne-terminated surface because of the absence of any bromine peak. The successful subsequent CuAAC reaction with an azido mannoside can be visualized by the changes in the C 1s narrow spectrum, with the additional peak at 288.6 eV, corresponding to the O- \underline{C} -O carbon of the carbohydrate, and the increase of the peak at 286.5 eV, corresponding to the \underline{C} -O and \underline{C} -N carbons (**Figures SI-2 and SI-3**). The presence of the alkyne on the **PAO-yne** surface can also be observed in the IR spectrum as a $\equiv\text{C-H}$ stretching at 3323 cm^{-1} (**Figure SI-4**).

Thiol-ene reaction on alkene-terminated PAO (PAO-ene)

In a similar manner as with the CuAAC click, the thiol-ene reaction can also be performed on PAO using either of two different approaches: with the alkene on the PAO surface and the thiol in solution or with the thiol on the surface and the alkene in solution. Both approaches are again possible starting from the initial **PAO-Br** surface. In the first approach, by reacting an alkene-containing amine with the bromo-terminated surface, we near quantitatively obtain alkene-terminated PAO surfaces (**PAO-ene**, **Figure SI-5**; no Br signal present after the reaction), which can further react with (bio)molecules containing a thiol group in solution in the presence of UV light (365 nm) and 2,2-dimethoxy-2-phenylacetophenone (DMPA) as photoinitiator.

As proof of principle, 1-thio- β -D-glucose tetraacetate was immobilized on **PAO-ene**, yielding the acetyl-protected glucose-terminated PAO surface (**PAO-ene-gluAcO**) with approximately 60% conversion, according to both wide scan XPS data (**Figure SI-6**) and the narrow scan C 1s spectrum. The XPS spectrum of the C 1s region of the **PAO-ene-gluAcO** surface presents four different types of carbon: \underline{C} -C (285.0 eV), \underline{C} -O/ \underline{C} -N/ \underline{C} -S (286.4 eV), O- \underline{C} -S (287.6 eV), and \underline{C} =O (289.7 eV) (**Figure 5a**). The attachment of the intact protected sugar can be observed from the \underline{C} -C to \underline{C} -O/ \underline{C} -N/ \underline{C} -S to O- \underline{C} -S to \underline{C} =O ratio of 66 / 20 / 5 / 9% (theory: 54 / 28 / 4 / 14% for 100% conversion). After the immobilization reaction, the glucose present on the PAO surface was deprotected by immersing the **PAO-ene-gluAcO** in a solution of sodium methoxide in methanol to obtain the deprotected carbohydrate, which is then suitable for use in biological experiments. The C 1s XPS spectrum of the surface after deprotection (**Figure 5b**) shows full deprotection of glucose by the absence of the C=O peak at 289.7 eV and a \underline{C} -

O/C-N/C-S to O-C-S ratio in line with expectations (both experiment and theory: 24 / 3%). The IR spectra of the same PAO surfaces confirm the full deprotection of the glucose present on the surface by the absence of the carbonyl band at 1760 cm^{-1} after the deprotection step (**Figure SI-7**). Interestingly, the monolayer does not show any signs of degradation under this basic deprotection conditions. For example, the ratio of Al compared to other elements is not increased, as shown in the XPS wide spectra of **PAO-ene-gluAcO** before and after deprotection (**Figures SI-6 and SI-8**).

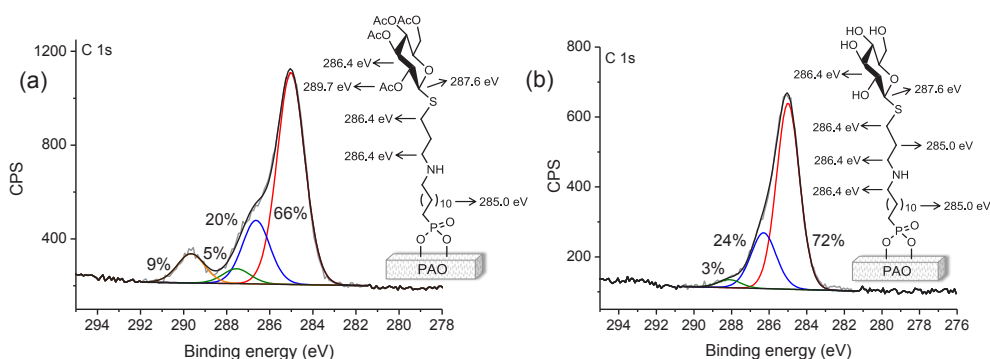


Figure 5. XPS C 1s narrow scan of PAO after reaction between **PAO-ene** and 1-thio- β -D-glucose tetraacetate (**PAO-ene-gluAcO**): (a) before and (b) after deprotection of the carbohydrate.

Thiol-ene reaction on thiol-terminated PAO (PAO-SH)

The second approach for the thiol-ene reaction involves a thiol-terminated surface, which can react with a solution containing (bio)molecules with a terminal alkene functionality. The thiol-terminated PAO surface (**PAO-SH**) was prepared from the **PAO-Br** surface via a two-step sequence: reaction with KSCN on the **PAO-Br** surface, yielding the thiocyanate-terminated PAO (**PAO-SCN**), followed by reduction with NaBH_4 to yield the surface-bound thiol groups (**PAO-SH**). The XPS survey scan of **PAO-SCN** shows complete conversion from PAO-Br, with a carbon / nitrogen / sulfur ratio that is close to the theory (experiment: 13 / 1 / 1; theory: 11 / 1 / 1), and the absence of Br peaks. The C 1s XPS spectrum of **PAO-SCN** (**Figure 6b**) shows three different peaks: C-C (285.0 eV), C-S (286.3 eV), and S-C \equiv N (287.0 eV), in a ratio fitting what is theoretically expected (experiment and theory both: 84 / 8 / 8%). Although we and others observe a chemical shift for C-S of 1.3 eV,³⁵⁻³⁸ we are aware that other authors have reported a chemical shift between 0.3 – 0.4 eV for a carbon atom adjacent to sulfur.³⁹ For the

reduction of the thiocyanate group, we initially tried to use LiAlH_4 as a reducing agent as previously reported.⁴⁰ Although different conditions were tried, the initial phosphonate modification of the surface degraded even when immersing the **PAO-SCN** surface in a 0.25 M LiAlH_4 solution in THF for only 5 min at 0 °C. We then decided to try NaBH_4 as a milder reducing agent and successfully obtained the **PAO-SH** surface. The complete reduction of the thiocyanate group without monolayer degradation could in that case be observed by the absence of the nitrogen peak in the wide range XPS spectrum (**Figure 6c**), and this was in line with the deconvoluted C 1s XPS spectrum shown in **Figure 6d**.

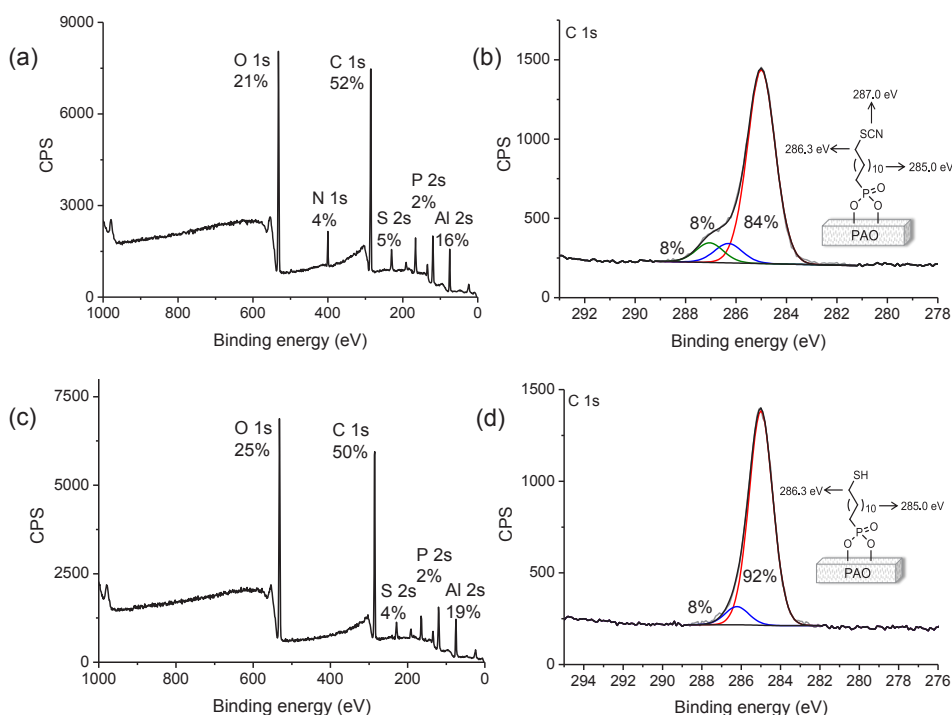


Figure 6. XPS spectra of **PAO-SCN** and **PAO-SH** surfaces: (a) **PAO-SCN** survey scan, (b) **PAO-SCN** C 1s narrow scan, (c) **PAO-SH** survey scan, and (d) **PAO-SH** C 1s narrow scan.

After the reduction, the thiol-ene reaction was performed with a fluorinated alkene ($\text{CH}_2=\text{CHOCH}_2\text{CF}_3$) for easy quantification of the reaction efficiency by XPS. The conversion of this reaction was approximately 20%, based on the amount of fluorine and carbon on the XPS survey scan (**Figure SI-9**). We considered that the formation of disulfide bridges between thiol groups present on the surface could be the reason for the low conversion. To circumvent this potential issue, we immersed the **PAO-SH** surface in a

0.1 M tris(2-carboxyethyl)phosphine (TCEP) solution in methanol for 30 min before the thiol-ene reaction. TCEP is known for reducing disulfide bonds and has been especially used with proteins.⁴¹ However, to our surprise, this step did not improve the conversion of the thiol-ene reaction. This considerably lower conversion for the thiol-ene reaction when the thiol is on the surface and the alkene is in solution might be related to the mechanism of the reaction. The initiation of the reaction involves the generation of a thiyl radical (RS^\bullet) by the treatment of the thiol with a photoinitiator. The propagation step involves first the direct addition of the RS^\bullet radical in the C=C bond, followed by the chain transfer of the radical to a second thiol moiety.⁴² This transfer of the radical to another thiol might be hampered when the thiols are on the surface, resulting in a limited conversion. In this case, considering that all of the other reactions under current study provide considerably better conversions, this approach of the thiol-ene reaction should be considered only for PAO if the other reactions are not possible.⁴³

Maleimide-thiol coupling on PAO-SH

As a proof of principle for the maleimide-thiol reaction, we reacted alkyne-PEG4-maleimide with the **PAO-SH** surface using conditions that are compatible with the attachment of biomolecules (**Figure 2f**). The conversion of this reaction was approximately 50%, based on the \underline{C} -C to \underline{C} -S/ \underline{C} -O/ \underline{C} -N to \underline{C} =O ratio (experimental: 74 / 22 / 4%; theory: 47 / 44 / 9%) (see **Figure SI-10** for the XPS spectra).

Isothiocyanate-terminated PAO (PAO-NCS)

Another reactive surface that can be obtained from **PAO-Br** is the isothiocyanate-terminated PAO (**PAO-NCS**). The first step to prepare **PAO-NCS** is the substitution with NaN_3 , as previously discussed. The transformation of the azide group into an isothiocyanate was based on a procedure described for this conversion in solution. When **PAO-N₃** is treated with triphenylphosphine, nitrogen is released due to the Staudinger reaction, and subsequent addition of carbon disulfide to the iminophosphorane-terminated intermediate surface yields **PAO-NCS**.⁴⁴ The conversion of **PAO-N₃** into **PAO-NCS** was observed by the appearance of the sulfur peak in the XPS survey scan and the presence of three carbon peaks in the XPS C 1s spectrum: \underline{C} -C (285.0 eV), \underline{C} -N (286.5 eV), and $N=\underline{C}=S$ (287.7 eV) (**Figure 7**). In a previous work, Lex and co-workers prepared isothiocyanate-terminated surfaces upon UV irradiation of

thiocyanate-terminated surfaces. However, only a limited amount of isothiocyanate (25 to 30%) was observed by them, even when almost all of the thiocyanate was consumed.²⁹ In our approach, the N 1s spectrum indicates complete conversion of the reactants because of the presence of only one peak in the N 1s spectrum, instead of the two peaks observed for the **PAO-N₃** surface. However, the slightly higher amount of nitrogen than sulfur in the XPS survey scan of **PAO-NCS** (Figure 7a) might indicate that a small part of the azide groups were converted to byproducts (most probably to amines via a Staudinger reduction due to adventitious water). The IR spectrum of the **PAO-NCS** surface shows the presence of the characteristic isothiocyanate stretching band at 2094 cm⁻¹ (**Figure SI-12**).^{29, 45} To our knowledge, this is the first time that an isothiocyanate-terminated surface was prepared via transformation of an azide group. As proof of principle for the use of **PAO-NCS**, we reacted a fluorinated amine with the **PAO-NCS** surface and obtained a moderate conversion of 18% (**Figure SI-13**). Although this conversion is not optimal yet, such an isothiocyanate-terminated surface is a possible alternative to the *N*-hydroxysuccinimide (NHS)-terminated surface. The limited conversion may be due to the formation of byproducts (mainly amine) in the azide-isothiocyanate reaction, yielding a mixed surface that is only partially reactive toward amines.

With further optimization, isothiocyanate-terminated surfaces can be used to immobilize amine-containing (bio)molecules, especially proteins. The isothiocyanate group is more stable than the NHS group, which renders it a good alternative when protein-reactive surfaces are not intended to be immediately used.

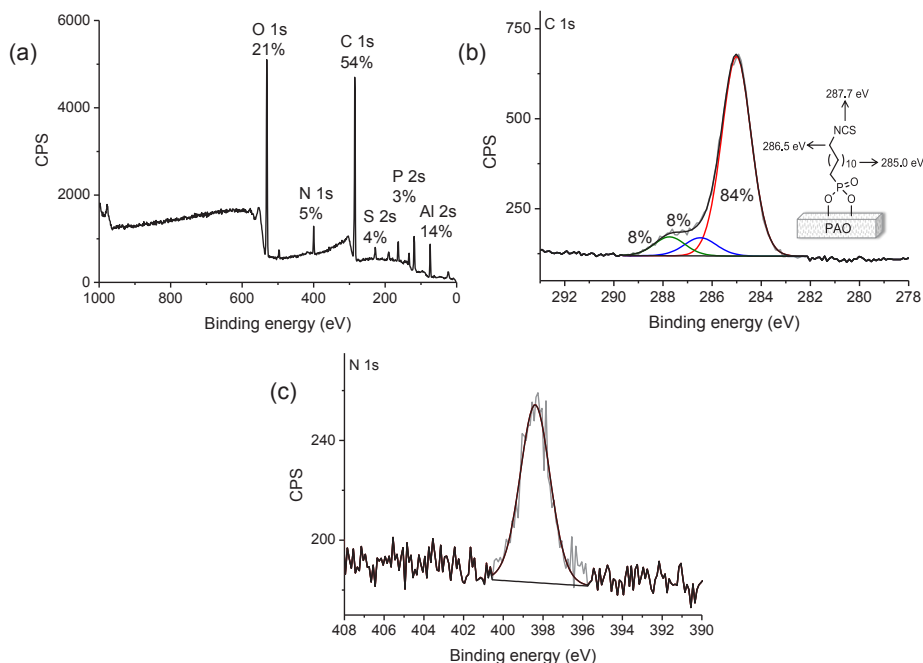


Figure 7. XPS spectra of **PAO-NCS**: (a) survey scan, (b) C 1s narrow scan, and (c) N 1s narrow scan.

Protein immobilization on NHS-terminated PAO (PAO-NHS)

Starting with a reaction of **PAO-Br** with tris(2-aminoethyl)amine, the resulting amine-terminated surface (**PAO-NH₂**) was treated with *N,N'*-disuccinimidyl carbonate (DSC) to provide the NHS-terminated PAO surface (**PAO-NHS**) (**Figure 8**). The complete substitution reaction with the amine on the **PAO-Br** surface was observed by XPS via the complete disappearance of the bromine peak in the survey scan (**Figure SI-14**). The reaction of the DSC reagent with the amine-terminated PAO surface was confirmed by the C 1s XPS spectrum (**Figure SI-15**), which presents an additional carbon peak at 288.6 eV, corresponding to the carbonyls' C atoms of **PAO-NHS**. As an additional confirmation, the IR spectrum of **PAO-NHS** presents a band at 1745 cm⁻¹, corresponding to the C=O stretching vibrations in the carbamate (**Figure SI-16**).⁴⁶

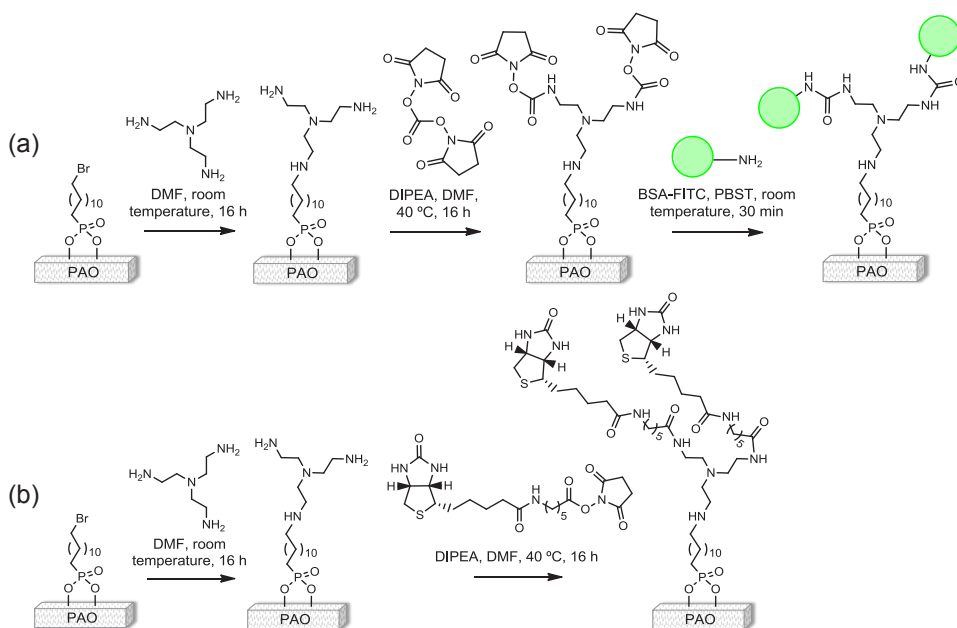


Figure 8. Immobilization of proteins on PAO: (a) BSA-FITC on **PAO-NHS** and (b) biotin-terminated PAO for binding of streptavidin.

For the immobilization of a protein on the **PAO-NHS**, we selected bovine serum albumin fluorescently labeled with fluorescein isothiocyanate (BSA-FITC) as proof of principle because the PAO surfaces with BSA-FITC can be easily visualized by fluorescence microscopy. **PAO-NHS** blocked with ethanolamine was used as a negative control to show that the BSA-FITC present on the surface was covalently attached to the surface and not just adsorbed. After immersion of both PAO surfaces in a BSA-FITC solution in PBS, pH 7.0, containing 0.05% Tween 20 and extensive washing of the surfaces, the BSA-FITC was present almost exclusively on the **PAO-NHS** surface (**Figure 9**). The same experiments were performed without Tween 20, and it was observed that the presence of Tween 20 in the BSA-FITC solution is necessary to prevent nonspecific adsorption of the protein on both surfaces (data not shown). We also tried to immobilize BSA-FITC directly on the **PAO-Br** surface, but this was not possible, probably due to the harsher reaction conditions necessary for the substitution of amines on **PAO-Br**.

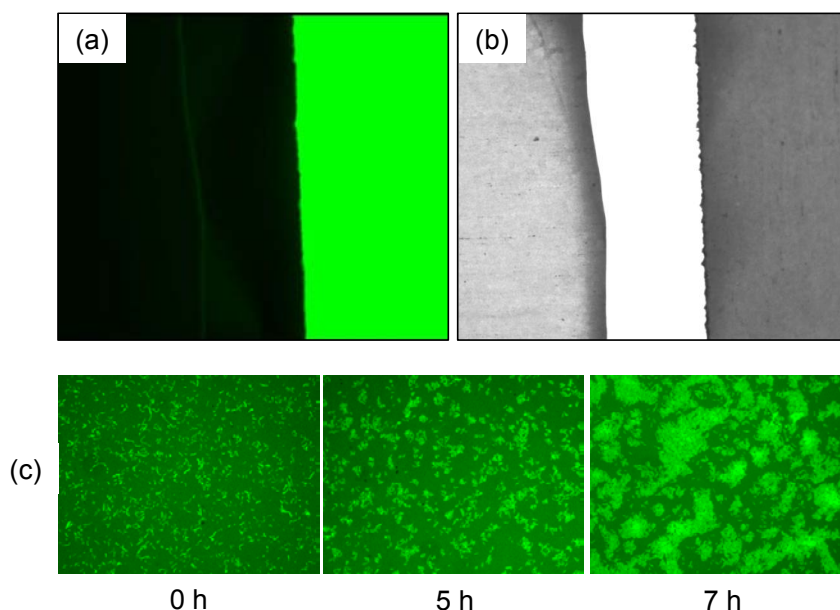


Figure 9. Immobilization of fluorescently-labeled bovine serum albumin (BSA-FITC) on **PAO-NHS** blocked with ethanolamine (left) and **PAO-NHS** (right) in PBS, pH 7.0, with 0.05% Tween 20: (a) fluorescence image and (b) transmission image; (c) growth of *L. plantarum* on **PAO-BSA** surfaces.

Immobilization of biotin on PAO and binding of streptavidin

The amine-terminated PAO surface can also be used to directly attach (bio)molecules containing a NHS group. In this case, we immobilized NHS-linked biotin onto PAO as a small recognition element for streptavidin (**Figure 8**). The attachment of the NHS-containing biotin in an >75 % yield was confirmed by the presence of a sulfur peak in the wide XPS spectrum and also the presence of three types of carbon in the XPS spectrum of the C 1s region: $\underline{\text{C}}\text{-C}$ (285.0 eV), $\underline{\text{C}}\text{-N}/\underline{\text{C}}\text{-S}$ (286.1 eV), and $\underline{\text{C}}\text{=O}$ (288.0 eV) in a 68 / 21 / 11% ratio (theory: 62 / 26 / 12%) (**Figure 10a, b**).

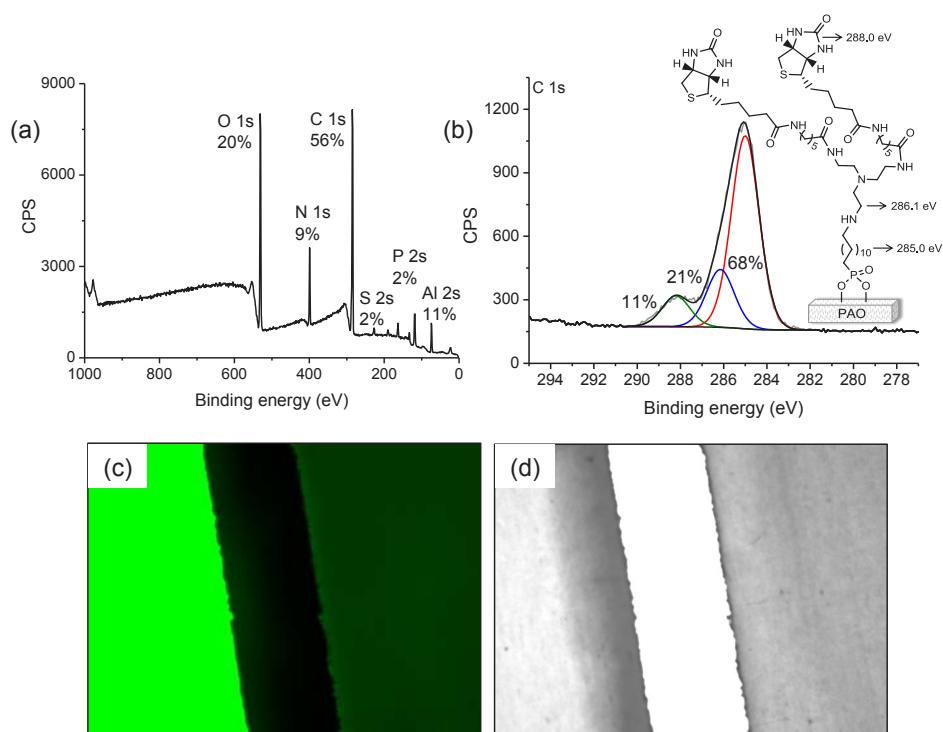


Figure 10. XPS spectra of amine-terminated PAO after reaction with biotin-NHS: (a) survey scan and (b) C 1s narrow scan. Binding of strep-FITC on biotin-terminated PAO (left) and **PAO-NHS** blocked with ethanolamine (right) in PBS, pH 7.0, with 0.05% Tween 20: (c) fluorescence image and (d) transmission image.

For the binding of streptavidin on the biotin-terminated PAO (**PAO-biotin**), any remaining amine groups present on the surface were blocked by sequential treatment with bifunctional NHS molecule and ethanolamine. The negative control for this experiment was the **PAO-NHS** surface blocked with ethanolamine, the same type of sample used as a negative control for BSA-FITC attachment. Both samples were immersed in a solution of streptavidin-fluorescein isothiocyanate conjugate (strep-FITC) in PBS, pH 7.0, containing 0.05% Tween 20 and extensively washed with PBS. The binding of strep-FITC on the biotin-terminated PAO surface was considerably higher when compared to that of the **PAO-NHS** surface blocked with ethanolamine (**Figure 10c**), indicating that the biotin present on the surface is available for binding with streptavidin.

Bacterial growth on PAO-BSA samples

In order to verify whether the immobilization of BSA on PAO does not block the pores and thereby affect its use as a culturing chip, we performed bacterial growth experiments on the **PAO-BSA** samples. Bacterial growth is possible only when the nutrients can diffuse via pores from the agar to the top PAO surface where the bacteria are located. In these experiments, we observed that the *L. plantarum* cells could still grow to microcolonies on the **PAO-BSA** surface (**Figure 9c** and **Figure SI-17**), showing that the pores are still available for the diffusion of nutrients. Additionally, the diffusion of cFDA, a small molecule fluorogenic vitality stain,⁴⁷ from the low-melting point agarose to the bacteria also shows the availability of the pores on the **PAO-BSA** surface and the viability of the bacteria present on the surface.

Conclusions and Prospects

In this study we show that porous aluminum oxide (PAO) that is modified with bromo-terminated phosphonic acid can function as a highly versatile platform for the (bio)functionalization of PAO for various applications. Using only mild reaction conditions, a range of terminal functional groups could be obtained (alkyne, azide, thiol, alkene, amine, *N*-hydroxysuccinimide (NHS), isothiocyanate, maleimide). These could be effectively and with high conversions used for a range of click reactions and as a bioconjugation handle, for example, to attach carbohydrates and proteins. Remarkably, the thiol-ene click reaction worked well with the alkene on the surface and the thiol in solution, but it worked poorly with the inverse reaction, i.e., with the thiol on the surface. In future work, we will use this **PAO-Br** platform to immobilize antibodies, lectins, and complex carbohydrates onto the PAO surface for our ongoing studies toward the selective capture and subsequent growth of bacteria on modified PAO.

Associated Content

XPS and IR spectra of the remaining modified PAO surfaces not given in the main text. The Supporting Information is available free of charge on the ACS Publications website at DOI: 10.1021/acs.langmuir.5b00853.

Acknowledgements

This work is supported by NanoNextNL, a micro and nanotechnology consortium of the Government of The Netherlands and 130 partners, ERC grant 250712 (MicrobesInside), and the Netherlands Organization for Scientific Research (NWO VENI grant 722.011.006 to T.W.).

Supporting Information

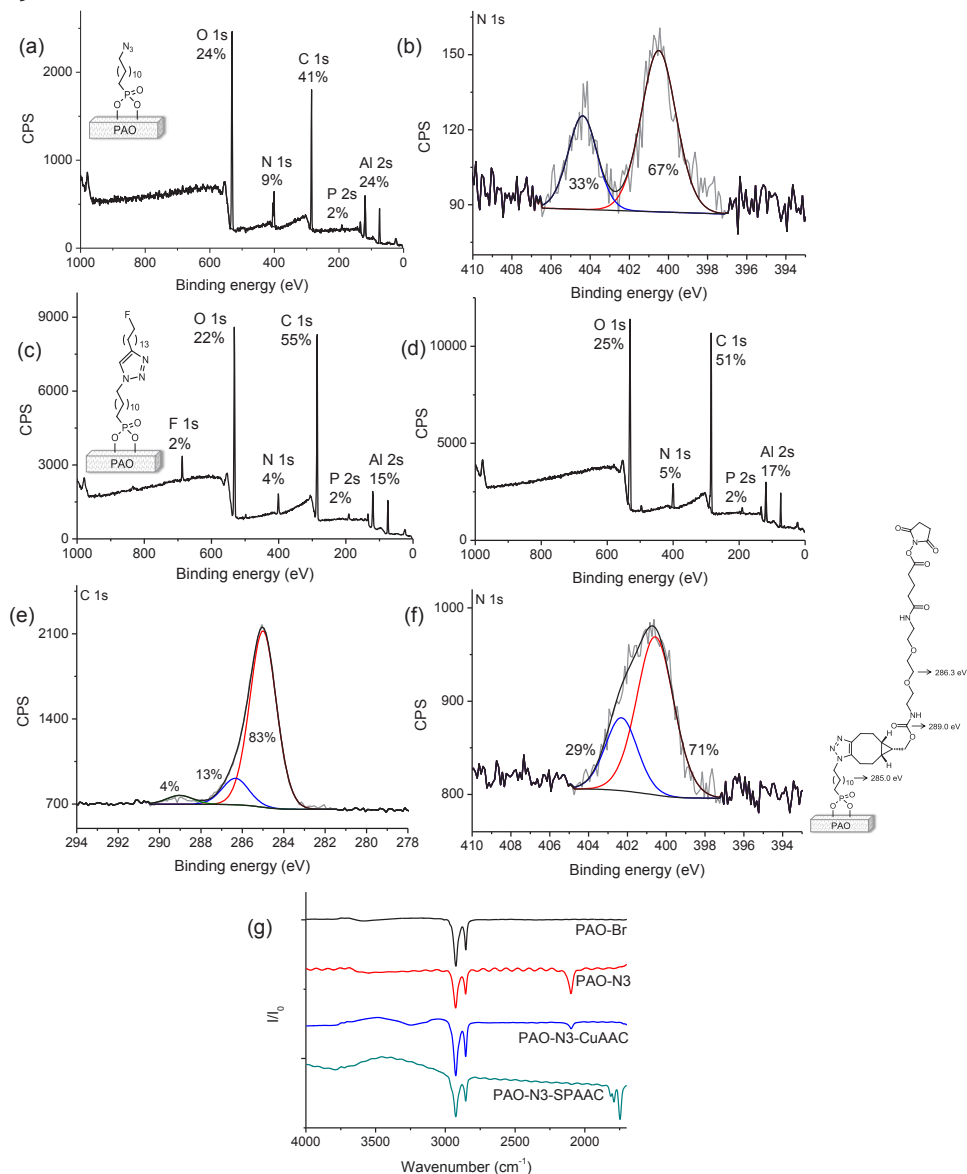
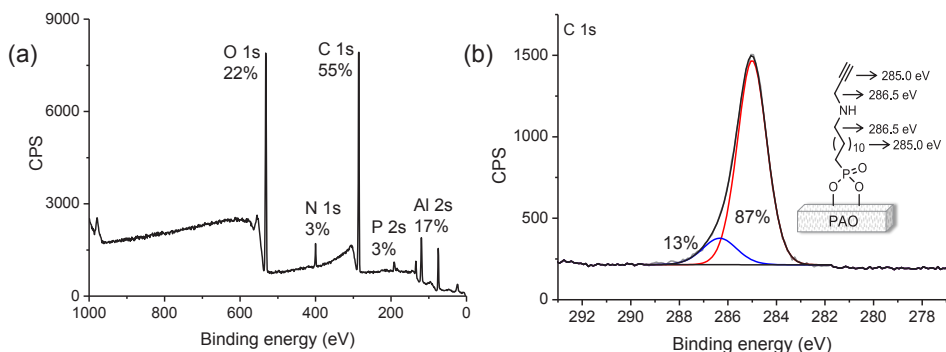
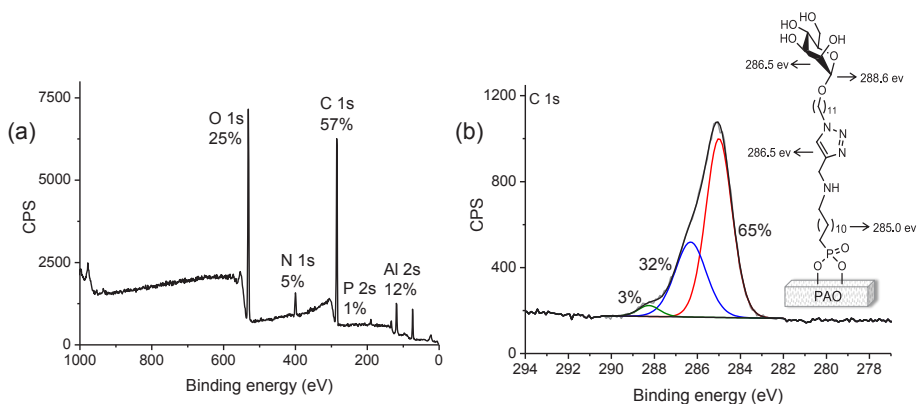
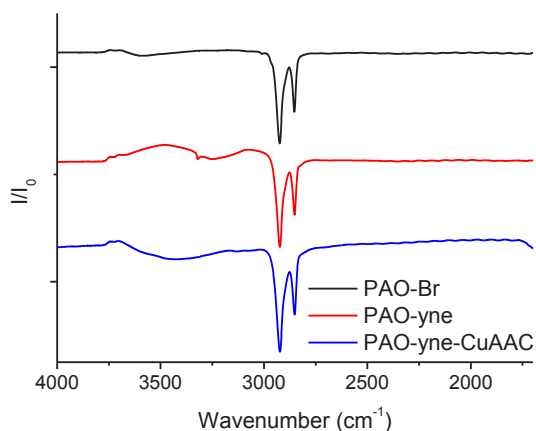
Copper-catalyzed azide-alkyne cycloaddition (CuAAC) and strain-promoted azide-alkyne cycloaddition (SPAAC) on azide-terminated porous aluminum oxide (PAO-N₃)

Figure SI-1. XPS spectra of **PAO-N₃** (a) survey scan and (b) N 1s narrow scan; (c) survey scan of **PAO-N₃** after CuAAC reaction with 1-fluorohexadec-1-yne (**PAO-N₃-CuAAC**); (d) survey scan, (e) C 1s narrow scan, and (f) N 1s narrow scan of **PAO-N₃** after SPAAC reaction with BCN-NHS (**PAO-N₃-SPAAC**); and (g) infrared (IR) spectra of bromo-terminated PAO (**PAO-Br**), **PAO-N₃**, **PAO-N₃-CuAAC**, and **PAO-N₃-SPAAC**.

CuAAC on alkyne-terminated PAO (PAO-yne)**Figure SI-2.** XPS spectra of **PAO-yne**: (a) survey scan and (b) C 1s narrow scan.**Figure SI-3.** XPS spectra of **PAO-yne** after CuAAC reaction with azido mannoside: (a) survey scan and (b) C 1s narrow scan.**Figure SI-4.** IR spectra of **PAO-Br**, **PAO-yne**, and **PAO-yne** after CuAAC reaction with azido mannoside (**PAO-yne-CuAAC**).

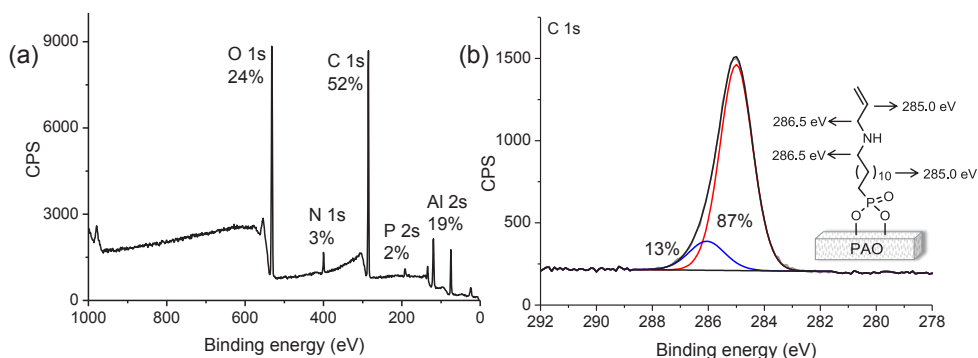
Thiol-ene on alkene-terminated PAO (PAO-ene)

Figure SI-5. XPS spectra of **PAO-ene**: (a) survey scan and (b) C 1s narrow scan.

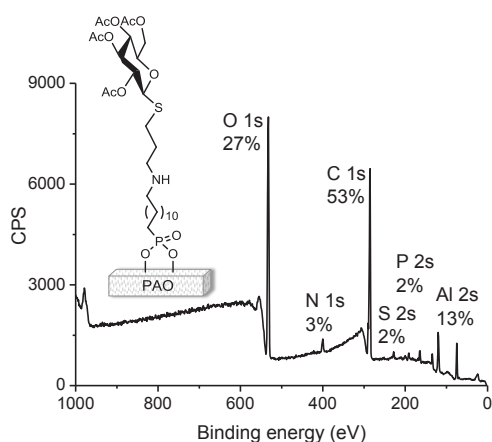


Figure SI-6. XPS survey scan of **PAO-ene** after reaction with 1-thio-β-D-glucose tetraacetate (**PAO-ene-gluAcO**).

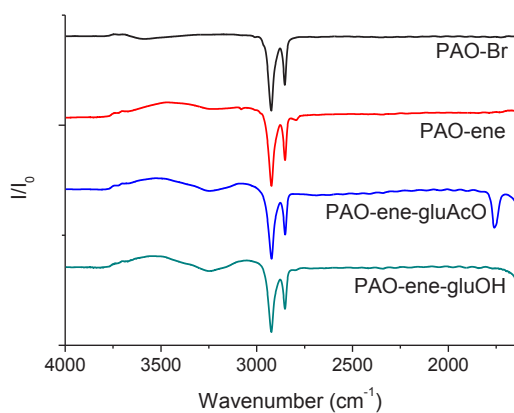


Figure SI-7. IR spectra of **PAO-Br**, **PAO-ene**, **PAO-ene-gluAcO**, **PAO-ene-gluAcO** after deprotection of the acetyl groups (**PAO-ene-gluOH**).

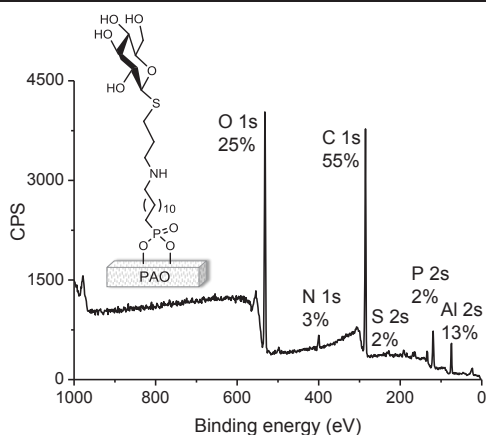


Figure SI-8. XPS survey scan of **PAO-ene-gluAcO** after deprotection of the acetyl groups.

Thiol-ene on thiol-terminated PAO (PAO-SH)

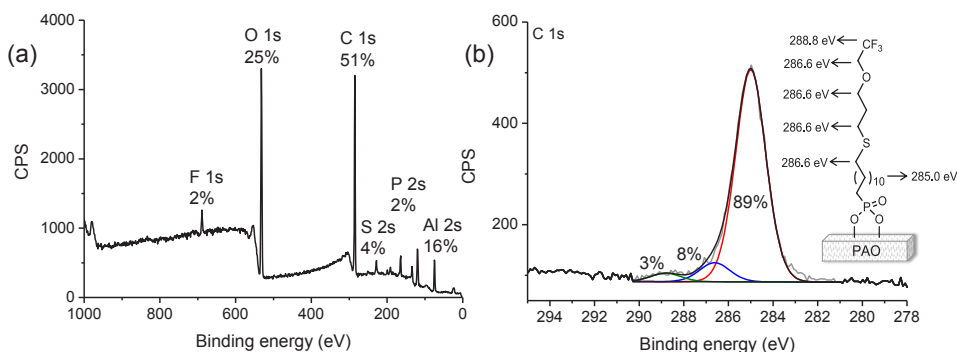


Figure SI-9. XPS spectra of **PAO-SH** after thiol-ene click reaction with fluorinated alkene: (a) survey scan and (b) C 1s narrow scan.

Maleimide-thiol coupling on PAO-SH

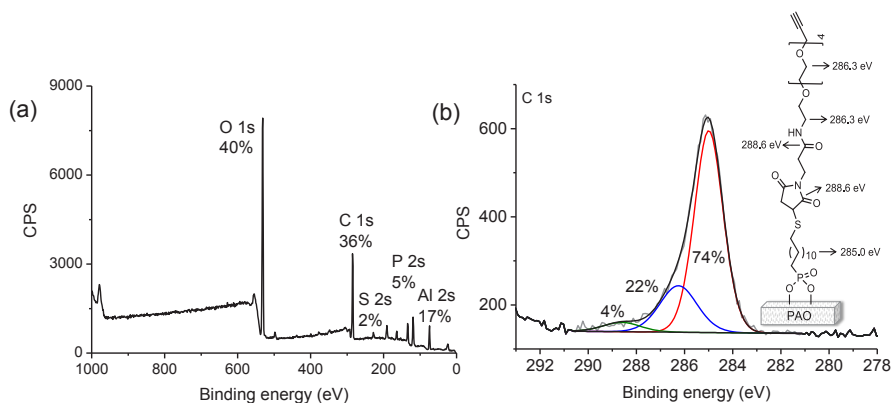


Figure SI-10. XPS spectra of **PAO-SH** after reaction with maleimide-PEG4-alkyne: (a) survey scan and (b) C 1s narrow scan.

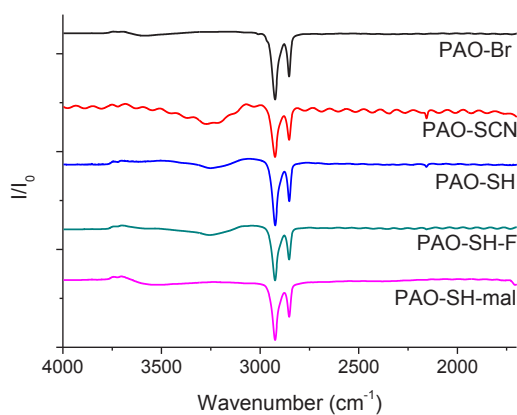


Figure SI-11. IR spectra of **PAO-Br**, thiocyanate-terminated PAO (**PAO-SCN**), **PAO-SH**, PAO-SH after thiol-ene click reaction with fluorinated alkene (**PAO-SH-F**), and **PAO-SH** after reaction with maleimide-PEG4-alkyne (**PAO-SH-mal**).

Isothiocyante-terminated PAO (**PAO-NCS**)

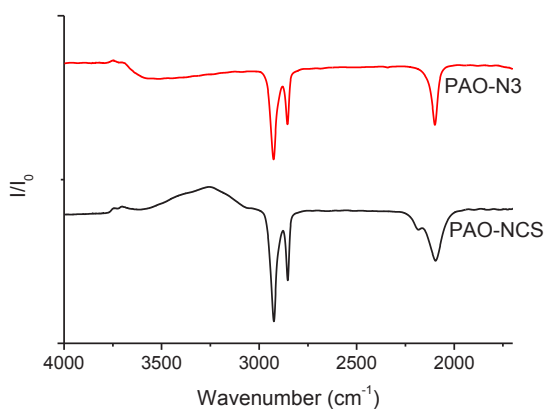


Figure SI-12. IR spectra of **PAO-NCS** compared to **PAO-N₃**.

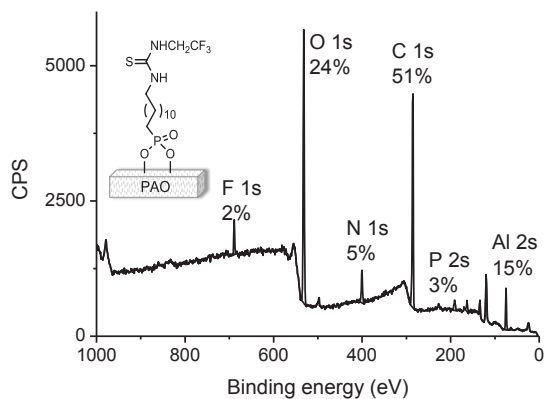
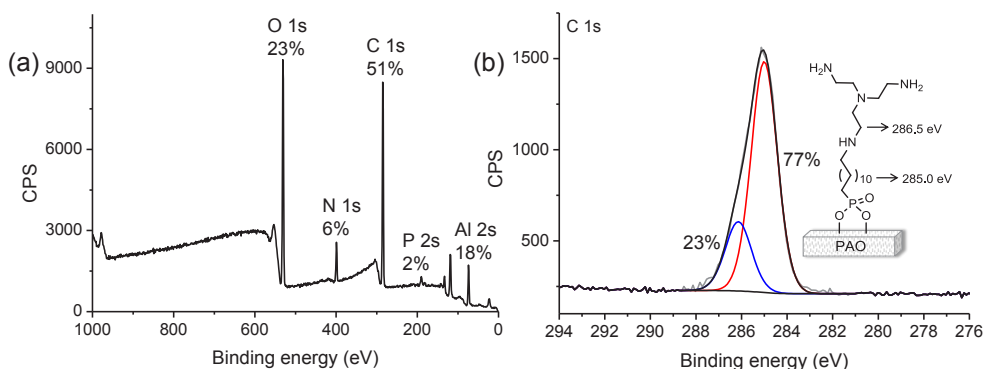
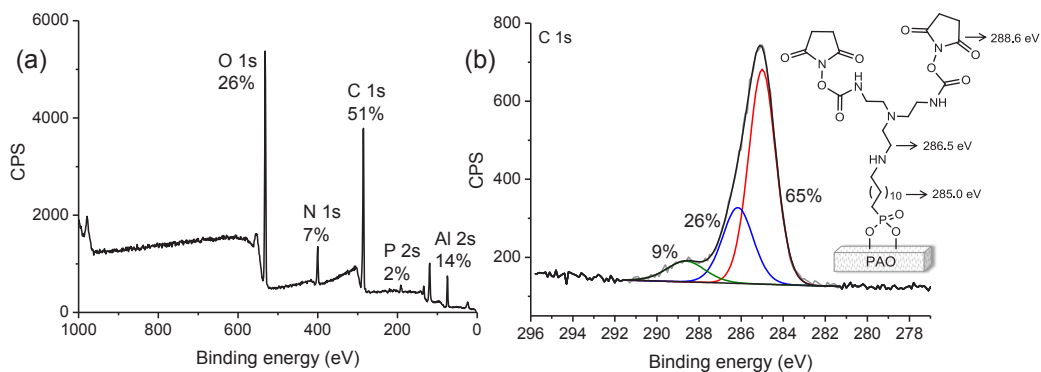
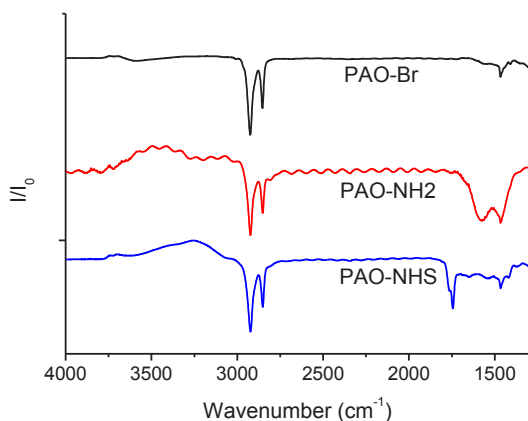


Figure SI-13. XPS survey scan of **PAO-NCS** after reaction with fluorinated amine.

Immobilization of protein on NHS-terminated PAO (PAO-NHS)**Figure SI-14.** XPS spectra of amine-terminated PAO: (a) survey scan and (b) C 1s narrow scan.**Figure SI-15.** XPS spectra of **PAO-NHS**: (a) survey scan and (b) C 1s narrow scan.**Figure SI-16.** IR spectra of **PAO-Br**, amine-terminated PAO (**PAO-NH₂**), and **PAO-NHS**.

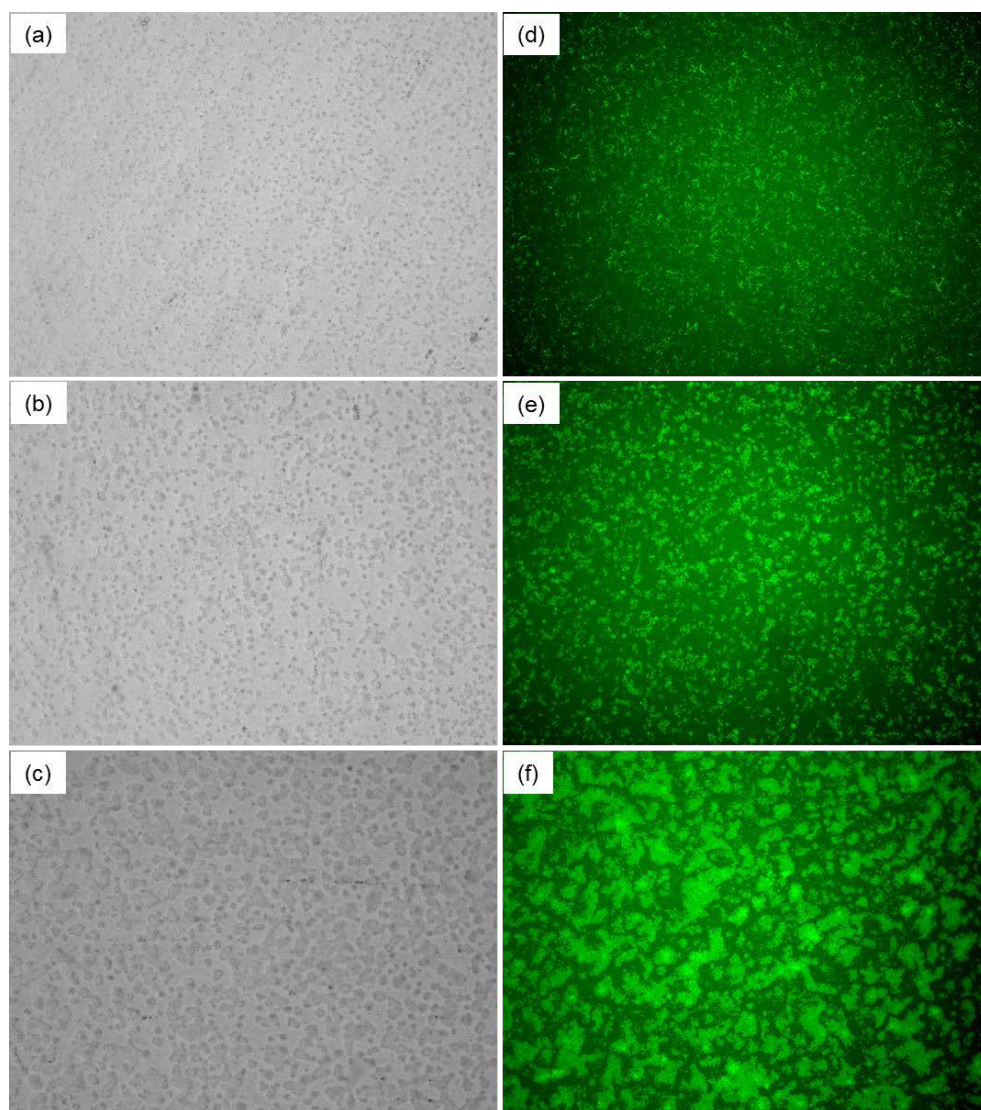
Bacterial growth on PAO-BSA

Figure SI-17. *Lactobacillus plantarum* on PAO-BSA after incubation at 37 °C: (a) and (d) 0 h; (b) and (e) 5 h; and (c) and (f) 7 h. Transmission images: (a), (b), and (c); fluorescence images: (d), (e), and (f). Total magnification 100 ×. Transmission and fluorescence images were taken from different individual samples.

References

1. Ingham, C. J.; ter Maat, J.; de Vos, W. M. Where bio meets nano: the many uses for nanoporous aluminum oxide in biotechnology. *Biotechnol. Adv.* **2012**, *30*, 1089-1099.
2. Feng, L.; Che, Y.; Liu, Y.; Qiang, X.; Wang, Y. Fabrication of superhydrophobic aluminium alloy surface with excellent corrosion resistance by a facile and environment-friendly method. *Appl. Surf. Sci.* **2013**, *283*, 367-374.

3. Joung, C. K.; Kim, H. N.; Lim, M. C.; Jeon, T. J.; Kim, H. Y.; Kim, Y. R. A nanoporous membrane-based impedimetric immunosensor for label-free detection of pathogenic bacteria in whole milk. *Biosens. Bioelectron.* **2013**, *44*, 210-215.
4. Chan, K. Y.; Ye, W. W.; Zhang, Y.; Xiao, L. D.; Leung, P. H. M.; Li, Y.; Yang, M. Ultrasensitive detection of *E. coli* O157:H7 with biofunctional magnetic bead concentration via nanoporous membrane based electrochemical immunosensor. *Biosens. Bioelectron.* **2013**, *41*, 532-537.
5. van Hattum, H.; Martin, N. I.; Ruijtenbeek, R.; Pieters, R. J. Development of a microarray detection method for galectin cancer proteins based on ligand binding. *Anal. Biochem.* **2013**, *434*, 99-104.
6. Ye, W. W.; Shi, J. Y.; Chan, C. Y.; Zhang, Y.; Yang, M. A nanoporous membrane based impedance sensing platform for DNA sensing with gold nanoparticle amplification. *Sens. Actuators, B* **2014**, *193*, 877-882.
7. Pera, N. P.; Brandhorst, H. M.; Kooij, R.; Maierhofer, C.; van der Kaaden, M.; Liskamp, R. M. J.; Wittmann, V.; Ruijtenbeek, R.; Pieters, R. J. Rapid screening of lectins for multivalency effects with a glycodendrimer microarray. *ChemBioChem* **2010**, *11*, 1896-1904.
8. ter Maat, J.; Regeling, R.; Ingham, C. J.; Weijers, C. A. G. M.; Giesbers, M.; de Vos, W. M.; Zuilhof, H. Organic modification and subsequent biofunctionalization of porous anodic alumina using terminal alkynes. *Langmuir* **2011**, *27*, 13606-13617.
9. Debrassi, A.; Ribbera, A.; de Vos, W. M.; Wennekes, T.; Zuilhof, H. Stability of (bio)functionalized porous aluminum oxide. *Langmuir* **2014**, *30*, 1311-1320.
10. Haensch, C.; Hoepfner, S.; Schubert, U. S. Chemical modification of self-assembled silane based monolayers by surface reactions. *Chem. Soc. Rev.* **2010**, *39*, 2323-2334.
11. Fryxell, G. E.; Rieke, P. C.; Wood, L. L.; Engelhard, M. H.; Williford, R. E.; Graff, G. L.; Campbell, A. A.; Wiacek, R. J.; Lee, L.; Halverson, A. Nucleophilic displacements in mixed self-assembled monolayers. *Langmuir* **1996**, *12*, 5064-5075.
12. Baker, M. V.; Watling, J. D. Functionalization of alkylsiloxane monolayers via free-radical bromination. *Langmuir* **1997**, *13*, 2027-2032.
13. Heise, A.; Stamm, M.; Rauscher, M.; Duschner, H.; Menzel, H. Mixed silane self assembled monolayers and their in situ modification. *Thin Solid Films* **1998**, *327*, 199-203.
14. Shyue, J. J.; De Guire, M. R. Acid-base properties and zeta potentials of self-assembled monolayers obtained via *in situ* transformations. *Langmuir* **2004**, *20*, 8693-8698.
15. Wang, Y. Y.; Cai, J.; Rauscher, H.; Belun, R. H.; Goedel, W. A. Maleimido-terminated self-assembled monolayers. *Chem.-Eur. J.* **2005**, *11*, 3968-3978.
16. Haensch, C.; Ott, C.; Hoepfner, S.; Schubert, U. S. Combination of different chemical surface reactions for the fabrication of chemically versatile building blocks onto silicon surfaces. *Langmuir* **2008**, *24*, 10222-10227.
17. Koloski, T. S.; Dulcey, C. S.; Haralson, Q. J.; Calvert, J. M. Nucleophilic displacement-reactions at benzyl halide self-assembled monolayer film surfaces. *Langmuir* **1994**, *10*, 3122-3133.
18. Sfez, R.; De-Zhong, L.; Turyan, I.; Mandler, D.; Yitzchaik, S. Polyaniline monolayer self-assembled on hydroxyl-terminated surfaces. *Langmuir* **2001**, *17*, 2556-2559.
19. Long, D. A.; Unal, K.; Pratt, R. C.; Malkoch, M.; Frommer, J. Localized "click" chemistry through dip-pen nanolithography. *Adv. Mater.* **2007**, *19*, 4471-4473.
20. Nebhani, L.; Barner-Kowollik, C. Orthogonal transformations on solid substrates: efficient avenues to surface modification. *Adv. Mater.* **2009**, *21*, 3442-3468.
21. Xi, W.; Scott, T. F.; Kloxin, C. J.; Bowman, C. N. Click chemistry in materials science. *Adv. Funct. Mater.* **2014**, *24*, 2572-2590.
22. Kantheti, S.; Narayan, R.; Raju, K. The impact of 1,2,3-triazoles in the design of functional coatings. *RSC Adv.* **2015**, *5*, 3687-3708.
23. Debrassi, A.; de Vos, W. M.; Zuilhof, H.; Wennekes, T. Carbohydrate-presenting self-assembled monolayers: preparation, analysis and applications in microbiology. In *Carbohydrate Nanotechnology*, Stine, K. J., Ed.; Wiley: Hoboken, NJ, 2015; *in press*.
24. Manova, R.; van Beek, T. A.; Zuilhof, H. Surface functionalization by strain-promoted alkyne-azide click reactions. *Angew. Chem., Int. Ed.* **2011**, *50*, 5428-5430.
25. Manova, R. K.; Pujari, S. P.; Weijers, C. A. G. M.; Zuilhof, H.; van Beek, T. A. Copper-free click biofunctionalization of silicon nitride surfaces via strain-promoted alkyne-azide cycloaddition reactions. *Langmuir* **2012**, *28*, 8651-8663.
26. Zimmermann, J. L.; Nicolaus, T.; Neuert, G.; Blank, K. Thiol-based, site-specific and covalent immobilization of biomolecules for single-molecule experiments. *Nat. Protoc.* **2010**, *5*, 975-985.
27. Jonkheijm, P.; Weinrich, D.; Schroeder, H.; Niemeyer, C. M.; Waldmann, H. Chemical strategies for generating protein biochips. *Angew. Chem., Int. Ed.* **2008**, *47*, 9618-9647.
28. Yu, Q.; Wang, Q.; Li, B.; Lin, Q.; Duan, Y. Technological development of antibody immobilization for optical immunoassays: progress and prospects. *Crit. Rev. Anal. Chem.* **2015**, *45*, 62-75.
29. Lex, A.; Pacher, P.; Werzer, O.; Track, A.; Shen, Q.; Schennach, R.; Koller, G.; Hlawacek, G.; Zojer, E.; Resel, R.; Ramsey, M.; Teichert, C.; Kern, W.; Trimmel, G. Synthesis of a photosensitive thiocyanate-functionalized trialkoxysilane and its application in patterned surface modifications. *Chem. Mater.* **2008**, *20*, 2009-2015.
30. Pujari, S. P.; van Andel, E.; Yaffe, O.; Cahen, D.; Weidner, T.; van Rijn, C. J. M.; Zuilhof, H. Mono-fluorinated alkyne-derived SAMs on oxide-free Si(111) surfaces: preparation, characterization and tuning of the Si workfunction. *Langmuir* **2013**, *29*, 570-580.
31. Smith, J. A. S.; Brisdon, B. J.; Brewer, S. A.; Willis, C. R. Synthesis of model organosiloxanes containing perfluoroether side-chains. *J. Mater. Chem.* **2000**, *10*, 1765-1769.
32. Pretzer, G.; Snel, J.; Molenaar, D.; Wiersma, A.; Bron, P. A.; Lambert, J.; de Vos, W. M.; van der Meer, R.; Smits, M. A.; Kleerebezem, M. Biodiversity-based identification and functional characterization of the mannose-specific adhesin of *Lactobacillus plantarum*. *J. Bacteriol.* **2005**, *187*, 6128-6136.
33. Ho, K. K. K.; Chen, R.; Willcox, M. D. P.; Rice, S. A.; Cole, N.; Iskander, G.; Kumar, N. Quorum sensing inhibitory activities of surface immobilized antibacterial dihydropyrrones via click chemistry. *Biomaterials* **2014**, *35*, 2336-2345.
34. Zhang, S.; Maidenberger, Y.; Luo, K.; Koberstein, J. T. Adjusting the surface areal density of click-reactive azide groups by kinetic control of the azide substitution reaction on bromine-functional SAMs. *Langmuir* **2014**, *30*, 6071-6078.
35. Techane, S. D.; Gamble, L. J.; Castner, D. G. X-ray photoelectron spectroscopy characterization of gold nanoparticles functionalized with amine-terminated alkanethiols. *Biointerphases* **2011**, *6*, 98-104.
36. Bhairamagi, N. S.; Gangarapu, S.; Campos, M. A. C.; Paulusse, J. M. J.; van Rijn, C. J. M.; Zuilhof, H. Efficient functionalization of oxide-free silicon(111) surfaces: thiol-yne versus thiol-ene click chemistry. *Langmuir* **2013**, *29*, 4535-4542.
37. Wang, H.; Zhou, H.; Gestos, A.; Fang, J.; Niu, H.; Ding, J.; Lin, T. Robust, electro-conductive, self-healing superamphiphobic fabric prepared by one-step vapour-phase polymerisation of poly(3,4-ethylenedioxythiophene) in the presence of fluorinated decyl polyhedral oligomeric silsesquioxane and fluorinated alkyl silane. *Soft Matter* **2013**, *9*, 277-282.

38. Huang, Y.; Candelaria, S. L.; Li, Y.; Li, Z.; Tian, J.; Zhang, L.; Cao, G. Sulfurized activated carbon for high energy density supercapacitors. *J. Power Sources* **2014**, *252*, 90-97.
39. Fujimori, T.; Morelos-Gomez, A.; Zhu, Z.; Muramatsu, H.; Futamura, R.; Urita, K.; Terrones, M.; Hayashi, T.; Endo, M.; Hong, S. Y.; Choi, Y. C.; Tomanek, D.; Kaneko, K. Conducting linear chains of sulphur inside carbon nanotubes. *Nat. Commun.* **2013**, *4*, 2162.
40. Balachander, N.; Sukenik, C. N. Monolayer transformation by nucleophilic-substitution: applications to the creation of new monolayer assemblies. *Langmuir* **1990**, *6*, 1621-1627.
41. Alzahrani, E.; Welham, K. Fabrication of a TCEP-immobilised monolithic silica microchip for reduction of disulphide bonds in proteins. *Anal. Methods* **2014**, *6*, 558-568.
42. Lowe, A. B. Thiol-ene "click" reactions and recent applications in polymer and materials synthesis. *Polym. Chem.* **2010**, *1*, 17-36.
43. Escorihuela, J.; Zuilhof, H. Metal-free "click" chemistry reactions on surfaces. *Adv. Mater. Interfaces* **2015**, in press.
44. Fesenko, A. A.; Dem'yachenko, E. A.; Fedorova, G. A.; Shutalev, A. D. A selective synthesis of beta-isothiocyanato ketones through a Staudinger/aza-Wittig reaction of beta-azido ketones. *Monatsh. Chem.* **2013**, *144*, 351-359.
45. Mendez-Ardoy, A.; Steentjes, T.; Kudemac, T.; Huskens, J. Self-assembled monolayers on gold of beta-cyclodextrin adsorbates with different anchoring groups. *Langmuir* **2014**, *30*, 3467-3476.
46. Yang, M.; Teeuwen, R. L. M.; Giesbers, M.; Baggerman, J.; Arafat, A.; de Wolf, F. A.; van Hest, J. C. M.; Zuilhof, H. One-step photochemical attachment of NHS-terminated monolayers onto silicon surfaces and subsequent functionalization. *Langmuir* **2008**, *24*, 7931-7938.
47. Tawakoli, P. N.; Al-Ahmad, A.; Hoth-Hannig, W.; Hannig, M.; Hannig, C. Comparison of different live/dead stainings for detection and quantification of adherent microorganisms in the initial oral biofilm. *Clin. Oral Invest.* **2013**, *17*, 841-850

Chapter 5

Carbohydrate-Protein Interactions for the Binding of Bacteria on Porous Aluminum Oxide

**Aline Debrassi¹, Nathalja Berghuis¹, Steven Aalvink², Willem M. de Vos^{2,3}, Han
Zuilhof^{1,4}, Tom Wennekes¹**

¹ Laboratory of Organic Chemistry, Wageningen University, 6703 HB Wageningen, The
Netherlands

² Laboratory of Microbiology, Wageningen University, 6703 HB Wageningen, The
Netherlands

³ RPU Immunobiology, Department of Bacteriology & Immunology and Department of
Veterinary Biosciences, University of Helsinki, 00014 Helsinki, Finland

⁴ Department of Chemical and Materials Engineering, King Abdulaziz University, 21589
Jeddah, Saudi Arabia

Manuscript in preparation

Abstract

Carbohydrate–protein interactions play an important role in various physiological and pathological processes. One possible tool to study these complex interactions is via carbohydrate-presenting surfaces, as reviewed in **Chapter 2**. With the results described in **Chapter 3** we showed that porous aluminum oxide (PAO) surfaces can be biofunctionalized with mannose derivatives and used for the binding of *Lactobacillus plantarum*, a potential probiotic bacterium that presents a mannose-specific binding adhesin. In this chapter the results are reported of a more in-depth investigation of the various parameters involved in the preparation of these surfaces and their binding with lectins, such as the nature of the spacer connected to the mannoside derivative and the presence of soluble carbohydrates and bovine serum albumin (BSA) in the medium. The mannose derivative with a long hydrophobic hydrocarbon chain (C11) as the spacer presented the best binding of *L. plantarum*. The presence of an α -glucoside in the suspension of bacteria did not prevent the binding of the bacteria to the mannose-presenting PAO, and similar results were observed when BSA was present in the bacterial suspension. Finally, the lack of binding of a mutant strain of *L. plantarum* that does not present the mannose-specific adhesin, proved that this carbohydrate–protein interaction is the main mechanism of binding in this system. Future work should involve the capture of *L. plantarum* from a mixture of various bacterial species using the mannose-presenting PAO surfaces.

Introduction

Carbohydrates are present on the surface of cells as part of a dense layer known as glycocalyx, either for the protection of the cells from harmful physical forces or for the regulation of interactions between cells and their environment.¹ Carbohydrate–protein interactions involve glycoproteins, glycolipids or polysaccharides present on the cell surface and carbohydrate-binding proteins. These interactions play a role in various biological processes, such as cell-to-cell interaction, ligand-receptor recognition, transport of biological macromolecules, immune response,² cancer metastasis,²⁻⁴ viral and bacterial infections.^{5, 6} The involvement of carbohydrate–protein interactions in various physiological and pathological processes makes them potential therapeutic targets for various diseases.⁷ However, the study of these interactions is still a challenge,

mainly due to the structural complexity and heterogeneity of carbohydrates in biological systems. To overcome this challenge, well-defined carbohydrate-presenting surfaces are an interesting type of material that can be used in the investigation of the interaction between carbohydrates and other biomolecules, mainly proteins.^{1, 8}

Carbohydrate-presenting surfaces can also be used to bind and sense bacteria via their carbohydrate-binding proteins called adhesins. In **Chapter 2**, a detailed overview was presented on how these carbohydrates-presenting surfaces can be prepared, characterized, and applied for the binding, capture, and sensing of bacteria and bacterial toxins. In **Chapter 3**, we have shown a proof-of-principle that mannose-presenting porous aluminum oxide (PAO) surfaces increase the binding of *Lactobacillus plantarum*, a potential probiotic bacterium, via its mannose-specific binding adhesin.^{9, 10}

After this initial proof-of-principle, our objective in the current study is to optimize the preparation of the carbohydrate-presenting PAO surfaces and further investigate the factors that influence the binding of *L. plantarum*. Various parameters that may influence this binding event were analyzed, such as the spacer that connects the carbohydrate to the PAO surface and the presence of soluble carbohydrates and bovine serum albumin (BSA). Finally, a mutant strain of *L. plantarum*⁹ devoid of the mannose-specific adhesin was used to prove that the binding of *L. plantarum* to the mannose-presenting PAO was mainly due to this carbohydrate-protein interaction.

Materials and Methods

Materials

Porous aluminum surfaces (PAO) surfaces were purchased from Microdish BV (Netherlands) with dimensions of $36 \times 8 \text{ mm}^2$ and an average pore size of 200 nm. 10-undecynylphosphonic acid was purchased from SiKÉMIA (France). 2,2,2-Trifluoro-*N*-phenylacetimidoyl chloride was purchased from TCI Europe NV. Methyl- β -D-galactopyranoside was purchased from Fisher Scientific BV. 2-[2-(2-(2-Azidoethoxy)ethoxy)ethoxy]ethanol (N₃-PEG4-OH) was obtained from Carbosynth (Berkshire, United Kingdom). The other chemicals were obtained from Sigma-Aldrich and used without further purification. Solvents were of analytical grade. Dichloromethane was purified using a Pure Solv 400 solvent purification system

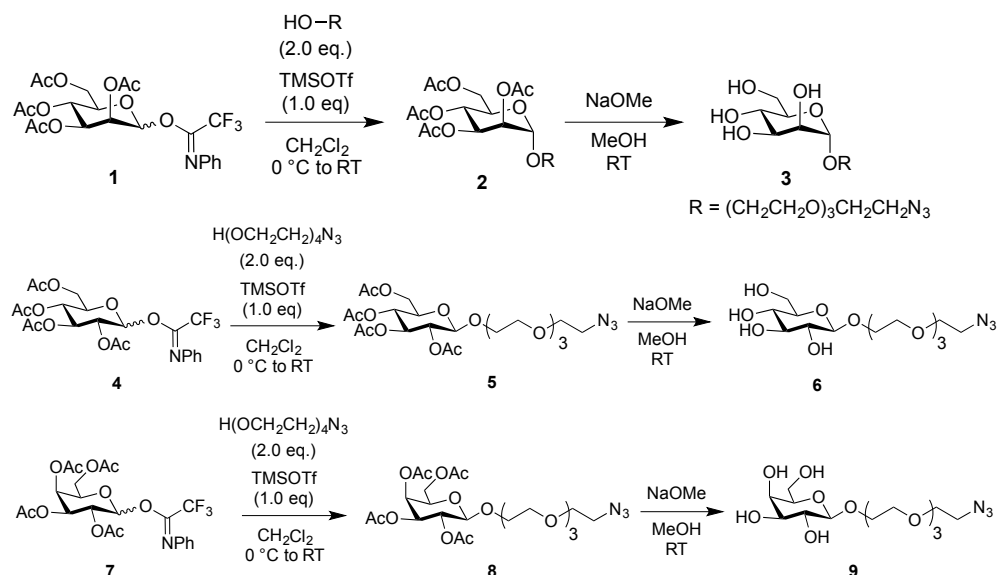
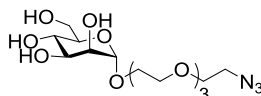
(Innovative Technology, USA). An Elmasonic P 30 H ultrasonic unit was used for the sonication steps at a frequency of 80 kHz. Nuclear magnetic resonance (NMR) spectra were obtained with a Bruker 400 MHz spectrometer, and peaks were assigned with COSY and HSQC experiments. Optical rotation was measured at 589 nm using a PerkinElmer 241 polarimeter. HRMS data were recorded on an Exactive high-resolution MS instrument (Thermo Scientific) equipped with a DART or ESI probe. For all microbiological experiments, surfaces with lectins and bacteria were imaged with an Olympus BX-41 fluorescence microscope equipped with U-MNIBA2 (for bacteria stained with 5-carboxyfluorescein diacetate, cFDA) and U-MWG2 (for rhodamine-labeled concanavalin A, conA-rho) filters (Olympus). Images were taken using a Kappa CCD camera. CellProfiler version 2 (Broad Institute) was used to calculate the area occupied by bacteria.

Modification of PAO With Phosphonic Acids

Substrates were prepared in the same way as previously reported by us.¹¹ Briefly, the PAO substrate was rinsed and sonicated in acetone (5 min) and ultrapure water (5 min). Then, it was immersed in a fresh mixture of methanol and 37% hydrochloric acid (1:1, v/v) for 30 min. The substrate was rinsed and sonicated in ultrapure water (5 min) and absolute ethanol (5 min). The substrate was rinsed with absolute ethanol and dried under vacuum for ~10 min. The PAO substrate was immersed in a 1 mM mixed solution of 1-octylphosphonic acid and 10-undecynylphosphonic acid (1:1) in absolute ethanol for 16 h at room temperature. Then, it was rinsed with absolute ethanol and heated at 140 °C under vacuum for 6 h. The substrate was rinsed and sonicated in absolute ethanol (2 × 5 min) and dichloromethane (5 min) and dried in air before storage.

Synthesis of Azido-Glycosides

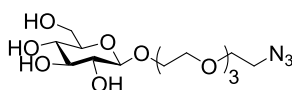
1-(11-Azidoundecanyl)- α -D-mannopyranoside¹¹ and 1-(3-azidopropyl)- α -D-mannopyranoside¹² were synthesized as previously described. Glycosyl trifluoroacetimidate donors were prepared according to a method previously described in the literature.¹³ The glycosyl donors were coupled to N₃-PEG4-OH (**Scheme 1**). The peracetylated mannoside was directly reacted with 3-bromopropanol, followed by reaction with sodium azide to obtain the azido-glycoside.¹² The products were deprotected with sodium methoxide to yield the azido-glycosides.

Scheme 1. Synthesis of azido-glycosides **3**, **6**, and **9**.**1-[2-[2-[2-(2-azidoethoxy)ethoxy]ethoxy]ethyl]- α -D-mannopyranoside (**3**)**

2,3,4,6-Tetra-*O*-acetyl- α -D-mannopyranosyl 1-(*N*-phenyl)-2,2,2-trifluoroacetimidate **1** was prepared according to a procedure previously described in the literature.¹³ A solution of donor **1** (0.401 g, 0.77 mmol), the 2-[2-[2-(2-azidoethoxy)ethoxy]ethoxy]ethanol acceptor (0.338 g, 1.54 mmol), and activated molecular sieves (0.5 g, 4 Å) in anhydrous dichloromethane (8 mL) was cooled to 0 °C and stirred for 30 min under argon atmosphere. TMSOTf (0.171 g, 0.771 mmol) was added and the mixture was stirred for 3 h, slowly warming up to room temperature in the ice bath. The reaction was monitored by thin layer chromatography (heptane, ethyl acetate, 1:3). Triethylamine (0.78 mL) was added and the reaction mixture was filtered over a Celite layer. Dichloromethane was added (80 mL) and the filtrate was washed with saturated NaHCO₃ solution (40 mL), dried over Na₂SO₄, filtered, and concentrated under reduced pressure. The crude product was purified by column chromatography (heptane/ethyl acetate 50:50 to 30:70) to yield 2,3,4,6-tetra-*O*-acetyl-1-[2-[2-[2-(2-azidoethoxy)ethoxy]ethoxy]ethyl]- α -D-mannopyranoside (**2**) as a yellowish syrup in

77% yield (0.328 g, 0.60 mmol). Intermediate **2** (0.328 g, 0.60 mmol) was then dissolved in dry methanol (5 mL) and a solution of sodium methoxide in methanol (25%, 64 μ L) was added. The mixture was stirred for 1.5 h and after complete conversion (monitored by TLC, eluent ethyl acetate), Dowex 50 (H^+ form) was added until the pH was 7. The suspension was filtered over a Celite layer and the solution was concentrated under reduced pressure to yield 1-[2-[2-[2-(2-azidoethoxy)ethoxy]ethoxy]ethyl]- α -D-mannopyranoside (**3**) as a yellowish oil in 91% yield (0.207 g, 0.54 mmol). $[\alpha]_D^{20} +27.7$ (c 1.0, MeOH). 1H NMR (400 MHz, MeOD): δ 4.80 (1H, s, H-1), 3.85 (3H, m), 3.69 (15H, m), 3.60 (2H, m), 3.38 (2H, t, $-CH_2-N_3$, $J = 4.0$ Hz). ^{13}C NMR (100 MHz, MeOD): δ 101.7 (CH, C-1), 74.6 (CH), 72.6 (CH), 72.1 (CH), 71.7 ($2 \times CH_2$), 71.6 (CH_2), 71.5 (CH_2), 71.4 (CH_2), 71.1 (CH_2), 68.6 (CH), 67.8 (CH_2), 62.9 (CH_2), 50.4 (CH_2 , $-CH_2N_3$). HRMS: m/z 404.1615; calcd for $C_{14}H_{27}N_3O_9Na$ ($[M + Na]^+$), 404.1640.

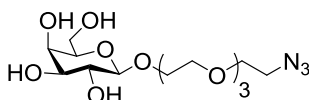
1-[2-[2-[2-(2-azidoethoxy)ethoxy]ethoxy]ethyl]- β -D-glucopyranoside (**6**)



2,3,4,6-Tetra-*O*-acetyl-D-glucopyranosyl 1-(*N*-phenyl)-2,2,2-trifluoroacetimidate **4** was prepared according to a procedure previously described in the literature.¹³ A solution of donor **4** (0.300 g, 0.58 mmol), the 2-[2-[2-(2-azidoethoxy)ethoxy]ethoxy]ethanol acceptor (0.250 g, 1.16 mmol), and activated molecular sieves (0.3 g, 4 Å) in anhydrous dichloromethane (10 mL) was cooled to 0 °C and stirred for 30 min under argon atmosphere. TMSOTf (0.129 g, 0.58 mmol) was added and the mixture was stirred for 3 h, slowly warming up to room temperature. The reaction was monitored by thin layer chromatography (heptane, ethyl acetate, 1:3). Triethylamine (0.58 mL) was added and the reaction mixture was filtered over a Celite layer. Dichloromethane was added (40 mL) and the filtrate was washed with saturated $NaHCO_3$ solution (40 mL), dried over Na_2SO_4 , filtered, and concentrated under reduced pressure. The crude product was purified by column chromatography (heptane/ethyl acetate 35:65) to yield 2,3,4,6-tetra-*O*-acetyl-1-[2-[2-[2-(2-azidoethoxy)ethoxy]ethoxy]ethyl]- β -D-glucopyranoside (**5**) as a yellowish syrup in 44% yield (0.140 g, 0.25 mmol). Intermediate **5** (0.140 g, 0.25 mmol) was then dissolved in dry methanol (5 mL) and a solution of sodium methoxide in methanol (25%, 35 μ L) was added. The mixture was

stirred for 1.5 h and after complete conversion (monitored by TLC, eluent ethyl acetate), Dowex 50 (H⁺ form) was added until the pH was 7. The suspension was filtered over a Celite layer and the solution was concentrated under reduced pressure to yield 1-[2-[2-[2-(2-azidoethoxy)ethoxy]ethoxy]ethyl]]-β-D-glucopyranoside (**6**) as a yellowish oil in 58% yield (0.053 g, 0.14 mmol). $[\alpha]_D^{20} -13.1$ (c 1.0, MeOH). ¹H NMR (400 MHz, MeOD): δ 4.30 (1H, d, H-1, *J* = 7.6 Hz), 4.02 (1H, s), 3.87 (1H, d, H-6a, *J* = 12.0 Hz), 3.75 – 3.66 (16H, m, H-6b, glycol moiety), 3.78 (1H, t, H-3, *J* = 4.4 Hz), 3.31 (2H, m, H-4, H-5), 3.22 (1H, t, H-2, *J* = 8.0 Hz). ¹³C NMR (100 MHz, MeOD): δ 102.9 (CH, C-1), 76.5 (CH), 74.0 (CH), 73.6 (CH), 70.2 (CH), 68.3 (CH₂), 61.4 (CH₂, C-6), 51.5 (CH₂, –CH₂N₃), 50.0 (2 × CH₂), 49.7 (CH₂), 49.5 (2 × CH₂), 49.3 (CH₂).

1-[2-[2-[2-(2-azidoethoxy)ethoxy]ethoxy]ethyl]]-β-D-galactopyranoside (**9**)



2,3,4,6-Tetra-*O*-acetyl-β-D-galactopyranosyl 1-(*N*-phenyl)-2,2,2-trifluoroacetimidate **7** was prepared according to a procedure previously described in the literature.¹³ A solution of donor **7** (0.400 g, 0.77 mmol), the 2-[2-[2-(2-azidoethoxy)ethoxy]ethoxy]ethanol acceptor (0.340 g, 1.54 mmol), and activated molecular sieves (0.4 g, 4 Å) in anhydrous dichloromethane (10 mL) was cooled to 0 °C and stirred for 30 min under argon atmosphere. TMSOTf (0.171 g, 0.77 mmol) was added and the mixture was stirred for 3 h, slowly warming up to room temperature. The reaction was monitored by thin layer chromatography (heptane, ethyl acetate, 1:3). Triethylamine (0.77 mL) was added and the reaction mixture was filtered over a Celite layer. Dichloromethane was added (40 mL) and the filtrate was washed with saturated NaHCO₃ solution (40 mL), dried over Na₂SO₄, filtered, and concentrated under reduced pressure. The crude product was purified by column chromatography (heptane/ethyl acetate 30:70) to yield 2,3,4,6-tetra-*O*-acetyl-1-[2-[2-[2-(2-azidoethoxy)ethoxy]ethoxy]ethyl]]-β-D-galactopyranoside (**8**) as a yellowish syrup in 40% yield (0.165 g, 0.30 mmol). Intermediate **8** (0.165 g, 0.30 mmol) was then dissolved in dry methanol (5 mL) and a solution of sodium methoxide in methanol (25%, 32 μL) was added. The mixture was stirred for 1.5 h and after complete conversion (monitored by TLC, eluent ethyl acetate), Dowex 50 (H⁺ form) was added until the pH was 7. The

suspension was filtered over a Celite layer and the solution was concentrated under reduced pressure to yield 1-[2-[2-[2-(2-azidoethoxy)ethoxy]ethoxy]ethyl)]- β -D-galactopyranoside (**9**) as a yellowish oil in 70% yield (0.080 g, 0.21 mmol). $[\alpha]_D^{20}$ -6.7 (c 1.0, MeOH). ^1H NMR (400 MHz, MeOD): δ 4.25 (1H, d, H-1, $J = 7.2$ Hz), 4.01 (1H, s), 3.82 (1H, d, $J = 2.4$ Hz), 3.76 – 3.66 (16H, m, H-6a, glycol moiety), 3.56 – 3.45 (2H, m, H-6b), 3.38 (2H, t, $-\text{CH}_2\text{N}_3$). ^{13}C NMR (100 MHz, MeOD): δ 105.5 (CH, C-1), 76.7 (CH), 75.2 (CH), 72.5 (CH), 70.2 (CH), 68.1 (CH_2), 61.2 (CH_2 , C-6), 50.4 (CH_2 , $-\text{CH}_2\text{N}_3$), 49.8 ($5 \times \text{CH}_2$), 48.4 (CH_2).

Copper-Catalyzed Azide-Alkyne Cycloaddition (CuAAC) Click Reaction

For all CuAAC click reactions, the reaction tubes were equipped with a stirring bar and a platform to prevent the stirring bar to break the fragile PAO substrate.¹¹ The optimization of the conditions for the CuAAC click reaction of the azido-mannosides was performed using N_3 -PEG4-OH. A solution containing N_3 -PEG4-OH (1.0 mM), sodium ascorbate (2.0 mM), and copper sulfate (2.0 mM) was prepared in different solvents (acetonitrile, ethanol/water 1:1, and methanol/DMF 1:1). The alkyne-terminated PAO surface was immersed in one of the solutions and heated at 50 or 60 °C for the desired time (from 30 min to 16 h) in a microwave oven, except for the reactions performed for 16 h (performed in oil bath). After the reaction, the substrates were rinsed and sonicated in an 0.1 M EDTA solution in water (5 min), ultrapure water (5 min), ethanol (5 min), and dichloromethane (5 min).

All the remaining CuAAC reactions (**Figure 1**) were performed as follows. A solution of azido-glycoside (mannose, glucose, and/or galactose) (1.0 mM), sodium ascorbate (2.0 mM), and copper sulfate (2.0 mM) was prepared in a mixture of methanol and DMF (1:1). The alkyne-terminated PAO was immersed in this solution and heated at 60 °C for 1 h in a microwave oven. After the reaction, the substrates were rinsed and sonicated in a 0.1 M EDTA solution in water (5 min), ultrapure water (5 min), ethanol (5 min), and dichloromethane (5 min).

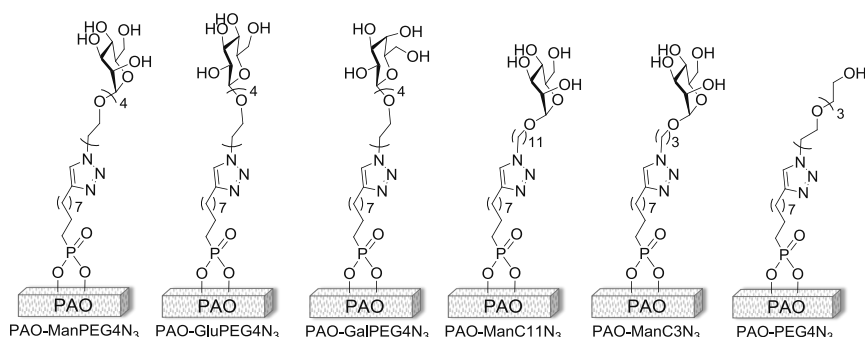


Figure 1. Carbohydrate-presenting PAO surfaces used in this study and PEG4-terminated PAO (PAO-PEG4N₃).

X-ray photoelectron spectroscopy (XPS)

XPS spectra were obtained with a JPS 9200 photoelectron spectrometer (JEOL) under ultrahigh vacuum conditions using monochromatic Al X-ray radiation at 12 kV and 20 mA with an analyser pass energy of 10 eV. The binding energy was calibrated for the C 1s peak at 285 eV as a reference. Irradiation with electrons with a kinetic energy of 2.8 eV and a filament current of 4.8 A was used to prevent surface charging. The spectra were processed using CasaXPS software (version 2.3.15).

Bacterial Strains

L. plantarum NZ7511 (MSA mutant) was derived from the wild-type strain WCFS1 and contains an insertionally inactivated *msa* gene for the mannose-specific adhesin, as previously described.⁹ Both strains were kindly provided by Prof. Michiel Kleerebezem (NIZO Food Research).

Binding of Rhodamine-Labeled Concanavalin A (conA-rho) on Carbohydrate-Terminated PAO

The carbohydrate-presenting PAO surfaces (PAO-ManPEG4N₃, PAO-GluPEG4N₃, and PAO-GalPEG4N₃) or a PEG4-terminated surface (PAO-PEG4N₃) were immersed in a 0.05 mg/mL solution of conA-rho in phosphate-buffered saline (PBS) containing 0.05% Tween 20 (PBST) and 1 mM of CaCl₂ for 30 min at room temperature. The surfaces were thoroughly washed with PBS, dried under vacuum, and imaged using fluorescence microscopy.

Binding of *L. plantarum* on Mannose-Presenting PAO With Different Spacers

An overnight culture of *L. plantarum* WCFS1 in MRS broth was diluted with water to obtain an optical density at 600 nm (OD_{600}) of 0.5. The mannose-presenting surfaces used for the experiment with different spacers were prepared with a PAO surface modified with a mixture of 1-octylphosphonic acid and 10-undecynylphosphonic acid 50:50 (w/w), followed by a CuAAC click reaction with either 1-(3-azidopropyl)- α -D-mannopyranoside (**PAO-ManC3N₃**), 1-(11-azidoundecanyl)- α -D-mannopyranoside (**PAO-ManC11N₃**) or 1-[2-[2-[2-(2-azidoethoxy)ethoxy]ethoxy]ethyl]- α -D-mannopyranoside (**PAO-ManPEG4N₃**) (**Figure 1**). The mannose-presenting surfaces were cut in four equal pieces and the samples were placed on a Petri dish covered with parafilm. The suspension of bacteria with $OD_{600} = 0.5$ was placed on the samples (3 μ L per one quarter of PAO) and the Petri dishes were incubated at 37 °C for 30 min with a wet cotton inside the Petri dishes. The top surface of the samples was washed various times (0, 5 or 15 times). Each washing step consisted of adding and removing 250 μ L of PBST three times, using a micropipette and a round support to contain the PBST. The bacteria were stained with 5-carboxyfluorescein diacetate (cFDA) by placing the PAO surfaces on low-melting point agarose (BioRad, USA) that contained 50 μ M cFDA for 30 min. The bacteria were imaged using fluorescence microscopy, and the area covered by bacteria was calculated using CellProfiler. For more details on the calculation of the area covered by bacteria, see the microbiology experiments in **Chapter 3**.

Binding of *L. plantarum* on Mannose-Presenting PAO in the Presence of Soluble Carbohydrates

An overnight culture of *L. plantarum* WCFS1 in MRS broth was diluted with an aqueous solution of methyl- α -D-mannopyranoside (α -mannoside, 35 mM), methyl- α -D-glucopyranoside (α -glucoside, 35 mM) or with water to obtain $OD_{600} = 0.5$. The mannose-presenting surfaces (**PAO-ManC11N₃**) were cut in four equal pieces and the samples were placed on a Petri dish covered with parafilm. The suspension of bacteria in the glycoside solutions or in water was placed on the samples (3 μ L per one quarter of PAO) and the Petri dishes were incubated at 37 °C for 30 min with a wet cotton inside the Petri dishes. The top surface of the samples was washed various times (0, 5 or 15 times). Each washing step consisted of adding and removing 250 μ L of PBST three times, using a micropipette and a round support to contain the PBST. The bacteria on the

surface were fluorescently stained with cFDA by placing the PAO on low-melting-point agarose containing 50 μM cFDA for 30 min. The bacteria were imaged and the area covered by bacteria was calculated.

Binding of *Lactobacillus plantarum* WCFS1 and MSA mutant on Mannose-Presenting PAO

Overnight cultures of *L. plantarum* strains WCFS1 and MSA mutant were prepared in MRS broth (Difco Lactobacilli MRS broth, BD, Amsterdam, The Netherlands), with 10 $\mu\text{g/mL}$ chloramphenicol for the MSA mutant strain. The cultures were diluted in water to obtain $\text{OD}_{600} = 0.5$. The mannose-presenting surfaces (**PAO-ManC11N₃**) were cut in four equal pieces and the samples were placed on a Petri dish covered with parafilm. The suspension of bacteria (either *L. plantarum* WCFS1 or MSA mutant) with $\text{OD}_{600} = 0.5$ was placed on the samples (3 μL per one quarter of PAO) and the Petri dishes were incubated at 37 °C for 30 min with a wet cotton inside the Petri dishes. The top surface of the samples was washed various times (0, 3, 5, 10 or 15 times). Each washing step consisted of adding and removing 250 μL of PBST three times, using a micropipette and a round support to contain the PBST. The bacteria on the surface were fluorescently stained with cFDA by placing the PAO on low-melting-point agarose containing 50 μM cFDA for 30 min. The bacteria were imaged and the area covered by bacteria was calculated. The same experiment was also performed in the presence of 0.5% bovine serum albumin (BSA) in the suspension of bacteria with $\text{OD}_{600} = 0.5$.

Results and Discussion

Optimizing the CuAAC Click Reaction for Glycosides

The first step in the preparation of the carbohydrate-presenting PAO surfaces was the synthesis of the azido-glycosides, which were prepared with as spacers either 4 ethylene oxide moieties (labelled as: PEG4), or a propyl (C3) or undecenyl (C11) alkyl chain. Glycosyl trifluoroacetimidates^{14, 15} were selected as glycosyl donors because of their overall efficiency in chemical glycosylations and storability. Glycosylation reactions with D-glucose, D-galactose, D-mannose derived peracetylated trifluoroacetimidate donors and N₃-PEG4-OH as an acceptor, yielded the glycosides in a 40 - 77% yield, with exclusive formation of the α -anomer for mannoside **3** and β -anomer for the glucoside **6**

and galactoside **9**). For the analogous synthesis of the azido-mannoside with the C3 spacer, the glycosylation using the trifluoroacetimidate donor gave a yield of only 30%. A more simple glycosylation method using directly the peracetylated mannose as previously described by Ladmiral and co-workers,¹² gave 1-(3-azidopropyl)- α -D-mannopyranoside in 61% yield.

PAO surfaces were modified with a 1:1 mixture of 1-octylphosphonic acid and 10-undecynylphosphonic acid to obtain the alkyne-terminated PAO (**Chapter 3**),¹¹ which can react with the azido-glycosides (**Figure 1**). However, the conditions that were successfully used for the CuAAC reaction of 1-(11-azidoundecanyl)- α -D-mannopyranoside with the alkyne-terminated PAO¹¹ in Chapter 3 proved to be inefficient for the other azido-mannosides. This lower reactivity might be due to the coordination of the copper ion to the ethylene glycol spacer. Increasing the concentration of CuSO₄ and sodium ascorbate led to degradation of the initial monolayer. Therefore, various solvents (acetonitrile, a mixture of water/ethanol 1:1,¹⁶ and a mixture of DMF/Methanol 1:1¹⁷), reaction times, and two temperatures were assessed for the optimization of the CuAAC reaction (**Table 1**), using fixed amounts of CuSO₄, sodium ascorbate and N₃-PEG4-OH.

The best results were found when using a mixture of DMF/Methanol (1:1) as the reaction solvent. When compared to the other solvents, the higher amount of nitrogen (from N₃-PEG4-OH), as judged by XPS, indicates a higher conversion for the CuAAC reaction and the higher amount of carbon indicates that there is only limited degradation of the initial alkyne-terminated monolayer. Thus, all the subsequent CuAAC reactions (including with 1-(11-azidoundecanyl)- α -D-mannopyranoside) were performed in DMF/Methanol (1:1) at 60 °C for 1 h. When using these optimized conditions, traces of copper were noticed on the PAO surface after the click reaction, because of the increased concentration of copper used in the reaction. By adding a sonication step in an aqueous EDTA solution to the work-up procedure, all the remaining traces of copper could, however, be removed from the PAO surfaces.

Table 1. Optimization of the CuAAC click reaction of N₃-PEG4-OH on alkyne-terminated PAO surfaces.

| Solvent | Time (h) | Temperature (°C) | %C compared to Al ^a | %N compared to Al ^b |
|---------------------|-----------------|------------------|--------------------------------|--------------------------------|
| Acetonitrile | 2 | 60 | 69 | 5 |
| | 4 | 60 | 73 | 13 |
| | 16 ^c | 50 | 73 | 2 |
| Water/Ethanol (1:1) | 2 | 60 | 66 | 19 |
| | 4 | 60 | 68 | 17 |
| | 16 ^c | 50 | 71 | 19 |
| DMF/Methanol (1:1) | 0.5 | 60 | 71 | 24 |
| | 1 | 60 | 76 | 28 |
| | 2 | 60 | 75 | 27 |
| | 4 | 60 | 79 | 25 |
| | 16 ^c | 50 | 75 | 24 |

^a %C was determined by integrating the XPS signals of C 1s and Al 2p.^b %N was determined by integrating the XPS signals of N 1s and Al 2p.^c Reactions performed in oil bath.

Binding of Rhodamine-Labeled Concanavalin A (conA-rho) on Carbohydrate-Terminated PAO

The next step was to evaluate the PEG-carbohydrate-presenting PAO surfaces for the binding of a fluorescently labeled lectin, as a simple proof-of-principle system to evaluate that the carbohydrates present on the surfaces are available to interact with carbohydrate-binding proteins. Rhodamine-labeled concanavalin A (conA-rho) was selected due to its well-documented selective interaction with mannosides and glucosides.¹⁸ Upon exposure of **PAO-ManPEG4N₃**, **PAO-GluPEG4N₃**, and **PAO-GalPEG4N₃** surfaces to a solution of conA-rho, it was clearly visible via fluorescence

microscopy that, as expected, the lectin is present mainly on the mannose- and glucose-presenting surfaces (**PAO-ManPEG4N₃** and **PAO-GluPEG4N₃**), with negligible adsorption on the galactose-terminated and PEGylated control surfaces (**PAO-GalPEG4N₃** and **PAO-PEG4N₃**) (**Figure 2**). With these proof-of-principle results, the carbohydrate-presenting PAO surfaces were then used to study the binding of bacteria via their adhesins.

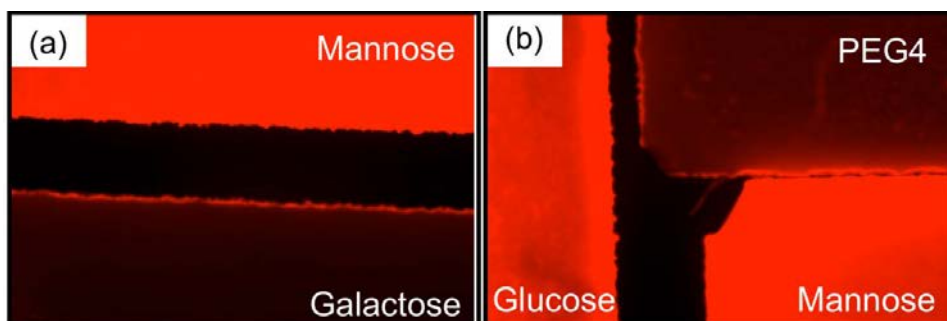


Figure 2. Binding of conA-rho on carbohydrate-presenting PAO: (a) **PAO-ManPEG4N₃** compared with **PAO-GalPEG4N₃** and (b) **PAO-GluPEG4N₃** and **PAO-ManPEG4N₃** compared with **PAO-PEG4N₃** as a negative control.

CuAAC Click Reaction for Mannosides With Different Spacers

After the successful proof-of-principle experiment with a soluble lectin and the PEG-carbohydrate-presenting PAO surfaces, a more complex system was chosen to study the binding, namely the mannose-specific adhesin present on the cell surface of *L. plantarum* to the PAO surfaces. Initial bacterial binding experiments on **PAO-ManPEG4** showed lower binding of *L. plantarum* WCFS1 to these surfaces than to the mannose-presenting surfaces studied in **Chapter 3**. This difference of binding motivated us to compare the bacterial binding on mannose-presenting PAO surfaces with different spacers connecting the mannoside to the surface. For this step, PAO surfaces presenting other two azido-mannosides with different spacers were prepared: **PAO-ManC11N₃** (C11 spacer, studied in **Chapter 3**, as a hydrophobic long spacer) and **PAO-ManC3N₃** (C3 spacer as a short spacer) (**Figure 1**).

The XPS survey scan spectra of the mannose-presenting PAO surfaces (**Figure 3a, c, and d**) clearly show the presence of a N 1s peak at 400 eV, in addition to the peaks corresponding to the other components of the substrate, the initial monolayer, and the carbohydrate (Al at 119 eV, P at 191 eV, C at 285 eV, and O at 531 eV). The C 1s narrow

scans (**Figure 3b, d, and e**) present three types of carbon: $\underline{\text{C}}\text{-C}$ (285.0 eV), $\underline{\text{C}}\text{-O}/\underline{\text{C}}\text{-N}$ (286.5 eV) and $\text{O}-\underline{\text{C}}\text{-O}$ (288.0 eV), with the percentage of $\underline{\text{C}}\text{-O}/\underline{\text{C}}\text{-N}$ varying in accordance with the spacer of the mannose derivative.

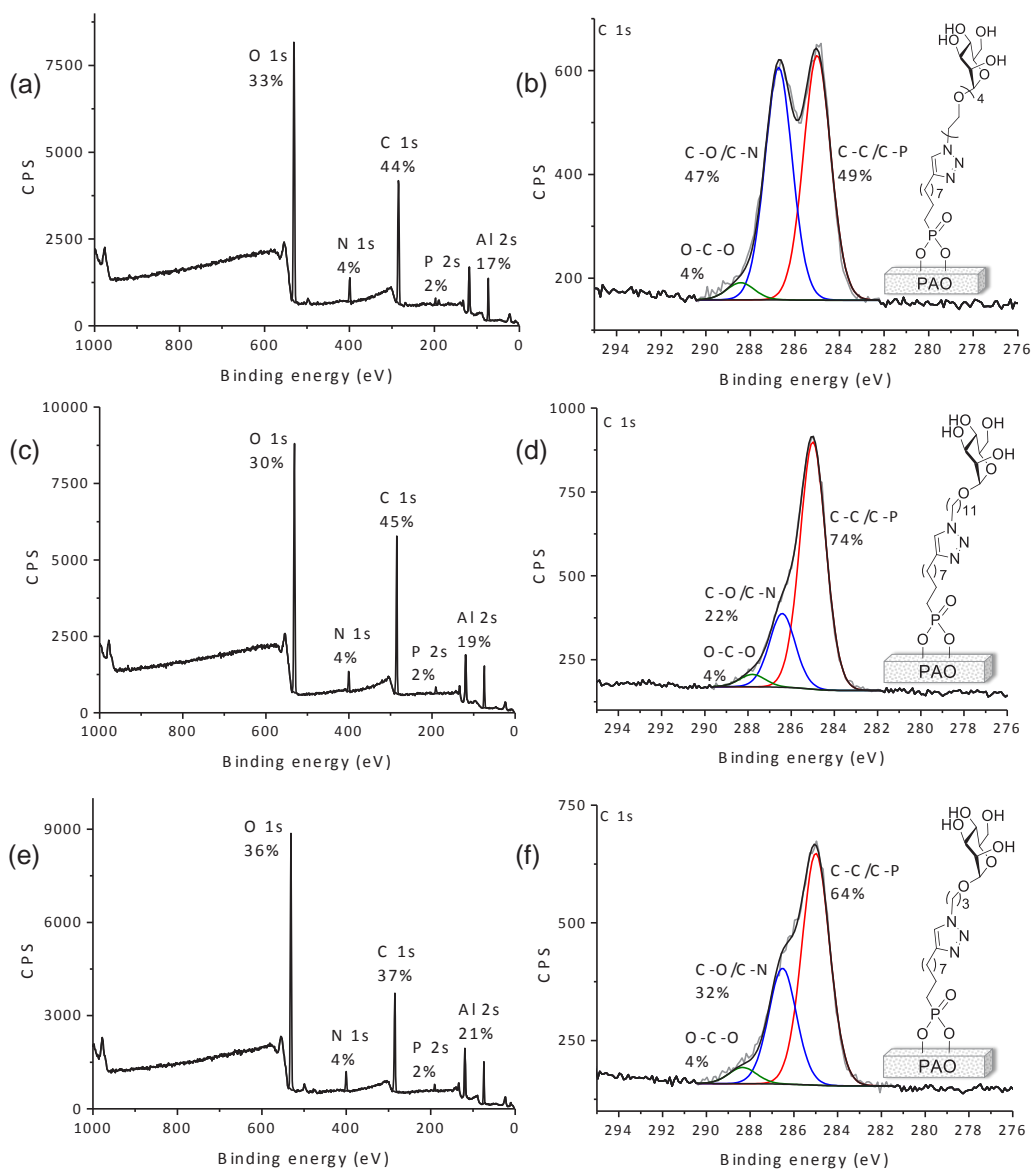


Figure 3. XPS spectra of mannose-presenting PAO surfaces: (a) survey scan and (b) C 1s narrow scan of PAO-ManPEG4N₃, (c) survey scan and (d) C 1s narrow scan of PAO-ManC11N₃, and (e) survey scan and (f) C 1s narrow scan of PAO-ManC3N₃.

Binding of *L. plantarum* on Mannose-Presenting PAO With Different Spacers

In **Chapter 3**, we have shown that the potential probiotic bacterium *L. plantarum* WCFS1 can bind to mannose-presenting PAO via its specific mannose-binding adhesin.⁹ To further explore this binding process and the parameters that may be involved in this interaction, we first assessed the binding of *L. plantarum* WCFS1 on PAO presenting mannose derivatives with different spacers: a long hydrophobic one (**PAO-ManC11N₃**, used in **Chapter 3**), a short one (**PAO-ManC3N₃**), and a long hydrophilic one (**PAO-ManPEG4N₃**). The highest bacterial binding was found on the surfaces containing the mannose derivative with the hydrophobic C11 spacer (**PAO-ManC11N₃**), with only a slightly lower binding on the surfaces with the hydrophilic PEG4 spacer (**PAO-ManPEG4N₃**) and a considerably lower binding on the surfaces with the short C3 spacer (**PAO-ManC3N₃**) (**Figure 4a**). Although ethylene glycol spacers have been used to decrease non-specific adsorption,^{19, 20} a high binding of *L. plantarum* WCFS1 was observed on mannose-free **PAO-PEG4N₃** control surfaces (data not shown), indicating that part of the binding on **PAO-ManPEG4N₃** may be due to non-specific adsorption. Previous studies also showed that the modification of stainless steel with PEG molecules was effective to prevent the adsorption of proteins, but did not prevent bacterial binding.²¹ The low binding on **PAO-ManC3N₃** might be due to the rigidity caused by the short spacer, making the carbohydrates on the surface less available to interact with the adhesin units of the bacteria. Because of the high binding of *L. plantarum* WCFS1 on the mannose-presenting surfaces with the C11 spacer, we decided to use the **PAO-ManC11N₃** surfaces for all subsequent experiments.

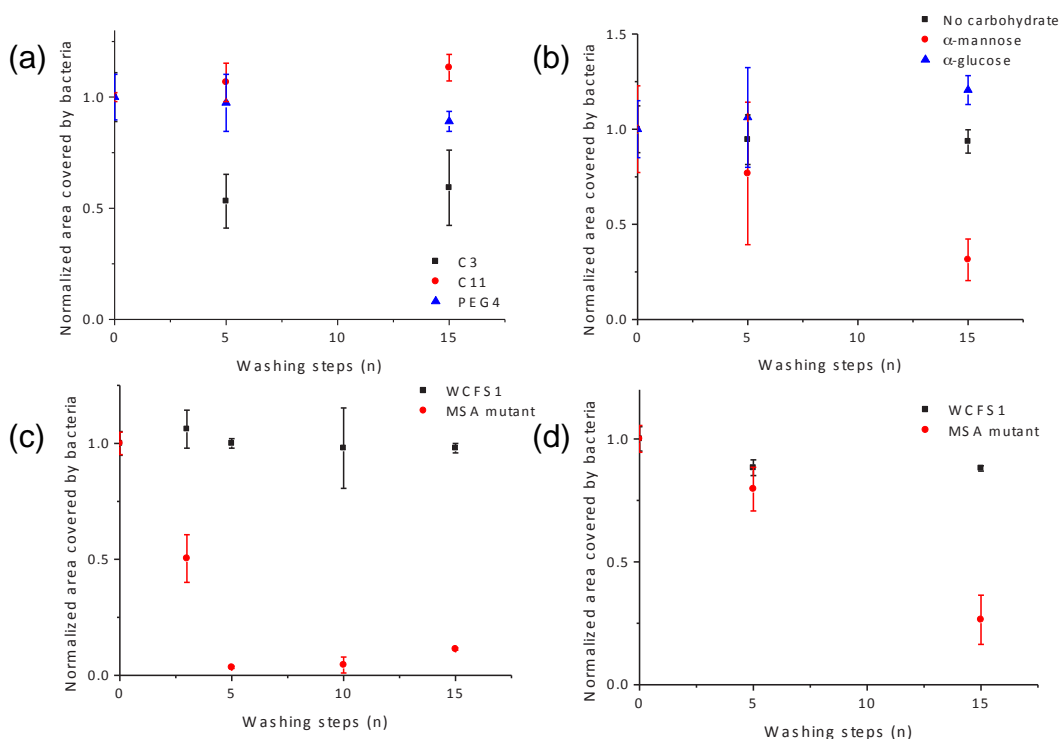


Figure 4. Binding of *L. plantarum* WCFS1 on mannose-presenting PAO surfaces: (a) Mannose-presenting PAO with different spacers, (b) on PAO-ManC11N₃ in the presence of soluble sugars, (c) binding of *L. plantarum* WCFS1 and MSA mutant strain on PAO-ManC11N₃, and (d) in the presence of BSA in solution.

Binding of L. plantarum on Mannose-Presenting PAO in the Presence of Soluble Carbohydrates

The effect of the presence of methyl- α -D-mannopyranoside in solution on the binding of *L. plantarum* WCFS1 to mannose-presenting PAO was shown in **Chapter 3**. This mannose derivative occupies the binding sites of the mannose-binding adhesin of *L. plantarum* WCFS1 and consequently hampers the binding of the bacteria to the carbohydrate-presenting PAO.¹¹ To verify whether the blocking of the adhesin was caused specifically by the mannose derivative, the same experiment was performed in the presence of methyl- α -D-glucopyranoside, an equivalent glucose derivative. When this glucose derivative is present in the suspension of bacteria, the binding of *L. plantarum* WCFS1 to the mannose-presenting PAO surfaces is similar to the binding in the absence of a soluble carbohydrate (**Figure 4b**). Not surprisingly, this shows that a

carbohydrate with a single but critical difference, the equatorial orientation of the hydroxyl group of C2, cannot block the mannose-binding adhesin of *L. plantarum*.⁹

Binding of L. plantarum WCFS1 and NZ7511 on Mannose-Presenting PAO

Finally, the binding of *L. plantarum* NZ7511, an isogenic mutant of strain WCFS1, which does not present the mannose-specific adhesin (MSA mutant)⁹ was also tested and compared with the binding of the strain WCFS1. Most of the *L. plantarum* MSA mutant was removed from the mannose-presenting **PAO-ManC11N₃** surface upon washing, whereas almost all the *L. plantarum* WCFS1 cells remained on the surface even when the surface was extensively washed (**Figure 4c**). These results showed that the mannose-specific adhesin of *L. plantarum* WCFS1 is essential for the binding on the mannose-presenting PAO surfaces and proved that this interaction is the main mechanism of the binding.

Considering that complex biological samples would be used for a future application of the carbohydrate-presenting PAO surfaces, this experiment was also performed in the presence of BSA to increase the complexity of the system. In this case, the same trend was observed (**Figure 4d**), but more washing steps were necessary to remove the MSA mutant from the surface. However, when the binding of *L. plantarum* WCFS1 was performed in the presence of methyl- α -D-mannopyranoside and BSA, the presence of the soluble mannose derivative did not prevent the binding of the bacteria to the surface. This may be due to interactions between methyl- α -D-mannopyranoside and BSA, which impede the blocking of the mannose-binding adhesin on the bacteria by the soluble mannose derivative. These results showed that although the adhesin-mannose plays the main role in the binding, there are more interactions with other proteins that may be relevant in complex mixtures.

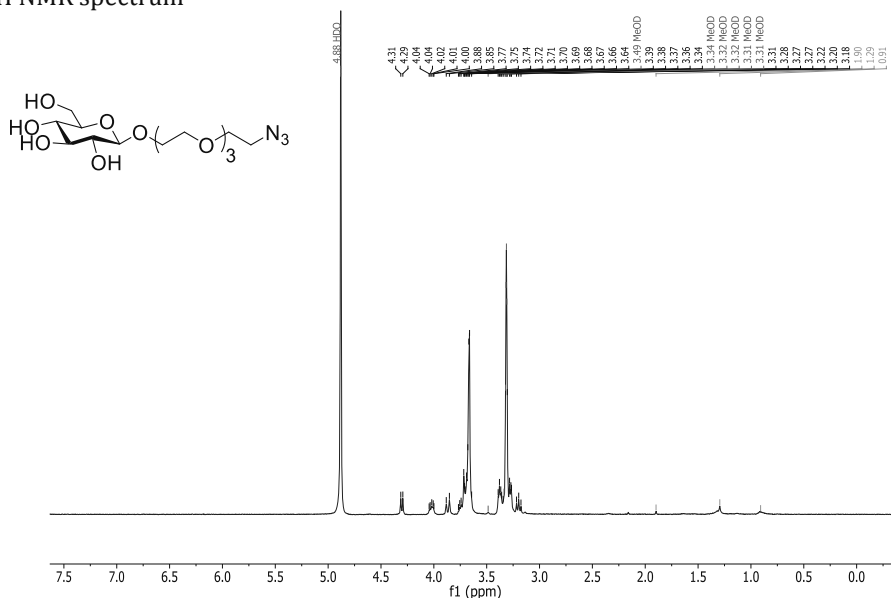
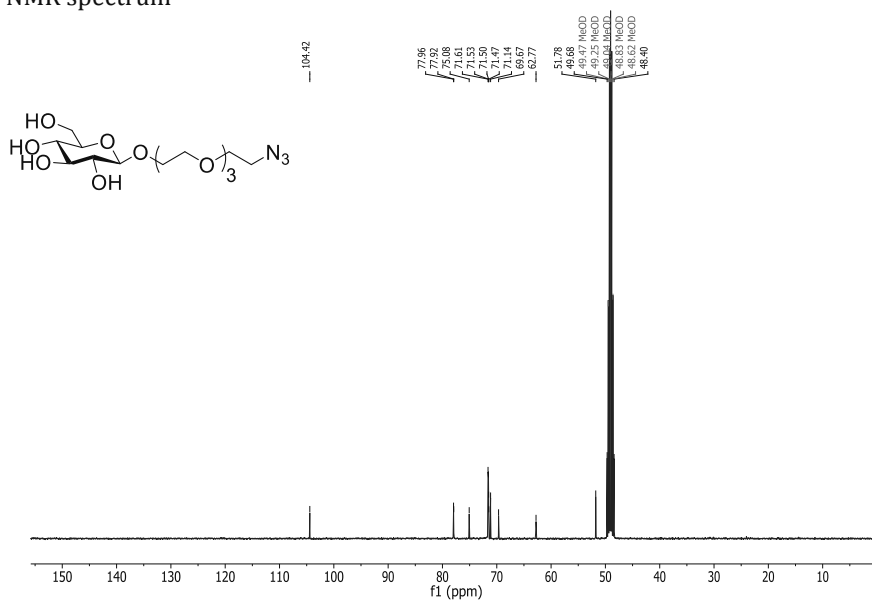
Conclusions

We immobilized with high efficiency azide-containing mannose derivatives with different spacers on alkyne-terminated PAO surfaces via the CuAAC click reaction. The mannose-presenting PAO surface containing the long hydrophobic C11 spacer presented the highest binding of *L. plantarum* WCFS1 and a low non-specific binding of the MSA mutant deficient for the production of the mannose-specific adhesin. The presence of a

soluble glucoside did not prevent the binding of *L. plantarum* to the mannose-presenting PAO whereas a soluble mannose did, showing the high specificity of the adhesin on the cell envelope of *L. plantarum*. Finally, the mannose-specific adhesin of *L. plantarum* showed to be essential for the binding on the mannose-presenting surface, demonstrating that this interaction is the main mechanism of binding.

Acknowledgements

This work is supported by NanoNextNL, a micro and nanotechnology consortium of the government of The Netherlands and 130 partners, and by ERC grant 250712 (MicrobesInside). We thank Frank W. Claassen (Wageningen University) for HRMS measurements.

1-[2-[2-[2-(2-azidoethoxy)ethoxy]ethoxy]ethyl)]- β -D-glucopyranoside (6) ^1H NMR spectrum**Figure SI-3.** ^1H NMR spectrum of 1-[2-[2-[2-(2-azidoethoxy)ethoxy]ethoxy]ethyl)]- β -D-glucopyranoside (6). ^{13}C NMR spectrum**Figure SI-4.** ^{13}C NMR spectrum of 1-[2-[2-[2-(2-azidoethoxy)ethoxy]ethoxy]ethyl)]- β -D-glucopyranoside (6).

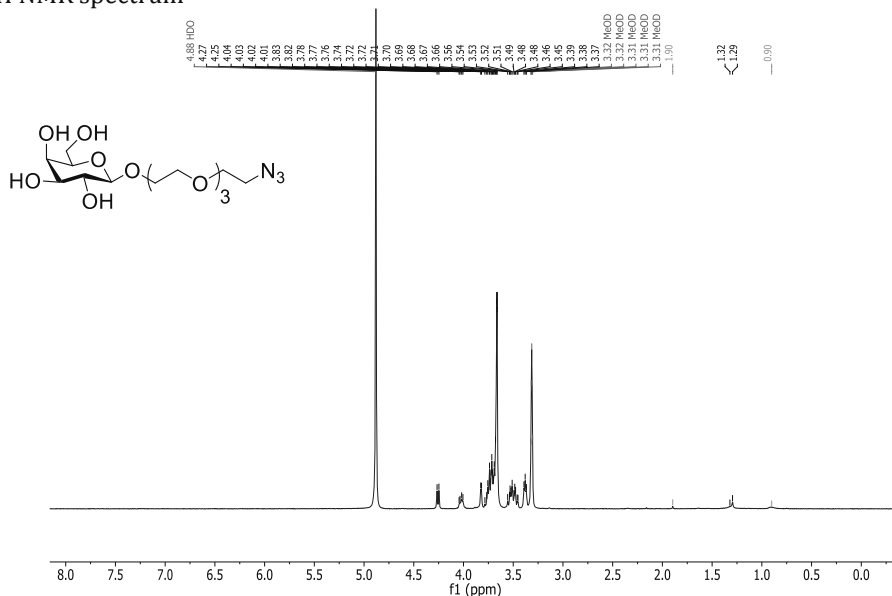
1-[2-[2-[2-(2-azidoethoxy)ethoxy]ethoxy]ethyl)]-β-D-galactopyranoside (9)¹H NMR spectrum

Figure SI-5. ¹H NMR spectrum of 1-[2-[2-[2-(2-azidoethoxy)ethoxy]ethoxy]ethyl)]-β-D-galactopyranoside (9).

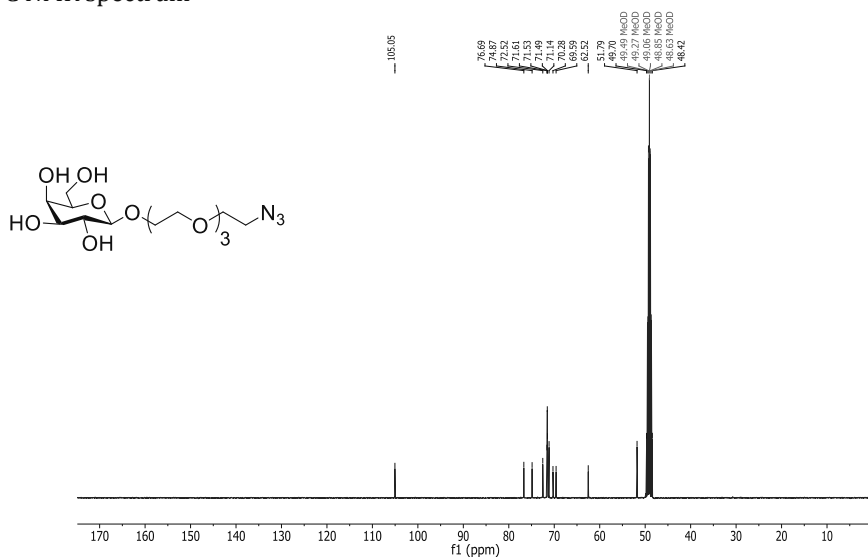
¹³C NMR spectrum

Figure SI-6. ¹³C NMR spectrum of 1-[2-[2-[2-(2-azidoethoxy)ethoxy]ethoxy]ethyl)]-β-D-galactopyranoside (9).

References

1. Horlacher, T.; Seeberger, P. H. Carbohydrate arrays as tools for research and diagnostics. *Chem. Soc. Rev.* **2008**, *37*, 1414-1422.
2. Kregel, U.; Bousquet, P. A. Molecular recognition of gangliosides and their potential for cancer immunotherapies. *Front. Immunol.* **2014**, *5*, 325.
3. Hakomori, S. Glycosylation defining cancer malignancy: new wine in an old bottle. *Proc. Natl. Acad. Sci. U.S.A.* **2002**, *99*, 10231-10233.
4. Berois, N.; Osinaga, E. Glycobiology of neuroblastoma: impact on tumor behavior, prognosis, and therapeutic strategies. *Front. Oncol.* **2014**, *4*, 114.
5. Hartmann, M.; Lindhorst, T. K. The bacterial lectin FimH, a target for drug discovery - carbohydrate inhibitors of type 1 fimbriae-mediated bacterial adhesion. *Eur. J. Org. Chem.* **2011**, *2011*, 3583-3609.
6. Kamhi, E.; Joo, E. J.; Dordick, J. S.; Linhardt, R. J. Glycosaminoglycans in infectious disease. *Biol. Rev.* **2013**, *88*, 928-943.
7. Kamiya, Y.; Yagi-Utsumi, M.; Yagi, H.; Kato, K. Structural and molecular basis of carbohydrate-protein interaction systems as potential therapeutic targets. *Curr. Pharm. Des.* **2011**, *17*, 1672-1684.
8. Zeng, X.; Andrade, C. A. S.; Oliveira, M. D. L.; Sun, X. L. Carbohydrate-protein interactions and their biosensing applications. *Anal. Bioanal. Chem.* **2012**, *402*, 3161-3176.
9. Pretzer, G.; Snel, J.; Molenaar, D.; Wiersma, A.; Bron, P. A.; Lambert, J.; de Vos, W. M.; van der Meer, R.; Smits, M. A.; Kleerebezem, M. Biodiversity-based identification and functional characterization of the mannose-specific adhesin of *Lactobacillus plantarum*. *J. Bacteriol.* **2005**, *187*, 6128-6136.
10. de Vos, W. M. Systems solutions by lactic acid bacteria: from paradigms to practice. *Microb. Cell Fact.* **2011**, *10*.
11. Debrassi, A.; Ribbera, A.; de Vos, W. M.; Wennekes, T.; Zuilhof, H. Stability of (bio)functionalized porous aluminum oxide. *Langmuir* **2014**, *30*, 1311-1320.
12. Ladmiral, V.; Mantovani, G.; Clarkson, G. J.; Cauet, S.; Irwin, J. L.; Haddleton, D. M. Synthesis of neoglycopolymers by a combination of "click chemistry" and living radical polymerization. *J. Am. Chem. Soc.* **2006**, *128*, 4823-4830.
13. Thomas, M.; Gesson, J.-P.; Papot, S. First O-glycosylation of hydroxamic acids. *J. Org. Chem.* **2007**, *72*, 4262-4264.
14. Yu, B.; Tao, H. Glycosyl trifluoroacetimidates. Part 1: Preparation and application as new glycosyl donors. *Tetrahedron Lett.* **2001**, *42*, 2405-2407.
15. Yu, B.; Tao, H. Glycosyl Trifluoroacetimidates. 2. Synthesis of dioscin and xiebai saponin I. *J. Org. Chem.* **2002**, *67*, 9099-9102.
16. Zhang, Y.; Luo, S. Z.; Tang, Y. J.; Yu, L.; Hou, K. Y.; Cheng, J. P.; Zeng, X. Q.; Wang, P. G. Carbohydrate-protein interactions by "clicked" carbohydrate self-assembled monolayers. *Anal. Chem.* **2006**, *78*, 2001-2008.
17. Kleinert, M.; Winkler, T.; Terfort, A.; Lindhorst, T. K. A modular approach for the construction and modification of glyco-SAMs utilizing 1,3-dipolar cycloaddition. *Org. Biomol. Chem.* **2008**, *6*, 2118-2132.
18. Madwar, C.; Kwan, W. C.; Deng, L.; Ramstrom, O.; Schmidt, R.; Zou, S.; Cuccia, L. A. Perfluorophenyl azide immobilization chemistry for single molecule force spectroscopy of the concanavalin A/mannose interaction. *Langmuir* **2010**, *26*, 16677-16680.
19. Kingshott, P.; Wei, J.; Bagge-Ravn, D.; Gadegaard, N.; Gram, L. Covalent attachment of poly(ethylene glycol) to surfaces, critical for reducing bacterial adhesion. *Langmuir* **2003**, *19*, 6912-6921.
20. Harris, L. G.; Tosatti, S.; Wieland, M.; Textor, M.; Richards, R. G. *Staphylococcus aureus* adhesion to titanium oxide surfaces coated with non-functionalized and peptide-functionalized poly(L-lysine)-grafted-poly(ethylene glycol) copolymers. *Biomaterials* **2004**, *25*, 4135-4148.
21. Wei, J.; Ravn, D. B.; Gram, L.; Kingshott, P. Stainless steel modified with poly(ethylene glycol) can prevent protein adsorption but not bacterial adhesion. *Colloid. Surface. B* **2003**, *32*, 275-291.

Chapter 6

Biofunctionalization of Porous Aluminum Oxide With Antibodies for the Binding of Bacteria

**Aline Debrassi¹, Hanne Tytgat², François Douillard³, Willem M. de Vos^{2,3}, Han
Zuilhof^{1,4}, Tom Wennekes¹**

¹ Laboratory of Organic Chemistry, Wageningen University, 6703 HB Wageningen, The
Netherlands

² Laboratory of Microbiology, Wageningen University, 6703 HB Wageningen, The
Netherlands

³ Department of Bacteriology & Immunology and Department of Veterinary Biosciences,
University of Helsinki, 00014 Helsinki, Finland

⁴ Department of Chemical and Materials Engineering, King Abdulaziz University, 21589
Jeddah, Saudi Arabia

Manuscript in preparation

Abstract

Porous aluminum oxide (PAO), a nanostructured material capable of culturing microorganisms, was biofunctionalized with antibodies against *Escherichia coli* and the binding of this bacterium on the biofunctionalized surfaces was studied. Initially, the surface modification chemistry and the experimental conditions used in the binding experiments were investigated and optimized. The optimization experiments showed that the incubation conditions were more important to decrease the non-specific adsorption of bacteria than the approach used for the chemical modification. The PAO biofunctionalized with the anti-*E. coli* antibodies showed increased binding of this bacterium, which can still grow on the antibodies-presenting PAO surfaces. Optimization for usage of this technique with *Lactobacillus rhamnosus* GG is currently ongoing.

Introduction

Porous aluminum oxide (PAO), also known as anodic aluminum oxide and nanoporous alumina, is a nanoporous material used for various biotechnological applications, including as a support to grow and count microorganisms and other types of cells.¹⁻⁸ In the previous chapters, we showed that it is possible to generate stable reactive phosphonate-based monolayers on PAO that can then be further biofunctionalized with carbohydrates and proteins to achieve the binding of a target bacteria.^{9, 10} Additionally, the captured bacteria can still grow on the biofunctionalized PAO, even when the surface is covalently modified with a protein.¹⁰

The immobilization of carbohydrates on the PAO surfaces enables the selective binding of bacteria, but in general the binding strength is weak and it does not provide a very specific binding of one single bacterial species or strain.¹¹ To achieve species- or strain-selective binding, a different biorecognition element needs to be used, such as antibodies, which are the most commonly used bioreceptor for the detection of bacterial cells.¹² The immobilization of antibodies on PAO has already been applied to detect biomarkers related to cancer progression¹³ and pathogenic bacteria.^{14, 15}

Our overall aim is to selectively capture and grow specific bacteria on PAO, as to optimally exploit the possibilities to functionalize this surface and use it to support growth of microorganisms.^{1,6,9} We selected *Lactobacillus rhamnosus* GG as model system as this strain is widely applied in probiotic and other functional foods¹⁶⁻¹⁹ because of its contribution to promoting the development of a healthy immune response²⁰ and

reducing inflammation.²¹ Moreover, it is known that the composition of the gut microbiota plays a major role in maintaining the homeostasis of the human metabolism.²² Therefore, it would be helpful to have a simple and quick way to identify, isolate, and quantify *L. rhamnosus* from faecal samples of healthy subjects or patients.

It has been shown that *L. rhamnosus* GG is capable of producing proteinaceous adhesive appendages, termed pili, on its surface that are composed of three pilin subunits: SpaA, SpaB, and SpaC (**Figure 1**). SpaA is the major fiber component building up the pilus shaft, while SpaB is considered to be the stop transfer protein that docks the pili to the peptidoglycan.²³⁻²⁵ The SpaC subunit plays a key role in the adhesion of *L. rhamnosus* GG to human intestinal mucus²⁴ and is located at the pilus tip and also along the length of the pilus shaft.²³ Recently, antibodies have been developed directed against the SpaC protein and its various domains as well as against whole *L. rhamnosus* GG cells. These are good candidates to be tested as surface-bound biomolecules to selectively capture cells of *L. rhamnosus* GG on the PAO surface while the specificity of the anti-SpaC antibodies can be validated by using the isogenic but non-pili producing derivative PB12.²⁶

In this study our aim is to immobilize antibodies generated against *L. rhamnosus* GG on PAO surfaces and to use the biofunctionalized surfaces for the selective binding and growth of the captured bacteria. Initially, the surface modification and especially the experimental conditions used for the bacterial binding experiments were extensively studied and optimized. A commercially available antibody against *Escherichia coli* was then immobilized on PAO and the binding of this bacterium was tested as a proof-of-principle. It is interesting to study both *Escherichia coli* and a gut-relevant bacterium, as this technique holds promise for the capture and growth of other bacteria and for screening of complex samples.

Materials and Methods

Materials

Porous aluminum oxide (PAO) substrates with dimensions of 36 × 8 mm² and average pore size of 200 nm were purchased from MicroDish BV (Netherlands). 12-Bromododecylphosphonic acid was purchased from SiKÉMIA (France). 2,5-dioxopyrrolidin-1-yl 1-(bicyclo[6.1.0]non-4-yn-9-yl)-3,14-dioxo-2,7,10-trioxa-4,13-

diazaoctadecan-18-oate (BCN-NHS) was obtained from SynAffix (The Netherlands). Alpha-amino-omega-hydroxy poly(ethylene glycol) (PEG-MW = 3.000 Dalton, PEG3000-amine) was purchased from Iris Biotech GmbH (Germany). Dichloromethane was purified using a Pure Solv 400 solvent purification system (Innovative Technology, USA). Dry DMF was purchased in SureSeal™ bottles and stored under argon. Ultrapure water was produced using a Milli-Q Integral 3 system (Millipore, France). Other solvents used were of analytical grade. Anti-*E. coli* antibodies were purchased from Abcam Antibodies (ab48416, generated against 6 strains of *E. coli*: TOP 10F, HB101, JM109, BL21, DH5 alpha and K12). Protein printing buffer (2×) was purchased from Arrayit Corporation. SYTO9 and hexidium iodide were purchased from Thermo Fisher Scientific (USA). The other chemicals were obtained from Sigma-Aldrich and used without further purification. Sonication steps were performed in an Elmasonic P 30 H ultrasonic unit at a frequency of 80 kHz. For the microbiological experiments, surfaces with bacteria were imaged with an Olympus BX-41 fluorescence microscope equipped with U-MNIBA2 (for bacteria stained with SYTO9) and U-MWG2 (for bacteria stained with hexidium iodide) filters (Olympus). Images were taken using a Kappa CCD camera. ImageJ was used to adjust the contrast and the color of the images.

Modification of PAO with 12-Bromododecylphosphonic Acid

The substrate preparation procedure was the same as previously reported by us.^{9, 10} In short, A PAO substrate was rinsed and sonicated in acetone (5 min) and ultrapure water (5 min). The substrate was immersed in a freshly prepared mixture of 37% hydrochloric acid and methanol (1:1 v/v) for 30 min. It was then rinsed and sonicated in ultrapure water (5 min) and absolute ethanol (5 min). The PAO substrate was immersed in a 1 mM solution of 12-bromododecylphosphonic acid in absolute ethanol for 16 h at room temperature. Afterward, it was rinsed with absolute ethanol and heated at 140 °C under vacuum for 6 h. Finally, the substrate was rinsed and sonicated in absolute ethanol (twice for 5 min) and dichloromethane (5 min) and dried under ambient conditions to obtain the bromo-terminated PAO (**PAO-Br**). The bromo-terminated PAO substrate that was used to obtain the azide-terminated PAO (**PAO-N₃**) itself was prepared using a 1 mM mixture of 12-bromododecylphosphonic acid and 1-octylphosphonic acid 50:50 (w/w) to obtain the **PAO-mix-Br** substrate.

N-Hydroxysuccinimide (NHS)-Terminated PAO From the Amine-Terminated PAO (PAO-NH₂-NHS)

The **PAO-Br** substrate was immersed in a 1.0 M solution of tris(2-aminoethyl) amine in dry DMF for 16 h at room temperature. It was then rinsed, sonicated in DMF (5 min), ethanol (5 min), and dichloromethane (5 min) and dried under ambient conditions to obtain the amine-terminated PAO (**PAO-NH₂**). The **PAO-NH₂** substrate was immersed in a solution containing 0.1 M *N,N'*-disuccinimidyl carbonate (DSC) and 0.1 M *N,N*-diisopropylethylamine (DIPEA) in DMF at 40 °C for 16 h. After the reaction, the substrate was rinsed, sonicated in DMF (5 min) and dichloromethane (5 min), and dried in air to obtain the **PAO-NH₂-NHS** substrate.

NHS-Terminated PAO From the Azide-Terminated PAO (PAO-N₃-NHS)

The **PAO-mix-Br** substrate was immersed in a 0.1 M NaN₃ solution in dry DMF for 16 h at 60 °C under argon. The substrate was rinsed, sonicated in DMF (5 min), ethanol (5 min), and dichloromethane (5 min), and dried under ambient conditions to obtain the azide-terminated PAO (**PAO-N₃**). The **PAO-N₃** substrate was immersed in a 5 mM solution of BCN-NHS in dichloromethane for 4 h at room temperature. The substrate was then rinsed, sonicated in dichloromethane (5 min), and dried in air.

Polyglycerol-Terminated PAO (PAO-PG)

A PAO substrate was rinsed and sonicated in acetone (5 min) and ultrapure water (5 min). The substrate was immersed in a freshly prepared mixture of 37% hydrochloric acid and methanol (1:1 v/v) for 30 min. It was then rinsed and sonicated in ultrapure water (5 min), absolute ethanol (5 min), and *N*-methyl-2-pyrrolidone (NMP, 5 min). The substrate was then immersed in a 10% (w/w) glycidol solution in NMP at 140 °C for 24 h. Afterward, the substrate was rinsed, sonicated in water (twice for 5 min), ethanol (5 min), dichloromethane (5 min), and dried under ambient conditions.²⁷

Blocking of PAO-NHS With Amines

The blocking of **PAO-NHS** was performed with ethanolamine, tetraethylene glycol amine (PEG4-amine) or PEG3000-amine. For ethanolamine and PEG4-amine, a 0.1 or 0.25 M solution of the amine was prepared in PBS and the pH of the solution was adjusted to 7 – 8 with 37% hydrochloric acid. The **PAO-NH₂-NHS** and **PAO-N₃-NHS**

surfaces were immersed in this solution for 1, 4 or 24 h at room temperature. The surfaces were then extensively rinsed with PBS pH 7. When used for infrared spectroscopy and for the optimization of the negative control in the microbiological experiments, the surfaces were additionally rinsed, sonicated in water (5 min), ethanol (5 min), and dichloromethane (5 min), and dried under ambient conditions. When used for the microbiological experiments, the following conditions were used: 0.1 M solution of the amine (pH 7 – 8) and 4 h of immersion of the surfaces, without the sonication steps, except when indicated. For PEG3000-amine, the **PAO-NH₂-NHS** and **PAO-N₃-NHS** surfaces were immersed in a 20 mg/mL solution of the amine in PBS pH 7 for 4 h at room temperature. Afterward, the surface was extensively rinsed with PBS pH 7.

X-ray photoelectron spectroscopy (XPS)

XPS measurements were performed using a JPS-9200 photoelectron spectrometer (JEOL). The spectra were obtained using a monochromatic Al K α X-ray radiation at 12 kV and 20 mA under ultrahigh vacuum conditions. The binding energies were calibrated at 531 eV for the O 1s peak as a reference for the PAO-PG surfaces and at 285.0 eV for the C 1s peak for the other modified PAO substrates. To counteract electrostatic surface charging, charge neutralization was used with electrons with a kinetic energy of 2.8 eV and a filament current of 4.8 A. High-resolution spectra were corrected using a linear background subtraction before fitting. The spectra were processed using CasaXPS software (version 2.3.15).

Immobilization of Anti-*E. coli* Antibody on PAO

The **PAO-NH₂-NHS** surfaces were covered with a 0.5 mg/mL of anti-*E. coli* antibodies in protein printing buffer (1 \times) (100 μ L of solution for each piece (36 \times 8 mm²) of PAO), kept for 10 min at room temperature and then for 16 h at 4 °C. The surfaces were washed with PBS pH 7 (5 \times 2 mL) and the blocking step was performed. The blocking step consisted of covering these surfaces with a 20 mg/mL solution of PEG3000-amine in PBS pH 7 at room temperature for 4 h and, subsequently, washing the surfaces with PBS pH 7 (5 \times 2 mL). The blocking step was also performed directly on the **PAO-NH₂-NHS** surfaces under the same conditions and these surfaces were used as the negative control for the bacterial binding experiments.

Optimization of the Negative Control for the Bacterial Binding Experiments

Initially, the **PAO-NH₂-NHS** and **PAO-N₃-NHS** surfaces blocked with ethanolamine, tetraethylene glycol amine (PEG4-amine), and PEG3000-amine were tested as negative controls. An overnight culture of *Lactobacillus plantarum* WCFS1 strain expressing a far-red fluorescent protein (*L. plantarum* FRFP) (François Douillard, unpublished results) in MRS broth containing 5 µg/mL chloramphenicol was diluted with fresh MRS with 5 µg/mL chloramphenicol (1:5, overnight culture/fresh medium) and incubated at 37 °C for 4 h. The bacteria were then diluted with water to obtain an optical density at 600 nm (OD₆₀₀) of 0.5. The **PAO-NH₂-NHS** or **PAO-N₃-NHS** surfaces blocked with the three different blocking agents (with or without the sonication step) (**Table 1**) were cut in four equal pieces (9 × 8 mm²). The bottom of a Petri dish was covered with a piece of parafilm and the surfaces were placed on top of it (**Figure 1**). The suspension of bacteria with OD₆₀₀ = 0.5 was placed on the surfaces (3 µL per one quarter of PAO) and the Petri dishes were incubated at 37 °C for 30 min. The top surface of the samples was washed various times (0, 1 or 15 times). Each washing step consisted of adding and removing 250 µL of PBS containing 0.05% of Tween 20 (PBST) three times, using a micropipette and a round support to contain the PBST. The bacteria were then imaged using fluorescence microscopy and the area covered by bacteria was calculated using CellProfiler.⁹

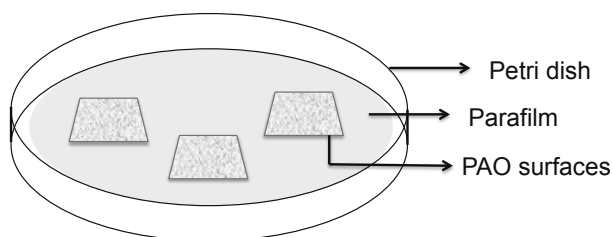


Figure 1. Schematic representation of experimental setup.

The second part of the optimization of the negative control was performed with the **PAO-PG** surfaces and *L. plantarum* FRFP and *E. coli* K12. An overnight culture of *L. plantarum* FRFP in MRS broth containing 5 µg/mL chloramphenicol was diluted in fresh MRS with 5 µg/mL chloramphenicol (1:5, overnight culture/fresh medium) and incubated at 37 °C for 4 h. The *E. coli* K12 was directly used from the overnight culture.

The bacteria were diluted to obtain $OD_{600} = 0.5$. The **PAO-PG** surfaces were cut in four equal pieces ($9 \times 8 \text{ mm}^2$) and the samples were placed on a Petri dish covered with parafilm. The suspension of bacteria with $OD_{600} = 0.5$ was added to the surfaces ($3 \mu\text{L}$ per one quarter of PAO) and the Petri dishes were incubated at 37°C for 30 min or directly washed (incubation time = 10 s). Two different washing methods were evaluated. In the pipette method, each washing step consisted of adding and removing $250 \mu\text{L}$ of PBST three times, using a micropipette and a round support to contain the PBST. This procedure was repeated 15 times with each surface. In the rotating method, each surface with bacteria was placed in a 1.5 mL tube containing 1 mL of PBST and agitated in a shaker at 100 rpm for 5 min. The PBST was removed and 1 mL of fresh PBST was added. This washing procedure was repeated three times for each surface. The bacteria were then further stained with hexidium iodide by placing the PAO on low-melting-point agarose containing $20 \mu\text{M}$ hexidium iodide for approximately 30 min in the dark. Imaging was performed using fluorescence microscopy, and the area covered by bacteria was calculated using CellProfiler.

The third part of the optimization was performed with the **PAO-PG** surfaces and *E. coli* K12. An overnight culture of *E. coli* K12 in LB broth was diluted to obtain $OD_{600} = 0.1$ or 0.5 . The **PAO-PG** surfaces were cut in four equal pieces ($9 \times 8 \text{ mm}^2$) and the samples were placed on a Petri dish covered with parafilm. The suspension of bacteria with $OD_{600} = 0.1$ or 0.5 was placed on the samples (100 or $250 \mu\text{L}$ per one quarter of PAO) and the Petri dishes were incubated at 37°C for 5, 15 or 30 min. Each surface with bacteria was placed in a 1.5 mL tube containing 1 mL of PBST and agitated in a shaker at 100 rpm for 5 min. The PBST was removed and 1 mL of fresh PBST was added. This washing procedure was repeated three times for each surface. The bacteria were then stained with hexidium iodide by placing the PAO on low-melting-point agarose containing $20 \mu\text{M}$ hexidium iodide for approximately 30 min in the dark, imaged using fluorescence microscopy, and the area covered by bacteria was calculated using CellProfiler.

Binding of E. coli to PAO Surfaces Containing Antibodies

An overnight culture of *E. coli* K12 in LB broth was stained with SYTO9. For the staining procedure, $2 \mu\text{L}$ of a 5 mM solution of SYTO9 was added to a 1 mL of the culture with $OD_{600} = 1.7$ and incubated in the dark at room temperature for 5 min. To remove

the excess of SYTO9, the stained bacteria were centrifuged for 3 min (12000 rpm) at 4 °C. The supernatant was removed and 1 mL of PBST was added and the cells were resuspended. This washing procedure was repeated three times, and in the third time the cells were resuspended in 1 mL of PBS pH 7 instead of PBST.

For the binding experiments, the bacteria stained with SYTO9 were diluted in PBS pH 7 to obtain $OD_{600} = 0.5$. The PAO surfaces with the immobilized anti-*E. coli* antibodies were cut in four equal pieces ($9 \times 8 \text{ mm}^2$) and the samples were placed on a Petri dish covered with parafilm. The suspension of bacteria with $OD_{600} = 0.5$ was placed on the samples (100 μL per one quarter of PAO) and the Petri dishes were incubated at 37 °C for 5 min. The top surface of the samples was washed various times (0, 1, 3 or 5 times). Each washing step consisted of adding and removing 250 μL of PBST three times, using a micropipette and a round support to contain the PBST. The bacteria were then imaged using fluorescence microscopy. The same procedure was performed with the **PAO-NH₂-NHS** surfaces directly blocked with PEG3000-amine as a negative control.

Growth of E. coli on PAO Surfaces Containing Antibodies

An overnight culture of *E. coli* K12 in LB broth was diluted with PBS pH 7 to obtain $OD_{600} = 0.1$. The PAO surfaces with the immobilized anti-*E. coli* antibodies were cut in four equal pieces ($9 \times 8 \text{ mm}^2$) and placed on LB agar plates. The suspension of bacteria with $OD_{600} = 0.1$ was placed on the samples (3 μL per one quarter of PAO) and the agar plates were incubated at 37 °C. The samples were imaged after 0, 1.5, and 3 h using transmission light.

Binding of L. rhamnosus GG and mutant strain PB12 to PEG-presenting PAO surfaces

Overnight cultures of *L. rhamnosus* strains GG and pili-less mutant PB12²⁶ were grown for 16h in MRS broth (Difco Lactobacilli MRS broth, BD, Amsterdam, The Netherlands) (OD_{600} of around 4.5, late exponential phase). The bacteria were diluted in PBS pH 7 to obtain $OD_{600} = 0.5$. The **PAO-NH₂-NHS** surfaces directly blocked with PEG3000-amine were cut in four equal pieces ($9 \times 8 \text{ mm}^2$) and the surfaces were placed on a Petri dish covered with parafilm. The suspension of bacteria with $OD_{600} = 0.5$ was placed on the samples (100 μL per one quarter of PAO) and the Petri dishes were incubated at 37 °C for 5 min. The surface of the samples was washed 25 times with 250 μL PBST. At least two surfaces with each strain were not washed for further comparison.

The bacteria on the surface were fluorescently stained with hexidium iodide by placing the PAO on low-melting-point agarose containing 20 μ M hexidium iodide for approximately 30 min. The bacteria were imaged using fluorescence microscopy.

Results and Discussion

N-Hydroxysuccinimide (NHS)-Terminated PAO and Blocking with Different Amines

First the surfaces that should act as a negative control in the binding experiments were prepared by blocking NHS-terminated PAO surfaces, their preparation is described in **Chapter 4 (Figure 2a)**,¹⁰ with three different amines. The NHS-terminated surfaces were prepared starting from bromo-terminated PAO surfaces (**PAO-Br** and **PAO-mix-Br**). The first NHS-terminated PAO was prepared by reacting tris(2-aminoethyl)amine to the **PAO-Br** surface, followed by a reaction with *N,N'*-disuccinimidyl carbonate (DSC), a bifunctional NHS molecule, to yield the **PAO-NH₂-NHS** surface. The other NHS-terminated PAO surface had a “diluted” version of **PAO-Br** as the starting point, which was prepared using a 1:1 mixture of 12-bromododecylphosphonic acid and octylphosphonic acid, yielding the **PAO-mix-Br** surface. A substitution reaction of this surface with NaN₃ generated the **PAO-N₃** surface, which reacted with BCN-NHS via strain-promoted azide-alkyne cycloaddition (SPAAC) reaction to form **PAO-N₃-NHS**.¹⁰ Both types of NHS-terminated surface were separately blocked with three types of amines (**Figure 2b**): ethanolamine, PEG4-amine, and PEG3000-amine. Ethanolamine was chosen to create a short hydroxy-terminated control and the short and long PEG-amines were selected because PEG-presenting surfaces are well established in their ability to suppress non-specific binding.²⁸

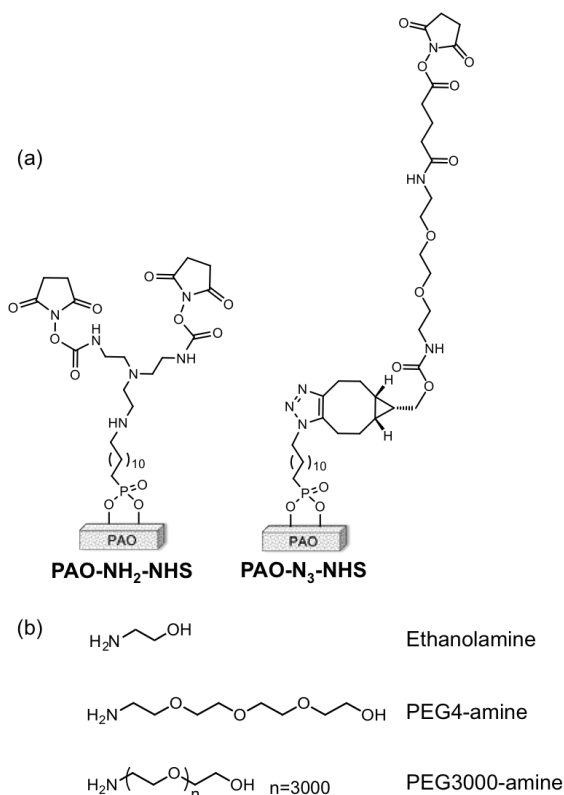


Figure 2. (a) NHS-terminated PAO surfaces and (b) amines used to block the NHS-terminated PAO surfaces.

Preliminary bacterial binding experiments pointed towards an influence of the work-up after the blocking step on the ability of the surfaces to prevent non-specific adhesion. Therefore, after the blocking step, the completed control surfaces were treated in two different ways to assess the extent in which the sample treatment affects the bacterial binding. One set of blocked surfaces was successively sonicated in water, ethanol, dichloromethane and finally dried. Another set was only washed with PBS after the blocking step and subsequently used directly for the microbiological experiments.

Polyglycerol-Terminated PAO (PAO-PG)

Another possible approach to generate surfaces that could prevent non-specific adsorption was with polyglycerol layers, which are a hyperbranched version of oligoethyleneglycol molecules.^{27, 29} These layers were generated on PAO as an attempt to circumvent the non-specific bacterial adsorption observed in the first step of the

optimization of the negative control on the NHS-blocked PAO surfaces. Polyglycerol-terminated PAO surfaces (**PAO-PG**) were prepared via ring-opening polymerization of glycidol, using the hydroxyl groups of the PAO surface as the nucleophile (**Figure 3**).²⁷

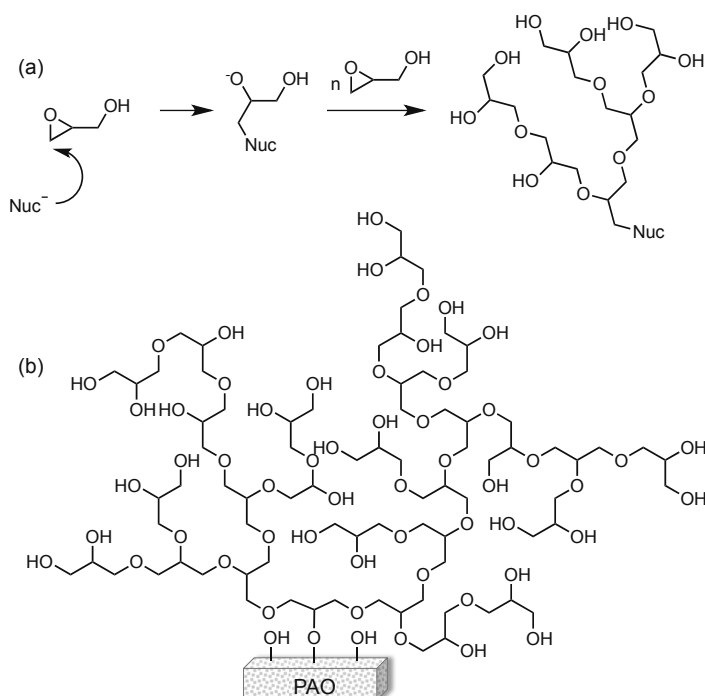


Figure 3. Formation of hyperbranched polyglycerol: (a) The reaction is initiated by the reaction of a nucleophile (Nuc^-) with glycidol through ring-opening polymerization and (b) scheme of **PAO-PG**.²⁷

The X-ray photoelectron spectroscopy (XPS) spectrum of **PAO-PG** (**Figure 4**) shows the almost complete disappearance of the aluminium peak at 119 eV, indicating a layer thickness of at least 20 nm.³⁰ The same reaction conditions generated a layer thickness of 17.6 nm on aluminum and silicon surfaces. According to previous studies on these surfaces,²⁷ a polyglycerol layer thickness of 5 nm was already sufficient to significantly decrease non-specific bacterial adsorption.

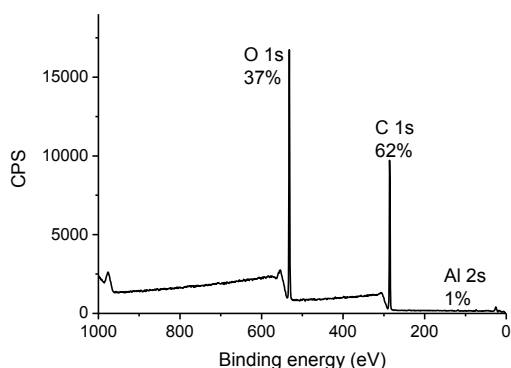


Figure 4. XPS survey scan of **PAO-PG**.

Optimization of the Negative Control for the Bacterial Binding Experiments

The next step was to select the most suitable modification of PAO to be used for the immobilization of the antibodies and, subsequently, for the bacterial binding experiments. Two different NHS-terminated PAO surfaces were tested in combination with three amines as the blocking agent: ethanolamine, PEG4-amine, and PEG3000-amine. The aim was to identify which combination of initial surface modification and blocking agent would present the lowest non-specific bacterial adsorption. Additionally, two surface treatments were tested in order to verify whether the washing, sonication, and drying step would influence the bacterial binding (**Table 1**).

For the bacterial binding experiment in this step of the optimization, an adapted strain of *Lactobacillus plantarum* WCFS1 was used that expresses far-red fluorescent protein (*L. plantarum* FRFP; F. Douillard et al., unpublished observations). This strain was selected because of the convenience of being fluorescent itself, enabling direct visualization by fluorescence microscopy, without the need of a subsequent staining step. The surfaces blocked with the amines were exposed to a small volume (3 μ L) of bacterial suspension for 30 min and then washed to remove the non-adherent bacteria. For the surfaces blocked with ethanolamine and PEG4-amine, the surfaces were washed once or 15 times. However, already for the first batch of surfaces we noticed that a single washing step did not significantly remove bacteria. Therefore, the surfaces blocked with PEG3000-amine were directly washed 15 times. Surprisingly, almost all the bacteria added to the surfaces were still present even after 15 washing steps for all the surfaces and conditions tested (**Figure 5**). Although PEG-presenting surfaces are known to prevent non-specific binding,²⁸ the short and long PEG molecules were not able to

prevent non-specific binding of *L. plantarum* under the tested conditions. The only exception being the **PAO-N₃-NHS** surface blocked with ethanolamine, treated with sonication and dried. However, this was an isolated case and no trend was observed regarding initial surface modification, blocking agent or surface treatment. Non-specific adsorption of bacteria was also found for other PEG-presenting surfaces, which showed a low non-specific adsorption of protein, but high adsorption of bacteria.³¹

Table 1. Surfaces and sample treatments tested in the first step of the optimization of the negative control for the bacterial binding experiments.

| NHS-terminated PAO | Blocking agent | Surface treatment |
|-------------------------------|-----------------------|--------------------------|
| PAO-N₃-NHS | Ethanolamine | Direct |
| PAO-N₃-NHS | Ethanolamine | Sonication |
| PAO-NH₂-NHS | Ethanolamine | Direct |
| PAO-NH₂-NHS | Ethanolamine | Sonication |
| PAO-N₃-NHS | PEG4-amine | Direct |
| PAO-N₃-NHS | PEG4-amine | Sonication |
| PAO-NH₂-NHS | PEG4-amine | Direct |
| PAO-NH₂-NHS | PEG4-amine | Sonication |
| PAO-N₃-NHS | PEG3000-amine | Direct |
| PAO-N₃-NHS | PEG3000-amine | Sonication |
| PAO-NH₂-NHS | PEG3000-amine | Direct |
| PAO-NH₂-NHS | PEG3000-amine | Sonication |

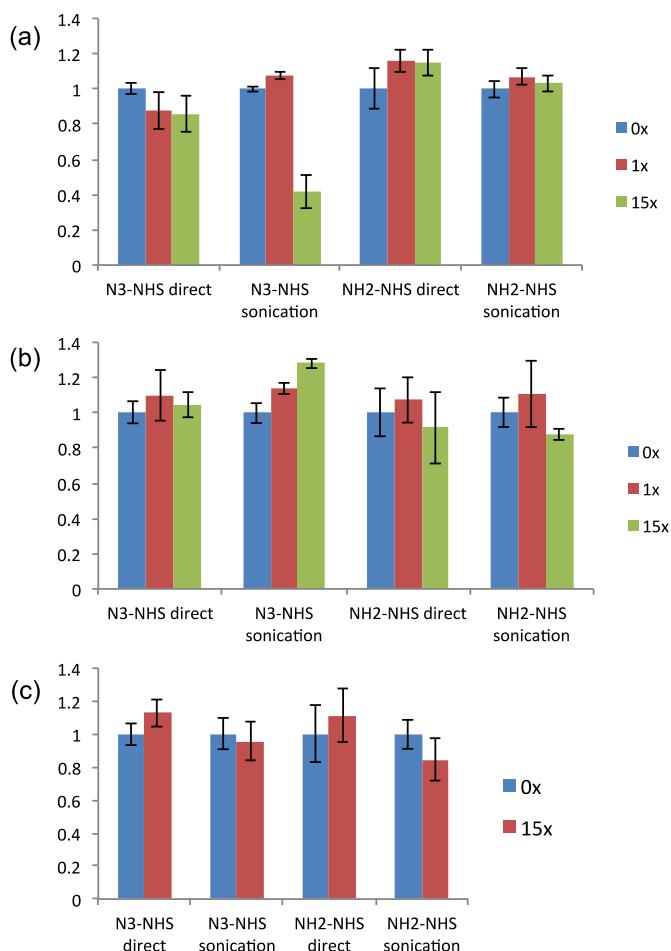


Figure 5. Binding of *L. plantarum* FRFP on NHS-terminated PAO surfaces blocked with different amines: (a) Ethanolamine, (b) PEG4-amine, and (c) PEG3000-amine.

In view of these unexpected results for the PEG surfaces, we considered that the surfaces might not present enough antifouling capacity. Therefore, we decided to try another type of surface modification, *viz.* by generating polyglycerol layers, which are known to be antifouling and have been used in several studies that successfully prevented bacterial binding.^{27, 29}

Another parameter tested in this optimization step together with the PAO-PG surfaces was the incubation time (10 s and 30 min). The incubation time was one of the parameters tested because we hypothesized that possibly the bacteria were starting

some defence mechanism due to lack of nutrients and water caused by the 30 min incubation time.³²

Additionally, a different washing method that kept the surface in contact with the washing solution (PBST) for a longer time was also evaluated to verify whether a more extensive washing method could assist in removing aspecifically adsorbed bacteria from the PAO surface.

Finally, two strains were tested (*L. plantarum* FRFP and *E. coli* K12, as models for Gram-positive and Gram-negative bacteria, respectively) to verify whether there was a strain-dependent trend in the non-specific adsorption. Both strains were tested for different incubation times (10 s and 30 min and washing methods (shaker and pipette).

The results for variation in the incubation time and the washing method showed a clear trend in the binding related to the incubation time (**Figure 6a**). When the bacteria were kept on the surfaces for a short time (10 s), most of the cells could be removed from the surfaces by washing. The opposite was observed when the incubation time was 30 min, after which nearly all the cells remained on the surfaces after extensive washing. Little difference was observed on the bacterial binding upon variation of the bacterial strains or the washing methods.

Although the short incubation time was suitable to prevent non-specific adsorption, in the actual experiment with the PAO surfaces with the antibody we aimed for a longer incubation time to allow the antibodies to bind to the antigens (on the bacterial cell). Considering this, in the next step of the optimization we decided to test various incubation times (5, 15, and 30 min) to verify what was the longest incubation time that could be used without resulting in significant non-specific adsorption. Additionally, two higher volumes of bacterial culture were tested (100 and 250 μL) to prevent the surfaces with bacteria from dehydration, which could increase non-specific adsorption. Finally, because the volume of bacterial culture was increased, a lower concentration of bacteria was also tested. This time, only the binding *E. coli* K12 was tested and the washing method using a shaker was selected due to the possibility of testing more conditions at once (**Figure 6b**).

The binding results for this step show that 5 min of incubation is optimal for balance between low non-specific adsorption and specific binding (**Figure 6b**). However, when increasing the incubation time to 15 or 30 min there is no visible trend, with some surfaces presenting low non-specific adsorption and others presenting high

amount of bacteria left on the surface. The volume and concentration of bacterial culture did not have a reproducible effect on the binding of the bacteria to the surface.

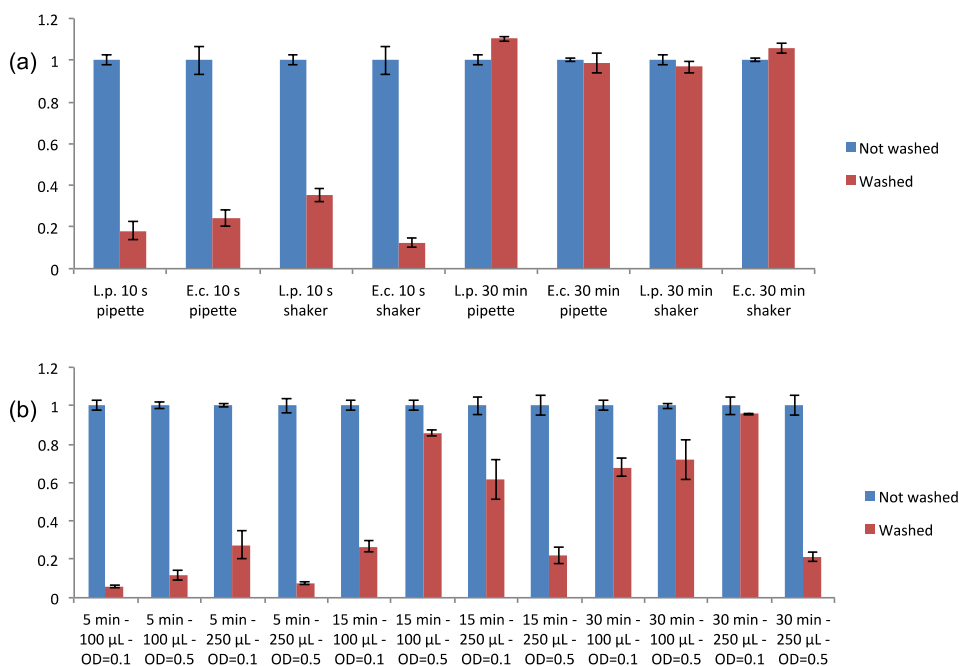


Figure 6. Binding of bacteria on **PAO-PG** surfaces under various conditions: (a) Binding of *L. plantarum* FRFP (L.p.) and *E. coli* K12 (E. c.) under different incubation times and washing methods and (b) binding of *E. coli* K12 under various incubation times, volume and concentration of bacteria.

After these optimization experiments, the conditions selected to perform the binding experiments on the PAO surfaces containing antibodies were the following: 100 μ L of bacterial culture with $OD_{600} = 0.5$, with 5 min of incubation at 37 $^{\circ}$ C, followed by washing the surfaces using the pipette method. These conditions were also tested with *E. coli* on **PAO-NH₂-NHS** surfaces blocked with PEG3000-amine and the same low non-specific bacterial adsorption was observed (**Figure 7**). Considering that the **PAO-NH₂-NHS** surfaces are better defined and the method to obtain these surfaces is more reproducible compared to the method to obtain the **PAO-PG** surfaces, the immobilization of the antibodies and the subsequent binding experiments were performed on **PAO-NH₂-NHS**.

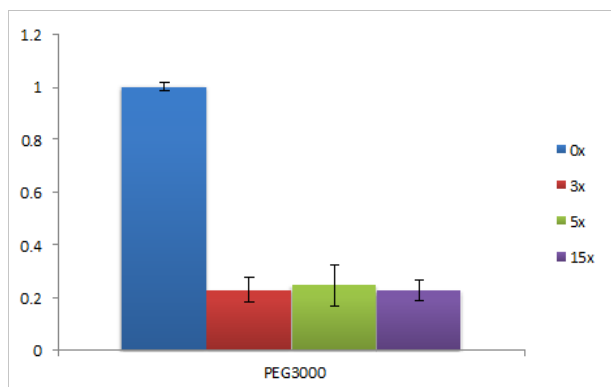


Figure 7. Binding of *E. coli* K12 on **PAO-NH₂-NHS** surfaces blocked with PEG3000-amine. The number of washings is indicated by the different colors.

Binding of E. coli to PAO Surfaces Containing Antibodies

After the optimization of the incubation and washing conditions, the bacterial binding was tested on the PAO surfaces containing the antibodies (**Figure 8**). Initially, a commercially available anti-*E. coli* antibody was selected as a proof-of-principle. The staining procedure with 5-carboxyfluorescein diacetate (cFDA) that was earlier successfully applied to *L. plantarum* in **Chapters 3**,⁹ **4**,¹⁰ and **5** was also evaluated for *E. coli*. However, only very weak fluorescence was observed. It was possible to increase the fluorescence of *E. coli* by adding glutaraldehyde to the staining solution in low-melting point agarose (data not shown). This increase of fluorescence in the staining of *E. coli* and other Gram-negative bacteria when using glutaraldehyde is due to two effects: the increase in the permeability of cFDA into the cell and the prevention of leakage of carboxyfluorescein (a hydrolysed product of cFDA) out of the cell.³³ However, when this staining procedure with cFDA and glutaraldehyde was performed on bacteria bound to modified PAO (**PAO-NH₂-NHS**), the background was too high to visualize the cells, probably due to crosslinking reactions with amine groups present on the surface. The staining with various fluorescent dyes (SYTO9, hexidium iodide, and DAPI) after the binding experiments by placing the surface with bacteria on low melting point agarose containing the dye was not suitable for *E. coli* on the **PAO-NH₂-NHS** surfaces. The most suitable staining procedure was to stain the bacteria with SYTO9 prior the binding experiments due to the high fluorescent background generated by the staining of the modified surfaces.

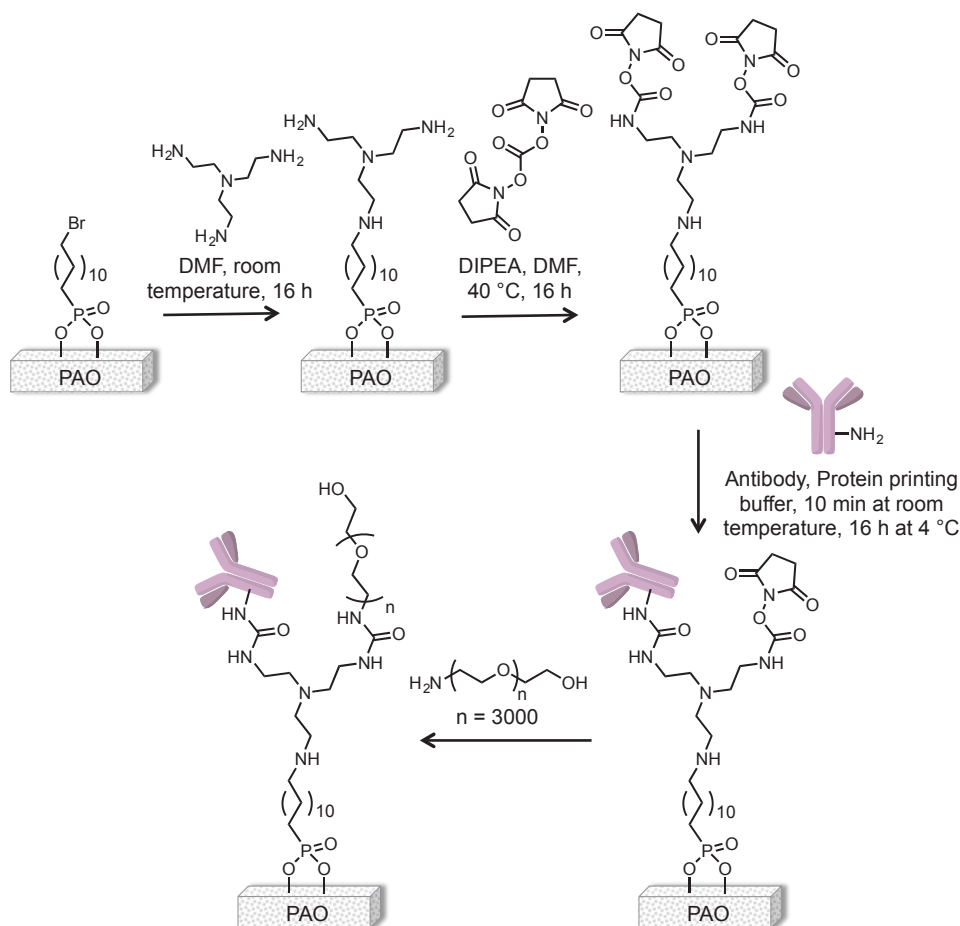


Figure 8. Preparation of the antibody-presenting PAO surfaces.

The binding of *E. coli* K12 was tested on a **PAO-NH₂-NHS** with immobilized antibodies, followed by blocking of the remaining NHS groups with PEG3000-amine. **PAO-NH₂-NHS** surfaces directly blocked with PEG3000-amine were used as the negative control. The same amount of bacteria was present when no washing step was performed (**Figure 9a and d**). However, there is a more pronounced decrease of cells after one and three washing steps on the control surface, directly blocked with PEG3000-amine, when compared to the antibody-presenting surfaces (**Figure 9b, c, e, and f**). The results indicate that the surface directly blocked with PEG3000-amine is antifouling enough for this bacterial strain, because the amount of cells drastically decreases even after one washing step, with further decrease after three washing steps. Although more cells stay on the surfaces containing the antibodies, there is also a significant decrease of the

number of cells when the surfaces are successively washed, especially after three washing steps. When the surfaces were further washed, the bacterial cells were also progressively removed even from the surfaces containing the antibodies (data not shown).

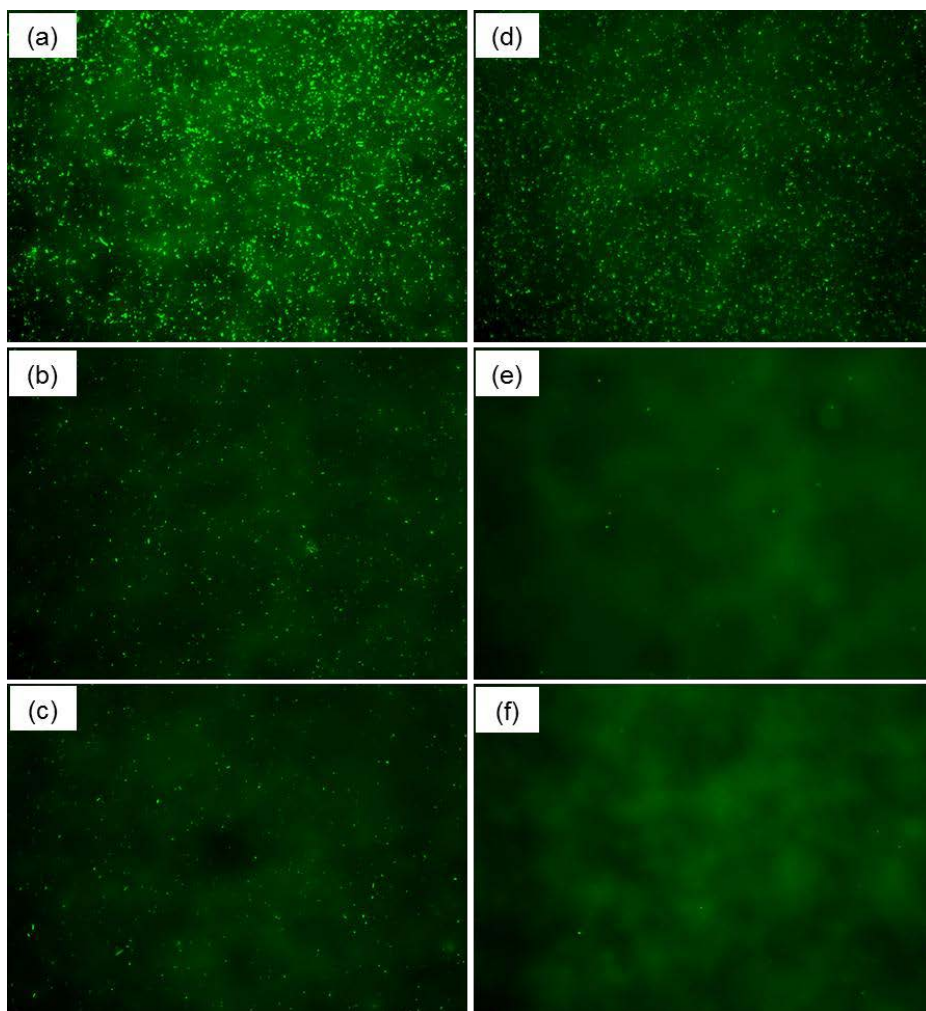


Figure 9. Binding of *E. coli* K12 on PAO surfaces containing antibodies and **PAO-NH₂-NHS** blocked with PEG3000-amine (negative control): (a) PAO with antibodies not washed, (b) PAO with antibodies washed once, (c) PAO with antibodies washed three times, (d) **PAO-NH₂-NHS** blocked with PEG3000-amine not washed, (e) **PAO-NH₂-NHS** blocked with PEG3000-amine washed once, and (f) **PAO-NH₂-NHS** blocked with PEG3000-amine washed three times. Total magnification is 200 \times .

Growth of *E. coli* on PAO Surfaces Containing Antibodies

After the binding experiments, the next step was to verify whether the *E. coli* cells were still able to grow on the antibody-functionalized PAO surfaces for them to work as a culturing chip. This experiment showed that the *E. coli* cells could still grow to microcolonies on the PAO surfaces containing antibodies (**Figure 10**), proving that the presence of the antibodies does not block the pores and the nutrients can still diffuse from the culture medium to the top PAO surface.

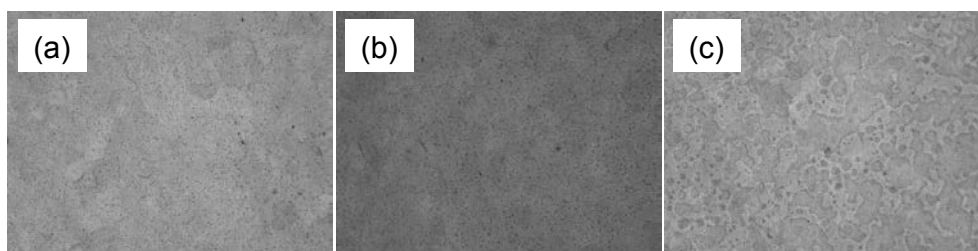


Figure 10. Growth of *E. coli* K12 on **PAO-NH₂-NHS** surfaces containing antibodies after incubation at 37 °C: (a) 0 h, (b) 1.5 h, and (c) 3 h.

Towards Antibody-based Capture & Growth of *L. rhamnosus* GG on PAO

After these promising proof-of-principle results with the optimized conditions for *E. coli*, the next step was to achieve capture and growth of *L. rhamnosus* GG and its pili-less derivative strain PB12, on antibody-biofunctionalized PAO. First, however, suitable control PAO surfaces had to be evaluated that contained a similar chemical modification as our target antibody-functionalized PAO, but that would not bind *L. rhamnosus*. This is not as straightforward as *L. rhamnosus* is well known for its ability to aspecifically adhere to surfaces.

As a negative control surface, **PAO-NH₂-NHS** was directly blocked with PEG3000-amine. In a first binding experiment with *L. rhamnosus* GG on this surface, the same washing conditions of the binding experiments with *E. coli* were used (0, 1, 3, and 5 washing steps), however, these were unable to sufficiently remove the cells (data not shown). Consequently, the experiment was repeated with 25 washing steps, which proved sufficient to almost completely remove both *L. rhamnosus* GG and PB12 strains from the control surfaces (**Figure 11**). The higher non-specific adhesion of *L. rhamnosus* GG compared to *E. coli* K12 is probably due to the presence of the pili on the cell surface

of *L. rhamnosus* GG. *L. rhamnosus* GG needed more washing steps than PB12 to be removed from the surfaces. This can be explained by the presence of the highly adhesive pili, in which the SpaC subunit of the pili likely plays a central role in the adhesion process.^{24, 34}

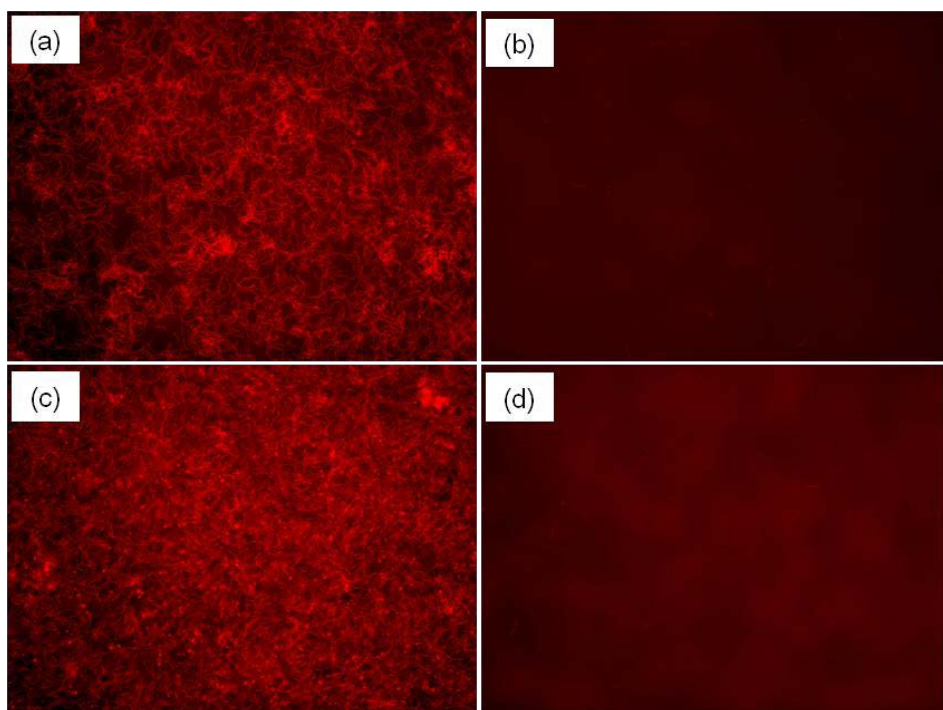


Figure 11. Binding of *L. rhamnosus* on **PAO-NH₂-NHS** blocked with PEG3000-amine: (a) *L. rhamnosus* GG not washed, (b) *L. rhamnosus* GG washed 25 times, (c) PB12 not washed, and (d) PB12 washed 25 times.

Our overall aim in this study is to immobilize two different antibodies (kindly provided by Reetta Satokari, UHelsinki) against *L. rhamnosus* GG on NHS-terminated PAO: one against the whole cell of *L. rhamnosus* GG (anti-LGG) and the other one against the pilin subunit SpaC (anti-SpaC). The binding of *L. rhamnosus* GG and the mutant strain PB12, which does not have the pili, will then be tested on the biofunctionalized PAO. *L. rhamnosus* GG cells are expected to bind to the surfaces functionalized with both antibodies. On the other hand, PB12 is expected to bind only to the PAO surfaces functionalized with the antibody against the whole cell of *L. rhamnosus* GG due to the absence of the pili and, consequently, the SpaC subunit. This next step is currently being

investigated. Preliminary data on the binding of *L. rhamnosus* GG to biofunctionalized PAO surfaces are presented in **Chapter 7**.

Conclusions

In this study, we optimized the bacterial binding experiments on PAO surfaces functionalized with antibodies. In the first optimization steps, various surfaces were prepared and analyzed in order to select the one that presented the lowest non-specific adsorption of bacteria. However, all these surfaces performed similarly poor, with a high non-specific adsorption that was not suitable for the binding experiments with antibodies. The non-specific adsorption only decreased when the incubation conditions of the bacteria on the surfaces were changed to higher volume of bacterial culture and shorter incubation time, showing that in this case the incubation conditions were more important than the chemical modification developed on the surfaces. The binding and growth of *E. coli* on PAO surfaces with antibodies was then studied as a proof-of-principle system, showing considerably higher binding of *E. coli* on the surfaces with antibodies. An effective negative control modified PAO-surface was developed for *L. rhamnosus*. Future work involves the immobilization of antibodies against *L. rhamnosus* GG using the same conditions to achieve increased binding and subsequent growth of this bacterium on biofunctionalized PAO surfaces.

Acknowledgements

This work is supported by NanoNextNL, a micro and nanotechnology consortium of the Government of The Netherlands and 130 partners, ERC grant 250712 (MicrobesInside), and the Netherlands Organization for Scientific Research (NWO VENI grant 722.011.006 to T.W.). We thank Reetta Satokari (UHelsinki) for providing the anti-LGG antibodies used in the preliminary experiments.

References

1. Ingham, C. J.; ter Maat, J.; de Vos, W. M. Where bio meets nano: the many uses for nanoporous aluminum oxide in biotechnology. *Biotechnol. Adv.* **2012**, *30*, 1089-1099.
2. Ingham, C. J.; van den Ende, M.; Pijnenburg, D.; Wever, P. C.; Schneeberger, P. M. Growth and multiplexed analysis of microorganisms on a subdivided, highly porous, inorganic chip manufactured from anopore. *Appl. Environ. Microbiol.* **2005**, *71*, 8978-8981.
3. Ferrari, B. C.; Binnerup, S. J.; Gillings, M. Microcolony cultivation on a soil substrate membrane system selects for previously uncultured soil bacteria. *Appl. Environ. Microbiol.* **2005**, *71*, 8714-8720.
4. Hoess, A.; Teuscher, N.; Thormann, A.; Aurich, H.; Heilmann, A. Cultivation of hepatoma cell line HepG2 on nanoporous aluminum oxide membranes. *Acta Biomater.* **2007**, *3*, 43-50.

5. Hu, J.; Tian, J. H.; Shi, J.; Zhang, F.; He, D. L.; Liu, L.; Jung, D. J.; Bai, J. B.; Chen, Y. Cell culture on AAO nanoporous substrates with and without geometry constraints. *Microelectron. Eng.* **2011**, *88*, 1714-1717.
6. Ingham, C. J.; Sprenkels, A.; Bomer, J.; Molenaar, D.; van den Berg, A.; Vlieg, J.; de Vos, W. M. The micro-Petri dish, a million-well growth chip for the culture and high-throughput screening of microorganisms. *Proc. Natl. Acad. Sci. U. S. A.* **2007**, *104*, 18217-18222.
7. Wang, P. Y.; Clements, L. R.; Thissen, H.; Tsai, W. B.; Voelcker, N. H. High-throughput characterisation of osteogenic differentiation of human mesenchymal stem cells using pore size gradients on porous alumina. *Biomater. Sci.* **2013**, *1*, 924-932.
8. Brueggemann, D. Nanoporous aluminium oxide membranes as cell interfaces. *J. Nanomater.* **2013**.
9. Debrassi, A.; Ribbera, A.; de Vos, W. M.; Wennekes, T.; Zuilhof, H. Stability of (bio)functionalized porous aluminum oxide. *Langmuir* **2014**, *30*, 1311-1320.
10. Debrassi, A.; Roeven, E.; Thijssen, S.; Scheres, L.; de Vos, W. M.; Wennekes, T.; Zuilhof, H. Versatile (bio)functionalization of bromo-terminated phosphonate-modified porous aluminum oxide. *Langmuir* **2015**, *31*, 5633-5644.
11. Zeng, X.; Andrade, C. A. S.; Oliveira, M. D. L.; Sun, X. L. Carbohydrate-protein interactions and their biosensing applications. *Anal. Bioanal. Chem.* **2012**, *402*, 3161-3176.
12. Ahmed, A.; Rushworth, J. V.; Hirst, N. A.; Millner, P. A. Biosensors for whole-cell bacterial detection. *Clin. Microbiol. Rev.* **2014**, *27*, 631-646.
13. van Hattum, H.; Martin, N. I.; Ruijtenbeek, R.; Pieters, R. J. Development of a microarray detection method for galectin cancer proteins based on ligand binding. *Anal. Biochem.* **2013**, *434*, 99-104.
14. Joung, C. K.; Kim, H. N.; Lim, M. C.; Jeon, T. J.; Kim, H. Y.; Kim, Y. R. A nanoporous membrane-based impedimetric immunosensor for label-free detection of pathogenic bacteria in whole milk. *Biosens. Bioelectron.* **2013**, *44*, 210-215.
15. Chan, K. Y.; Ye, W. W.; Zhang, Y.; Xiao, L. D.; Leung, P. H. M.; Li, Y.; Yang, M. Ultrasensitive detection of *E. coli* O157:H7 with biofunctional magnetic bead concentration via nanoporous membrane based electrochemical immunosensor. *Biosens. Bioelectron.* **2013**, *41*, 532-537.
16. Bernardeau, M.; Guguen, M.; Vernoux, J. P. Beneficial lactobacilli in food and feed: long-term use, biodiversity and proposals for specific and realistic safety assessments. *FEMS Microbiol. Rev.* **2006**, *30*, 487-513.
17. Saxelin, M.; Tynkkynen, S.; Mattila-Sandholm, T.; de Vos, W. M. Probiotic and other functional microbes: from markets to mechanisms. *Curr. Opin. Biotechnol.* **2005**, *16*, 204-211.
18. Hatakka, K.; Savilahti, E.; Ponka, A.; Meurman, J. H.; Poussa, T.; Nase, L.; Saxelin, M.; Korpela, R. Effect of long term consumption of probiotic milk on infections in children attending day care centres: double blind, randomised trial. *BMJ* **2001**, *322*, 1327.
19. Kalliomaki, M.; Salminen, S.; Arvilommi, H.; Kero, P.; Koskinen, P.; Isolauri, E. Probiotics in primary prevention of atopic disease: a randomised placebo-controlled trial. *Lancet* **2001**, *357*, 1076-1079.
20. Nermes, M.; Kantele, J. M.; Aatosuo, T. J.; Salminen, S.; Isolauri, E. Interaction of orally administered *Lactobacillus rhamnosus* GG with skin and gut microbiota and humoral immunity in infants with atopic dermatitis. *Clin. Exp. Allergy* **2011**, *41*, 370-377.
21. Sagar, S.; Morgan, M. E.; Chen, S.; Vos, A. P.; Garssen, J.; van Bergenhenegouwen, J.; Boon, L.; Georgiou, N. A.; Kraneveld, A. D.; Folkerts, G. *Bifidobacterium breve* and *Lactobacillus rhamnosus* treatment is as effective as budesonide at reducing inflammation in a murine model for chronic asthma. *Respir. Res.* **2014**, *15*, 46.
22. Kootte, R. S.; Vrieze, A.; Holleman, F.; Dallinga-Thie, G. M.; Zoetendal, E. G.; de Vos, W. M.; Groen, A. K.; Hoekstra, J. B. L.; Stroes, E. S.; Nieuwdorp, M. The therapeutic potential of manipulating gut microbiota in obesity and type 2 diabetes mellitus. *Diabetes Obes. Metab.* **2012**, *14*, 112-120.
23. Reunanen, J.; von Ossowski, I.; Hendrickx, A. P.; Palva, A.; de Vos, W. M. Characterization of the SpaCBA pilus fibers in the probiotic *Lactobacillus rhamnosus* GG. *Appl. Environ. Microbiol.* **2012**, *78*, 2337-2344.
24. Kankainen, M.; Paulin, L.; Tynkkynen, S.; von Ossowski, I.; Reunanen, J.; Partanen, P.; Satokari, R.; Vesterlund, S.; Hendrickx, A. P.; Lebeer, S.; De Keersmaecker, S. C.; Vanderleyden, J.; Hamalainen, T.; Laukkanen, S.; Salovuori, N.; Ritari, J.; Alatalo, E.; Korpela, R.; Mattila-Sandholm, T.; Lassig, A.; Hatakka, K.; Kinnunen, K. T.; Karjalainen, H.; Saxelin, M.; Laakso, K.; Surakka, A.; Palva, A.; Salusjarvi, T.; Auvinen, P.; de Vos, W. M. Comparative genomic analysis of *Lactobacillus rhamnosus* GG reveals pili containing a human- mucus binding protein. *Proc. Natl. Acad. Sci. U. S. A.* **2009**, *106*, 17193-17198.
25. Douillard, F. P.; Rasinkangas, P.; von Ossowski, I.; Reunanen, J.; Palva, A.; de Vos, W. M. Functional identification of conserved residues involved in *Lactobacillus rhamnosus* strain GG sortase specificity and pilus biogenesis. *J. Biol. Chem.* **2014**, *289*, 15764-15775.
26. Rasinkangas, P.; Reunanen, J.; Douillard, F. P.; Ritari, J.; Uotinen, V.; Palva, A.; de Vos, W. M. Genomic characterization of non-mucus-adherent derivatives of *Lactobacillus rhamnosus* GG reveals genes affecting pilus biogenesis. *Appl. Environ. Microbiol.* **2014**, *80*, 7001-7009.
27. Weber, T.; Bechthold, M.; Winkler, T.; Dauselt, J.; Terfort, A. Direct grafting of anti-fouling polyglycerol layers to steel and other technically relevant materials. *Colloid. Surf. B* **2013**, *111*, 360-366.
28. Kingshott, P.; Wei, J.; Bagge-Ravn, D.; Gadegaard, N.; Gram, L. Covalent attachment of poly(ethylene glycol) to surfaces, critical for reducing bacterial adhesion. *Langmuir* **2003**, *19*, 6912-6921.
29. Weber, T.; Gies, Y.; Terfort, A. Bacteria-repulsive polyglycerol surfaces by grafting polymerization onto aminopropylated surfaces. *Langmuir* **2012**, *28*, 15916-15921.
30. Joshi, S.; Pellacani, P.; van Beek, T. A.; Zuilhof, H.; Nielen, M. W. F. Surface characterization and antifouling properties of nanostructured gold chips for imaging surface plasmon resonance biosensing. *Sensor. Actuat. B-Chem.* **2015**, *209*, 505-514.
31. Wei, J.; Ravn, D. B.; Gram, L.; Kingshott, P. Stainless steel modified with poly(ethylene glycol) can prevent protein adsorption but not bacterial adhesion. *Colloids Surf. B Biointerfaces* **2003**, *32*, 275-291.
32. Katsikogianni, M.; Missirlis, Y. F. Concise review of mechanisms of bacterial adhesion to biomaterials and of techniques used in estimating bacteria-material interactions. *Eur. Cell Mater.* **2004**, *8*, 37-57.
33. Morono, Y.; Takano, S.; Miyana, K.; Tanji, Y.; Unno, H.; Hori, K. Application of glutaraldehyde for the staining of esterase-active cells with carboxyfluorescein diacetate. *Biotechnol. Lett.* **2004**, *26*, 379-383.
34. Tripathi, P.; Beaussart, A.; Alsteens, D.; Dupres, V.; Claes, I.; von Ossowski, I.; de Vos, W. M.; Palva, A.; Lebeer, S.; Vanderleyden, J.; Dufrene, Y. F. Adhesion and nanomechanics of pili from the probiotic *Lactobacillus rhamnosus* GG. *ACS Nano* **2013**, *7*, 3685-3697.

Chapter 7

General Discussion

Aline Debrassi

This thesis describes the research that was carried out towards the ultimate goal of selectively capturing and growing various relevant bacteria that occur in the human gut microbiome on nanoporous aluminum oxide (PAO) culturing chips. To achieve this goal, various (bio)functionalization approaches for PAO surfaces were developed, to achieve stable monolayer formation as well as to allow secondary and tertiary reactions for the immobilization of biomolecules on the surface. In this chapter, the most important achievements are discussed, together with additional ideas and recommendations for further research. Finally, in connection to the NanoNextNL consortium, which funded this study, and to outline realistic perspectives on the potential for application of this research, some reflections are provided in the context of risk analysis and technology assessment.

Biofunctionalization of surfaces usually requires a stepwise approach, in which a monolayer is first generated, followed by a secondary reaction to install the biomolecule of interest. In this case, the initial monolayer needs to be stable under the conditions of the intended application. In the beginning of this project, it was already known that various functional groups are able to react with (porous) aluminum oxide, however, there was no comprehensive stability study of modified PAO under the conditions that are important for microbial growth. An overview of the relevant literature is provided in **Chapter 2**.

In **Chapter 3**, the stability of PAO modified with various functional groups (carboxylic acid, α -hydroxycarboxylic acid, alkyne, alkene, phosphonic acid, and silane) is reported. The modification with phosphonic acids proved to be the most stable one, and was therefore assessed under various pH and temperature conditions that are relevant for microbial growth. In general, it was observed that the PAO surfaces modified with a hydrophobic phosphonic acid monolayer were stable for at least two weeks in buffer solutions with pH values between 4 and 8, and at temperatures up to 40 °C. However, the stability of the same monolayer on PAO significantly decreased at 60 °C and 80 °C under hydrolytic conditions. Interestingly, a similar hydrophobic phosphonate monolayer on PAO was stable at temperatures even higher than 500 °C when heated under vacuum, probably due to the formation of multidentated structures generated by optimal curing and the absence of hydrolysis reactions.¹ This exceptionally high stability of phosphonate monolayers on PAO under vacuum may enable their use in other fields, such as in organic electronic devices that require stability at high temperatures.²

After the formation of a stable monolayer, the next step for the biofunctionalization of PAO is to perform a secondary and, in some cases, even a tertiary reaction to immobilize the biomolecule of interest. Various approaches to achieve (bio)functionalization of PAO were explored in **Chapter 4**, starting from a straightforward initial modification with a bromo-terminated phosphonic acid. PAO surfaces presenting different terminal reactive groups were prepared, such as azide, alkyne, alkene, thiol, isothiocyanate, and *N*-hydroxysuccinimide (NHS), and used to immobilize (bio)molecules, including carbohydrates and proteins. On the surface with immobilized bovine serum albumin (BSA), the growth of bacteria was still possible, showing that the nutrients can diffuse from the culture medium to the top of PAO even when the PAO surface is biofunctionalized with an organic monolayer and big biomolecules, such as a protein. Most of the reactive surfaces prepared in **Chapter 4** presented a high conversion in the subsequent reaction, showing that a versatile “tool-box” was developed for the use in the later chapters. It was not the scope of that study to compare the conversion yields of all the reactions since to achieve this it would be necessary to use more comparable molecules, with the same chain length and similar electronic properties, for example, with the one single difference being the functional group involved in the reaction. Additionally, not all the molecules used to functionalize the PAO surfaces were biologically relevant (notably the fluorinated molecules are toxic), and similarly not all the reactions were performed under biologically compatible conditions. The fluorinated molecules were used for an improved quantification of the conversion yield by X-ray photoelectron spectroscopy (XPS). However, it would be also interesting if the same reactions were performed with biologically relevant molecules, such as complex carbohydrates, proteins, and nucleic acid derivatives.

With our reaction “tool-box” in hand, the next step was to immobilize biomolecules using the stable reactive PAO surfaces developed in **Chapters 3 and 4** so as to construct the biofunctionalized PAO for the binding and growth of bacteria in **Chapters 5 and 6**. In **Chapter 3**, an azido-mannoside was immobilized on alkyne-terminated PAO via the copper(I)-catalyzed alkyne-azide cycloaddition (CuAAC) click reaction, and the mannose-presenting surfaces showed increased binding of the probiotic bacterium *Lactobacillus plantarum*, which has a mannose-specific adhesin on its surface. The bacteria were also still able to growth on the mannose-presenting PAO. After this proof-of-principle study, the parameters involved in the preparation of these

surfaces and their binding with *L. plantarum* were further investigated in **Chapter 5**, such as the nature of the spacer connected to the mannoside derivative and the presence of soluble carbohydrates and bovine serum albumin (BSA) in the medium. The binding of a mutant strain of *L. plantarum* that does not present the mannose-specific adhesion was also studied on the mannose-presenting PAO and the lack of binding of this strain proved that this carbohydrate–protein interaction is the main mechanism of binding in this system.

Considering the complex multivalent interactions between carbohydrate-binding proteins on bacteria and glycosurfaces,³ it is important to further investigate the influence of various parameters involved in the binding and thereby develop a better understanding of these events. A way by which the specificity of the interaction can be tested is by performing more extensive bacterial binding studies on a range of PAO surfaces that present mono- (glucose, galactose, fructose, *N*-acetylglucosamine or arabinose for example) or disaccharides (lactose, maltose). As a trial to go one step further in mimicking the complex natural glycosurfaces, surfaces presenting a mixture of two or more carbohydrates could also be tested (**Figure 1a**).

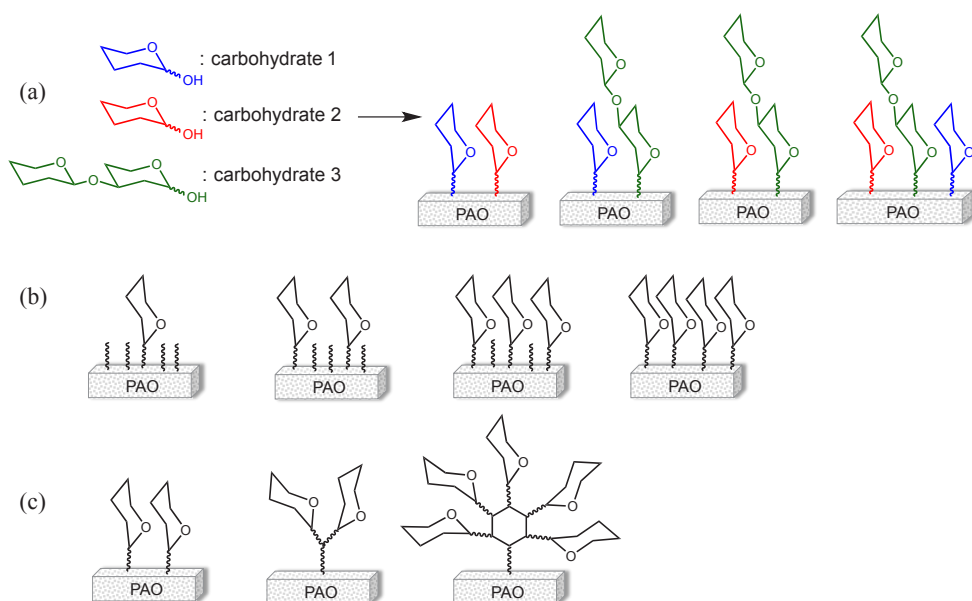


Figure 1. Parameters to investigate in bacteria-carbohydrate binding studies: (a) Mixture of carbohydrates, (b) carbohydrate density, and (c) carbohydrate presentation.

Another important parameter that influences the binding of soluble and bacterial lectins to carbohydrate-functionalized surfaces is the carbohydrate density (**Figure 1b**),⁴⁻⁷ as more extensively discussed in **Chapter 2**. Although preliminary binding experiments were performed on mannose-presenting PAO surfaces with different carbohydrate densities, no trend was observed so far under the conditions studied. However, the suboptimal binding conditions used for that experiment might have caused this. New binding studies using the incubation conditions optimized in **Chapter 6** (higher volume of bacterial culture and shorter incubation time) may provide more enlightening results. Not only is the amount of carbohydrate on a surface important, but also the manner in which it is present on the surface, considering that many of these carbohydrate-protein interactions are multivalent.⁴ Carbohydrate-presenting dendrimers or dendrons (**Figure 1c**)⁸ can be immobilized on PAO and the influence of the carbohydrate presentation on the bacterial binding can be tuned to achieve the best binding with the least non-specific adsorption possible.

Other combinations of carbohydrates and bacteria can also be studied. A well-known example of carbohydrate-mediated bacterial adhesion process is the binding of *Pseudomonas aeruginosa* via two lectins, LecA (or PA-IL) and LecB (or PA-IIL). LecA binds D-galactose and N-acetyl-D-galactosamine and LecB binds L-fucose. Both lectins bind to oligosaccharides on human glycoproteins, strongly suggesting that these lectins are directly involved in the adhesion on *P. aeruginosa* to human tissues and, consequently, to its pathogenesis.⁹ It would be interesting to study the binding of *P. aeruginosa* on PAO surfaces presenting different mixtures of these carbohydrates. Another combination of carbohydrate and bacteria that can be studied on PAO is between *Enterococcus faecalis* and galactose, which was previously analyzed on a glycopolymer-presenting surface.¹⁰

At a later stage, carbohydrate-functionalized PAO surfaces can be used to identify the type of bacteria present in a complex mixture by their carbohydrate-binding “fingerprint”.¹¹ An advantage of PAO when compared to carbohydrate microarrays on other surfaces is that the bacterial growth can directly be performed on the same surface because of the nanoporous structure. The influence of small molecules (antibiotics or nutrients, for example) on the growth of bacteria can also directly be studied on the same surface used for the binding experiments.^{12, 13} By using the micro-Petri dish mentioned in **Chapter 1**,¹⁴ it is feasible that the isolation of certain types of

bacteria can be achieved based on a combination of the carbohydrate-binding “fingerprint” and the bacterial susceptibility or resistance to antibiotics.

Carbohydrate-presenting PAO surfaces can be used to enhance the binding of certain types of bacteria, but to achieve a species- or strain-selective binding or capture it is necessary to modify PAO with more specific biomolecules, such as antibodies or DNA aptamers.¹⁵ In **Chapter 6**, PAO was biofunctionalized with antibodies to achieve selective binding of bacteria. After an extensive optimization of the incubation and washing conditions, the proof-of-principle using a commercial anti-*Escherichia coli* antibody showed more binding of *E. coli* on the antibody-functionalized surfaces. As described in **Chapter 6**, our aim was to immobilize two different antibodies against *L. rhamnosus* GG on NHS-terminated PAO: one against the whole cell of *L. rhamnosus* GG (anti-LGG) and the other one against the pilin subunit SpaC, present on the cell surface of *L. rhamnosus* GG (anti-SpaC). After successfully developing negative control surfaces for the sticky *L. rhamnosus* GG, as described in Chapter 6, preliminary binding experiments between PAO surfaces presenting anti-LGG antibodies and *L. rhamnosus* GG were performed (**Figure 2**). Although these preliminary results are promising, this system still needs further optimization and currently still has some reproducibility issues. Additionally, the PAO surfaces also need to be biofunctionalized with the anti-SpaC antibodies and to be tested against a mixture of bacteria to determine whether the biofunctionalized PAO is capable to selectively capture *L. rhamnosus* GG.

The reproducibility issues observed in these preliminary experiments may be related to several factors. The rabbit antiserum used here, instead of isolated antibodies as in the *E. coli* proof-of-concept experiments, contains many other (protein) components that will probably also be immobilized on the PAO surface and might have an influence. Additionally, the (non-oriented) immobilization step used will result in blocking of the binding region (Fab portion) of an unknown fraction of the antibodies. A possible way to overcome the blocking of the binding region of the antibodies is to use one of the known oriented (or site-specific) immobilization approaches, such as protein A/G,¹⁶ biotin-streptavidin,¹⁷ using a nitriloacetic acid-terminated surface and polyhistidine-conjugated antibodies,¹⁸ boronic acid-¹⁹ and hydrazide-terminated surfaces²⁰ (see **Chapter 1** for more extensive discussion).^{21, 22} Alternatively, bio-orthogonal reactions can also be used for the oriented immobilization of the antibodies, such as the Diels-Alder cycloaddition,²³ Staudinger ligation,²⁴ copper(I)-catalyzed azide-

alkyne cycloaddition (CuAAC), strain-promoted azide-alkyne cycloaddition (SPAAC), click sulfonamide reaction (CSR),²⁵ or thiol-ene reaction.^{26, 27} Most of these approaches, however, require modification of the antibody to insert the reactive functional groups prior the immobilization step. The exceptions are protein A/G and boronic acids that do not require prior modification, and hydrazide-terminated surfaces, which requires a simple oxidation step of the antibody *N*-glycans.²⁰

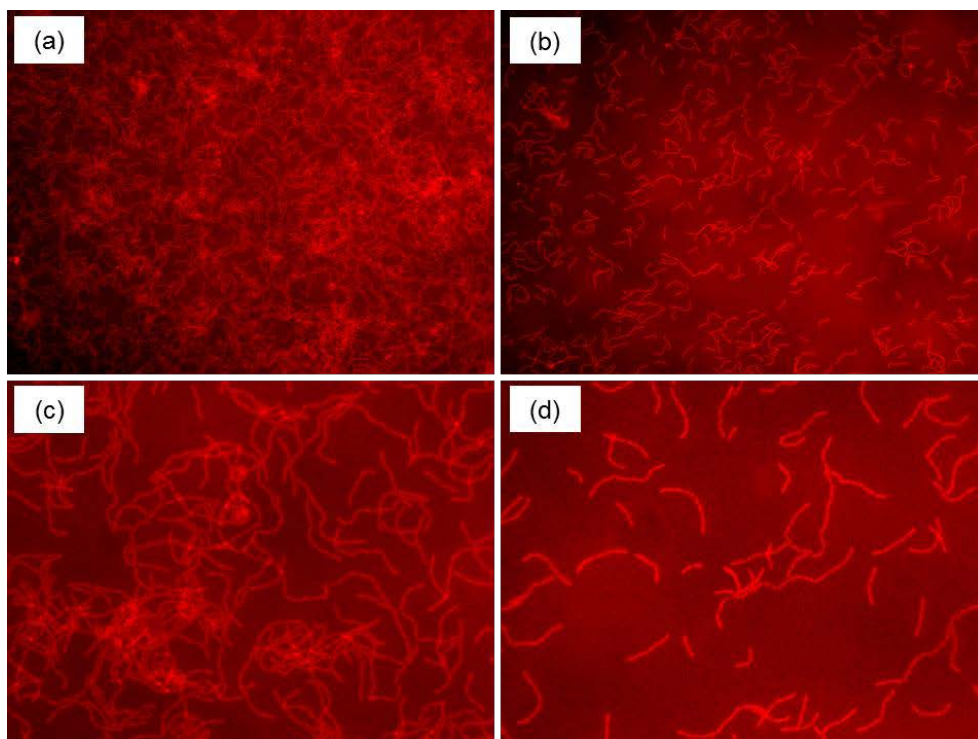


Figure 2. Binding of *L. rhamnosus* GG on PAO with immobilized anti-LGG antibodies: (a) surface not washed, (b) surface washed 25 times, (c) digital magnification of a fragment of (a), and (d) digital magnification of fragment of (b). We are grateful to Dr. Reetta Satokari for a kind gift of the anti-LGG antibodies.

After further optimization of both the carbohydrate- and antibody-presenting PAO surfaces, bacterial binding experiments with mixed bacterial cultures containing one or more strains will need to be successfully performed to achieve our overall aim of specific bacterial capture and growth from a complex biological sample. These experiments will require bacterial strains expressing different protein fluorophores or selective fluorescent or fluorogenic staining reagents to distinguish the bacterial strains

using fluorescence microscopy and quantify their capture efficiency. Fluorescent strains were used in **Chapter 6** for the optimization of the incubation and washing conditions. These strains, however, presented low and/or irreproducible fluorescence that turned out to be unsuitable for our planned experiments with mixed cultures, at least not with the available fluorescence microscopes. Some strains were homogeneously fluorescent, but the intensity was too low, whereas other strains had good fluorescence intensity, but only approximately half of the cells were fluorescent, possibly as a result of growth-phase dependent expression. In order to improve the fluorescence intensity or homogeneity, different concentrations of antibiotics and incubation times were tested, without any significant improvement. Considering that the fluorescence may be growth phase-dependent,²⁸ it would be necessary to measure the fluorescence intensity of these strains at various points of the growth phase in order to obtain the best fluorescence possible with the available strains.

Fluorescent and fluorogenic stains were used to visualize the bacteria by fluorescence microscopy in all the experimental chapters of this thesis. Various combinations of chemical modification of PAO, bacterial strains, and fluorescent or fluorogenic stains were tested and overall it can be concluded that the efficiency of cell staining compared to background needs to be tested and optimized for each new combination. Although most of the staining reagents were able to efficiently stain the bacteria on non-modified PAO (except 5-carboxyfluorescein diacetate, cFDA, for *E. coli*), the same combination of bacteria and staining reagent was not suitable on modified PAO surfaces due to the high background generated by the adsorption of the fluorescent dye on the organic modification of the surface. Interestingly, even when the PAO modification and the fluorescent dye were the same (PAO modified with antibodies or a PEG molecule and hexidium iodide as the staining reagent in **Chapter 6**), the suitability of the staining reagent was strain-dependent. Whereas this system presented a very good staining for *L. rhamnosus* GG, it was completely unsuitable to stain *E. coli* under the same conditions. Future work in this area should involve testing various combinations of relevant bacteria and fluorescent dyes for each PAO modification in order to create a database with this information for the end users.

In this thesis, PAO was biofunctionalized only with carbohydrates and antibodies, but the immobilization of other biomolecules can be explored, such as lectins. The immobilized lectins can then be used to selectively bind certain bacteria based on the

carbohydrates present on the bacterial cell surface. Preliminary experiments were performed with wheat germ agglutinin (WGA) immobilized on PAO for the selective binding of Gram-positive bacteria based on the interaction with mainly *N*-acetylglucosamine present in the peptidoglycan layer on the Gram-positive bacterial cells (**Figure 3**). The cell wall of Gram-positive bacteria has a thick peptidoglycan layer, whereas Gram-negative bacteria have a much thinner peptidoglycan layer, which is located in between two cell membranes.²⁹ The thicker and more accessible peptidoglycan layer of the Gram-positive bacteria could then lead to a higher binding of these bacteria on the WGA-functionalized PAO. The binding of the Gram-positive bacterium *L. plantarum* was tested on the WGA-functionalized PAO. Unfortunately, low binding was observed under these initially studied conditions. The low binding may be related to the presence of lipids and other proteins on the peptidoglycan layer. The selectivity of this binding may also encounter problems due to the presence of lipopolysaccharides (LPS) on the outer membrane of the Gram-negative bacteria, which may also bind to WGA. Although further experiments still need to be performed to validate this system, it would be an interesting approach to quickly identify and capture Gram-positive bacteria from a complex mixture.

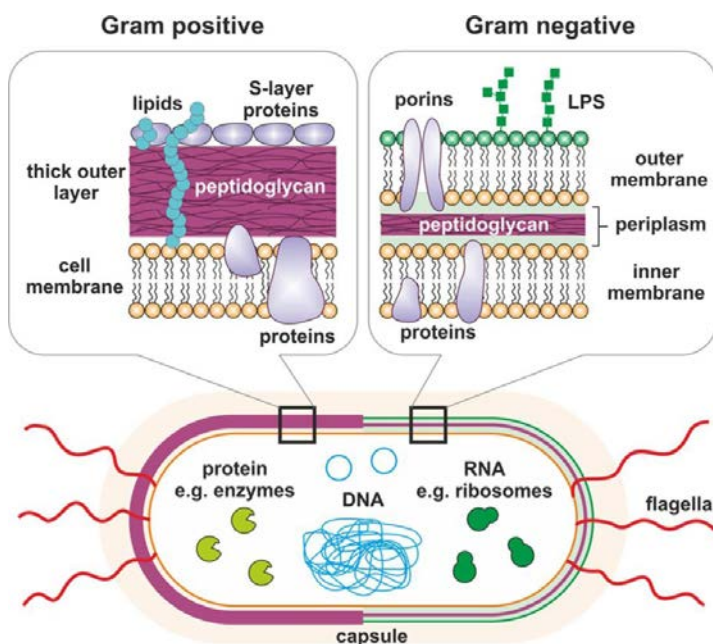


Figure 3. Gram-positive and Gram-negative bacterial cells. Adapted from reference.²⁹

Finally, besides the aim in itself of specific capture of a target bacterium via an immobilized biomolecule, the other challenge is to minimize non-specific adsorption. Antifouling layers can be generated on PAO as an approach to decrease this. One of the up and coming approaches to prevent non-specific adsorption by chemical modification of surfaces is via the growth of zwitterionic polymers on the surface.³⁰ The antifouling properties of these polymers are based on the balance of their charged groups³¹ and also on their strong binding to water, creating a hydration layer that prevents proteins from adhering to the surface.³² Biofunctionalization of zwitterionic polymers can be performed by reacting amines with the remaining terminal bromine groups of the polymer chains³³ or by their conversion into an azide group (**Figure 4**).³⁴

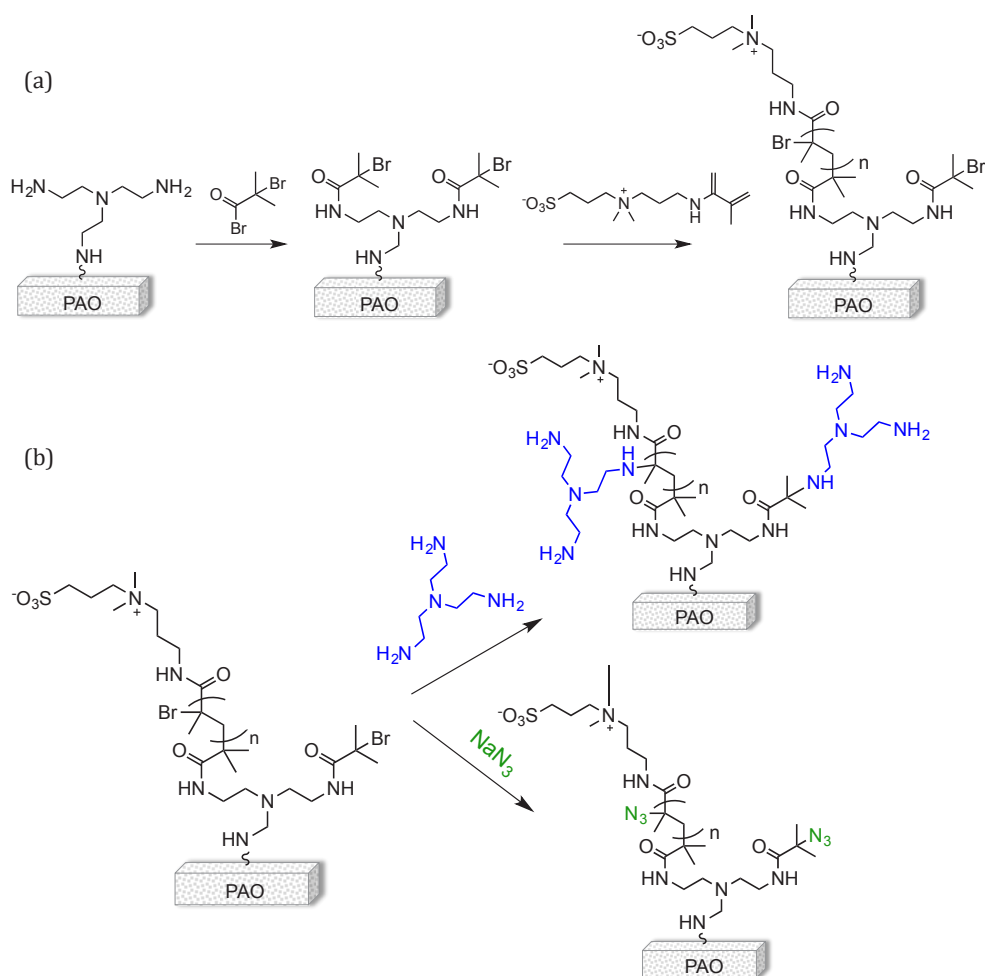


Figure 4. Zwitterionic polymers on PAO: (a) Polymer growth and (b) subsequent functionalization.

In conclusion, the research described in this thesis focused on the covalent stable biofunctionalization of PAO surfaces with carbohydrates and antibodies for the binding and subsequent growth of bacteria. The selective binding of bacteria on biofunctionalized PAO still has plenty of room left to explore and this is worthwhile as it has potential application in microbiological research laboratories for the screening of bacterial strains and also for diagnosis of bacterial infections, with the possibility to be combined with resistance or susceptibility tests for antibiotics.

Risk Analysis & Technology Assessment (RATA)

The research described in this thesis aimed to achieve the selective capture and growth of various relevant bacteria that occur in the human gut microbiome on PAO culturing chips. This research was part of the Integrated Microsystems for Biosensing program (3E), within the Nanomedicine theme in the NanoNextNL consortium. The cluster within which this research was carried out aims at the development of microsystems-based lab-on-a-chip systems for the improved detection of microbial pathogens. The researchers participating in the NanoNextNL program have the responsibility of addressing potential risks involved in their research for human health and the environment.

The use of PAO surfaces for capture and growth of bacteria present a very low risk for human health, considering that it would not be in contact with the patient. However, the person who is manipulating the PAO surfaces needs to be aware of the fragility of the material to avoid its breakage in smaller pieces, which could be inhaled or released to the environment. Specifically, the nanometer-sized pores in this material, which makes it fit within the realm of nanomedicine, is only relevant with respect to the micron-sized bacteria, as these cannot penetrate the membrane whereas nutrients can. Finally, PAO has a thickness in the hundreds of microns or even thicker, and neither normal use nor extensive heating (used in the cleaning of chemical waste) is not expected to lead to free nanometer-sized aluminum oxide-based particles.

Another potential risk of the use of PAO is related to its disposal. Despite the inherent risks of bacterial samples and the suitable methods for their inactivation and disposal, the biofunctionalized PAO surfaces are prepared for a single use. Disposal of

the surfaces after autoclave treatment should follow the protocols for the disposal of solid chemical waste.

The development of biofunctionalized PAO as a platform for diagnosis of bacterial infections could lead to rapid results for identification of the pathogenic strain as well as for the susceptibility or resistance to certain antibiotics. The use of the proper antibiotic to treat the infection would lead to faster recovery for the patient and could also avoid antibiotic resistance.

The evaluation of the RATA aspects in this stage of the research indicate few risks, which can be circumvented if suitable information and training is provided the end users of biofunctionalized PAO surfaces. Additional risks and long-term societal impact need to be evaluated during the course of the research.

References

1. Bhairamadi, N. S.; Pujari, S. P.; Trovela, F. G.; Debrassi, A.; Khamis, A. A.; Alonso, J. M.; Al Zaharani, A. A.; Wennekes, T.; Al-Turaif, H. A.; van Rijn, C.; Alhamed, Y. A.; Zuilhof, H. Hydrolytic and thermal stability of organic monolayers on various inorganic substrates. *Langmuir* **2014**, *30*, 5829-5839.
2. Kuribara, K.; Wang, H.; Uchiyama, N.; Fukuda, K.; Yokota, T.; Zschieschang, U.; Jaye, C.; Fischer, D.; Klauk, H.; Yamamoto, T.; Takimiya, K.; Ikeda, M.; Kuwabara, H.; Sekitani, T.; Loo, Y.-L.; Someya, T. Organic transistors with high thermal stability for medical applications. *Nat. Commun.* **2012**, *3*.
3. Horlacher, T.; Seeberger, P. H. Carbohydrate arrays as tools for research and diagnostics. *Chem. Soc. Rev.* **2008**, *37*, 1414.
4. Bernardi, A.; Jimenez-Barbero, J.; Casnati, A.; De Castro, C.; Darbre, T.; Fieschi, F.; Finne, J.; Funken, H.; Jaeger, K. E.; Lahmann, M.; Lindhorst, T. K.; Marradi, M.; Messner, P.; Molinaro, A.; Murphy, P. V.; Nativi, C.; Oscarson, S.; Penades, S.; Peri, F.; Pieters, R. J.; Renaudet, O.; Reymond, J. L.; Richichi, B.; Rojo, J.; Sansone, F.; Schaffer, C.; Turnbull, W. B.; Velasco-Torrijos, T.; Vidal, S.; Vincent, S.; Wennekes, T.; Zuilhof, H.; Imbert, A. Multivalent glycoconjugates as anti-pathogenic agents. *Chem. Soc. Rev.* **2013**, *42*, 4709-4727.
5. Huskens, J. Multivalent interactions at interfaces. *Curr. Opin. Chem. Biol.* **2006**, *10*, 537-543.
6. Slaney, A. M.; Wright, V. A.; Meloncelli, P. J.; Harris, K. D.; West, L. J.; Lowary, T. L.; Buriak, J. M. Biocompatible Carbohydrate-functionalized stainless steel surfaces: a new method for passivating biomedical implants. *ACS Appl. Mater. Inter.* **2011**, *3*, 1601-1612.
7. Szunerits, S.; Niedziolka-Joensson, J.; Boukherroub, R.; Woisel, P.; Baumann, J.-S.; Siriwardena, A. Label-free detection of lectins on carbohydrate-modified boron-doped diamond surfaces. *Anal. Chem.* **2010**, *82*, 8203-8210.
8. Lindhorst, T. K.; Dubber, M. Octopus glycosides: multivalent molecular platforms for testing carbohydrate recognition and bacterial adhesion. *Carbohydr. Res.* **2015**, *403*, 90-97.
9. Grishin, A. V.; Krivozubov, M. S.; Karyagina, A. S.; Gintsburg, A. L. *Pseudomonas aeruginosa* lectins as targets for novel antibacterials. *Acta Naturae* **2015**, *7*, 29-41.
10. Yang, Q.; Strathmann, M.; Rumpf, A.; Schaule, G.; Ulbricht, M. Grafted glycopolymers-based receptor mimics on polymer support for selective adhesion of bacteria. *ACS Appl. Mater. Inter.* **2010**, *2*, 3555-3562.
11. Disney, M. D.; Seeberger, P. H. The use of carbohydrate microarrays to study carbohydrate-cell interactions and to detect pathogens. *Chem. Biol.* **2004**, *11*, 1701-1707.
12. den Hertog, A. L.; Menting, S.; Smienk, E. T.; Werngren, J.; Hoffner, S.; Anthony, R. M. Evaluation of a microcolony growth monitoring method for the rapid determination of ethambutol resistance in *Mycobacterium tuberculosis*. *BMC Infect. Dis.* **2014**, *14*, 9.
13. Tsou, P. H.; Sreenivasappa, H.; Hong, S. M.; Yasuike, M.; Miyamoto, H.; Nakano, K.; Misawa, T.; Kameoka, J. Rapid antibiotic efficacy screening with aluminum oxide nanoporous membrane filter-chip and optical detection system. *Biosens. Bioelectron.* **2010**, *26*, 289-294.
14. Ingham, C. J.; Sprengels, A.; Bomer, J.; Molenaar, D.; van den Berg, A.; Vlieg, J.; de Vos, W. M. The micro-Petri dish, a million-well growth chip for the culture and high-throughput screening of microorganisms. *Proc. Natl. Acad. Sci. U. S. A.* **2007**, *104*, 18217-18222.
15. Song, S.; Wang, L.; Li, J.; Fan, C.; Zhao, J. Aptamer-based biosensors. *Trends Anal. Chem.* **2008**, *27*, 108-117.
16. van Hattum, H.; Martin, N. I.; Ruijtenbeek, R.; Pieters, R. J. Development of a microarray detection method for galectin cancer proteins based on ligand binding. *Anal. Biochem.* **2013**, *434*, 99-104.
17. Kumeria, T.; Kurkuri, M. D.; Diener, K. R.; Parkinson, L.; Losic, D. Label-free reflectometric interference microchip biosensor based on nanoporous alumina for detection of circulating tumour cells. *Biosens. Bioelectron.* **2012**, *35*, 167-173.
18. Wang, C.; Feng, B. Research progress on site-oriented and three-dimensional immobilization of protein. *Mol. Biol.* **2015**, *49*, 1-20.
19. Adak, A. K.; Li, B. Y.; Huang, L. D.; Lin, T. W.; Chang, T. C.; Hwang, K. C.; Lin, C. C. Fabrication of antibody microarrays by light-induced covalent and oriented immobilization. *ACS Appl. Mater. Inter.* **2014**, *6*, 10452-10460.
20. Shrestha, D.; Bagosi, A.; Szollosi, J.; Jenéi, A. Comparative study of the three different fluorophore antibody conjugation strategies. *Anal. Bioanal. Chem.* **2012**, *404*, 1449-1463.
21. Jonkheijm, P.; Weinrich, D.; Schroeder, H.; Niemeyer, C. M.; Waldmann, H. Chemical strategies for generating protein biochips. *Angew. Chem. Int. Ed.* **2008**, *47*, 9618-9647.

22. Trilling, A. K.; Beekwilder, J.; Zuilhof, H. Antibody orientation on biosensor surfaces: a minireview. *Analyst* **2013**, *138*, 1619-1627.
23. Palomo, J. M. Diels-Alder cycloaddition in protein chemistry. *Eur. J. Org. Chem.* **2010**, 6303-6314.
24. Kalia, J.; Abbott, N. L.; Raines, R. T. General method for site-specific protein immobilization by staudinger ligation. *Bioconjugate Chem.* **2007**, *18*, 1064-1069.
25. Govindaraju, T.; Jonkheijm, P.; Gogolin, L.; Schroeder, H.; Becker, C. F. W.; Niemeyer, C. M.; Waldmann, H. Surface immobilization of biomolecules by click sulfonamide reaction. *Chem. Commun.* **2008**, 3723-3725.
26. Jonkheijm, P.; Weinrich, D.; Koehn, M.; Engelkamp, H.; Christianen, P. C. M.; Kuhlmann, J.; Maan, J. C.; Nuesse, D.; Schroeder, H.; Wacker, R.; Breinbauer, R.; Niemeyer, C. M.; Waldmann, H. Photochemical surface patterning by the thiol-ene reaction. *Angew. Chem. Int. Ed.* **2008**, *47*, 4421-4424.
27. Weinrich, D.; Lin, P.-C.; Jonkheijm, P.; Nguyen, U. T. T.; Schroeder, H.; Niemeyer, C. M.; Alexandrov, K.; Goody, R.; Waldmann, H. Oriented immobilization of farnesylated proteins by the thiol-ene reaction. *Angew. Chem. Int. Ed.* **2010**, *49*, 1252-1257.
28. Josenhans, C.; Friedrich, S.; Suerbaum, S. Green fluorescent protein as a novel marker and reporter system in *Helicobacter* sp. *FEMS Microbiol. Lett.* **1998**, *161*, 263-273.
29. Ahmed, A.; Rushworth, J. V.; Hirst, N. A.; Millner, P. A. Biosensors for whole-cell bacterial detection. *Clin. Microbiol. Rev.* **2014**, *27*, 631-646.
30. Schlenoff, J. B. Zwitteration: coating surfaces with zwitterionic functionality to reduce nonspecific adsorption. *Langmuir* **2014**, *30*, 9625-9636.
31. Chen, S.; Li, L.; Zhao, C.; Zheng, J. Surface hydration: principles and applications toward low-fouling/nonfouling biomaterials. *Polymer* **2010**, *51*, 5283-5293.
32. Banerjee, I.; Pangule, R. C.; Kane, R. S. Antifouling coatings: recent developments in the design of surfaces that prevent fouling by proteins, bacteria, and marine organisms. *Adv. Mater.* **2011**, *23*, 690-718.
33. Nguyen, A. T.; Baggerman, J.; Paulusse, J. M. J.; Zuilhof, H.; van Rijn, C. J. M. Bioconjugation of protein-repellent zwitterionic polymer brushes grafted from silicon nitride. *Langmuir* **2012**, *28*, 604-610.
34. Li, Y.; Giesbers, M.; Gerth, M.; Zuilhof, H. Generic top-functionalization of patterned antifouling zwitterionic polymers on indium tin oxide. *Langmuir* **2012**, *28*, 12509-12517.

Summary

Porous aluminum oxide (PAO) is a nanostructured material used for various biotechnological applications, including the culturing microorganisms and other types of cells. The ability to chemically modify the PAO surface and tailor its surface properties is a promising way to expand and refine its applications. The immobilization of biomolecules on PAO that specifically interact with and bind to target bacteria would enable the capture and subsequent growth of bacteria on the same surface, and this was the ultimate goal of the research presented in this thesis (**Figure 1**).

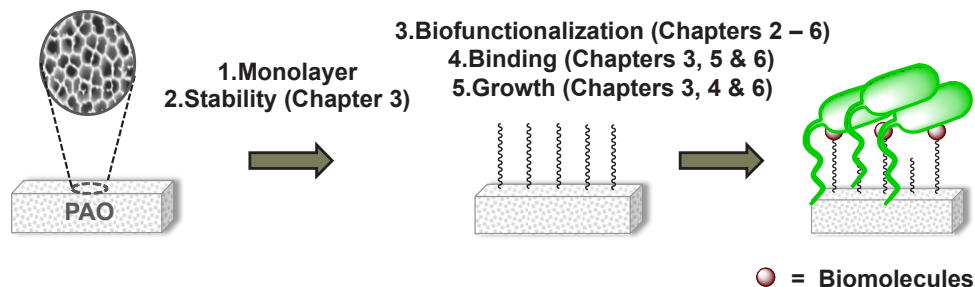


Figure 1. Outline of the thesis.

After a general introduction to the overall subject of this thesis, presented in **Chapter 1**, the most commonly used and recent methods to prepare glycosurfaces are reviewed and compared on their merits and drawbacks in **Chapter 2**. Although there are a great number of techniques, the main challenge that still remains is to develop an accessible, reproducible and inexpensive approach that produces well-defined and stable glycosurfaces using as few steps as possible. The most used analytical techniques for the characterization of glycosurfaces and several applications of these surfaces in the binding, capture, and sensing of bacteria and bacterial toxins were also discussed in **Chapter 2**.

Biofunctionalization of surfaces in general requires a stepwise approach, in which it is very important to have a stable monolayer as the first step. At the beginning of this research it was known that various functional groups were able to react with

(porous) aluminum oxide, but there was no comprehensive study comparing the stability of these modified surfaces under the conditions that are important for microbiological applications. In **Chapter 3**, the PAO surface was modified with various functional groups known to react with PAO (carboxylic acid, α -hydroxycarboxylic acid, alkyne, alkene, phosphonic acid, and silane), and the stability of these modified surfaces was assessed over a range of pH and temperatures that are relevant for microbial growth. Silane and phosphonate-modified PAO surfaces with a hydrophobic monolayer proved to be the most stable ones, but the phosphonate modification was both more easily applied and reproducible. This modification was stable for at least two weeks in buffer solutions with pH values between 4 and 8, and at temperatures up to 40 °C. Only at elevated temperatures of 60 °C and 80 °C under hydrolytic conditions it was observed that the stability of the same monolayer on PAO decreased gradually. As a proof-of-principle for the biofunctionalization and bacterial capture on this PAO phosphonate monolayer, an alkyne-terminated monolayer was biofunctionalized via a CuAAC click reaction with an azido-mannoside and the binding and growth of *Lactobacillus plantarum* was successfully demonstrated.

In **Chapter 4** various approaches to install reactive groups onto the phosphonate-modified PAO surface were developed, creating a (bio)functionalization “tool-box”. PAO surfaces presenting different terminal reactive groups were prepared, such as azide, alkyne, alkene, thiol, isothiocyanate, and *N*-hydroxysuccinimide (NHS), starting from a single, straightforward and stable initial modification with a bromo-terminated phosphonic acid. These reactive surfaces were then used to immobilize (bio)molecules, including carbohydrates and proteins. Fluorescently labeled bovine serum albumin (BSA) was covalently immobilized on the PAO surface as a proof-of-principle, and it was shown that a range of bacteria could still grow on the BSA-functionalized PAO surface.

With a PAO (bio)functionalization tool-box in hand, the successful proof-of-principle mannoside-dependent binding and growth of *L. plantarum* on PAO (**Chapter 3**) was further investigated and expanded upon (**Chapter 5**). The parameters involved in the preparation of these surfaces and in the binding with *L. plantarum* were investigated in more detail in **Chapter 5**, such as the nature of the spacer connected to the mannoside derivative and the presence of soluble carbohydrates and bovine serum albumin (BSA) in the medium. The surfaces with the azido-mannoside with the long

hydrophobic spacer showed the best binding of *L. plantarum* when compared to a long PEG-based hydrophilic spacer and a short hydrophobic one. The presence of a soluble α -glucoside did not prevent the binding of the bacteria to the mannose-presenting PAO, and similar results were obtained when BSA was present. Additionally, a mutant strain of *L. plantarum* that does not have the mannose-specific adhesion was not able to bind to the mannose-presenting PAO. When taken together, this proves that the mannoside–adhesin interaction is the main mechanism of binding the bacteria to the mannose-biofunctionalized PAO in this system.

In **Chapter 6**, the NHS-terminated PAO developed in **Chapter 4** was used for the immobilization of antibodies against *Escherichia coli*. After an extensive optimization of the modification chemistry of the surfaces and the incubation conditions, commercially available anti-*E. coli* antibodies were immobilized on the PAO surface. Binding and washing experiments indeed demonstrated increased binding of *E. coli* on the antibody-presenting PAO surfaces, providing avenues for testing other bacteria such as *Lactobacillus rhamnosus* GG widely used in probiotic formulations worldwide.

In **Chapter 7**, the most important achievements of this project are discussed, together with additional ideas and recommendations for further research. Most notably some preliminary results are presented on the immobilization of two antibodies against *L. rhamnosus* GG: anti-*L. rhamnosus* GG, against the whole bacterial cell, and anti-SpaC, against only the SpaC part of the pili present on the cell surface of *L. rhamnosus* GG. Anti-*L. rhamnosus* GG antibody showed promising but not yet optimal increased binding of *L. rhamnosus* GG. Finally, some reflections on PAO and its (bio)functionalization are provided in the context of a risk analysis and technology assessment.

Acknowledgements

The PhD project has given me the opportunity to meet many great people who have contributed in various ways to the completion of this thesis.

I would like to thank Prof. Han Zuilhof, my thesis promoter at the Laboratory of Organic Chemistry (ORC), for giving me the opportunity to perform my PhD research at ORC. Thank you for your support and for all the scientific discussions and advices.

Many thanks also to Prof. Willem de Vos, my thesis promoter at the Laboratory of Microbiology (MIB), for the opportunity to learn more about this field that scared me at the beginning. Thank you for your patience in explaining concepts and for all the ideas and contributions to the project.

I would most like to thank Dr. Tom Wennekes, my thesis co-promoter and my daily supervisor. Tom, your positive attitude and enthusiasm towards science helped me keeping motivated during the years of my PhD. Thank you for being so helpful and understanding and for all the great ideas that you contributed to my thesis. I wish you a lot of success in this new step of your career at Utrecht University.

Many thanks to the people from MIB who helped me in this project. Thanks to Steven Aalvink for always being so helpful and for preparing everything that I needed for my experiments there. Thanks to Dr. Angela Ribbera for helping me in the beginning of the microbiological part of the project. Thanks to Dr. Hanne Tytgat for the help in the final months of experimental work and also for the corrections and suggestions in Chapter 6.

I would like to thank Dr. Colin Ingham and Dr. Zalan Szabo from MicroDish for our meetings and discussions about the project. Thanks also to the NanoNextNL team, especially the ones in the 3E Program, for the interesting discussions.

Thanks to the members of ORC for the discussions and suggestions, especially during group meetings. Thanks to Ton, Teris, Maurice, Michel, and Maarten. Thanks to Barend, Marcel, Ronald, Remco, Elbert, Pepijn, Frank, and Judith for all the technical expertise and support. Thanks also to the education staff: Cees, Carel, Erik, and Anne-Marie for their help with the teaching duties. Many thanks to Elly, Aleida, Anita, and Linda for the help with the official and financial matters.

Thanks to all my PhD and postdoc colleagues at ORC: Alexandre, Nagesh, Sourav, Jaime, Wouter, Sidhu, Radostina, Nagendra, Satesh, Umesh, Saurabh, Peter, Yao, Yan Li, Steven, Florine, Bas, Wilco, Sweccha, Kuldeep, Txema, Bram, Frank, Jorin, Tjerk, Rick, Christie, Esther, Wang, Fatima, Medea, Sjoerd, Digvijay, Fred, Stefanie, and Jorge. Alexandre and Dani, thanks for telling Angela and Cristiani about the PhD position. If it was not for this networking, my adventure in Wageningen would have never happened. Alexandre, additional thanks for being positive and encouraging in all coffee and lunch breaks. Tjerk and Sweccha, special thanks for being my paranymphs. Sweccha, additional thanks for the fun during the zumba lessons. I really miss them! Tjerk, Sjoerd, and Jaime, thanks for the nice atmosphere in the office and in the lab. Umesh and Satesh, thanks for being great friends and for all the support during this challenging PhD journey. Sidhu, thanks for answering so many questions, especially about XPS. Wang, thanks for the nice coffee breaks, especially at the end of my PhD time.

Thanks a lot to the Surfix team: Luc, Esther, Anke, Jelmer, and Carole. Luc, Esther, and Anke, thanks for all the nice ideas and suggestions for this PhD project and for being part of Chapter 4.

Ai and Jacob, thanks for all the lunch breaks and squash matches. I hope we will be able to play together again some day.

Many thanks to my students Marleen de Kool, Selina Thijssen, and Nathalja Berghuis for their contributions to my thesis. Marleen, thanks for teaching me how to be more assertive. Selina, thanks for all the work that you did for Chapter 4. Nathalja, thanks for the help in Chapter 5 with all those microbiological experiments and washing steps, and also for introducing me to zumba.

I would also like to thank my former supervisor, Dr. Clóvis Antonio Rodrigues, for introducing me to scientific research. Thanks for always encouraging me to pursue my dreams. I would like to extend my gratitude to Dr. Angela Malheiros and Dr. Cristiani Bürger, who told me about this PhD position at ORC after a trip to Wageningen. Thanks for all the support and encouragement.

I also want to thank my friends outside the lab: Suraj, Alice, Hilda, Leonie, Sam, Jenny, Violeta, Suzanne. Thanks for welcoming me in your group and for the great dinners together.

Thanks to all my friends from Brazil for the support despite the distance. Special thanks to Thaisa, Luiz, and Zhelmy, who visited me in the Netherlands. I hope we can meet again soon.

I would like to thank my love Cezary. We met in the second month of my PhD and you have supported me since then. Thanks for your love, patience, and understanding, and for making my days happier. I would like to extend my gratitude to my Polish family, who welcomed me so warmly.

Finally, many thanks to my family, especially to my parents, Adalberto and Mara, and my grandparents, Dalva (*in memoriam*), Vicente, and Ana. Obrigada por entenderem minhas decisões, pelo enorme amor e apoio. Eu sinto saudades de vocês todos os dias. Thanks for understanding my decisions, for the huge love and support. I miss you everyday.

Thank you!

Curriculum vitae

Aline Debrassi was born in Joinville, Brazil, on 7th October 1987. After finishing the high school at Colégio São Luiz in Brusque in 2004, she started her study in Pharmacy at Universidade do Vale do Itajaí (UNIVALI). After obtaining her BSc degree, she started her master studies in Pharmaceutical Sciences at the same university under the supervision of Dr. Clóvis Antonio Rodrigues. There she worked on the synthesis and characterization of magnetic nanoparticles for targeted drug delivery. In 2011, she joined the Laboratory of Organic Chemistry at Wageningen University under the supervision of Dr. Tom Wennekes, Prof. Han Zuilhof, and Prof. Willem de Vos. The most important findings of this research are described in this thesis. In August 2015, Aline joined the company Surflay Nanotec, in Berlin, Germany, to work on the Marie Curie Project SYNCHRONICS.



List of Publications

Debrassi, A.; de Vos, W. M.; Zuilhof, H.; Wennekes, T. (2015) *Carbohydrate-presenting self-assembled monolayers: preparation, analysis and applications in microbiology*. In Stine, K. ed. **Carbohydrate Nanotechnology**, Hoboken, NJ, Wiley.

Debrassi, A.; Roeven, E.; Thijssen, S.; Scheres, L. M. W.; de Vos, W. M.; Wennekes, T.; Zuilhof, H. (2015) *Versatile (bio)functionalization of bromo-terminated phosphonate-modified porous aluminum oxide*. **Langmuir** 31, 5633-5644.

Demarchi, C. A.; **Debrassi, A.**; Dal Magro, D.; Nedelko, N.; Ślawska-Waniewska, A.; Dłużewski, P.; Greneche, J. M.; Rodrigues, C. A. (2015) *Adsorption of Cr(VI) on crosslinked chitosan-Fe(III) complex in fixed-bed systems*. **Journal of Water Process Engineering** 7, 141-152.

Debrassi, A.; Ribbera, A.; de Vos, W. M.; Wennekes, T.; Zuilhof, H. (2014) *Stability of (bio)functionalized porous aluminium oxide*. **Langmuir** 30, 1311-1320.

Bhairamadgi, N. S.; Pujari, S. P.; Trovela, F. G.; **Debrassi, A.**; Khamis, A. A.; Alonso, J. M.; Zahrani, A. A. A.; Wennekes, T.; Al-Turaif, H. A.; van Rijn, C.; Alhamed, Y. A.; Zuilhof, H. (2014) *Hydrolytic and thermal stability of organic monolayers on various inorganic substrates*. **Langmuir** 30, 5829-5839.

Manova, R.; Joshi, S.; **Debrassi, A.**; Bhairamadgi, N.; Roeven, E.; Gagnon, J.; Nazir, M.; Claassen, F.; Scheres, L.; Wennekes, T.; Schroen, K.; van Beek, T.; Zuilhof, H.; Nielen, M. (2014) *Ambient surface analysis of organic monolayers using direct analysis in real time orbitrap mass spectrometry*. **Analytical Chemistry** 86, 2403-2411.

Demarchi, C. A.; **Debrassi, A.**; Buzzi, F. C.; Correa, R.; Cechinel Filho, V.; Rodrigues, C. A.; Nedelko, N.; Demchenko, P.; Ślawska-Waniewska, A.; Dłużewski, P. (2014) *A magnetic nanogel based on O-carboxymethylchitosan for antitumor drug delivery: Synthesis, characterization and in vitro drug release*. **Soft Matter** 10, 3441-3450.

Tocci, N.; D'Auria, F. D.; Simonetti, G.; Panella, S.; Palamara, A. T.; **Debrassi, A.**; Rodrigues, C. A.; Cechinel Filho, V.; Sciubba, F.; Pasqua, G. (2013) *Bioassay-guided fractionation of extracts from *Hypericum perforatum* in vitro roots treated with carboxymethylchitosans and determination of antifungal pathogens*. **Plant Physiology and Biochemistry** 70, 342-347.

Debrassi, A.; Correa, A.; Baccarin, T.; Nedelko, N.; Ślawska-Waniewska, A.; Sobczak, K.; Dłużewski, P.; Greneche, J. M.; Rodrigues, C. A. (2012) *Removal of cationic dyes from*

aqueous solutions using N-benzyl-O-carboxymethylchitosan magnetic nanoparticles. Chemical Engineering Journal 183, 284-293.

Rosa, T. R. O.; **Debrassi, A.**; Lucinda-Silva, R. M.; Bressan, C.; Freitas, R. A.; Rodrigues, C. A. (2012) *Synthesis of N-benzyl-O-carboxymethylchitosan and application in the solubilization enhancement of a poorly water-soluble drug (triamcinolone). Journal of Applied Polymer Science* 124, 4206-4212.

Demarchi, C. A.; **Debrassi, A.**; Rodrigues, C. A. (2012) *The use of jatoba bark for removal of cationic dyes. Review of Progress in Coloration and Related Topics* 128, 208-217.

Debrassi, A.; Baccarin, T.; Demarchi, C. A.; Nedelko, N.; Ślawska-Waniewska, A.; Dłużewski, P.; Bilska, M.; Rodrigues, C. A. (2012) *Adsorption of Remazol Red 198 onto magnetic N-lauryl chitosan particles: equilibrium, kinetics, reuse and factorial design. Environmental Science and Pollution Research* 19, 1594-1604.

Debrassi, A.; Rodrigues, C. A. (2011) *Adsorption of cationic dyes from aqueous solution by termite feces, a non-conventional adsorbent. Clean – Soil Air Water* 39, 549-556.

Debrassi, A.; Burger, C.; Rodrigues, C. A.; Nedelko, N.; Ślawska-Waniewska, A.; Dłużewski, P.; Sobczak, K.; Greneche, J. M. (2011) *Synthesis, characterization and in vitro drug release of magnetic N-benzyl-O-carboxymethylchitosan nanoparticles loaded with indomethacin. Acta Biomaterialia* 7, 3078-3085.

Debrassi, A.; Largura, M. C. T.; Rodrigues, C. A. (2011) *Adsorption of congo red dye by hydrophobic O- carboxymethylchitosan derivatives. Química Nova* 34, 764-770.

Largura, M. C. T.; **Debrassi, A.**; Santos, H. H.; Marques, A. T.; Rodrigues, C. A. (2010) *Adsorption of rhodamine B onto O-carboxymethylchitosan-N-lauryl. Separation Science and Technology* 45, 1490-1498.

Dusza, A.; Wojtyniak, M.; Nedelko, N.; Ślawska-Waniewska, A.; Greneche, J. M.; Rodrigues, C. A.; Bürger, C.; Stringari, C.; **Debrassi, A.** (2010) *Magnetic behavior of O-carboxymethylchitosan bounded with iron oxide particles. IEEE Transactions on Magnetism* 46, 459-462.

Klepka, M. T.; Nedelko, N.; Greneche, J. M.; Lawniczak-Jablonska, K.; Demchenko, I. N.; Ślawska-Waniewska, A.; Rodrigues, C. A.; **Debrassi, A.**; Bordini, C. (2008) *Local atomic structure and magnetic ordering of iron in Fe-chitosan complexes. Biomacromolecules* 9, 1586-1594.

Overview of Completed Training Activities



Discipline Specific Activities

| | | |
|--|-----------------------|------------|
| Advanced Organic Chemistry | VLAG | 2011-2015 |
| MicroNano Conference (3×) | MinacNed / NanoNextNL | 2011-2013 |
| NWO CHAINS Conference (2×) | NWO-Chemistry / KNCV | 2011, 2014 |
| NWO-Chemistry Meeting (2×) | NWO-Chemistry / KNCV | 2012, 2013 |
| Advanced Drug Delivery and Drug Targeting Course | GUIDE / LACDR / UIPS | 2013 |
| Biodetection & Biosensors | SELECTBIO | 2015 |

General Courses

| | | |
|--|-------------|------|
| VLAG PhD Week | VLAG | 2012 |
| PhD Competence Assessment | WGS | 2012 |
| Techniques for Writing and Presenting a Scientific Paper | WGS | 2013 |
| Scientific Artwork | WUR Library | 2013 |
| Scientific Integrity | WGS | 2013 |
| Communication in Interdisciplinary Research | WGS | 2013 |
| Career Perspectives | WGS | 2014 |

Optionals

| | | |
|--|-----|------------|
| Preparation of Research Proposal | ORC | 2011 |
| Research Methods in Microbiology | MIB | 2012 |
| PhD Study Trips: Germany and Switzerland (2013) and Canada (2015) | ORC | 2013, 2015 |
| Group Meetings Organic Chemistry | ORC | 2011-2015 |
| Weekly Colloquium Organic Chemistry | ORC | 2011-2015 |
| Monthly Literature Club (Synthetic Organic Chemistry and Chemical Biology) | ORC | 2013-2015 |

The research presented in this thesis was financially supported by NanoNextNL.

Financial support from Wageningen University for printing this thesis is gratefully acknowledged.

Design and layout by Aline Debrassi and Cezary Smaczniak

Printed by GVO drukkers & vormgevers B.V.